

BIOPROCESS DEVELOPMENT
FOR THE CELL-BASED TREATMENT OF DIABETES

by

Corinne Hoesli

B. A. Sc. and B. Sc., The University of Ottawa, 2003 and 2002

A THESIS SUBMITTED IN PARTIAL FULFILLMENT OF
THE REQUIREMENTS FOR THE DEGREE OF
DOCTOR OF PHILOSOPHY

in

The Faculty of Graduate Studies
(Chemical & Biological Engineering)

THE UNIVERSITY OF BRITISH COLUMBIA

(Vancouver)

November 2010

© Corinne Hoesli, 2010

ABSTRACT

The widespread cellular treatment of type 1 diabetes by islet transplantation is limited by tissue shortage and graft rejection. This work describes two novel bioprocesses to immobilize pancreatic cells in alginate using: (1) hollow fiber bioreactors or (2) alginate bead generation by an adapted emulsion and internal gelation process. After optimization, live cell recovery rates and growth rates were not significantly different between these more scalable processes and conventional methods of alginate immobilization. After 10 days of alginate-immobilized culture, the insulin content of neonatal porcine cells cultured in a hollow fiber bioreactor increased by 4 fold, while the insulin expression of human islet-depleted tissue cultured in emulsion beads increased by 67 ± 32 fold, matching previous reports that used small-scale cultures. Solutions with >100 Pa·s viscosity could be used with the emulsion process to generate beads with higher concentration and greater antibody exclusion than has been so far permitted by nozzle-based encapsulators. The 5% alginate beads generated by the emulsion process led to blood glucose normalization of allogeneic β -cells transplanted into diabetic mice within 2 weeks, while mice transplanted with 1.5% alginate beads generated by a conventional encapsulator remained hyperglycemic after 20 days. The improved result with the 5% alginate emulsion beads was associated with lower graft-specific antibody plasma levels. These results suggest that the 5% alginate beads provided improved immune isolation of the graft. If human pancreatic progenitors are to be used for the large-scale generation of insulin+ cells in alginate, their expansion in serum-free medium will be a prerequisite. Pancreatic duct-like cells are expected to have more potential to generate insulin+ cells than the fibroblast-like cells that overgrow unsorted cultures of islet-depleted human pancreatic tissue. The last part of this thesis describes the magnetic-activated depletion of CD90-expressing cells, which reduced the fraction of CD90+ fibroblast-like cells from $34 \pm 20\%$ to $1.3 \pm 0.6\%$. This allowed the expansion of the duct-like cell population in an optimized serum-free medium. These novel pancreatic cell culture methods could be used to generate and/or offer immune protection to insulin+ cells for the clinical-scale cellular treatment of diabetes.

PREFACE

Each chapter of the body of this thesis represents a manuscript that either has been published or accepted for publication, or will be submitted for publication. I was a major contributor along with James Piret in deciding the general direction of all of the projects. I contributed most of the experimental design, except for Chapter 2, to which Minh Luu contributed the initial work during her M.A.Sc. thesis. I also supervised two excellent undergraduate students, Roger Kiang and Kamini Raghuram, who contributed creatively and manually to Chapters 3 and 4. James Piret was the main supervisor for all chapters with important input from Timothy Kieffer (UBC), James Johnson (UBC) and Igor Lacík (Slovak Academy of Sciences) on alginate properties and cell encapsulation. The detailed contributions were as follows:

Chapter 2: “A Novel Alginate Hollow Fiber Bioreactor Process for Cellular Therapy Applications” was published in 2009 in *Biotechnology Progress* 25(6): 1740-1751, Copyright © 2009 by the American Institute of Chemical Engineers. Note that in this chapter, the author that generated the data shown is provided in the figure legend.

Corinne A. Hoesli: Contributed ~30% of experimental design, ~50% of experimental work, ~80% of the final data and text in the manuscript. Bioreactor cultures of CHO cells and primary porcine tissue.

Minh Luu (equal contribution): Rest of experimental design, work and final data and text. Process development with CHO cells.

James M. Piret: Supervision of Corinne and Minh, edited the manuscript.

Chapter 3: “Pancreatic Cell Immobilization in Alginate Beads Produced by Emulsion and Internal Gelation” was published in an abbreviated form online ahead of print in *Biotechnology and Bioengineering* on October 11th, Copyright © 2010 by Wiley-Blackwell.

Corinne A. Hoesli: Overall experimental design, ~50% of experimental work, supervised Kamini (2nd and 4th year undergraduate Co-op, 4th year thesis project) and Roger (4th year Co-up), writing of the manuscript

Kamini Raghuram: ~25% of the experimental design and work, developed the non-optimized process and determined the variables that should be optimized

Roger Kiang: ~10% of the experimental design and work, contributed to the MIN6 the growth and secretion experiments

Dušana Mocinecová: ~10% of the experimental design and work, performed the compression measurements
Xiaoke Hu: ~5% of the experimental design and work, performed all perfusions
James D. Johnson: Advice, edited the manuscript, supervised Xiaoke Hu.
Igor Lacík: Discussions with CH on internal gelation and bead properties, edited the manuscript, supervised Dušana Mocinecová.
Timothy J. Kieffer: Advice and ~20% of project supervision, edited the manuscript
James M. Piret: ~80% of the project supervision, edited the manuscript

Chapter 4: “Reversal of diabetes by β TC3 cells encapsulated in alginate beads generated by emulsion and internal gelation” will be submitted to a peer-reviewed journal.

Corinne A. Hoesli: Overall direction of the project, ~60% of experimental design, ~25% of experimental work, wrote the manuscript
Roger Kiang: ~20% of experimental design, ~55% of experimental work, transplantations, animal monitoring, *in vitro* analysis, edited the manuscript
Dušana Mocinecová: ~10% of experimental design and work, performed compression measurements and size exclusion chromatography
Madeleine Speck: ~5% of experimental design and work, performed transplantations, helped design the transplantation experiments
Daniela Jochek Moskova: ~2.5% of experimental design and work, viscosity tests
Christine Donald: ~2.5% of experimental design & work, transplantation pilot study
Igor Lacík: Advice and input on bead strength, porosity and stability, supervised Dušana
Timothy J. Kieffer: ~50% of the project supervision, supervised Madeleine and Christine
James M. Piret: ~50% of the project supervision, supervised Corinne and Roger

Chapter 5: “A serum-free high content imaging platform to identify pancreatic duct mitogens after CD90+ fibroblast depletion”. An abbreviated version will be submitted to a peer-reviewed journal.

Corinne A. Hoesli: Experimental work, experimental design, wrote the manuscript.
Garth L. Warnock: Provided islet tissue, general advice and perspective.
James D. Johnson: Advice on experimental design and interpretation, edited the manuscript.
James M. Piret: Supervision of the project, corrected the manuscript.

Ethical approval

Work with biohazards (level 2) in all Chapters was approved by the UBC BioSafety Committee (protocol # B09-0105).

All animal procedures were approved by the Canadian Council on Animal Care and the UBC Animal Care Committee (protocol A07-0091.).

The use of tissue from human organ donors at the Vancouver General Hospital was approved by the hospital Clinical Research Ethics Board (certificates C03-0453 beginning in 2003 and H03-70453 beginning in 2010).

TABLE OF CONTENTS

Abstract	ii
Preface	iii
Table of contents	vi
List of tables	x
List of figures	xi
Nomenclature	xv
Acknowledgements	xviii
1 Introduction	1
1.1 Islet transplantation.....	2
1.2 Sources of tissue to generate surrogate β -cells.....	4
1.2.1 Expanded human β -cells.....	4
1.2.2 β -cells derived from non-islet cells.....	5
1.2.2.1 Adult pancreatic stem cells.....	5
1.2.2.2 Duct-derived β -cell progenitors	8
1.2.2.3 Acinar-derived β -cell progenitors	9
1.2.2.4 Mesenchymal β -cell progenitors	10
1.2.2.5 Genetic re-programming of mature pancreatic cell types	10
1.2.3 Insulin+ cells from embryonic or induced pluripotent stem cells.....	11
1.2.4 Xenogeneic islets	12
1.3 Cell immobilization in alginate	13
1.3.1 Alginate gel properties	13
1.3.2 Alginate influence on pancreatic cell differentiation	16
1.3.3 Alginate beads as an immune barrier	18
1.3.3.1 The immune system and encapsulated islet survival.....	19
1.3.3.2 Non-immune factors affecting encapsulated islet survival.....	23
1.3.3.3 Current state of microencapsulated islet transplantation.....	25
1.4 Bioprocesses to scale up alginate immobilization.....	27
1.4.1 Extrusion-based alginate bead generators.....	27
1.4.2 Alginate immobilization in a hollow fiber bioreactor.....	28
1.4.3 Alginate immobilization by emulsion and internal gelation.....	29
1.4.4 Challenges of scaled-up <i>in vitro</i> culture of alginate-immobilized insulin+ cells.....	31
1.5 Research goals.....	32
2 Pancreatic cell immobilization in an alginate-filled hollow fiber bioreactor	35
2.1 Introduction.....	35
Materials and methods	38
2.1.1 CHO cell line.....	38
2.1.2 The effect of process solutions on CHO cell survival	38

2.1.3	The effect of alginate type on CHO cell growth	38
2.1.4	Alginate slab immobilization and recovery	39
2.1.5	AHFBR apparatus and set-up	39
2.1.6	AHFBR process.....	40
2.1.7	AHFBR ICS obstruction	42
2.1.8	AHFBR degree of gelling and cell recovery	42
2.1.9	CHO growth kinetics.....	42
2.1.10	CHO aggregate size distribution	43
2.1.11	NPCC isolation and shipment.....	44
2.1.12	NPCC cell culture.....	44
2.1.13	Cell enumeration.....	45
2.1.14	Insulin and DNA content.....	45
2.1.15	Statistical Analysis	45
2.2	Results and discussion.....	46
2.2.1	The effect of process solutions on CHO cell survival	46
2.2.2	The effect of alginate type on CHO cell growth	47
2.2.3	Complete gelling of alginate in the ECS	47
2.2.4	Higher ICS flow rates reduced fiber obstruction by alginate	49
2.2.5	Five degelling passes yielded >80% cell recovery from the AHFBR	50
2.2.6	AHFBR immobilized culture of CHO cells	52
2.2.7	AHFBR capacity to produce islet-sized CHO cell aggregates.....	55
2.2.8	AHFBR immobilized culture of NPCCs	57
2.2.9	Potential applications	58
2.3	Conclusions	61
3	Pancreatic cell immobilization in alginate beads generated by emulsion and internal gelation.....	63
3.1	Introduction.....	63
3.2	Materials and Methods.....	65
3.2.1	Alginate and cells.....	65
3.2.2	Emulsion process	66
3.2.3	Extrusion process using a vibrating nozzle bead generator	67
3.2.4	Alginate bead size distribution	68
3.2.5	Bead liquefaction and cell enumeration.....	69
3.2.6	Testing the effect of alginate, oil, CaCO ₃ , and acetic acid on MIN6 cell survival	69
3.2.7	Measurement of the initial and final process pH	70
3.2.8	Bead mechanical properties.....	70
3.2.9	MIN6 alginate-immobilized culture and growth parameters	71
3.2.10	Live/dead staining of MIN6 cells in alginate beads	72
3.2.11	Perifusion of immobilized or trypsinized non-immobilized MIN6 cells.....	72
3.2.12	Immobilized culture of human pancreatic exocrine tissue and quantitative PCR.....	73

3.2.13	Statistical analysis.....	74
3.3	Results.....	75
3.3.1	Bead size distribution and control of the average bead diameter.....	75
3.3.2	The effect of alginate, oil, CaCO ₃ , and acetic acid on MIN6 survival.....	77
3.3.3	Process optimization.....	78
3.3.4	Comparison of the emulsion processes with the extrusion process.....	83
3.3.5	Bead strength.....	83
3.3.6	MIN6 cell survival and alginate-immobilized growth.....	84
3.3.7	MIN6 cell glucose-stimulated insulin secretion after immobilized growth.....	87
3.3.8	Culture of primary islet-depleted pancreatic cells in emulsion-generated beads.....	88
3.4	Discussion.....	90
3.5	Conclusions.....	99
4	Transplantation of β -cells in alginate beads generated by emulsion and internal gelation.....	100
4.1	Introduction.....	100
4.2	Materials and methods.....	103
4.2.1	Cell culture.....	103
4.2.2	Alginate.....	104
4.2.3	Microencapsulation by emulsion and internal gelation.....	104
4.2.4	Microencapsulation by extrusion and external gelation.....	105
4.2.5	Alginate bead size distribution.....	105
4.2.6	Alginate viscosity.....	105
4.2.7	Cryo-scanning electron microscopy (cryo-SEM).....	105
4.2.8	Inverse size exclusion chromatography and data analysis.....	106
4.2.9	Bead mechanical properties.....	107
4.2.10	Transplantation, animal monitoring and sampling.....	107
4.2.11	Bead liquefaction and cell enumeration.....	108
4.2.12	Live/dead staining of cells in alginate beads.....	109
4.2.13	Peritoneal lymphocyte quantification.....	109
4.2.14	Quantification of graft-reactive antibodies in mouse serum.....	110
4.2.15	Histology.....	110
4.2.16	Statistical analysis.....	111
4.3	Results.....	111
4.3.1	Emulsion process alginate concentration and viscosity operating range.....	111
4.3.2	Bead porosity, surface topography and strength.....	113
4.3.3	<i>In vivo</i> function of β TC3 cells in emulsion-generated beads.....	118
4.3.4	Adaptive immune response to the grafts.....	122
4.4	Discussion.....	124
4.5	Conclusions.....	131
5	Optimization of primary CK19+ cell cultures.....	132

5.1	Introduction.....	132
5.2	Materials and methods	135
5.2.1	Cell culture.....	135
5.2.2	Conditioned medium	137
5.2.3	Cell dispersion.....	137
5.2.4	Magnetic-activated cell sorting (MACS).....	137
5.2.5	Flow cytometry.....	138
5.2.6	Staining of live cells in 96-well plates.....	139
5.2.7	Immunocytochemistry and Cellomics	140
5.2.8	Alginate immobilization	141
5.2.9	Quantitative reverse transcription polymerase chain reaction	141
5.2.10	Design of experiments and statistical analysis	142
5.3	Results.....	143
5.3.1	Characterization of the main cell types in adherent cultures of unsorted human islet-depleted pancreatic cells.....	143
5.3.2	Effects of depleting CD90-expressing cells from pancreatic islet-depleted cultures	146
5.3.3	Development of a screening platform to optimize CK19+ cell proliferation.....	149
5.3.4	Multifactorial screening of the effects of bFGF, EGF, HGF, KGF and VEGF	151
5.3.5	Effect of alginate immobilization of CD90 sorted cells on insulin expression ..	155
5.4	Discussion.....	156
5.5	Conclusions	164
6	Conclusions and future directions.....	166
	References	176
	Appendix A – Supplementary methods.....	208
	A1. Simplified calculation of CaCO ₃ and acetic acid requirements for complete internal gelation of 1.5% alginate.....	209
	A2. Islet-like cell cluster generation by Matrigel overlay	210
	A3. Cellomics imaging and analysis.....	211
	A4. Quantification of stained cells by ImageJ.....	212
	Appendix B – Supplementary data	213
	B2. Supplementary tables	214
	B3. Supplementary figures	223

LIST OF TABLES

Table 1.1. Long-term encapsulated islet trials in rodents & outcomes in larger mammals or humans.....	26
Table 2.1. Operating conditions of different AHFBR experiments.....	40
Table 2.2. Effect of alginate and flow on average azoalbumin ICS residence times.....	49
Table 2.3. AHFBR CHO growth parameters summary.....	53
Table 5.1. Fractions of cells obtained at different culture times before and after sorting on day 1	147
Table 6.1. Characteristics of alginate immobilization bioprocesses.....	169
Table B1. Protocols to expand adult human pancreatic tissue.....	214
Table B2. q-PCR primers.....	220
Table B3. Human pancreas donor information	220
Table B4. Yield of islet equivalents from the non-islet fraction by adherent culture followed by alginate-immobilized culture in emulsion-generated beads	221
Table B5. Cellomics algorithms and parameters	222

LIST OF FIGURES

Figure 1.1. Physiology of the pancreas.	1
Figure 1.2. Pancreas organogenesis.	7
Figure 1.3. Simplified schematic of the immune response in the context of encapsulated islet transplantation	20
Figure 1.4. Internal gelation reaction steps during the emulsion/internal gelation process.	29
Figure 2.1. AHFBR process flow diagram.	39
Figure 2.2. CHO cell survival in the alginate processing solutions.	46
Figure 2.3. Reduced growth rate of CHO cells due to alginate immobilization.	47
Figure 2.4. Correction of ICS obstruction by alginate by increasing the ICS flow rate during gelling.	48
Figure 2.5. Cumulative viable CHO cell recovery from the AHFBR after each degelling pass.	51
Figure 2.6. CHO cell concentration, pH and metabolite profiles in the AHFBR compared to slab and suspension cultures.	54
Figure 2.7. Aggregate formation by CHO cells in the AHFBR and the control slabs.	56
Figure 2.8. Insulin content of NPCCs during suspension or alginate-immobilized culture.	57
Figure 3.1. Schematic of the emulsion process adapted to mammalian cell immobilization.	66
Figure 3.2. Size distribution of HEPES emulsion alginate beads.	75
Figure 3.3. Cell survival as a function of time for the HEPES emulsion process and omitting various process components (alginate, CaCO ₃ , oil and/or acid).	77
Figure 3.4. Process pH operating range.	79
Figure 3.5. Effects of changes in process time on bead diameter and CaCO ₃ dissolution.	80
Figure 3.6. Effect of process modifications on MIN6 cell survival.	81

Figure 3.7. Cell survival dependence on bead diameter, process buffer and process time.....	82
Figure 3.8. Initial bead bursting force and bead recovery after 21 days agitation at 136 rpm.....	83
Figure 3.9. MIN6 cell expansion in MOPS emulsion-generated 2% alginate beads, MOPS extrusion-generated 2% alginate beads and control adherent cultures.....	85
Figure 3.10. Live/dead stained MIN6 aggregates after of 2 weeks of expansion.....	86
Figure 3.11. Insulin secretion of MIN6 cell aggregates in emulsion-generated beads.....	87
Figure 3.12. Insulin gene expression of islet-depleted human pancreatic tissue before and after 10 days of immobilized culture in emulsion-generated alginate beads.....	90
Figure 4.1. Effect of alginate concentration on the solution zero-shear viscosity and on the surface area moment emulsion bead diameter.....	112
Figure 4.2. Bead permeability measured by size exclusion chromatography.....	114
Figure 4.3. Cryo-scanning electron micrographs of the alginate bead surface.....	115
Figure 4.4. Bead rupture strength before and after size exclusion chromatography.....	116
Figure 4.5. (A) Blood glucose (B) body weight and (C) plasma insulin profiles of C57BL/6 mice transplanted with encapsulated β TC3 cells.....	117
Figure 4.6. Staining of β TC3 cells in alginate beads before and after 20 days <i>in vitro</i> or <i>in vivo</i>	119
Figure 4.7. Beads retrieved from animals 56 days after transplantation.....	120
Figure 4.8. DNA yield in the alginate beads after 20 days <i>in vivo</i> or <i>in vitro</i>	121
Figure 4.9. Adaptive immune response to the β TC3 graft.....	122
Figure 5.1. Phenotype of dispersed unsorted islet-depleted pancreatic cells.....	144
Figure 5.2. Depletion of CD90- cells on day 1 leads to CD90-/Ca19-9+ cell cultures on day 7 as shown by flow cytometry.....	145
Figure 5.3. Morphology of cultures generated by CD90 sorted cells compared to Ca19-9 sorted cells.....	148
Figure 5.4. Validation of a screening platform to identify CK19+ cell mitogens.....	150

Figure 5.5. 2 ⁵ full factorial effects of bFGF (F), EGF (E), HGF (H), KGF (K) and VEGF (V) on the BrdU incorporation by CD90- purified CK19+ cells.....	152
Figure 5.6. Fold expansion of CK19+ cells or vimentin- cells in basal medium or basal medium + bFGF, EGF, HGF and KGF, all at 20 ng/mL.	155
Figure 5.7. Insulin expression of alginate-immobilized CD90 sorted cells.....	156
Figure B1. Insulin staining of NPCCs in the AHFBR.....	223
Figure B2. Bead image analysis by Cell Profiler after toluidine blue staining.	224
Figure B3. Time course q-PCR data for dispersed human non-islet tissue during adherent culture.	225
Figure B4. Human islet-depleted cell survival during serum-free culture between day 7 and day 17.	226
Figure B5. Cell morphology and insulin expression during Matrigel-induced islet-like cluster formation by NPCCs and human islet-depleted pancreatic cells.....	227
Figure B6. Pdx-1 gene expression of islet-depleted human pancreatic tissue before and after 10 days of immobilized culture in emulsion-generated alginate beads.....	228
Figure B7. Insulin and gapdh gene expression of islet-depleted human pancreatic tissue before and after 10 days of immobilized culture in emulsion-generated alginate beads with or without poly-L-lysine and FBS.....	229
Figure B8. Correlation between total dispersed human islet-depleted pancreatic cell concentrations (live + dead cells), packed cell volume and DNA.....	230
Figure B9. Dynamic viscosity of alginate samples as a function of shear stress.....	231
Figure B10. Relationship between the log of the zero-shear viscosity and the surface area moment average emulsion bead diameter.....	232
Figure B11. Insulin and glucagon stained pancreas sections obtained after sacrificing the mice on day 19.....	232
Figure B12. Visualization of mouse immunoglobulins (IgGs) in alginate beads.....	233
Figure B13. Cellomics image analysis.....	234
Figure B14. Quantification of BrdU and CK19 staining by the Cellomics algorithm.....	235

Figure B15. Impact of seeding density and dissociation into single cells on the yield of cells during monolayer culture.	236
Figure B16. CK19 and vimentin expression levels in CD90-sorted populations.	237
Figure B17. Pre-plating to eliminate vimentin+ cells from human islet-depleted pancreatic tissue	238
Figure B18. Changes in total cell number with time for unsorted dispersed islet-depleted pancreatic cells cultured in 96-well screening plates.....	239
Figure B19. Effect of Matrigel surface coating on the seeding efficiency of CD90-depleted cells.	240
Figure B20. bFGF, EGF, KGF and HGF dose-dependent effects on the proliferation of human CK19+ pancreatic cells.	241
Figure B21. Effects of bFGF, EGF, KGF, HGF and VEGF on apoptosis measured on day 3 based on YoPro permeability of the Ca19-9+ cells.....	242

NOMENCLATURE

α 1-3Gal	Gal α 1-3Gal β 1-4GlcNAc
bFGF	basic fibroblast growth factor (FGF-2)
BG	blood glucose
BrdU	bromodeoxyuridine
BSA	bovine serum albumin
AHFBR	Alginate-filled hollow fiber bioreactor
Ca19-9	carbohydrate antigen 19-9
CD	cluster of differentiation (e.g. CD90, CD4, CD8)
CHO	Chinese Hamster Ovary
CK19	cytokeratin 19
C-Met	mesenchymal epithelial transition factor
cryo-SEM	cryological scanning electron microscopy
DNA	deoxyribonucleic acid
ECS	extra-capillary space
EDTA	ethylenediamine tetraacetic acid
EGF	epidermal growth factor
ES	embryonic stem
FACS	fluorescent-activated cell sorting
FBS	fetal bovine serum
G	guluronic acid
gapdh	glyceraldehyde 3-phosphate dehydrogenase
HEPES	4-(2-hydroxyethyl)-1-piperazineethanesulfonic acid
HGF	hepatocyte growth factor
HFBR	hollow fiber bioreactor
ICS	intra-capillary space
IgG	immunoglobulin
iPS	induced pluripotent stem
KGF	keratinocyte growth factor
KRB	Krebs Ringer buffer
LVM	low viscosity high mannuronic acid content
M	mannuronic acid
MACS	magnetic-activated cell sorting
MANOVA	multiple analysis of variance
MHC	major histocompatibility complex
MIN	mouse insulinoma
MOPS	3-(N-morpholino)propanesulfonic acid
MTT	3-(4,5-Dimethylthiazol-2-yl)-2,5-diphenyltetrazolium bromide
MVG	medium viscosity high guluronic acid content
MW	molecular weight
MWCO	molecular weight cut-off
NCAM	neural cell adhesion molecule

NGN3	neurogenin 3
NK	natural killer
NPCCs	porcine neonatal pancreatic cell clusters
NPS	neonatal porcine serum
PBS	phosphate buffered saline
PCNA	proliferating cell nuclear antigen
PCV	packed cell volume
PDX-1	pancreatic duodenal homeobox 1
PLL	poly-L-lysine
PLO	poly-L-ornithine
q-PCR	quantitative (real-time) polymerase chain reaction
SD	standard deviation
SEM	standard error of the mean
STZ	streptozotocin
Thy1	thymus cell antigen 1 (also CD90)
Tx	transplantation
VEGF	vascular endothelial growth factor

Symbols

A_i	area of the bead or cell aggregate in the 2D picture
B_n	Huggins-like equation fitting parameter
c	alginate concentration
C	constant
C_i	growth factor concentration
D_{32}	surface area moment average diameter
D_{43}	volume moment average diameter
d_{max}	maximum stable droplet diameter
F	bFGF subscript
E	EGF subscript
H	HGF subscript
K	KGF subscript
R_η	viscous radius
K_C	Cross time constant
K_H	Huggins constant
K_{SEC}	partition coefficient measured by size exclusion chromatography
m	Cross rate constant
n	lumped order of higher orders of the Huggins-like equation
N	number of replicates, beads or cell aggregates
N_i	impeller agitation rate
P_i	perimeter of the bead or cell aggregate in the 2D picture
R_η	protein viscous radius
SD_{32}	surface area moment standard deviation (SD of D_{32})

$s_{D_{43}}$	volume moment standard deviation (SD of D_{43})
V_e	elution volume of the solute during size exclusion chromatography
V_0	void volume between beads in the size exclusion chromatography column
V_t	total liquid volume of the size exclusion chromatography column
$t_{R,ave}$	average residence time
V	VEGF subscript
x_i	scaled growth factor concentration
Y	model response
\hat{Y}	measured response
β_0	model intercept
β_i	model parameter for factor “i”
ε	energy dissipation
$\dot{\gamma}$	shear rate applied
η	dynamic viscosity
η_0	zero-shear viscosity
η_∞	infinite shear viscosity
$\eta_{solvent}$	viscosity of the solvent
$[\eta]$	intrinsic viscosity
μ_d	viscosity of the discontinuous phase
ρ_c	density of the continuous phase
σ	surface tension

ACKNOWLEDGEMENTS

I thank my supervisor Jamie for his unwavering patience, support and guidance. I am very grateful for the invaluable advice and help provided by Dr. Timothy Kieffer and Dr. James Johnson. I thank Dr. Igor Lacík for his enthusiastic collaboration and insightful discussions. Dr. Garth Warnock guided and was very supportive of this project. I thank Dr. Gregory Korbitt at the Department of Surgery of the University of Alberta for helpful input and for the contribution of porcine neonatal pancreatic cell clusters.

Ohne meine Eltern hätte ich diese Doktorarbeit nie vertiggebracht: erstens wäre ich nicht gebohren, zweitens wäre ich vielmals verhungert und drittens waren sie immer verständnisvoll wann ich dafür bis spät oder am anderen ände des Kontinents studieren wollte. Merci Isabel – évidemment parce que tu es la meilleure soeur que j'aie jamais eue. Merci Nicolas de tes conseils, de ta tendresse et de ta ptience. Merci Stéphane et Julie de me supporter quand je suis insupportable. Merci Antho pour le support PC. Thank you Ted, Chris and Daša for keeping me sane. Bref, « merci à tous ceux qui m'ont nourrie! »

I thank Roger Kiang and Kamini Raghuram, two creative and dedicated undergraduate students that significantly contributed to this work. Marta Szabat was always ready to offer creative and technical with experiments. Yu Huan Liao heard and shared my primary tissue woes but always provided a positive perspective. I am particularly thankful to Dr. Ziliang Ao and Dr. Garth Warnock at the Ike Barber Human Islet Transplant Laboratory for providing the human exocrine tissue. The transplantation experiments would not have been possible without Madeleine Speck, Christine Donald and Dr. Majid Mojibian, from the Kieffer lab. Dušana Mocinecová performed all the alginate bead mechanical testing and size exclusion chromatography experiments. Daniela Moskova performed the alginate rheological measurements. Xiaoke Hu performed the perfusion experiments and helped with preliminary animal studies. James Lyon isolated and analyzed the insulin and DNA content of porcine neonatal pancreatic cell clusters at the Department of Surgery of the University of Alberta. Derrick Horne patiently performed the cryo-scanning electron microscopy experiments. Ali Asadi provided technical support with immunohistochemistry. I am thankful to Jill Osborne for initiating experiments related to the emulsion project, as well as Lauren Wilkinson and Michael Lee for technical support. Timothy Vitalis and Dr. Malcolm L. Kennard reviewed and proofread respectively Chapters 2 and 3. I also thank all Piret, Johnson and Kieffer lab members for their support and input. In particular, I thank Christopher Sherwood for his assistance and moral support, as well as Mario Jardón and Pascal Beauchesne for their numerous suggestions related to the project.

I received fellowships from the University of British Columbia, the Michael Smith Foundation for Health Research, the Fonds québécois de la recherche sur la nature et les technologies, the Natural Sciences and Engineering Research Council of Canada. The collaboration with the Slovak Academy of Sciences was initiated at the XVII International Conference on Bioencapsulation through a COST 865 travel award. The Canadian Stem Cell Network also granted funding for the project.

1 INTRODUCTION

Diabetes is a chronic disease afflicting ~5% of Canadians (Statistics Canada 2009) that, if left untreated, results in elevated blood glucose levels due to a lack of insulin production and/or sensitivity to insulin. Among diabetic patients, ~10% suffer from type 1 diabetes (Canadian Diabetes Association 2010), an auto-immune disease where the patient's

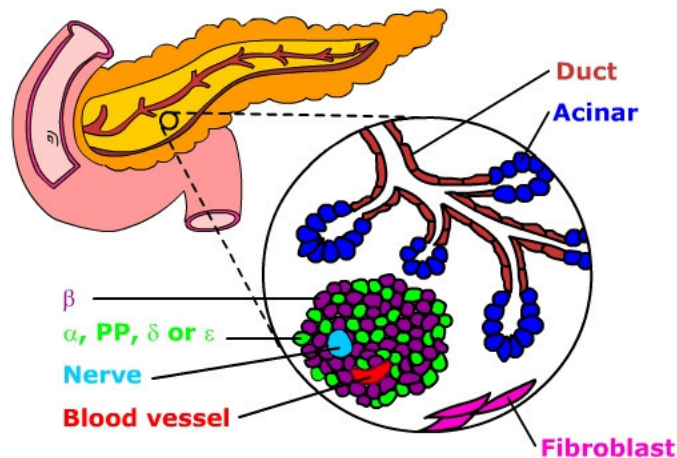


Figure 1.1. Physiology of the pancreas.

The pancreas is both an exocrine and an endocrine gland. Pancreatic digestive enzymes secreted by exocrine acinar cells (expressing amylase, cholecystinin receptor type A) are delivered into the small intestine through pancreatic ducts (which express cytokeratin 19, carbohydrate antigen 19-9, carbonic anhydrase). Endocrine hormones are produced by β -cells (secreting insulin, glucose receptor 2), α -cells (secreting glucagon), PP cells (secreting pancreatic polypeptide), δ -cells (secreting somatostatin) and ϵ -cells (secreting ghrelin) cells clustered in islets of Langerhans. Other cells present in the pancreas that do not originate from the pancreatic primordium during development include vascular cells, nerve cells and mesenchymal cells (fibroblasts).

immune system targets and destroys the insulin-producing β -cells of the pancreas. Insufficient β -cell mass also plays an important role in the pathology of type 2 diabetes. As a result, type 1 diabetic patients and many type 2 patients regulate their blood glucose levels by exogenous administration of insulin. Most type 1 diabetic patients rely on several daily injections of insulin or insulin analogues modified to be slower- or faster-acting. The blood glucose control achieved by these injections is imperfect compared to physiological insulin release, leading to the many devastating complications of the disease such as blindness, loss

of limbs and premature death. More aggressive insulin therapy aimed at minimizing these side effects increases the risks of severe hypoglycemia (The Diabetes Control and Complications Trial Research Group 1993). Insulin pumps allow a more precise and flexible administration of insulin. To mimic the physiological basal insulin secretion, rather than using long-lasting insulin analogues, the insulin pump continuously infuses low levels of fast-acting insulin, reducing the risk of hypoglycemia. Currently available insulin pumps remain open-loop, i.e. they require that the patient estimate the amount of carbohydrates to be consumed so as to adjust the insulin bolus to be provided by the pump. This requires frequent blood glucose monitoring and input by the patient. Other disadvantages of insulin pumps include their higher cost compared to injections, risks of pump failure, infection at the site of the cannula and the inconvenience of constantly wearing the pump, which needs to be removed during bathing/swimming for at most 2 h. Closed-loop pumps with continuous blood glucose monitoring and feed-back control by insulin infusion rather than patient input are being developed. Many challenges limit this technology, including the inaccuracy of continuous blood glucose monitors, the lag in insulin action by subcutaneous injection (45 min for maximum action even with fast-acting analogues) and safety concerns related to risks of hypoglycemia (Aye et al. 2010).

1.1 ISLET TRANSPLANTATION

Physiological blood glucose control could be achieved by β -cell rather than insulin replacement. The insulin-producing β -cells reside in endocrine cell clusters of 50~2000 cells in the human pancreas, termed islets of Langerhans (Figure 1.1). Islet transplantation using the Edmonton protocol (Shapiro et al. 2000) eliminated the requirement for insulin injections for a median duration of 1 year in ~80% of the type 1 diabetic patients treated (Registry 2009; Shapiro et al. 2006). A subset of ~7% of the patients have remained insulin-free for over 5 years (Ryan et al. 2005). Islets currently used for transplantation originate from human cadavers, with two to three donors required per patient. The islets make up ~2% of the pancreas and can be isolated from the acinar (~85%) and duct (10%) cells (Figure 1.1) by enzymatic digestion, mechanical dissociation and density separation. This generates an islet

graft of <10 mL per donor that is infused into the liver portal vein of patients during a short surgical procedure that is much less invasive than whole organ transplantation.

Compared to insulin infusion by mechanical devices, a cell-based treatment of diabetes would minimize risks related to inadequate insulin infusion. Islet transplantation allows independence from an exogenous device and avoids the need for regular replenishment of exogenous insulin. Implantable insulin pumps are available, but currently require surgical replacement after a median time of ~2 years (Haveman et al. 2010). With the currently available methods, islet transplantation has been shown to lead to improved blood glucose control compared to intraperitoneal insulin infusion by an insulin pump (Vantyghem et al. 2009). Mechanical devices can fail unexpectedly and software algorithms cannot perfectly mimic the complex mechanisms of physiological insulin release by β -cells. However, the benefits of islet transplantation have to be weighted against the detriments associated with chronic immunosuppression. Side effects of the immune suppressants used include increased risks of malignancies (Gutierrez-Dalmau and Campistol 2007), mouth ulcers, pneumonia and opportunistic infections, increased blood cholesterol and triglycerides, as well as impaired wound healing (Cravedi et al. 2010; Hakeam et al. 2008). The direct costs of intensive insulin therapy by injections are ~5000 \$/year, ~6000 \$/year for insulin pumps with subcutaneous insulin infusion and 13 000\$/year for implantable insulin pumps with intraperitoneal insulin infusion (Haardt et al. 1994; Logtenberg et al. 2010). The direct costs of islet transplantation are ~100 000\$ in the first year (Guignard et al. 2004) and ~14 000 \$ per year thereafter related to the cost of immunosuppression. However, these costs do not include the potential reduction of complications related to diabetes by islet transplantation, and these represent the main portion of diabetes-related costs. Islet transplantation has the potential to increase the lifespan and quality of life of the patients (Chicago Diabetes Project 2010, Patient Testimonies).

The potential of islet transplantation as a therapeutic option is currently most limited by (1) the amount of cadaveric donor tissue available for transplantation, (2) the requirement for lifelong immune suppression and (3) graft failure over time, in part due to rejection despite the use of immune suppressants (Hilbrands et al. 2009). This thesis

describes novel culture methods that could be used either to generate more β -cells or to isolate the cells from the immune system after transplantation. Three model cell types were used to develop these culture methods. First, neonatal porcine pancreatic cells were used because they contain islet progenitors, likely among the duct cell population (Street et al. 2004b). The insulin content of this tissue is known to increase over time *in vivo* (Trivedi et al. 2001) and under certain *in vitro* conditions (Tatarkiewicz et al. 2001). Second, duct-like cells derived from adult human pancreatic tissue were studied based on several reports of *in vitro* generation of insulin-producing cells from duct-rich cultures. These cells were derived from the cells left unused after islet transplantation, which are ~50 times more abundant than islets. Lastly, two insulinoma cell lines, mouse insulinoma 6 (MIN6) cells and β TC3 cells, were used as mouse β -cell models during the development of a novel cell encapsulation process, assuming that maximizing the survival of these cells should also improve primary β -cell survival in similar processing conditions.

1.2 SOURCES OF TISSUE TO GENERATE SURROGATE β -CELLS

Widespread application of islet transplantation to all currently diagnosed type 1 diabetic patients would require an estimated 100-fold increase in donated tissue supply (Ricordi 2003). Alternate methods to obtain insulin-producing cells being considered include expanding human β -cells *in vitro*, generating β -cells from other cells in the pancreas, from embryonic stem (ES) cells or induced pluripotent stem (iPS) cells (Street et al. 2004b), as well as using xenogeneic islets.

1.2.1 Expanded human β -cells

Expansion of functional β -cells has proven to be challenging. In the normal adult pancreas, the β -cell proliferation rate is very low, leading to a half-life of 1~3 months in young adult rats (Finegood et al. 1995) and > 1 year in aged mice (Teta et al. 2005) and no significant β -cell turnover in lean humans after the age of ~30 (Perl et al. 2010). β -cell mass does increase in response to the increased metabolic demand resulting from weight gain (Butler et al. 2003) or pregnancy (Rieck and Kaestner 2010) in humans, but this adaptive

capacity decreases with age (Rankin and Kushner 2009). In islet-derived *in vitro* cultures, glucose-responsive insulin secretion is lost in the first few passages and insulin expression disappears within 4 weeks, although other β -cell markers such as PDX-1 remain expressed (Beattie et al. 1999; Schmied et al. 2001). Many studies have focused on inducing insulin re-expression in the expanded cells (Ouziel-Yahalom et al. 2006). Some impressive results achieved in this field (Abraham et al. 2002; Zulewski et al. 2001) remain controversial since they could not be reproduced by others (Kayali et al. 2007).

1.2.2 β -cells derived from non-islet cells

Instead of expanding β -cells, insulin-producing cells could potentially be generated from non-islet cell types that are not used for islet transplantation. Duct, acinar and mesenchymal cells have all been investigated as potential sources of stem cells or progenitor cells capable to give rise to new β -cells.

1.2.2.1 Adult pancreatic stem cells

The existence of pancreatic stem cells has been surmised based on the impressive β -cell recovery following injury in rodents (Bonner-Weir et al. 1993; Fernandes et al. 1997; Hayashi et al. 2003; Li et al. 2003). Young adult rats that have undergone 90% pancreatectomy reach 45% of the β -cell mass of sham-operated controls within 4 weeks (Bonner-Weir and Sharma 2002). Islet neogenesis following injury also occurs in primates (Wolfe-Coote et al. 1998) including humans when >85% pancreatectomy is required to treat nesidioblastosis in infancy (Berrocal et al. 2005; Schonau et al. 1991).

Mounting evidence suggests that β -cell replication rather than neogenesis from stem cells is the main mechanism of β -cell replenishment during normal pancreas maintenance or after injury in adult mice. The progeny of β -cells were distinguished from non β -cells (Dor et al. 2004) by permanent labeling of insulin-expressing cells with alkaline phosphatase when the mice reached 6-8 weeks of age. Over the following year, there was no significant change in the fraction of labelled cells although a daily turnover (i.e. label dilution) of 0.7% of the β -cells is expected in mice of this age (Teta et al. 2005). The labelled fraction of β -cells was undiluted by β -cell formation from putative insulin- progenitors 2 months after 70%

pancreatectomy. Another group later showed that all β -cells had a uniform replication potential (Brennand et al. 2007). Therefore, in most situations, normal mouse β -cell homeostasis and expansion after injury were attributed to the uniform proliferation of pre-existing β -cells rather than the differentiation of stem cells. These conclusions were supported by the lack of cells undergoing multiple rounds of cell division in the pancreas, even after partial pancreatectomy (Teta et al. 2007).

These studies did not preclude the existence of a facultative stem cell that is activated in other injury models or selected *in vitro* culture conditions. For example, the islets generated during the recovery from pancreatic duct ligation arise from progenitors that express neurogenin 3 (NGN3), a transcription factor expressed by endocrine precursors during pancreas development (Xu et al. 2008). Knocking down NGN3 expression also reduced islet regeneration in this model. Interestingly, the NGN3⁺ cells did not express any of the islet hormones and were found to be associated with but not part of the pancreatic (Kim et al. 2009) duct lining. These progenitors were purified by flow cytometry and expressed insulin *in vitro* after being placed in contact with embryonic mouse pancreatic explants. Pancreatic duct ligation was also shown to lead to the generation of insulin⁺ cells from progenitors expressing carbonic anhydrase, a pancreatic duct marker (Inada et al. 2008), although this observation was contradicted by lineage tracing of HNF1 β ⁺ cells, another pancreatic duct marker (Solar et al. 2009). It is possible that pancreatic stem cells found in close association with ducts only express subsets of ductal markers, explaining some of the confusion in the field. A recent study (Liu et al. 2010) failed to reproduce the results by Dor et al. (2004) and suggested that insulin⁻ cells indeed contribute to insulin⁺ cell homeostasis or regeneration after injury with streptozotocin, a β -cell toxin. A mathematical model indicated that insulin⁻ cells generated >80% of new β -cells in a rat model of type 2 diabetes (Manesso et al. 2009). A recent lineage tracing study has also suggested that non- β -cells contribute to the increased β -cell mass observed in pregnant mice (Abouna et al. 2010), contrary to the observations of Teta et al. (2007). Reactivation of progenitors found among duct cells during pregnancy has also been suggested to occur in humans (Butler et al.). Lastly, given the difference between rodent and human islets architecture (Kim et al. 2009)

and β -cell development (Piper et al. 2004), conclusions drawn from rodent models may not necessarily translate to humans.

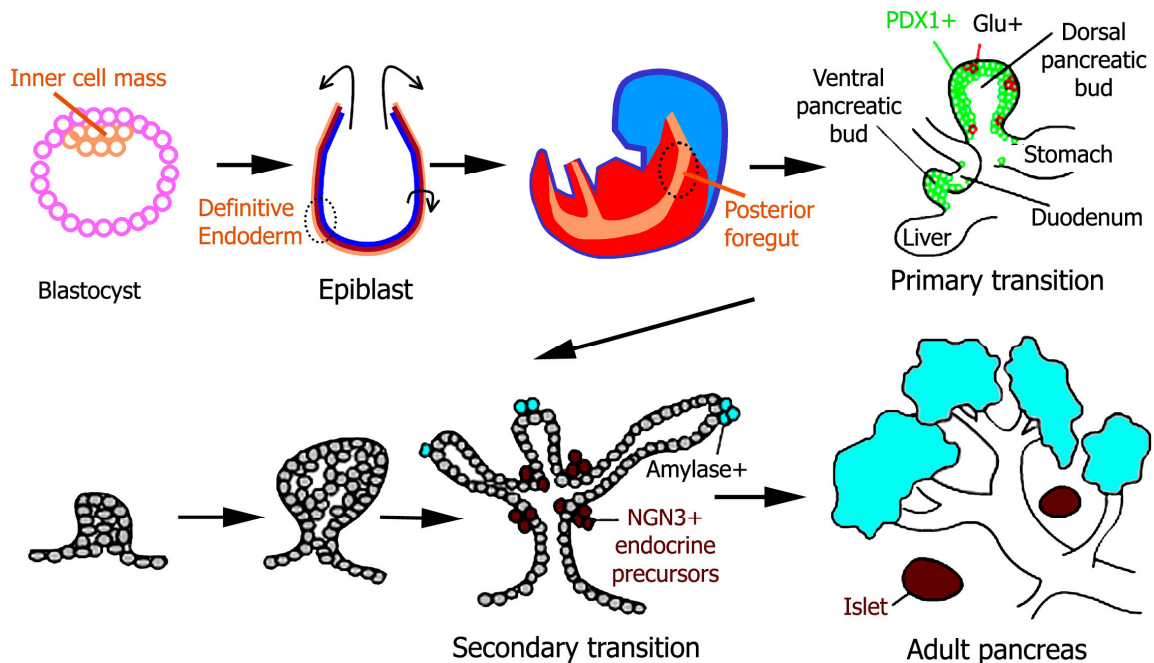


Figure 1.2. Pancreas organogenesis.

During development, the inner cell mass of the blastocyst gives rise to all of the adult tissues. The pancreas is generated by cells in the posterior foregut, which stem from the definitive endoderm cells formed during gastrulation. Two key transitions lead to the formation of the pancreas and then the β -cells. The primary transition denotes the first appearance of pancreatic structures in the form of two thickenings in the gut tube. These structures strongly express PDX-1. Dorsal bud development is guided by signals (e.g. FGF, TGF β , VEGF) from the notochord. Ventral bud development depends on signals from the liver, whose development in turn depends on signals from the cardiac mesoderm. Without the latter, liver cells attain a “default” pancreatic fate. The epithelial thickenings form multilayered evaginations expand into the pancreatic mesenchyme and fuse into a single organ. These evaginations thin during expansion and form ducts through microlumen fusion. The secondary transition marks a sudden increase in β -cells and acinar cells. Thereafter, PDX-1 expression is restricted to δ and β -cells. All endocrine cells stem from NGN3+ progenitors derived from ductal epithelial cells. The endocrine cells proliferate, aggregate, but remain in proximity to the ducts until they are pushed away by rapidly proliferating acinar cells shortly after birth. (The illustration is based on mouse development and adapted from Grapin-Botton and Melton 2000.; Jensen 2004.; Wells 2003)

Most of the evidence for the existence of an islet stem or progenitor cell comes from *in vitro* experiments. Using a colony-forming assay, multipotent progenitors that gave rise to pancreatic endocrine (Seaberg et al. 2004; Suzuki et al. 2004) and non-pancreatic – notably

neural – cell lineages (Choi et al. 2004) were identified in pancreatic tissue. The differentiated cell colonies derived from these progenitors contained 1/3 the amount of insulin found in islets and secreted insulin in response to elevated glucose concentrations. The frequency of these multipotent progenitors was 0.02%~0.03% among both the islet and duct pancreatic cells (Seaberg et al. 2004). In addition, numerous studies (reviewed in Table B1 and in Sections 1.2.2.1 to 1.2.2.5) report the generation of insulin+ cells *in vitro* from islet-rich or islet-depleted pancreatic tissue, suggesting that either duct, acinar or mesenchymal human pancreatic cells could act as β -cell progenitors.

1.2.2.2 Duct-derived β -cell progenitors

During development, all endoderm-derived pancreatic cells arise from common epithelial progenitors that express the transcription factor PDX-1 (Jonsson et al. 1994) and reside in the pancreatic ducts (Figure 1.2). An early wave of PDX-1 expression patterns the primitive endoderm to a pancreatic fate. This expression then becomes more and more restricted to β -, δ -, plus perhaps sparse duct cells of the newborn that become less frequent with aging (McKinnon and Docherty 2001; Street 2004). PDX-1 is a co-activator of the insulin promoter essential for normal islet function. Pancreatic injury (Kritzik et al. 2000; Sharma et al. 1999) and *in vitro* culture conditions (Gmyr et al. 2000; Rooman et al. 2000) can trigger PDX-1 re-expression in adult pancreatic cells of duct phenotype. Insulin expression can be induced by exposure to the incretin glucagon-like peptide-1 if the duct cells express PDX-1 (Hui et al. 2001). A subset of adult duct cells perhaps residing in intercalated ducts (Bonner-Weir et al. 1993; Hardikar et al. 1999; Hayashi et al. 2003) may have retained their primitive proliferation and differentiation capacity. In human (Bogdani et al. 2003) and porcine (Trivedi et al. 2001; Yoon et al. 1999) pancreatic grafts transplanted into mice, duct cell content decreases up to 90%, while the β -cell mass increases. A positive correlation exists between the duct fraction in human-to-human islet transplantation and the transplant outcome after 2 years (Street et al. 2004a), suggesting that the duct cells either act as progenitors or that they increase β -cell survival or self-duplication.

Islet-like cell clusters can be generated *in vitro* from duct-like epithelial cells that arise in adherent cultures of islet-depleted pancreatic tissue. Insulin expression has been

induced by serum-free culture and aggregation of duct-like (CK19+) adherent human pancreatic cells either in suspension (Todorov et al. 2006) or by immobilization in matrices such as collagen (Kerr-Conte et al. 1996) and Matrigel (Bonner-Weir et al. 2000; Gao et al. 2007; Gao et al. 2005; Gao et al. 2003; Kikugawa et al. 2009). Islet-like clusters obtained from cultured mouse duct cells normalized the blood glucose levels of non-obese diabetic mice for at least 3 months (Ramiya et al. 2000). Cultures of purified human duct cells have also been used to generate insulin+ islet-like cell clusters (Gao et al. 2005; Yatoh et al. 2007), though diabetes reversal by human duct-derived insulin+ cells has not been demonstrated (Gao et al. 2007; Todorov et al. 2006). Another weakness of human duct cell culture protocols is that at most ~3 fold expansion of the CK19+ cells has been reported (Table B1), compared to 10-100 fold for rodent duct cells (Agbunag and Bar-Sagi 2004; Chen et al. 2009). Both of these observations may reflect the limited proliferation capacity of adult human pancreatic cells compared to rodents (Cnop et al. 2010). Several growth factors (reviewed by Luu, 2004) have been individually shown to increase the expansion of pancreatic duct-like cells in culture. However, the effects of these factors have not been systematically examined in multifactorial experiments.

1.2.2.3 Acinar-derived β -cell progenitors

In vitro, acinar cells yield cultures of duct phenotype without evidence of any confounding selective duct survival or expansion (Baeyens et al. 2005; Hall and Lemoine 1992; Rooman et al. 2000; Sanchez et al. 2004). The trans-differentiation of acinar cells into cells with duct markers as well as insulin+ cells was confirmed by lineage tracing *in vitro* (Means et al. 2005; Minami et al. 2005) but not during the regeneration process after pancreas injury *in vivo* (Desai et al. 2007). However, acino-ductal transdifferentiation can occur during the formation of the duct-like tubular complexes that are precursors of pancreatic cancers (Bockman et al. 2003; De La O et al. 2008; Habbe et al. 2008; Strobel et al. 2007). In both mouse models (Song et al. 1999; Zhu et al. 2007) and human biopsies (Campbell-Thompson et al. 2009; Tezel et al. 2002) of pancreatic ductal adenocarcinomas, some neoplastic cells express β -cell transcription factors such as PDX-1 and small islets or single β -cells appear to “bud” from the tubular complexes. These reports suggest not only a

certain plasticity of acinar cells, but also underline the difficulty in judging whether cultured cells of duct phenotype are of ductal or acinar origin.

1.2.2.4 Mesenchymal β -cell progenitors

Highly proliferative cultures obtained after passaging primary pancreatic tissue usually consist mostly of spindle-shaped cells resembling fibroblasts (Gershengorn et al. 2004; Ouziel-Yahalom et al. 2006; Zulewski et al. 2001). These may in fact represent a mesenchymal stem cell population present in the pancreas (Seeberger et al. 2006). Reports where cells are expanded > 10 fold prior to differentiation document a mesenchymal phenotype of the expanding cells (Table B1). These cells appear more difficult to differentiate into functional islets *in vitro* (Treutelaar et al. 2003) than the less proliferative PDX-1+ cells of ductal phenotype (Bonner-Weir et al. 2000; Gao et al. 2007; Gao et al. 2003; Hao et al. 2006; Todorov et al. 2006). These fibroblast-like cells express nestin (Zulewski et al. 2001), a neural stem cell marker, which can be expressed by mesenchymal stem cells in certain culture conditions (Wislet-Gendebien et al. 2005). Several studies (Atouf et al. 2007; Chase et al. 2007; Morton et al. 2007; Moss and Rhodes 2007) have now demonstrated that fibroblast-like nestin+ cells derived from islet-rich cultures do not stem from PDX-1 or insulin-expressing cells. Nestin+ cells do not contribute to endocrine cell development and homeostasis *in vivo* (Delacour et al. 2004). However, specific culture conditions or genetic manipulation may allow the differentiation of these mesenchymal cells into insulin+ cells (Li et al. 2007).

1.2.2.5 Genetic re-programming of mature pancreatic cell types

Most studies aiming to obtain insulin+ cells from adult pancreatic cell types have focused on manipulating *in vitro* culture conditions to induce insulin expression. Another approach has been to genetically reprogram adult pancreatic cell types into β -cells. Insulin+ cells were obtained by over-expressing PDX-1, NGN3 and MafA in adult mouse pancreatic exocrine cells (Zhou et al. 2008). In human duct-like cells, the over-expression of NGN3 (Heremans et al. 2002) or PDX-1 (Zhao et al. 2005) alone may be sufficient to induce insulin expression, perhaps because subpopulations may already express β -cell transcription factors

such as Nkx6.1 and PDX-1. After transplantation, human duct-like cells transfected with PDX-1 generated grafts with 15% insulin+ cells that reduced the blood glucose levels of diabetic mice (Zhao et al. 2005). The potential of genetic manipulations has been demonstrated by the reprogramming of adult fibroblasts into iPS cells (Takahashi and Yamanaka 2006) that can generate entire embryos and viable mice, similar to ES cells (Boland et al. 2009; Kang et al. 2009; Zhao et al. 2009). The extent of reprogramming required should be less extensive between developmentally related (Figure 1.2) pancreatic cell types than between fibroblasts and iPS cells.

1.2.3 Insulin+ cells from embryonic or induced pluripotent stem cells

ES or iPS cells are readily accessible and can currently be produced at larger scales than cells derived from primary tissue. Cells with an insulin content similar to adult islets were obtained by a multi-step protocol designed to recapitulate the steps required for β -cell formation from ES cells during development (D'Amour et al. 2006). However, the purity of the insulin+ cells was low, at ~7% at the end of this protocol. In addition, the cells were not fully mature based on co-expression of several endocrine hormones in the same cells and the high levels of unprocessed insulin in the cells. Insulin+ cells derived from ES cells transplanted into streptozotocin-treated diabetic nude mice normalized the blood glucose levels of only ~30% of the animals transplanted (Jiang et al. 2007). Kroon et al. (2008) postulated that the *in vivo* environment could provide better differentiation cues than the current *in vitro* protocols. Indeed, after 3 months *in vivo*, the grafts consisted of >50% endocrine cells without co-expression of insulin and other endocrine hormones. The grafts appeared to be functional, preventing the development of diabetes when the β -cells of the mice were ablated by streptozotocin. The *in vivo* signals responsible for this improved differentiation are unknown, but may be related to the three-dimensional environment that is absent from *in vitro* cultures. During development, tissue architecture and signals from the extracellular matrix play an important role in specifying pancreatic cell types and directing β -cell delamination from the pancreatic epithelium (Gittes 2009). Immobilized culture in the presence of extracellular matrix components has been shown to increase the fraction of ES-derived insulin+ cells *in vitro* (Mason et al. 2009; Wang and Ye 2009). Insulin+

cells have recently been generated by similar protocols using iPS lines (Tateishi et al. 2008), including iPS cells derived from type 1 diabetic patients (Maehr et al. 2009). This could be useful for disease modeling and also allow autologous transplants to avoid allorejection. However, concerns surrounding the purity and safety of ES-derived cells will need to be addressed before ES or iPS-derived cells can be of clinical relevance, since teratoma formation has been observed in some of the animals transplanted (Kroon et al. 2008). In addition, autoimmune rejection will not be avoided by this strategy.

1.2.4 Xenogeneic islets

Xenografts are relatively easy to procure, do not require complex differentiation protocols, but can cause strong rejection of the graft and may lead to xenoinfections. Pig islets have been considered as the prime candidate for xenotransplantation in particular because porcine insulin was used for many years to treat diabetes before recombinant sources became available. The normal blood glucose levels in pigs are similar to humans and pigs are easier to breed than non-human primates (Yang and Sykes 2007). However, humans possess pre-formed antibodies against the Gal α 1-3Gal β 1-4GlcNAc (α 1-3Gal) carbohydrate, present on epithelial cells of most other species. These antibodies and then complement proteins bind to porcine islets transplanted by portal injection, contributing to islet destruction within 72 h (Dufrane and Gianello 2009). In addition, the isolation of adult porcine islets with reproducibility (Dufrane et al. 2006a) and their *in vitro* maintenance without loss of function (Davalli et al. 1993) is challenging. Contrary to adult islets, neonatal porcine pancreatic cell clusters (NPCCs) can be isolated with consistently high yields (Rayat et al. 1999) and β -cells within the NPCCs are proliferative (Vizzardelli et al. 2002). However, due to the immaturity of this tissue, up to 12 weeks can be required before the tissue becomes fully functional (Korbitt et al. 1996; Weir et al. 1997). Also, NPCCs express higher levels of α 1-3Gal than adult islets (Rayat et al. 2003). Key advances towards the use of pig islets for the treatment of diabetic patients are the genetic engineering of pig strains to reduce their immunogenicity (d'Apice and Cowan 2009) and the breeding of pigs depleted of infectious agents such as porcine endogenous retrovirus in pathogen-free facilities (Schuurman 2009). Ethical issues such as informed consent and adequate international

regulatory oversight remain problematic (Cozzi et al. 2009). Insulin independence of pancreatectomized monkeys for >4 months has been achieved both by transplanting adult porcine islets (Hering et al. 2006) or NPCCs (Cardona et al. 2006). In both cases, the immunosuppressive regimen led to severe side effects such as opportunistic infections and thrombosis, hindering the application of these protocols to humans. Pig-to-human islet transplants without immunosuppression have been performed in Mexico (Valdes-Gonzalez et al. 2005), Russia and New Zealand (Elliott et al. 2007; Living Cell Technologies 2010). Encapsulation devices, including alginate beads, were used instead of immunosuppression to protect the islets from rejection. No adverse effects were reported and some level of islet survival was demonstrated after up to 9.5 years post-transplant (Elliott et al. 2007), as discussed in Section 1.3.3.3.

1.3 CELL IMMOBILIZATION IN ALGINATE

1.3.1 Alginate gel properties

Alginate is a polysaccharide derived from seaweed used in the cosmetic and food industries as a thickening, stabilizing or gelifying agent (Ertesvag and Valla 1998), as well as to chelate heavy metals for water treatment (Davis et al. 2003). Alginate is also widely used as a biomaterial (Augst et al. 2006) because of its biocompatibility and gelation under mild conditions (de Vos et al. 2006). In its native form, alginate is a co-polymer of β -D-mannuronic acid (M) and its epimer, guluronic acid (G), arranged in sequences of M-rich, G-rich or alternating M-G “blocks” (Smidsrod and Skjakraek 1990). Divalent ions such as calcium and barium (but not magnesium) lead to gel formation by alginate solutions through the cooperative formation of salt bridges between G-blocks of neighbouring alginate chains. Cells do not adhere to unmodified alginate gels due to their negative surface charge, although cell adhesion can be induced by the grafting of cell adhesion peptides (Rowley et al. 1999). X-ray diffraction studies have shown that most of the gel structure can be explained by the formation of “egg-box” structures of 4 guluronic acid residues surrounding one divalent ion (Grant et al. 1973; Morris et al. 1978). Recent studies have

confirmed this general model (Sikorski et al. 2007) and refined it by modeling the lateral interaction between G-rich chains, determined by the residues present in the chain junctions and the divalent ion saturation of the gel (Stokke et al. 2000). In general, the egg-box model explains why alginates with higher G content and longer G blocks lead to stronger (Martinsen et al. 1989; Skjakbraek et al. 1986; Smidsrod et al. 1972) but more brittle (Morch et al. 2008) gels than alginates with high M content.

The viscosity of alginate decreases as a function of shear rate. This shear-thinning behavior can be described by the Cross model:

$$\eta = \eta_{\infty} + \frac{\eta_0 - \eta_{\infty}}{1 + (K_c \dot{\gamma})^m} \quad (\text{Equation 1.1})$$

where η is the apparent viscosity measured for the solution, $\dot{\gamma}$ is the shear rate applied, η_0 is the zero-shear viscosity, η_{∞} is the infinite shear viscosity, m is the Cross rate constant that provides an indication of the importance of the shear-thinning effect and K_c is the Cross time constant, which provides an indication of the onset of shear-thinning (occurring at $1/K_c$). The dependency of the zero-shear viscosity on the alginate concentration can be approximated by a Huggins-type equation (1942) with higher order terms combined into a single “ n ” order term (Kulicke et al. 1990; Storz et al. 2009; Storz et al. 2010):

$$\eta_0 = \eta_{\text{solvent}} \left(c \cdot [\eta] + K_H \cdot c^2 \cdot [\eta]^2 + B_n \cdot c^n \cdot [\eta]^n + 1 \right) \quad (\text{Equation 1.2})$$

where η_{solvent} is the viscosity of the solvent, $[\eta]$ is the intrinsic viscosity of the solution, c is the alginate concentration and K_H is the Huggins constant that can be estimated by neglecting the higher order term at low alginate concentrations. B_n and n are the higher order fitting parameters. Increasing the alginate concentration leads to an exponential increase in the viscosity of the solution when the alginate chains start to become entangled (Kulicke and Kniewske 1984).

The pore size of alginate beads decreases non-linearly as the bead gel concentration increases. For example, doubling the alginate concentration from 1.5% to 3% decreased the average pore size estimated from hindered diffusion rates by ~20% (Li et al. 1996). In alginate + cellulose sulfate beads with 1:1 weight ratio, doubling the alginate as well as the cellulose sulfate concentrations from 1.2% to 2.4% decreased the molecular weight (MW)

cut-off (MWCO) from molecules with a 12 nm viscous radius (R_η) to molecules with a 7.5 nm viscous radius (Brissova et al. 1998). This corresponds to a change from a MWCO of 1800 kDa to 500 kDa with respect to globular proteins, if it is assumed that their $R_\eta \propto (\text{MW})^{0.4}$ (Brissova et al. 1996). Gel gradients and lateral associations between alginate chains will also significantly affect pore sizes. The effects of the pore sizes on the access of solutes to beads can be assessed indirectly by determining the size exclusion chromatography partition coefficient K_{SEC} of solutes between the stationary liquid phase accessible to the molecule and the total liquid volume in the beads:

$$K_{SEC} = \frac{V_e - V_0}{V_t - V_0} \quad (\text{Equation 1.3})$$

where V_e is the elution volume of the solute, V_0 is the void volume of the column and V_t is the total liquid volume of the column. The assumption that the partition coefficient gives an indication of the fraction of the “pores” of a given size or larger is valid if the elution time is sufficiently low to avoid effects related to hindered diffusion (Brissova et al. 1996). It is also assumed that interactions between the solutes and beads are non-significant, which is not the case for most proteins. If alginate beads are used as the stationary phase, the value of $1 - K_{SEC}$ for a given solute provides the average fraction of the liquid volume in the beads from which this solute is excluded.

The two main methods of alginate gel formation are external gelation and internal gelation. The industrial production of monodisperse alginate beads such as those used for islet encapsulation relies on external gelation (Ahmad and Khuller 2008; Rokka and Rantamaki 2010). Internal gelation has been mainly used to generate larger gel structures (Johansen and Flink 1986; Mouquet et al. 1997). Biological molecules and microbial cells have also been immobilized in polydisperse alginate beads generated by emulsion and internal gelation (described in more detail in Section 1.4.3). External gelation occurs when divalent ions enter the alginate solution through the surface. In internal gelation, a salt with low solubility (e.g. calcium citrate, calcium EDTA or calcium carbonate) that is first mixed with the alginate solution provides the divalent ions. To release the divalent ions, the solution is acidified, for example by the slow hydrolysis of lactones mixed with the calcium

salt and alginate solution (Draget et al. 1990; Pelaez and Karel 1981). During external gelation, alginate can counter-diffuse into the gelled region and create gradients with higher gel concentration towards the surface (Skjakbraek et al. 1989; Thu et al. 2000). The gel gradients can be reduced if high concentrations of non-gelling ions are present. For transplantation applications, inhomogeneous beads are advantageous because this increases the elastic modulus and reduces the porosity of the beads (Moe et al. 1994; Thu et al. 1996b). For external gels, the elastic modulus correlates with the square of the alginate concentration (Smidsrod et al. 1972). The elastic modulus of calcium-limited internally set gels was found to be lower than for calcium-saturated externally set gels (Draget et al. 1993). Gel gradients are reduced but also observed in internally set gels, although the mechanism by which these are formed have not been investigated (Quong et al. 1998).

1.3.2 Alginate influence on pancreatic cell differentiation

Protocols aimed at maintaining or inducing islet function in cultured pancreatic tissue typically involve the addition of one or two growth factors (reviewed by Luu, 2004 and Garcia-Ocana *et al.*, 2001) and cell immobilization in a three-dimensional matrix. The effects of these matrices are largely mediated by integrin adhesion to extracellular matrix elements, leading to integrin clustering and signal transduction to intracellular pathways (Giancotti and Ruoslahti 1999). The shape and stiffness of the matrix surrounding the cells affect the contractility and organization of the cell cytoskeleton (Discher et al. 2005; Ghosh and Ingber 2007; Rehfeldt et al. 2007). Matrix properties can therefore influence fate decisions by various cell types both *in vitro* (Engler et al. 2006; Saha et al. 2008) and during development (Rozario and DeSimone 2010). In general, increased matrix stiffness appears to reduce cell growth rate, while differentiation towards a given cell type is optimal at the stiffness measured for the microenvironment of the same cell type *in vivo* (Banerjee et al. 2009; Engler et al. 2004). Matrices can also promote proximity between cell progeny, enhancing cell-cell signalling and local concentrations of paracrine molecules. Examples of matrices that increased the insulin expression or content of pancreas-derived cells include collagen (Katdare et al. 2004), laminin (Nagata et al. 2002), fibrin (Beattie et al. 2002), and basement membrane extracts such as Matrigel (Banerjee and Bhonde 2003; Bonner-Weir et

al. 2000; Gao et al. 2003; Lechner et al. 2005). The gels formed are effectively irreversible, complicating both the recovery and the analysis of the immobilized cells. Several of these matrices are animal-derived and poorly characterized, an additional hurdle for clinical applications. Alginate is a logical alternative that is non-animal-derived that could provide similar mechanical signals while allowing cell recovery.

Alginate has been used to promote insulin expression by pancreatic progenitors from different sources. Alginate immobilization was shown to increase the insulin content of NPCCs when these were cultured in the presence of serum (Korbutt et al. 1997b; Lopez-Avalos et al. 2001; Tatarkiewicz et al. 2001). One function of alginate in these cultures was to avoid the formation of large cell aggregates with central necrosis when serum is added to suspension cultures. More recently, the immobilization of expanded human islet-derived cells in alginate beads coated with poly-L-lysine (PLL), followed by the liquefaction of the bead core, led to the re-aggregation of the cells into islet-like structures (Tsang et al. 2007). Cells within the aggregates were insulin⁺ and the transplantation of the encapsulated aggregates led to blood glucose normalization in streptozotocin-induced immunocompromised diabetic mice 5 weeks after transplantation, associated with progressively increasing human C-peptide levels. Blood glucose levels were normalized for at least 2 weeks. Mouse ES cells immobilized in alginate did not lead to visible teratoma formation 3 months after allogeneic transplantation, while non-immobilized cells formed teratomas in some mice after 2 weeks (Dean et al. 2006). Alginate immobilization also promoted the differentiation of human ES cells towards endoderm (Chayosumrit et al. 2010; Dean et al. 2006). Alginate-immobilized ES cells were able to generate insulin⁺ cells 14 days after encapsulation and exposure to differentiation factors (Wang et al. 2009). The yield of insulin⁺ cells in alginate-immobilized cultures could be optimized by alginate matrix engineering to change the mechanical (Boonthekul et al. 2005; Donati et al. 2005), cell signaling (Perets et al. 2003) or adhesion (Huebsch et al. 2010; Rowley et al. 1999) properties of the gel. For example, the growth rate of β TC3 cells can be controlled by adjusting the gel strength and stiffness (Constantinidis et al. 1999).

1.3.3 Alginate beads as an immune barrier

Alginate has also been used to micro-encapsulate cells and protect them from immune rejection (Lim and Sun 1980). This strategy could eliminate or reduce the need for immune suppression following xenogeneic or allogeneic islet transplantation. Immune suppression is undesirable due to the side effects from the long-term use of immunosuppressive drugs (Marcen 2009) and their negative effects on islet function and survival (Hui et al. 2005; Johnson et al. 2009). The basic principle of immune isolation devices such as alginate microcapsules is to exclude harmful immune cells and molecules such as antibodies (~150 kDa), while allowing the diffusion of smaller molecules required for graft survival and function such as insulin (5.8 kDa), nutrients and waste products. Ideally, harmful cytokines (e.g. TNF- α homotrimers, 51 kDa) would also be excluded. However, this may hinder the access of some growth factors that affect islet survival, growth or function (e.g. hepatocyte growth factor, 83 kDa) (Dai et al. 2005), as well as proteins such as albumin (67 kDa) or transferrin (80 kDa) that carry fatty acids, hormones and metal ions important in cell metabolism. Uncoated calcium alginate beads at the typical concentrations used (1% to 3.5%) do not exclude antibodies (Kulseng et al. 1997; Nurdin et al. 2000; Strand et al. 2002). To reduce the molecular weight cut-off (MWCO) to below 100 kDa, the beads can be coated with cationic polymers such as PLL or poly-L-ornithine (PLO). This can be followed by an additional outer alginate layer to shield the cationic polymers from the host cells and reduce the fibrotic overgrowth caused by their exposure at the bead surface (de Vos et al. 2007; King et al. 2001). However, such size exclusion of antibodies may not necessarily be required since allogeneic (Duvivier-Kali et al. 2001) and xenogeneic (Schneider et al. 2005) islets encapsulated in uncoated barium cross-linked alginate beads with MWCOs of ~600 kDa were able to reverse diabetes in mice for >7 months. The MWCO is relevant for alginate capsules with a liquid core covered by relatively uniform pore sized membranes, where molecules access the entire inner bead volume once they pass the membrane. The MWCO may be less pertinent for uncoated gelled beads where much of the antibody access is hindered but not blocked (Morch 2008). For gelled beads, even if a molecule is excluded only from ~50% of the gel pores, the overall

concentration of this molecule in the gel will be reduced, potentially altering its effects on the immobilized cells. The optimization of bead properties for transplantation applications requires an understanding of the many factors that determine encapsulated islet survival *in vivo*.

1.3.3.1 The immune system and encapsulated islet survival

The immune response to encapsulated cells can be divided into three categories: (1) the non-specific innate response, (2) the specific adaptive response and (3) in type 1 diabetic recipients, the recurring autoimmune response. The innate and adaptive response are illustrated by a simplified schematic in Figure 1.3.

Transplantation surgery alone triggers the innate immune response to the graft. Tissue injury at the site of the surgery leads to the release of fibrinogen, thrombin, histamine, fibronectin and other chemo-attractants that recruit granulocytes, macrophages and other cells of the innate immune system to the site of injury within 24 h (de Vos et al. 2002). Activated macrophages and other cells then secrete pro-inflammatory cytokines such as IL-1 β , TNF- α and TGF- β that also reduce β -cell function, proliferation and survival (Blandino-Rosano et al. 2008; de Vos et al. 2003a; Rabinovitch and Suarez-Pinzon 1998). The effects of these cytokines may be lesser for xenogeneic than for allogeneic islet transplants (Piro et al. 2001) because of the reduced capacity of cells with xenogeneic receptors to bind and endocytose human cytokines. In the case of encapsulated islet transplantation, proteins released from ruptured blood vessels, injured cells or inflammatory cells can adsorb onto the encapsulation material and form a matrix conducive to the proliferation of cells involved in wound healing such as fibroblasts and macrophages (Anderson et al. 2008). This fibrotic overgrowth has been associated with bead surface irregularity (Bunger et al. 2003), protruding islets, impurities in the alginate (van Schilfgaarde and de Vos 1999) and higher positive surface charge (de Vos et al. 2007; Ponce et al. 2006). Overgrowth is usually only observed on a subset of the beads, which may be related to islet protrusion from these beads (van Schilfgaarde and de Vos 1999) or the location the beads occupied in the transplant site. Fibrotic overgrowth can be an indication of the immunogenicity of the graft independent of the bead material (Rokstad et al. 2001). Fibrotic overgrowth may not only affect the islets in

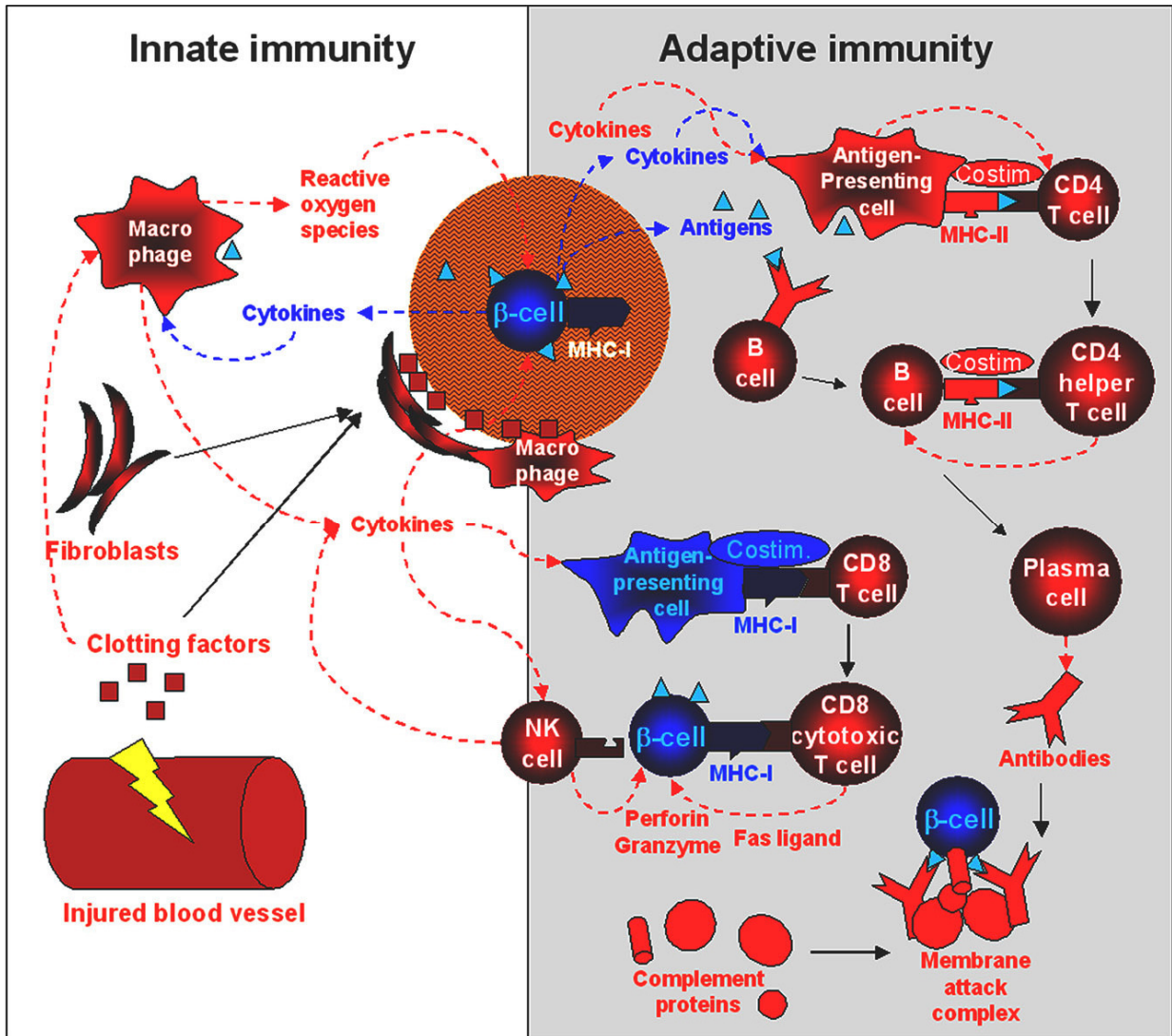


Figure 1.3. Simplified schematic of the immune response in the context of encapsulated islet transplantation

Cells and molecules from the graft are shown in blue while host cells and molecules are shown in red. The innate response to encapsulated islet transplants includes cell adhesion to the surface of the beads, recruitment of macrophages and release of cytokines that stress β -cells, in turn leading to increased production of cytokines by the β -cells (Cardozo et al. 2003). Natural killer cells recruited to the transplant site can eliminate non-encapsulated cells based on the lack of their expression of self-MHC molecules. Antigens released by β -cells can be endocytosed by macrophages and other antigen-presenting cells, activating the adaptive response to the graft. This includes the activation of T helper cells, which in turn activate cytotoxic cells, macrophages and B cells. Antibodies produced by B cells can bind to non-encapsulated cells and lead to cell death through complement activation or NK cell binding. Other cells that are not depicted but have an effect on graft survival include regulatory T cells, mast cells and granulocytes. "Costim" signifies up-regulation of co-stimulatory molecules on antigen-presenting cells. Note that auto-immunity is not explicitly addressed by this schematic.

the subset of overgrown beads, but also islets in neighboring beads due to cytokines secreted by macrophages (de Vos et al. 2003a). In the presence of these pro-inflammatory cytokines, islets themselves start to produce molecules that attract and activate macrophages (Cardozo et al. 2003).

When alginates of high purity are used in bead manufacturing, most infiltrating leukocytes disappear from the transplant site within two weeks after the surgery (de Vos et al. 2002), which is typical of innate immunity. An important function of the bead protection during these first two weeks is to shield the graft cells from being endocytosed by antigen-presenting cells such as macrophages and dendritic cells that help initiate the adaptive response (Gray 2001). The beads also reduce the direct cell contact between the graft and natural killer (NK) cells. NK cells can be activated by antibodies bound to cells and by the absence of self-MHC molecules on the surface of the transplanted cells. NK-mediated cell lysis may be more problematic for xenografts due to the lower inactivating signals provided by xenogeneic compared to allogeneic MHC molecules (Sharland et al. 2002), the presence of preformed antibodies against xenogeneic cells as well as NK cell receptor ligands on xenogeneic cells (Forte et al. 2005; Schneider et al. 2001a).

The adaptive response can be caused by both the direct and indirect pathways of antigen presentation (Game and Lechler 2002; Gokmen et al. 2008). In the first case, T cells from the host recognize allogeneic major histocompatibility complex (MHC) molecules as “self” MHC molecules presenting a foreign peptide. Without cell encapsulation, graft antigen-presenting cells can enter the host lymphatic system, activating CD8⁺ T cells that bind allogeneic MHC class I (MHC-I) molecules and CD4⁺ T cells that bind allogeneic MHC class II (MHC-II) molecules. The frequency of the naïve T cells reactive to allogeneic MHCs is much higher than the frequency of T cells reactive to minor histocompatibility antigens (Matis et al. 1987). If none of the graft cells protrude from the beads and the beads remain intact after transplantation, cell encapsulation should greatly reduce T cell activation via the direct pathway. It should however be noted that direct antigen presentation has become less problematic with the use of protocols such as low-temperature culture of islets prior to transplantation to deplete graft antigen-presenting cells (Lacy and Davie 1984). T cells can

also be activated through an indirect pathway involving the uptake and MHC-II presentation of foreign graft molecules by host antigen-presenting cells, followed by the binding and activation of naïve CD4⁺ T cells. This then leads to a CD8⁺ T-cell mediated response to the graft and/or an antibody/B cell-mediated humoral response to the graft. In both the direct and indirect pathways, CD4⁺ T cell activation requires the expression of co-stimulatory molecules. The absence of co-stimulation has the opposite effect and can lead to graft tolerance through T-cell anergy (Luo et al. 2000). Encapsulation, by reducing the production of pro-inflammatory cytokines (for example by avoiding contact between graft cells and host natural killer cells), may reduce expression levels of co-stimulatory molecules by antigen-presenting cells. Alginate beads should also deflect cytotoxic CD8⁺ T cells from the graft. However, the CD4⁺/B cell-mediated humoral response was found to be more crucial in allogeneic and xenogeneic (Kobayashi et al. 2006) graft rejection than the CD8⁺ cell-mediated response.

In the context of encapsulated islet transplantation, the humoral response results from B cell receptor binding by a “foreign” protein or molecule from the graft, which is then endocytosed and presented on the major histocompatibility complex (MHC) class II (MHC-II) proteins at the B cell surface. B cell differentiation into antibody-producing plasma cells generally requires B cell activation by CD4⁺ T cells recognizing the same antigen. Alginate itself can act both as an antigen and an adjuvant, directly activating B cells (Shapiro et al. 1967). Beads with high M content are more immunogenic than beads with high G content (Kulseng et al. 1999), presumably because chains with high M content are weakly bound by calcium and may leach from the beads and/or because M causes higher macrophage activation (Espevik et al. 1993). This underlines the importance of *in vitro* bead stability and the need to remove unreacted alginate from the beads prior to transplantation. The beads may reduce the humoral response to the graft by retaining some of the antigens from nonviable cells within the beads, but leaking of smaller antigenic peptides from the beads cannot be avoided. Therefore, graft-specific antibody generation is generally observed even when the cells are encapsulated (Kulseng et al. 1999), though the beads may still reduce complement-mediated cell lysis (Rayat et al. 2000).

Recurrence of the autoimmune β -cell destruction must also be avoided to achieve long-term transplanted islet function. Autoreactive T cells and antibodies have been observed in type 1 diabetic allogeneic islet transplant recipients (Vendrame et al. 2010). The absence of auto-reactive T cells has been correlated with improved clinical islet transplant outcomes (Huurman et al. 2008). Syngeneic islet grafts are rejected faster in non-obese diabetic (NOD) mice that develop auto-immunity than in NOD mice treated with streptozotocin, since this delays or prevents the development of auto-immunity (Huurman et al. 2008). CD4⁺ T cells and MHC-II molecules appear to play a pivotal role in the development and recurrence of auto-immunity (Roep 2003). MHC-II mismatched allografts (Makhlouf et al. 2002) or even xenografts (Koulmanda et al. 2003) may therefore elude mechanisms associated with autoimmune rejection. However, other islet cell antigens including insulin are targeted by autoantibodies in type 1 diabetic patients (Srikanta et al. 1986; Tsirogianni et al. 2009) and hence autoimmunity cannot be completely avoided. Nonetheless, by preventing antibody penetration and T-cell access to the graft, alginate beads should offer significant protection of the graft against autoimmunity.

To appropriately shield transplanted islets from the immune system, it is essential that the beads be strong and stable enough to maintain their structure for years. Being reversible hydrogels, alginate beads are greatly sensitive to ion exchange effects. The alginate gel volume is smaller than the original alginate solution due to de-watering during calcium cross-linking of the alginate chains (syneresis). Non-gelling ions can be exchanged with the divalent ions in the gel, leading to reduced gel strength and bead swelling. Stronger gels will exhibit less syneresis (Draget et al. 2001) and swelling (Thu et al. 1996b). Bead swelling after transplantation is undesirable since this increases the bead porosity.

1.3.3.2 Non-immune factors affecting encapsulated islet survival

Encapsulated islet survival can also be affected by nutrient limitations and other factors that are not directly related to immune rejection. In the normal pancreas, a dense network of sinusoidal capillaries irrigates the islets and allows their rapid blood glucose sensing, high oxygenation and response to endocrine factors (Olsson and Carlsson 2006). Without blood flow, islet cells have reduced access to nutrients and secreted factors, leading

to reduced function and survival (Dionne et al. 1993; Lau et al. 2009). Re-vascularization requires one week (rodent islets) or longer (human islets) for non-encapsulated islets (Jansson and Carlsson 2002; Lau and Carlsson 2009). Re-vascularization within the beads is undesirable since this would eliminate immune isolation. The access of encapsulated cells to oxygen is particularly problematic due to its low water solubility compared to other nutrients. β -cells are sensitive to hypoxic environments, leading to impaired insulin secretion at oxygen partial pressures <7 mmHg (Dionne et al. 1989; Papas et al. 1996). For ~ 600 μm diameter beads with one islet/bead, a rough approximation of the average parameters chosen for cell encapsulation trials (Table 1.1), the size of the graft is approximately 1 mL/kg body weight. To accommodate this graft size, the peritoneal cavity has been the most common transplantation site for encapsulated islets. Nutrient limitations are clearly responsible for some of the cell losses in peritoneal encapsulated islet transplantation (de Vos et al. 1996). The oxygen partial pressure at the surface of alginate beads transplanted into the peritoneal cavity (Noth et al. 1999) is typical of vascularized tissues, at ~ 40 mmHg (Klossner et al. 1974). This is also the oxygen partial pressure islets experience in the normal pancreas (Carlsson et al. 2000). At the typical islet encapsulation densities in alginate (i.e. $\sim 2\%$ cell/bead volume), the maximum diffusion length to avoid cell necrosis has been calculated to be ~ 600 μm for uniformly dispersed single cells in beads (Avgoustiniatos and Colton 1997) or ~ 400 μm for islets of 200 μm diameter in alginate cylinders (Dulong and Legallais 2007). Under these conditions, the alginate bead does not significantly contribute to the oxygen limitations experienced by transplanted islets. Even without encapsulation, hypoxia of avascular islets has been observed *in vitro* (Lehmann et al. 2007) and *in vivo* (Carlsson et al. 2001). The diffusion limitations offered by the beads would become more important if beads aggregate in the peritoneal cavity, in beads with fibrotic overgrowth or perhaps during the hypoxic period during and shortly after anesthesia. To reduce diffusion distances and the total graft volume, the bead size could be reduced, albeit this can increase islet protrusion from the beads (de Vos et al. 1996).

1.3.3.3 Current state of microencapsulated islet transplantation

The original report of blood glucose normalization for 2 to 3 weeks by encapsulated allogeneic rat islets by Lim and Sun (1980) sparked high enthusiasm for this strategy of immune isolation, especially after subsequent reports of >3 months blood glucose normalization for both allogeneic (O'Shea et al. 1984) and xenogeneic (O'Shea and Sun 1986) grafts. The findings were replicated using other bead types and animal models (Fritschy et al. 1991; Korbitt et al. 1997b; Lanza et al. 1995), but the results were highly variable between groups (Wilson and Chaikof 2008). Much of this early variation in the results was attributed to purity differences between alginate preparations (van Schilfgaarde and de Vos 1999). Most groups now use in-house purification methods or commercially available alginates that greatly reduce endotoxin and polyphenol levels (Dusseault et al. 2006) although protein contaminants may still be an issue (Langlois et al. 2009). These advances have led to more consistent blood glucose normalization for 6 months to ~1 year in chemically-induced or autoimmune rodent models of diabetes (Figure 1.4). Trials quickly progressed to larger mammals, with up to 70 weeks normoglycemia achieved with allogeneic canine islets (Soon-Shiong et al. 1993; Soonshiong et al. 1992). In non-human primates, the results are highly disparate, ranging from slight reductions in exogenous insulin requirements (Elliott et al. 2005) to insulin independence for 1 to >2 years (Sun et al. 1996). In the study by Elliott *et al.* (2005), there was evidence of graft immunogenicity since beads could be recovered from monkeys transplanted with empty beads but not graft-containing beads. Clinical trials of allogeneic (Calafiore et al. 2007; Soon-Shiong 1999; Tuch et al. 2009) and xenogeneic (Elliott et al. 2007) islets in humans have so far indicated that the beads are safe without measured adverse effects. However, the efficacy of the transplants has not been demonstrated. The most promising outcomes were detectable C-peptide after 2.5 years, live cell recovery in the beads after 9.5 years (Elliott et al. 2007), and ~30% reduction in exogenous insulin needed, as well as reduced glycated hemoglobin levels (Calafiore et al. 2006a). The trials of allogeneic islet transplantation in alginate-PLO-alginate beads are still ongoing in Perugia, Italy. Patients are also being recruited for a new clinical trial with encapsulated neonatal porcine islets in New Zealand (Living Cell Technologies 2010). The exact formulation of the beads

Table 1.1. Long-term encapsulated islet trials in rodents & outcomes in larger mammals or humans

Recipient	Graft type	Bead description (Type, concentration & Manufacturer, %G, diameter, MWCO)	Duration of BG normalization by the graft (weeks)	References
Chemically-induced nude mice	Xenogeneic	Uncoated Ca-alginate, 1.5% Metabolex, 72%G, D =150-350 µm	>14	(Korbitt et al. 2004; Rayat et al. 2000)
Chemically-induced diabetic mice	Allogeneic	Uncoated Ba-alginate	>72	(Duvivier-Kali et al. 2001)
	Xenogeneic	Alginate-PLO-alginate, 1.5% LVCR, 25%G, D = 400–500 µm	11 with Sertoli's cells; 6 without	(Luca et al. 2001)
		Uncoated Ba alginate, Pharmacia, 39%G	20	(Omer et al. 2003)
		Uncoated Ba-alginate, D = 700~800 µm	38	(Schneider et al. 2005)
Immuno-suppressed NOD mice	Xenogeneic	Uncoated Ba alginate, 3.3% FMC Biopolymer, 63%G, D = 854 µm, MWCO 77 – 150 kDa	43	(Cui et al. 2009)
NOD mice	Allogeneic	Uncoated Ba alginate	>72	(Duvivier-Kali et al. 2001)
	Xenogeneic	Alginate-PLO-alginate, 1.5% Stern Italia, 100 kDa MWCO	26	(Calafiore et al. 2004)
Chemically-induced diabetic rats	Syngeneic & allogeneic rat	Uncoated Ba-alginate, Pharmacia alginate, 39%G, D = 500~700 µm; 600 kDa MWCO	Syngeneic: 28 Allogeneic: 8	(Omer et al. 2005)
Autoimmune diabetic dogs	Allogeneic + cyclosporin	Alginate-PLL-alginate, >64%G, ~70 kDa MWCO	9 (N=4) 70 after 2 nd Tx	(Soon-Shiong et al. 1992, 1993)
	Xenogeneic	Alginate-PLO-alginate 1.5% Stern Italia, 100 kDa MWCO	7 (N=1 dog)	(Calafiore et al. 2004)
Non-diabetic monkeys	Xenogeneic	Uncoated Ca-alginate, 1% SLM 100 from FMC BioPolymer, 44%G, D = 754 µm	Porcine C-peptide detected at 9 weeks (N=2)	(Dufrane et al. 2006b)
Chemically-induced diabetic monkeys	Xenogeneic	Alginate-PLL-alginate, 1.5% Kelco, ~39%G, D = 250–350 µm, ~50 kDa MWCO	>17 (N=9)	(Sun et al. 1996)
		Alginate-PLO-alginate, D = 500 – 600 µm, 70 kDa MWCO	0 (N=7) 24 weeks of improved BG control	(Elliott et al. 2005)
Autoimmune diabetic humans	Allogeneic	Alginate-PLL-alginate, 64%G, ~70 kDa MWCO	4 (N=1) 44 months of improved BG control	(Soon-Shiong 1999)
		Uncoated Ba-alginate 2.2% MVG, FMC Biopolymer, 60%G, D = ~340 µm, 250 kDa MWCO	0 (N=4) C-peptide detected at 2.5 years	(Tuch et al. 2009)
		Alginate-PLO-alginate, 1.5% Stern Italia, 100 kDa MWCO	0 (N=2) C-peptide secretion at 1 year	(Calafiore et al. 2006a)
	Xenogeneic	Alginate-PLL-alginate, >64%G, ~70 kDa MWCO	0 (N=1) C-peptide detected at 4 months; live cells at 9.5 years	(Elliott et al. 2007)

*Unless otherwise specified, the cross-linking agent is CaCl₂ and the transplant is peritoneal. BG: blood glucose; G: guluronic acid content, LVCR: pharmaceutical-grade Kelco alginate; N: number of subjects; NOD: non-obese diabetic; PLL: poly-L-lysine; PLO: poly-L-ornithine; Tx: transplantation

used is proprietary but consist of alginate-PLO-alginate beads of ~70 kDa MWCO (Elliott 2008; Thanos et al. 2006; Thanos et al. 2007). In these trials, islet encapsulation was performed drop-wise by extrusion of islets and alginate from a nozzle and external gelation. The scalability of this encapsulation process may become problematic if larger clinical trials were attempted, with patients preferably treated from the same batch of encapsulated cells.

1.4 BIOPROCESSES TO SCALE UP ALGINATE IMMOBILIZATION

Several gel geometries have been investigated for the immobilization of mammalian cells in alginate (Uludag et al. 2000). Alginate sheets (slabs) are adequate for small-scale, but not large-scale *in vitro* cultures. Alginate cylinders encased in hollow fiber ultrafiltration membranes have been investigated as macroencapsulation immune isolation devices (Lacy et al. 1991). Most scale-up approaches have relied on the production of alginate microbeads that can be used in suspension cultures and maximize the surface/volume ratio in cultures or transplanted grafts.

1.4.1 Extrusion-based alginate bead generators

Mammalian cell immobilization in alginate is generally performed by extrusion from an orifice and external gelation. Typically, a mixture of alginate and cells is extruded from a nozzle and the droplets fall into an agitated solution containing divalent ions, resulting in the external gelation of the droplets. Coaxial gas flow (Anilkumar et al. 2001; Wolters et al. 1992), nozzle vibration (Heinzen et al. 2002), electrostatic repulsion (Poncelet et al. 1994) or rotating wires (Prusse et al. 2000) facilitate droplet formation at the nozzle tip. Rotating disks with orifices (Senuma et al. 2000) have also been proposed but their use has not been reported for mammalian cell encapsulation. Vibrating, air-jet and electrostatic bead generators rely on laminar jet break-up in the wind-induced regime that allows the generation of droplets of uniform diameter similar to the diameter of the nozzle. The alginate flow rate varies between ~10 mL/h for the air-jet or electrostatic (Klokk and Melvik 2002) cell encapsulators and ~600 mL/h for the vibrating nozzle (Serp et al. 2000). At higher flow rates, the jet breaks up into droplets smaller than the nozzle diameter and of less

predictable sizes. Multi-nozzle bead generators can be used to increase this throughput, but the distribution of equal flow among the nozzles and the use of solutions >0.2 Pa·s is problematic (Brandenberger and Widmer 1998). In addition, the vibrating and air-jet devices cannot be used for alginate solutions of more than ~ 1.2 Pa·s zero-shear viscosity (Koch et al. 2003; Prusse et al. 2008). This is due to an increase in the viscous and surface tension forces in the liquid, leading to a transition from the wind-induced to the Rayleigh jet break-up regime and eventually to the absence of jetting (i.e. dripping) (Brandenberger 1999; Heinzen et al. 2002).

The JetCutter was proposed as a technology that could achieve throughputs of ~ 500 mL/h (Koch et al. 2003; Prusse et al. 2000) while at the same time allowing the use of more viscous alginate solutions, with 11 Pa·s the highest reported (Prusse et al. 2008). Viscosities >0.15 Pa·s are required to generate beads of ~ 800 μm with the JetCutter, with no bead generation or the generation of misshaped beads at lower viscosities (Prusse et al. 2008). Moreover, the encapsulation of islets, other primary cells, cell aggregates or β -cell lines has not been reported with the JetCutter.

Overall, the throughput of nozzle-based devices is limited to ~ 600 ml/h for alginate viscosities of 0.05 – 11 Pa·s, ~ 10 mL/h for low-viscosity alginates and has not been reported for solutions of higher than 11 Pa·s viscosity (see Table 6.1. in Chapter 6). In addition, all of these devices are expected to impart some damage to islets, since the diameter of the nozzles used is between 100 μm and 500 μm , while $\sim 15\%$ of human islets from typical isolations are larger than 200 μm (Merani et al. 2008). Also, islets tend to aggregate in culture.

1.4.2 Alginate immobilization in a hollow fiber bioreactor

For *in vitro* applications, pancreatic progenitors or other mammalian cells could be cultured in hollow fiber bioreactors containing alginate and cells in the extra-capillary space (ECS). A method for immobilizing Chinese Hamster Ovary (CHO) cells was developed by Minh Luu, a Master's student in the laboratory of Dr. James Piret (Luu 2004). For this process, CHO cells and alginate were injected into the ~ 130 mL ECS of a hollow fiber bioreactor unit, followed by gelation of the alginate using flow of a calcium-containing solution through the intra-capillary space (ICS) and subsequent cell culture by medium flow

through the ICS. The cells could then be recovered with <20% losses by adding citrate to the ICS and then the ECS to chelate the calcium and degel the alginate. This hollow fiber system has the potential to be scaled up to several litres of alginate with the cells immobilized within ~30 min gelling time. The system should allow the use of high-viscosity alginates since bead generation or flow through small orifices is not required. However, the bioreactor method had not been fully validated for mammalian cell culture and had not been tested with primary cells.

1.4.3 Alginate immobilization by emulsion and internal gelation

Alginate bead generation by emulsification/internal gelation would allow the mass-production of beads with high sphericity using a broad range of alginate viscosities. This method has been used to immobilize DNA (Alexakis et al. 1995), proteins (Vandenberg and De La Noue 2001) including insulin (Silva et al. 2006) and bacteria (Larisch et al. 1994a). The process was also suggested to be applicable to plant and mammalian cells (Lencki et al. 1989). For this method, the encapsulant (e.g. cells) is dispersed in an alginate solution

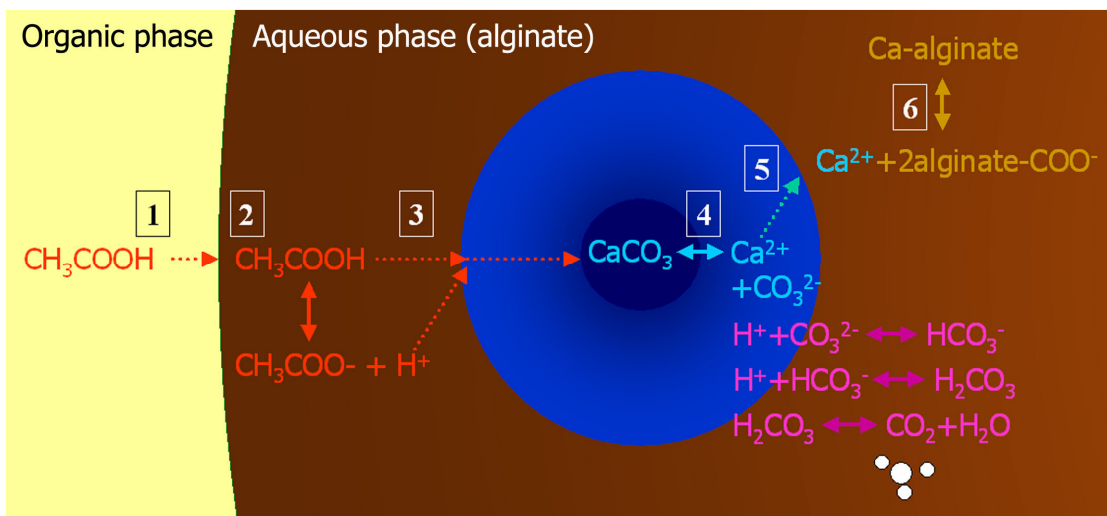


Figure 1.4. Internal gelation reaction steps during the emulsion/internal gelation process.

(1) The organic acid is added to the agitated organic phase where it is transported to the bead surface by convection. (2) The organic acid partitions into the aqueous phase. (3) The acid dissociates and diffuses through the alginate solution or gel to the surface of dissolving salt granules (in this case calcium carbonate) depicted in light blue. (4) Near the surface, the solid dissolves into calcium ions as well the conjugate base of the salt (e.g. CO_3^{2-}) with which the H^+ reacts. (5) The calcium ions diffuse until they encounter unreacted alginate, leading to the cross-linking (6) of neighbouring alginate chains.

containing a finely grained insoluble calcium or barium salt. The alginate mixture is agitated in an organic phase to create an emulsion, usually in the presence of a surfactant. The pH is then reduced using an oil-soluble acid that partitions into the aqueous phase to ionize the salt, releasing the divalent ions. For example, acetic acid, which has a mineral oil/water partition coefficient <0.005 (Reinsel et al. 1994), can be pre-dissolved in oil, then added to the emulsion where it is evenly mixed with the oil phase but rapidly partitions into the aqueous phase (Xiu-Dong et al. 2007). Various steps (depicted in Figure 1.4) during this internal gelation reaction can limit the overall reaction kinetics. For calcium carbonate grains larger than $\sim 2.5 \mu\text{m}$, the rate of carbonate dissolution has been shown to be rate-limiting for emulsion-based processes (Poncelet et al. 1995) or for internal gelation by slowly hydrolyzing lactones (Draget et al. 1990).

Potential drawbacks of using emulsion and internal gelation for encapsulating pancreatic tissue include: (1) the necessity for transient exposure to low pH, (2) the need to remove residual oil, (3) the polydisperse bead size distribution, (4) the potential shear stress during alginate droplet formation and (5) the higher porosity of internally gelled beads compared to externally gelled beads (Quong et al. 1998). Islet function may be particularly sensitive to transient changes in pH because glucose-responsive insulin release is modulated by the β -cell intracellular pH (Gunawardana and Sharp 2002).

As discussed in Section 1.2.3.2, uniform bead size distributions are desirable for transplantation applications. Whereas small bead sizes can lead to islet protrusion, large beads can hinder nutrient or insulin diffusion. During emulsification in turbulent flow, pressure fluctuations act to disrupt droplets (Hinze 1955; Kolmogorov 1949), counteracting the surface tension and the viscous forces in the dispersed phase (Davies 1985). Viscous forces are non-negligible if the viscosity of the dispersed phase is much higher than that of the continuous phase. Assuming that the maximum local energy dissipation rate is proportional to the average energy dissipation rate in the vessel, the maximum stable droplet diameter d_{max} (if \gg than the Kolmogorov scale) can be calculated as follows (Davies 1985; Pacek et al. 1999; Steiner et al. 2006; Tcholakova et al. 2008) :

$$\frac{\rho_c \varepsilon^{2/3} d_{\max}^{5/3}}{\sigma} = C \left(1 + \frac{1}{2^{3/2}} \frac{\eta_d (\varepsilon d_{\max})^{1/3}}{\sigma} \right) \quad (\text{Equation 1.4})$$

where ρ_c is the density of the continuous phase, ε is the average energy dissipation rate in the vessel, σ is the interfacial tension between the two fluids, η_d is the viscosity of the dispersed phase and C is a proportionality constant. When surface tension forces predominate over viscous forces, the right-hand side simplifies to C , whereas if the viscous forces predominate it simplifies to $C \frac{1}{2^{3/2}} \frac{\eta_d (\varepsilon d_{\max})^{1/3}}{\sigma}$. In stirred vessels, the energy input under turbulent flow scales proportionally to the power input, i.e. to $N_i^3 D_i^2$, where N_i is the agitation rate and D_i is the impeller diameter. Therefore, combined with Equation 1.4 and given a constant D_i , the d_{\max} is predicted to be proportional to $N_i^{-1.2}$ if surface tension forces predominate, while it is proportional to $N_i^{-0.75}$ if viscous forces within the beads predominate as the main retentive force. Since it can be impractical to determine d_{\max} experimentally, high quantile values (e.g. the 95th quantile) of the diameter or the surface area-moment mean diameter (D_{32}) have been used instead, as they generally are proportional to d_{\max} (Lagisetty et al. 1986).

1.4.4 Challenges of scaled-up *in vitro* culture of alginate-immobilized insulin+ cells

In addition to the factors that may affect cell survival during immobilization, the *in vitro* scaled-up culture of alginate-immobilized insulin-producing cells also presents particular challenges. As with other mammalian cell culture systems, access to nutrients, removal of harmful waste products, shear stress experienced by the cells, pH and temperature have to be taken into account. As mentioned in Section 1.3.3.2, the alginate matrix will hinder the diffusion of nutrients and secreted products, including insulin. Insulin can exert anti-apoptotic and mitogenic effects on β -cells (Beith et al. 2008; Johnson et al. 2006). Whereas this may be beneficial to the immobilized cells up to a certain local concentration, it would be undesirable for transplantation applications where insulin release is necessary for graft function. In hollow fiber bioreactor systems, diffusion limitations through alginate would be compounded with the nutrient and waste product gradients expected from the pressure gradients in these systems (Piret et al. 1991). In addition, large

proteins secreted by the cells that do not cross the ultrafiltration membrane of the hollow fiber bioreactor will accumulate in the extra-capillary space (Koska et al. 1997). In stirred suspension cultures of pancreatic cells entrapped in alginate beads, shear stress to the cells may be of less concern than for free-floating cells. Shear-induced damage of the beads themselves may however be problematic (Vogelsang et al. 2000). Lastly, the local pH in the negatively charged alginate matrix may be lower than in the surrounding medium. Finally, temperature gradients may affect hollow fiber bioreactor cultures unless the bioreactor, tubing and medium reservoirs are well insulated or placed in a temperature-controlled environment.

1.5 RESEARCH GOALS

The clinical use of islet transplantation as a treatment for type 1 diabetes is currently limited by the lack of donor tissue and the rejection of the transplanted islets. Clinical trials with embryonic stem cell-derived cells can be anticipated, especially given the recent lifting of the hold placed by the United States Food and Drug Administration on the first clinical trial of human embryonic stem-cell derived tissue for the treatment of spinal cord injury (Krassowska 2010). Clinical trials with encapsulated islets are also ongoing. A combination of the two approaches can be envisioned, since encapsulation in a gel matrix may promote the differentiation of embryonic-derived progenitors by providing mechanical cues (see Section 1.3.2), as well as provide immune protection. Alternatively, adult human pancreatic progenitors could be expanded and differentiated or re-programmed into insulin-producing cells. Numerous protocols reporting the generation of islet-like cell clusters from adult human pancreatic tissue have been published, but none have been consistently replicated by other groups and the expansions reported are insufficient for clinical applications (Bonner-Weir et al. 2000; Boretti and Gooch 2006; Todorov et al. 2006; Tsang et al. 2007). There is a need for novel technologies enabling both robust large-scale cell production and immune isolation to address the great need for improved diabetes therapy.

The overall goal of the proposed work was to optimize and scale up protocols allowing the generation or immune isolation of insulin+ cells. Two novel scalable

processes for alginate-immobilized culture of pancreatic cells were developed. Neonatal pancreatic porcine cell clusters and human islet-depleted pancreatic tissue were the primary tissues used to validate these bioprocesses. Also, a high content imaging platform to optimize serum-free cultures of primary human pancreatic duct-like cells was developed and implemented.

The objective of Chapter 2 was to determine whether a hollow fiber bioreactor could be used for the alginate-immobilized culture of β -cell progenitors. The first aim was to achieve gel formation in the extra-capillary space of the bioreactor without obstruction of the intra-capillary space. The second aim was to develop a method to recover >80% of the cells after degelling the alginate. The expansion of CHO cells in the hollow fiber bioreactor was then compared to small-scale alginate slab cultures. Lastly, the survival and insulin content of NPCCs after alginate-immobilized culture in the bioreactor were compared to slab cultures.

The objective of Chapter 3 was to adapt the emulsion and internal gelation alginate bead generation process to mammalian cell and, in particular, pancreatic cell immobilization. The first aim was to determine whether MIN6 cells could survive the process and to determine the main causes of cell losses. The second aim was to minimize these losses based on an empirical understanding of the emulsification and internal gelation kinetics. The third aim was to determine whether cell growth and function would be similar to beads generated by nozzle extrusion, including whether there would be increased cell survival and/or insulin expression by primary human pancreatic islet-depleted tissue.

The objective of Chapter 4 was to determine whether the alginate beads produced by emulsion and internal gelation could also protect transplanted β -cells from allorejection. It was hypothesized that high-concentration beads achievable by the emulsion process could improve the *in vivo* immunoisolation properties of the beads without the use of cationic polymers. The approach was to first determine the range of alginate concentrations and viscosities allowing bead generation by the emulsion process. The next step was to compare the strength, stability and porosity of high-concentration emulsion beads with standard lower-concentration beads generated nozzle extrusion. β TC3 insulinoma cells were then

encapsulated in the two bead types and transplanted into allogeneic diabetic mice to compare transplantation outcomes and cell survival. Lastly, the cellular and humoral immune response to the grafts was assessed.

The objective of Chapter 5 was to develop methods to expand cells of ductal phenotype from primary human islet-depleted pancreatic tissue in serum-free medium. The first aim was to develop a method to remove fast-cycling fibroblast-like cells that overgrow the cultures. It was hypothesized that these are from a mesenchymal developmental origin, and hence that they could less easily be prompted to express insulin than duct-like cells. The second aim was to develop, validate and apply a serum-free high content screening platform to identify pancreatic duct mitogens.

2 PANCREATIC CELL IMMOBILIZATION IN AN ALGINATE-FILLED HOLLOW FIBER BIOREACTOR¹

The first scale-up method considered for alginate-immobilized pancreatic cell cultures was a hollow fiber bioreactor process that would allow batch-wise gel formation without requiring droplet generation or exposing the cells to high shear. Hollow fiber bioreactors have been used for the high-density culture of non-immobilized mammalian cells that secrete the product into the intra-capillary space (ICS). Gel-immobilized culture presents new challenges related to the adequacy of gelling and cell recovery from between the bundle of fibers. A methodology was developed whereby (1) alginate obstruction of the ICS medium flow was negligible, (2) extra-capillary alginate gelling was complete and (3) $83 \pm 4\%$ of the cells seeded and immobilized were recovered from the bioreactor. Chinese Hamster Ovary (CHO) cells were used as a model aggregate-forming cell line that grew from mostly single cells to pancreatic islet-sized spheroids in 8 days of alginate-filled hollow fiber bioreactor (AHFBR) culture. CHO cell growth and metabolic rates in the AHFBR were comparable to small-scale alginate slab controls. The process was then successfully applied to the culture of primary neonatal pancreatic porcine cells, without significant differences in cell viability compared to slab controls. Similar to previous reports in the literature, alginate-immobilized culture in the AHFBR increased the insulin content of these cells compared to suspension culture.

2.1 INTRODUCTION

Immobilized gel-matrix mammalian cell culture is thought to have greater potential than traditional surface culture to mimic the *in vivo* environment and to induce or maintain differentiated cell function (Griffith and Swartz 2006). Alginate immobilization has been

¹ A version of Chapter 2 has been published: A Novel Alginate Hollow Fiber Bioreactor Process for Cellular Therapy Applications, Hoesli CA, Luu M, Piret JM, *Biotechnology Progress* 25(6): 1740-1751, Copyright © 2009 by the American Institute of Chemical Engineers. Link to the article: <http://onlinelibrary.wiley.com/doi/10.1002/btpr.260/abstract>.

shown to promote the differentiation of various types of cells along specific lineages depending on the gel properties and culture conditions. Alginate immobilization of mouse ES cells allowed the high-density generation of well-separated embryoid bodies that could generate cardiomyocytes and smooth muscle cells after release from the gel and culture in the presence of retinoic acid (Magyar et al. 2001). In another study, mouse embryoid bodies formed from single cells seeded in alginate microbeads had increased hepatocyte functions (Maguire et al. 2006). In the presence of Activin A or upon transplantation into mice, alginate immobilization promoted the differentiation of human ES cells towards endoderm (Chayosumrit et al. 2010; Dean et al. 2006). Alginate immobilization also induced chondrogenesis of mesenchymal (Ma et al. 2003) or adipose-derived (Awad et al. 2004) stem cells. Alginate immobilization has long been known to allow chondrocytes to retain functionality much longer than monolayer culture (vanSusante et al. 1995). Insulin+ cells can be generated directly in alginate beads from ES cells by following a β -cell differentiation protocol developed for adherent cultures (Wang et al. 2009). Alginate has been shown to increase the insulin content of neonatal pancreatic porcine cell clusters (NPCCs) *in vitro* (Tatarkiewicz et al. 2001) and hence to reduce the time required for diabetic mice to achieve normoglycemia following the transplantation of encapsulated NPCCs (Korbitt et al. 1997a). Similarly, insulin-expressing islet-like cell clusters were generated from expanded human islet-rich tissue by aggregation in alginate microcapsules (Tsang et al. 2007).

One challenge that can be anticipated for the clinical implementation of gel-matrix cell culture is the need for larger-scale cell immobilization technology. In the case of islet transplantation using the Edmonton Protocol (Shapiro et al. 2000), widespread treatment of type 1 diabetes would require the generation of 10^8 islet-like cell clusters per donor pancreas to transplant ~100 patients (Porrett et al. 2007; Ricordi 2003). It can be expected that each donor pancreas would be processed individually, due to their sporadic availability, to enable safety validation of lots and HLA matching. This donor-scale would represent ~10 L alginate volumes for each donated pancreas, assuming final cell concentrations on the order of 10^4 islets/mL or 10^7 cells/mL. Currently used single nozzle bead generators would typically require ~1 day to encapsulate this amount of cells (Serp et al. 2000). More rapid

batch cell immobilization would be preferable to avoid compromising the quality of the cells by exposure to longer-term processing conditions and delays. Even larger batches could be needed if islet transplantation was envisioned for type 2 diabetics, since they constitute the majority of diabetic patients who suffer from insufficient islet mass (Porrett et al. 2007). The potential use of virtually unlimited cell sources such as xenogeneic progenitors or embryonic stem cells for the treatment of diabetes or a variety of other cellular therapies adds to the motivation to develop larger-scale cell immobilization processes.

Micro- or ultra-filtration HFBRs of >10 L are used as membrane bioreactors in water treatment (Brindle and Stephenson 1996) and as recombinant protein concentration units. The 0.5~1 mm fibers of these units should be sufficient for the relatively dilute cell density and low oxygen demand of slowly dividing primary cells such as pancreatic cells in islet-like clusters (Piret and Cooney 1990). Cell immobilization in a matrix irrigated by hollow fibers has been reported for bioartificial pancreata designed to isolate transplanted islets from the host immune system (Maki et al. 1993; Ohgawara et al. 1998). Agarose or gelatin/agarose cell immobilization has been used to investigate mass transfer or cell concentration gradients in HFBRs (Koska et al. 1997; Sardonini and Dibiasio 1992; Wei and Russ 1977). However, these systems were not designed for cell recovery.

We describe a novel scalable and low-shear alginate hollow fiber bioreactor (AHFBR) process for immobilized mammalian cell culture and recovery. This process relied on diffusion of molecules from the ICS into the alginate-containing ECS to (1) externally gel the alginate, (2) provide nutrients during immobilized culture and (3) chelate the alginate at the end of cultures to recover the cells from the bioreactor. Azoalbumin tracer studies were performed to develop a methodology to minimize fiber blockage by alginate. Then, the alginate gel concentration and gelling time were selected to ensure effective gelling throughout the AHFBR. CHO cells were used as a practical model cell type because of their tendency to form aggregates similar to islets when cultured in suspension or in alginate. Islet-sized CHO cell aggregates should offer similar resistance to diffusion as would be the case for islet-like clusters generated from primary cells. However, their nutrient consumption would constitute a “worst-case scenario” for process development, since lower

nutrient demands are expected from primary cells. For example, the oxygen consumption of islets is ~0.13 pmol/cell/h (Dulong and Legallais 2007) compared to 0.31 pmol/cell/h for CHO cells (Jorjani and Ozturk 1999). These CHO cells were used to test the culture and develop the cell recovery methods, ultimately providing a proof-of-concept for this AHFBR process. Finally, the AHFBR was used to successfully culture primary pancreatic cells.

MATERIALS AND METHODS

2.1.1 CHO cell line

Chinese hamster ovary (CHO) suspension cells (Angepat et al. 2005) were grown in a serum-free medium (SFM 2.1b, Cangene, Winnipeg, MB). The cells were maintained in spinner flasks or in shake flasks (Corning, Corning, NY) in a shaking incubator (Minitron Infors, Bottmingen, Switzerland).

2.1.2 The effect of process solutions on CHO cell survival

CHO cells were incubated at room temperature (24° C) in ambient air for up to 2 h in gelling (75 mM CaCl₂, 75 mM NaCl, 10 mM HEPES), saline rinsing (170 mM NaCl, 10 mM HEPES) or degelling (55 mM sodium citrate, 10 mM HEPES) solutions at an initial density of 1.7 x 10⁶ cells/mL. Another chelator, ethylenediaminetetraacetic acid (EDTA) was compared to the citrate degelling agent by using an equimolar 82.5 mM solution in 10 mM HEPES. The number of viable cells was quantified by trypan blue exclusion (see *cell enumeration*) at different time points.

2.1.3 The effect of alginate type on CHO cell growth

CHO cells were seeded at 1 x 10⁵ cells/total mL of culture in 3 types of alginate: (1) high molecular weight (231 kDa) composed of 73% guluronic acid (Pronova MVG, Novamatrix, Sandvika, Norway), (2) intermediate molecular weight (189 kDa) but similar guluronic acid content (Pronova LVG) and (3) low molecular weight (12~80 kDa) 65-70% guluronic acid (A0682, plant cell culture tested, Sigma, St-Louis, MO). The cells were maintained for 5 days with daily cell enumeration.

2.1.4 Alginate slab immobilization and recovery

To create alginate slabs of 0.4 mm nominal thickness, one volume of 10-fold concentrated cell stock was added to 9 volumes of 0.83% MVG Pronova alginate for the NPCC experiments and 1.11% or 3.33% Sigma alginate for the CHO experiments, prepared in saline solution. The slabs generated were of final 0.75% alginate concentration for the NPCC cultures and 1% or 3% alginate for the CHO experiments. The surface of 10 cm treated dishes (Sarstedt, Germany) was wetted with saline solution and 2.5 mL of cell-alginate solution was added. To gel the alginate, 10 mL gelling solution was added drop-wise to each plate and left for ~5 min. The resulting alginate slabs were washed twice with saline solution and covered with 10 mL culture medium. After a given culture period at 37°C in humidified air containing 5% CO₂, the cells were recovered from the slabs by replacing medium with 5 mL degelling solution and rotary shaking (35 rpm) for 15 min.

2.1.5 AHFBR apparatus and set-up

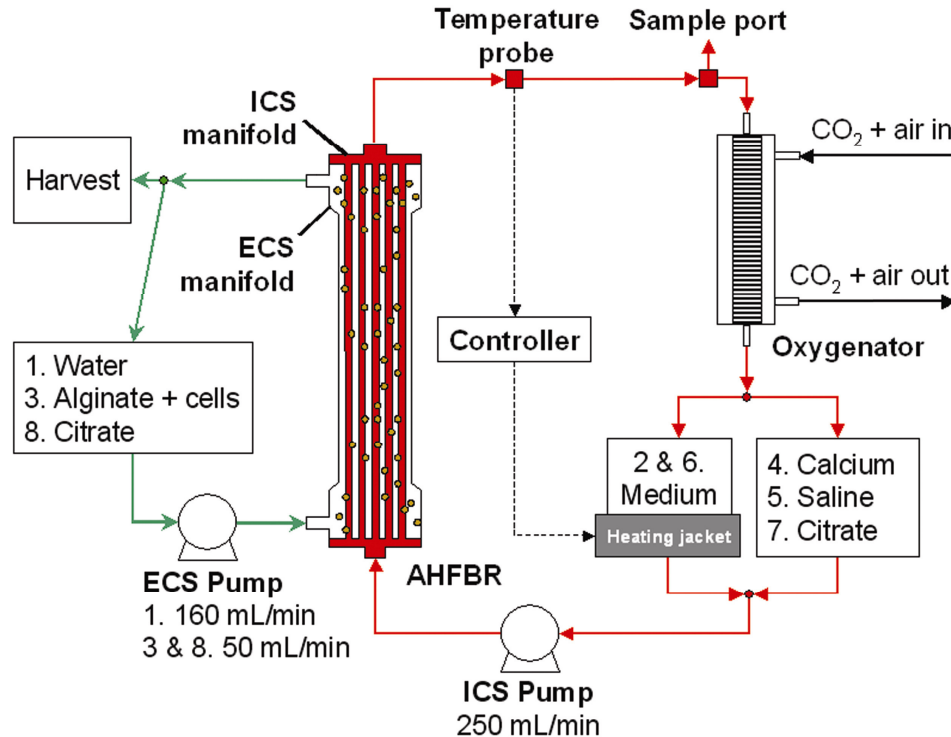


Figure 2.1. AHFBR process flow diagram.

Numbers indicate the order in which processing solutions are circulated through the HFBR unit (refer to Materials and methods, AHFBR process for details).

The AHFBR process flowchart for the cell growth experiment is shown in Figure 2.1. A Gambro 16 dialyzer (Stockholm, Sweden) was used as the HFBR. The pumps were peristaltic (Masterflex Cole-Parmer, Vernon Hills, IL). Masterflex Pharmed tubing was used throughout, except in the aeration unit, which consisted of 4 parallel lengths (2 m each) of silicon tubing (1/8" OD, Cole-Parmer) coiled inside a plastic box ventilated with 90% air mixed with CO₂ at 1 L/h. The heating jacket of a Cell-Pharm System 1500 (Unisyn Technologies, Hopkinton, MA) biocontroller unit controlled the temperature between 35.0 and 37.2°C. Adding cheesecloth and plastic insulation reduced temperature gradients near the edges of the AHFBR cartridge. To assemble the system aseptically, autoclaved sections of tubing and bottles were assembled in a laminar flow hood or connected with a SCD IIB sterile tubing welder (Terumo, Elkton, MD). All AHFBR experiments without cell growth were carried out at room temperature and the azoalbumin pulse-chase experiments also excluded the aeration unit.

2.1.6 AHFBR process

For each run, the extracapillary space (ECS) of a new HFBR cartridge was rinsed with 2 L of deionized water (Figure 2.1 step 1). This and other processing steps were performed without temperature control unless otherwise specified. The ECS ports were then closed and 2 L of deionized water or culture medium (at 37°C) was re-circulated for >24 h through the

Table 2.1. Operating conditions of different AHFBR experiments

Experiment	Alginate concentration	Gelling solution	Gelling time (h)	ICS flowrate (mL/min)
Alginate plugging	0.75% Pronova MVG	100 mM CaCl ₂ 100 mM NaCl	1	30, 115, 300
Degree of gelling	1%, 1.25%, 3% Sigma	75 mM CaCl ₂ 75 mM NaCl	0.5, 1	300
CHO recovery	1%, 3% Sigma	75 mM CaCl ₂ 75 mM NaCl 10 mM HEPES	0.5	250
CHO growth	1% Sigma	75 mM CaCl ₂ 75 mM NaCl 10 mM HEPES	0.5	250
NPCC culture	0.75% Pronova MVG	75 mM CaCl ₂ 75 mM NaCl 10 mM HEPES	0.5	250

intracapillary space (ICS) to flush out bubbles in the fibers and as a sterility test when medium was used (Figure 2.1 step 2). The ECS was emptied by flushing with air and subsequently loaded with alginate through the bottom port at 160 mL/min without cells and 50 mL/min with cells (Figure 2.1 step 3). The alginate was agitated with a magnetic stirrer at ~100 rpm while loading cells and re-circulated for 5 to 10 min while gently tapping the cartridge to remove bubbles. The ECS pump was stopped and the ECS outlet clamped before re-circulating a calcium-containing gelling solution in the ICS (Figure 2.1 step 4) using the solutions and flowrates specified in Table 2.1. It was essential to enumerate the cells left in the alginate solution after seeding the AHFBR because the bundle of fibers acts as a sieve. For 150 mL of initial alginate stock, the actual cell concentration seeded in the bioreactor and in the leftover stock were respectively $109\% \pm 1$ and $\sim 55\% \pm 2$ of the cell concentration in the initial seed stock. After gelation, 2 L of saline solution was flushed through the ICS at the flowrate provided in Table 2.1 to remove any excess Ca^{2+} that would form a precipitate with the phosphate in the medium (Figure 2.1 step 5). The cells were then cultured by circulating medium at 37°C through the ICS (Figure 2.1 step 6). For the CHO culture experiments, 1.6 L medium was re-circulated through the ICS and then (in the second AHFBR growth experiment) changed to 1.7 L of fresh medium at day 5.8 and to 0.8 L of fresh medium at day 7.7. For the NPCC culture, the ratio of medium to alginate was kept the same between the AHFBR, slab and suspension cultures and the medium was fully replenished every second day. To assess AHFBR culture performance, pH, glucose, lactate, glutamine, glutamate and dissolved gases were measured daily by a YSI 7100 MBS (Yellow Springs, OH) or RapidLab 348 (Bayer, Tarrytown, NY). The alginate was degelled by re-circulating 2 L degelling solution through the ICS for 1 h (Figure 2.1 step 7) at the flowrate given in Table 2.1. Air was then pumped into the ECS, pushing out 116 ± 2 mL of liquefied alginate for the 1% alginate case. Further degelling passes consisted of adding citrate solution directly into the ECS to $\sim 3/4$ fill (Figure 2.1 step 8), manually rotating the cartridge and pumping out the degelled alginate and cells. The air remaining in the unfilled $1/4$ of the ECS facilitated ECS mixing and degelling upon manual rotation.

2.1.7 AHFBR ICS obstruction

Fiber obstruction due to alginate egressing from the ECS to gel in the ICS was determined by analyzing the residence time of azoalbumin (Sigma, 5 g/L in saline) pulsed for 5 s through the ICS of the HFBR before and after loading alginate (without cells). Thorough ICS rinsing (>48 h at 300 mL/min) prior to alginate loading was necessary to flush out air bubbles (Labecki et al. 1998). ICS outlet samples were collected at 2 s intervals using an Advantec SF2120 fraction collector (Dublin, CA). Azoalbumin concentrations were determined from absorbance at 450 nm. The average residence time ($t_{R,ave}$) was calculated from the absorbance time distribution by numerical integration using the trapezoidal rule. It was assumed that the protein did not interact with the fibers or alginate and hence would move at the same velocity as the fluid. However, the cartridge did retain some red colour, indicating that there was some binding of azoalbumin. At the flow rates (≥ 30 mL/min) used, it was assumed that the contribution of binding kinetics on the shape of the elution peaks was negligible.

2.1.8 AHFBR degree of gelling and cell recovery

The degree of gelling was assessed visually at 3 concentrations and 2 gelling times (Table 2.1) by sawing the AHFBR cartridges open. In the cell recovery experiments, CHO cells were suspended at $20 \pm 1 \times 10^5$ cells/mL of alginate. The alginate was loaded, gelled and degelled within 4 h at room temperature with air and 5% CO₂ supplied to the oxygenator. The cell recovery was defined as the number of live cells retrieved after degelling divided by the number of live cells loaded (cells in the seeding flask before loading – cells in the seeding flask after loading). The number of islet equivalents that would correspond to the CHO cell aggregates produced during AHFBR growth was estimated by dividing the total live cell number by the number of CHO cells in a 150 μ m diameter aggregate.

2.1.9 CHO growth kinetics

The maximum specific growth rate was determined from the exponential portion of the growth curve. During culture, exit of up to 20% of the cells from the alginate slabs into suspension was observed, which is common for cell lines cultured in alginate (Seifert and

Phillips 1997). It was difficult to distinguish the rate of slab exit from the rate of cell division in suspension. Therefore total cell numbers, including cells in the supernatant, were used to calculate the growth rates in alginate slabs. This was only applied to slab cultures as the confined space of the AHFBR avoided cell exit from the alginate. The cell yield per gram of glucose consumed was obtained from the slope of the curve of ΔX versus ΔS , which was linear once the cultures exited the lag phase. The maximum specific growth rate and specific metabolic rates (data not shown) were determined by fitting the data to Richard's equation (Lopez et al. 2004), which provided high goodness-of-fit. For the AHFBR growth experiment, seeding densities were $6.3 \pm 0.8 \times 10^5$ cells/mL alginate for the AHFBR, $2.5 \pm 0.3 \times 10^5$ cells/mL alginate for the slabs and $4 \pm 2 \times 10^5$ cells/mL for the suspension cultures.

2.1.10 CHO aggregate size distribution

Bright field images of CHO cell aggregates were captured using a Nikon D100 camera mounted onto a TMS inverted microscope (Nikon, Tokyo, Japan) at an overall 40-fold magnification. Images were captured at the end of 8.3 days of AHFBR or alginate slab cultures. The seed stock images were taken the same day as other images from a maintenance suspension culture. The number of aggregates analyzed (N) was >200 for each sample. Aggregate area was determined using the Analyze Particles function of the ImageJ 1.34b (National Institutes of Health, USA) freeware. The volume moment average aggregate diameter (D_{43}) and the volume-weighted standard deviation (s_D) were calculated using respectively Equations 2.1 and 2.2. The individual diameters D_i and volumes V_i were based on the diameter of a circle occupying the same area as the aggregate in the 2D photograph. Equation 2.3 defined the circularity, where A_i and P_i are the aggregate area and perimeter in the 2D image.

$$D_{43} = \frac{\sum_{i=1}^N D_i^4}{\sum_{i=1}^N D_i^3} \quad (\text{Equation 2.1})$$

$$s_{D43} = \sqrt{\frac{\sum_{i=1}^N D_i^3 (D_i - \bar{D})}{(N-1) \sum_{i=1}^N D_i^3}} \quad (\text{Equation 2.2})$$

$$\text{Circularity} = 4\pi \frac{A_i}{P_i^2} \quad (\text{Equation 2.3})$$

2.1.11 NPCC isolation and shipment

NPCCs from 1-3 day old pigs were obtained from the University of Alberta Department of Surgery (Korbitt et al., 1996). Briefly, each pancreas was cut into pieces, digested with collagenase, washed four times with Hank's balanced salt solution (HBSS), and re-suspended in 100 mL Ham's F10 medium supplemented with 10 mM glucose, 50 mM isobutylmethylxanthine, 0.5% (w/v) bovine serum albumin (Sigma), 2 mM L-glutamine, 10 mM nicotinamide, 100 U/mL penicillin, and 100 mg/mL streptomycin (Ham's F10+). Cells were shipped overnight to the University of British Columbia without temperature control in 50 mL conical tubes with 0.5 to 1 cm headspaces. Viability after two rinses in medium was 75~90% based on trypan blue staining.

2.1.12 NPCC cell culture

Upon arrival (day 1), each pancreas yielded $2 \pm 1 \times 10^8$ cells. NPCCs were washed twice in Ham's F10+ and cultured in Ham's F10+ at 37°C in humidified air containing 5% CO₂ in 15 cm non-treated dishes (Thermo Fisher Scientific, Waltham, MA) with medium exchange every second day. A concentrated stock ($\sim 5 \times 10^7$ cells/mL) was used to ensure consistent seeding of fast settling NPCCs. Seeding densities were 1 to 5×10^6 cell/mL. At day 8, the tissue was divided between suspension cultures and alginate immobilized cultures, seeded at $0.9 \pm 0.1 \times 10^5$ viable cells/total mL of culture ($4.5 \pm 0.5 \times 10^5$ cells/mL alginate). This seeding density was ~10-fold lower than published protocols of NPCC culture in alginate since only two pancreata were available to seed the ~200 mL alginate required for the experiment. Alginate slabs were seeded at both the same and 5-fold this concentration to control for seeding density effects. Suspension cultures were kept in Ham's F10+ while

NPCCs in alginate were cultured in Ham's F10+ with 5% neonatal porcine serum (NPS) except for one slab culture without serum.

2.1.13 Cell enumeration

If a single cell suspension could be obtained, viable and nonviable cells were counted based on trypan blue exclusion in a hemocytometer or using an automated Cedex AS20 system (Roche Innovatis AG, Bielenfeld, Germany). CHO cell aggregates were dissociated in 1 volume 0.25% trypsin-EDTA (Invitrogen, Carlsbad, CA) medium to one volume of medium by incubating 10 min at 37°C and triturating prior to cell enumeration.

2.1.14 Insulin and DNA content

Intracellular insulin and DNA concentrations were measured respectively using a competitive radioimmunoassay (Linco, St. Charles, MO) and the Picogreen dye DNA binding assay (Invitrogen Molecular Probes) according to the manufacturers' instructions. Briefly, for insulin analysis, 1 mL of azol (11.4% v/v glacial acetic acid, 0.25% BSA) was added to duplicate or triplicate 200 µL culture samples. Samples were stored at -20°C, sonicated, lyophilized and re-suspended in PBS for the insulin radioimmunoassay. For DNA quantification, duplicate or triplicate 200 µL culture samples were washed twice in citrate buffer (150 mM NaCl, 15 mM citric acid, 3 mM EDTA, pH 7.4) and cell pellets were stored at -20°C. After thawing, the samples were sonicated in 0.5% Triton X in TE buffer (pH 7.4) and diluted with TE buffer. Picogreen reagent was added and the sample fluorescence compared to measurements of a 0 to 1000 ng/mL lambda phage DNA standard curve.

2.1.15 Statistical Analysis

Unless otherwise stated, reported values are averages \pm standard errors of the mean (SEM). Significant differences were determined by using the two-tailed Student's t-test with pooled variance if the Fisher ratio of squared standard deviations was less than $F_{v2, v1, 0.05}$. P-values ≤ 0.05 were considered to be statistically significant. For comparison of single AHFBR data to replicate reference cultures, 95% confidence intervals around the reference mean are reported. In the time course experiment with CHO cells incubated in various processing solutions, multivariate analysis of variance (MANOVA) was conducted using JMP IN 5.1.2

software (SAS Institute, NC). The repeated measures option allowed the assessment of the in-between impact of the processing solutions.

2.2 RESULTS AND DISCUSSION

2.2.1 The effect of process solutions on CHO cell survival

Prior to process development, the effects of the gelling (CaCl_2), saline (NaCl) and degelling (citrate or EDTA) solutions on CHO cell survival were tested (Figure 2.2) at room temperature without CO_2 control. Little growth or change in cell viability was observed for control cells in medium. MANOVA analysis confirmed a significant negative trend of viable cell number with time when any of the 4 processing solutions was used, while a significant positive trend was observed in the medium control. No significant difference in cell survival was observed between the two degelling solutions, citrate or EDTA. Citrate was chosen for further experiments because it is medically innocuous (Nishioka et al. 2002; Ramirez et al. 1993). Visual assessment ascertained that the citrate did not disrupt cell aggregates.

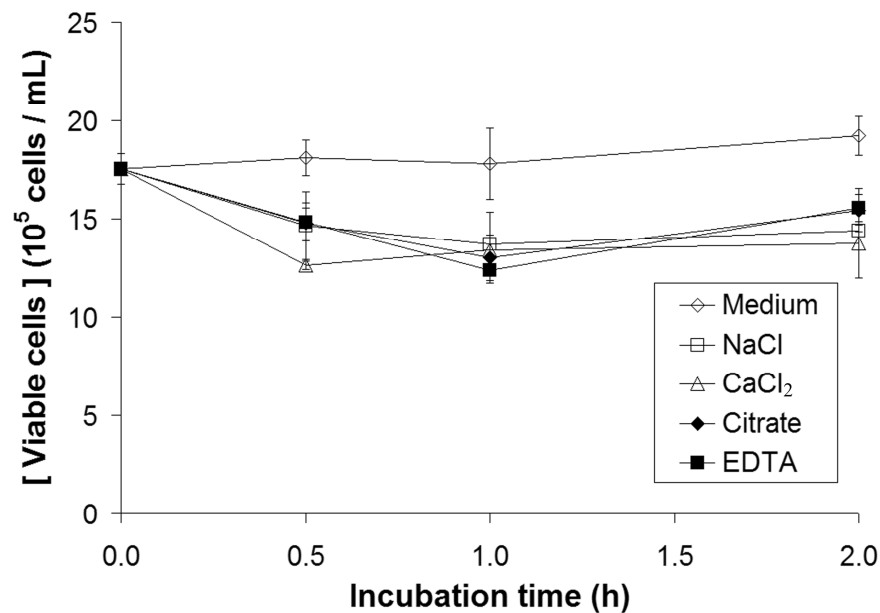


Figure 2.2. CHO cell survival in the alginate processing solutions.

2.2.2 The effect of alginate type on CHO cell growth

Alginate significantly reduced cell growth rates by 30% over a 5-day culture period compared to suspension controls (Figure 2.3). This could arise from direct effects of the matrix, with potential influences from nutrient and waste product gradients inherent to immobilized and aggregated cell growth. As could be expected for alginates of similar guluronic acid content (Stabler et al. 2001), no significant difference in CHO growth rate was observed between Pronova MVG, Pronova LVG and the Sigma LVG alginate. The lower cost alginate from Sigma was used to develop the AHFBR process, including the cultures with CHO cells, but was replaced by Pronova MVG for the NPCC AHFBR experiment, to be consistent with previously published NPCC protocols.

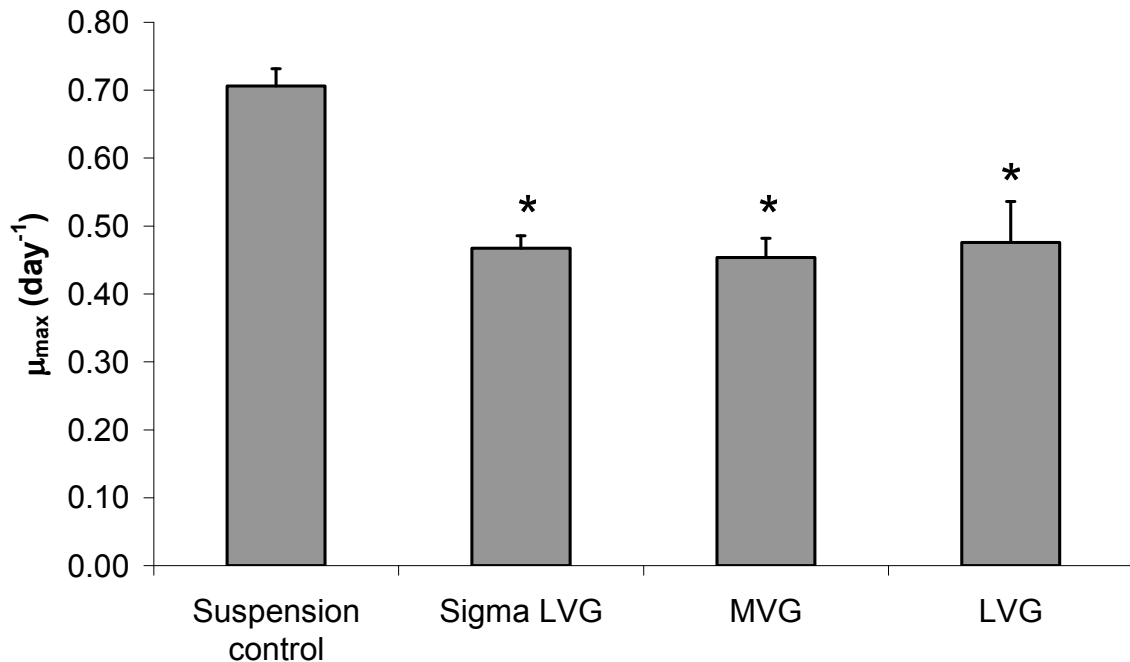


Figure 2.3. Reduced growth rate of CHO cells due to alginate immobilization.

The maximum cell growth rate measured during 5 days of CHO cell expansion was compared between control suspension cultures and immobilized culture in alginate slabs of 1% Sigma LVG alginate or 0.75% Pronova MVG or LVG alginate. * $p < 0.05$

2.2.3 Complete gelling of alginate in the ECS

Free calcium ions bind to the negatively charged guluronic acid monomers in alginate chains. In the AHFBR, calcium ions bind first near the membranes and diffuse over

time to the alginate chains furthest from the fibers. The critical regions where alginate gelling may be incomplete in the AHFBR are the ECS manifolds and the centre of the largest spaces created by fiber sinuosity. Visual inspection of sawed cartridges confirmed complete

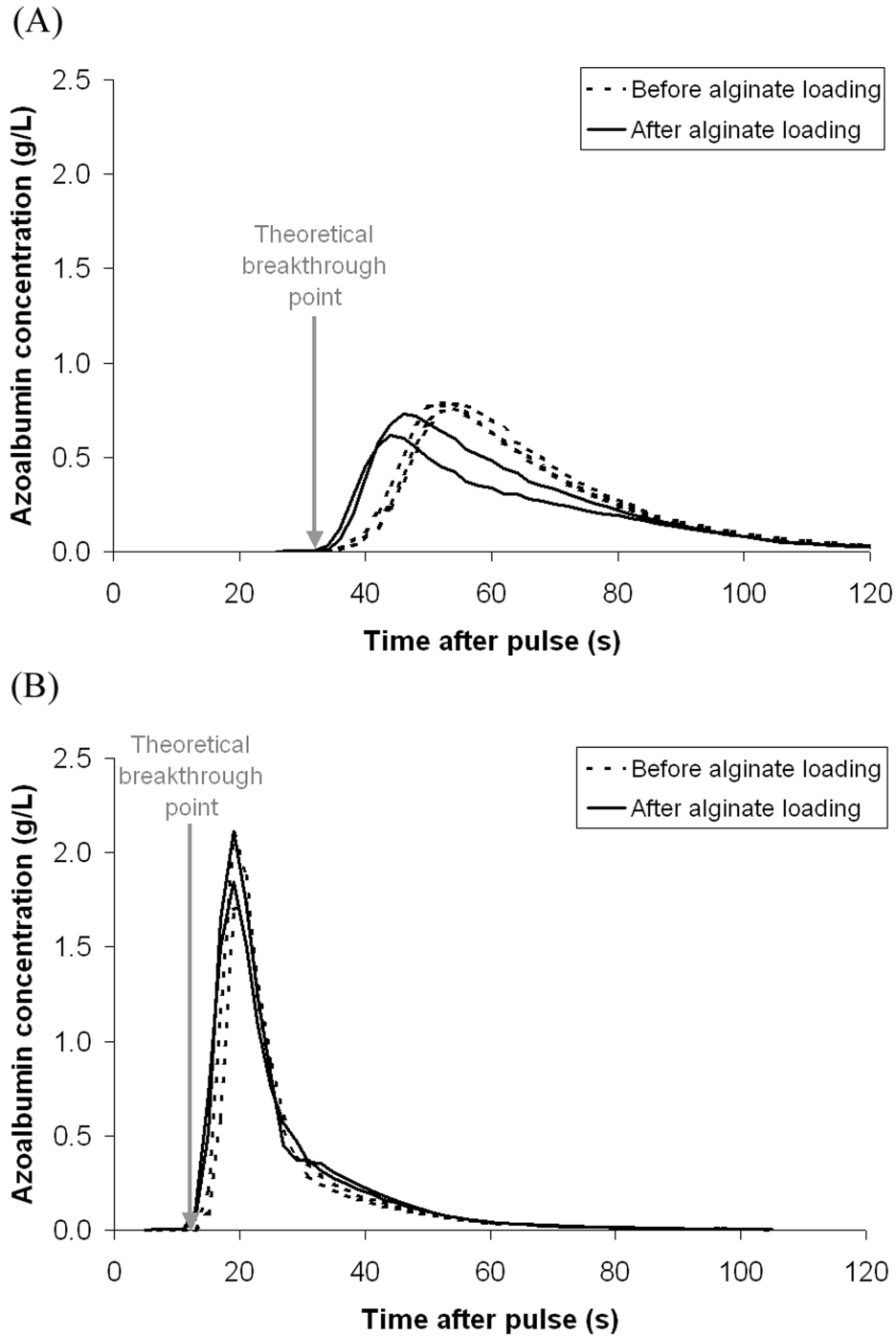


Figure 2.4. Correction of ICS obstruction by alginate by increasing the ICS flow rate during gelling.

A) ICS flow rate = 115 mL/min. B) ICS flow rate = 300 mL/min.

gelling between the fibers, around the bundle of fibers and into the ECS manifolds with either 1% or 3% alginate after a minimum of 0.5 h of gelling solution re-circulation. Thereafter, 0.5 h gelling time was used to reduce the potential adverse effects on the cells of gelling conditions in the absence of medium.

2.2.4 Higher ICS flow rates reduced fiber obstruction by alginate

A portion of the alginate was expected to cross the membranes into the ICS and gel there, causing obstructions to the ICS flow. The nominal MWCO of the fiber membrane used was 18 kDa for globular proteins, while alginate chains are not globular and had molecular weights down to 16 kDa. The ICS obstruction was assessed by measuring the azoalbumin (70 kDa MW) residence time in the ICS. The Poisson-shaped distribution of the elution curve (Figure 2.4) can be attributed to azoalbumin diffusion during the ~1 min residence time, as well as the parabolic velocity profiles associated with laminar flow. There could also be influences from the uneven distribution of azoalbumin among fibers at the ICS manifolds and some hydrophobic interaction of azoalbumin with the cellulose fibers (Clark et al. 1995). Alginate loading without ICS flow followed by a 115 mL/min ICS gelling solution flow decreased the azoalbumin ICS residence time by 6%, indicating a decrease in ICS volume (Table 2.2). At higher 300 mL/min flow rates, the azoalbumin ICS residence time was unaffected, indicating negligible obstruction of the ICS (Figure 2.4B). Sufficiently high ICS flow likely dislodged and diluted any alginate in the remaining saline rinsing solution before the gelling solution reached the ICS. However, these observations should have been confirmed using 300 mL/min during alginate gelling but 115 mL/min when measuring the azoalbumin elution profile.

Table 2.2. Effect of alginate and flow on average azoalbumin ICS residence times

ICS flow rate (mL/min)	ICS flow during loading	$t_{R,ave}$ before loading (s)	$t_{R,ave}$ after loading (s)	Decrease in $t_{R,ave}$ ^a (%)	Significant difference in $t_{R,ave}$ ^a
115	No	63.0 ± 0.8	59.3 ± 0.2	6.0 ± 0.1	Yes
300	Yes	27.4 ± 0.3	25.1 ± 0.6	8.2 ± 0.2	Yes
300	No	26.4 ± 0.4	25.8 ± 0.2	2.08 ± 0.03	No

^aCompared to the residence time of azoalbumin prior to alginate loading and gelling.

Simultaneous ECS alginate loading and ICS gelling solution flow was also tested to determine if the alginate could be gelled prior to crossing the fiber membrane into the ICS. However, this caused an 8% decrease in azoalbumin residence time. Without ICS flow, the ICS pressure would rise to roughly the average of the ECS pressure, while co-current flows open to the atmosphere at the downstream end would yield greater ECS to ICS pressure gradients, which could displace alginate into the ICS and explain the increased ICS obstruction. This pressure gradient would be aggravated by the highly viscous (>100 Pa·s for 1% Sigma LVG) and progressively gelling alginate. Precise calculation of HFBR pressure gradients is complex (Labecki et al. 1996). Nevertheless, based on a simple non-obstructed Krogh cylinder model neglecting transmembrane flux, the ECS pressure drop for 160 mL/min alginate ECS flow could be as high as 490 kPa, compared to 2 kPa for gelling solution flow in the ICS. The actual ECS pressure drop is expected to be much lower than this estimation due to the variable fiber packing that leaves greater spaces for flow. Based on these results, the ICS flow rate was set to 300 mL/min for immobilized mammalian cell culture, with no ICS flow during alginate loading.

2.2.5 Five degelling passes yielded >80% cell recovery from the AHFBR

Retrieval of cells from the alginate gel dispersed between the $\sim 10\,000$ fibers in each bioreactor is essential for cell production applications. Cells were loaded and recovered within 4 h to measure the yield of a known number of cells from an AHFBR. After 1 h of re-circulating sodium citrate through the ICS, visible amounts of ungelled alginate were left in the ECS. The initial degelled alginate fraction was then pumped out of the ECS. This first degelling pass recovered $37.5 \pm 0.2\%$ of the total number of viable cells seeded and alginate-immobilized in the AHFBR. The cell concentration (cells/mL), however, was only $39 \pm 1\%$ of the concentration seeded in the bioreactor after the first degelling pass. This indicated that the cells were not evenly distributed in the AHFBR, maybe locally concentrated in regions between the capillaries that were more difficult to degel. This was consistent with the cell sieving effect observed during alginate and cell loading (see Section 2.1.6).

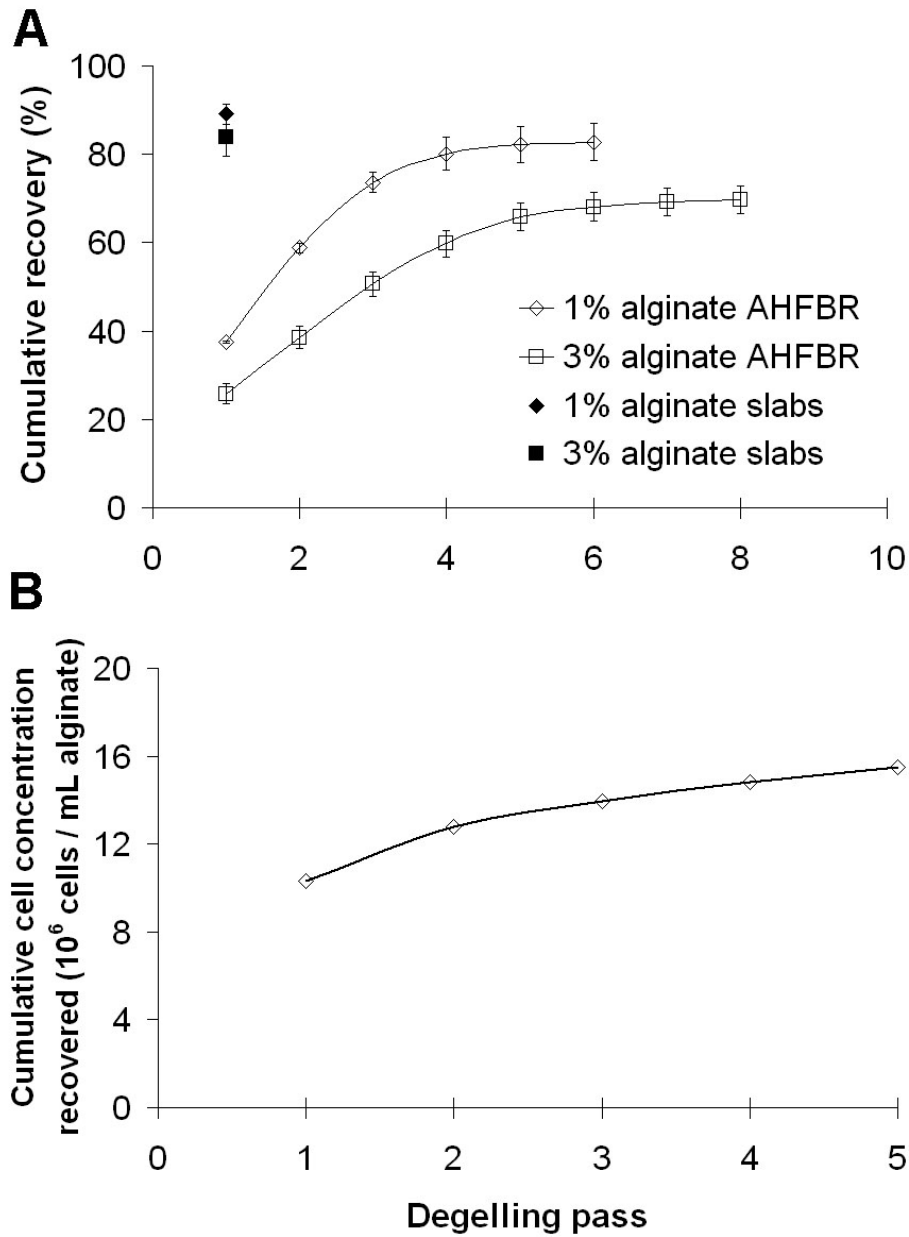


Figure 2.5. Cumulative viable CHO cell recovery from the AHFBR after each degelling pass.

Pass 1 is obtained after ICS circulation of sodium citrate; subsequent passes consist of filling, rotating and removing sodium citrate from the ECS. A) Cell seeding and degelling within 4 h. N = 3 for the 1% AHFBR and slabs; N = 1 for the 3% AHFBR and slabs. Error bars represent the SEM of 3 experiments except for the 3% AHFBR data where the error represents the standard deviation of analytical replicates. B) Cell concentration retrieved at the end of the CHO growth experiment.

The space liberated by the harvested cells and alginate was then partly filled with sodium citrate and the AHFBR cartridge was manually rotated to increase contact between

the chelating agent and the gelled alginate. An air space (~ 30 mL) was maintained in the ECS to improve mixing and visualization of the remaining gelled regions. Repeating this procedure up to 5 times (6 total degelling passes) allowed retrieval of $83 \pm 4\%$ of the cells seeded in 1% alginate and 70 ± 3 (standard deviation, SD)% of the cells seeded in 3% alginate (Figure 2.5). The recovery rates for the 1% AHFBR were not significantly different from the alginate slab controls and were consistent with expectations based on the effects of the gelling and degelling solutions on cell viability (Figure 2.2). Recovery profiles in the AHFBR reached a plateau (the increase in the cell yield from one further degelling pass ceased to be significant) after 4 degelling passes for 1% alginate and 5 degelling passes for 3% alginate. Compared to the 1% alginate HFBR and slabs and to the 3% alginate slabs, lower cell retrieval from the 3% AHFBR could be due to a greater resistance to flow by the higher viscosity 3% degelled alginate solution and/or due to insufficient chelation of the higher calcium concentration in the gel. For the 3% AHFBR, large gelled regions were visible after 8 degelling passes, giving more weight to the latter explanation. In the following growth experiments, 1% alginate and 5 degelling passes were selected to maximize cell recovery.

2.2.6 AHFBR immobilized culture of CHO cells

Immobilized CHO cells were grown in 2 separate AHFBR cultures. Metabolite profiles from the first experiment indicated that the cells underwent a 3~4 day lag phase. The experiment was ended after 5 days, yielding a 2-fold increase in cell number (data not shown). For the next experiment, the gelling solution and medium were warmed to 37°C prior to being re-circulated through the ICS. In this case, suspension controls experienced an 8 ± 4 h lag phase in contrast to undetectable lag phases in the alginate slabs (Figure 2.6A) and in the AHFBR, based on metabolic profiles (Figure 2.6C-D). In the alginate cultures, despite gas exchange, the pH decreased to ~6.8 (Figure 2.6B) due to lactate levels of ~20 mM. A complete medium exchange was therefore performed on days 5.8 and 7.7 for both the AHFBR and the slabs. The intracellular pH of CHO cells should not be affected at pH 6.8 (Wu et al. 1993) but their growth rate may have been reduced during the last day of culture at pH <7.0 (Yoon et al. 2005).

CHO cells in alginate slabs grew exponentially at least until day 7.8, just before harvest on day 8.3 (Figure 2.6A). The growth rate in the AHFBR estimated from the final cell number measured after 5 degelling passes was actually higher, but fell within the 95% confidence range for the slabs (Table 2.3). Similarly, the metabolite profiles in the AHFBR closely matched those in the slabs (Figure 2.6C-D). The yield of CHO cells per mol of glucose (Table 2.3), glutamine, lactate or glutamate (data not shown) of the AHFBR were within the 95% confidence interval of the yields in the alginate slabs. These results indicate that there were no substantially different growth limitations in the AHFBR compared to slab controls.

Table 2.3. AHFBR CHO growth parameters summary

System	μ_{\max} (d ⁻¹)	Doubling time (h)	Cell yield by glucose consumed (cell / μ mol)	8-day expansion	\bar{D} day 8 ^a aggregates (μ m)	D_{cell} day 8 ^a \pm S. D. (μ m)
AHFBR	0.40	1.8	0.036	24.6	142 \pm 101 ^b	11.7 \pm 0.8
Slabs	0.33 \pm 0.05	2.1 \pm 0.3	0.03 \pm 0.01	16.2 \pm 0.3	166 \pm 34	N/A ^c
Suspension	0.73 \pm 0.02	0.95 \pm 0.03	0.091 \pm 0.005	N/A	56 \pm 1 ^b	19.0 \pm 0.3

^aFor the suspension cells, the maintenance culture kept at constant cell density for 8 days from which the slabs and AHFBR had been seeded was used as a reference.

^bVolume-weighted standard deviation of one experiment.

^cAlthough the cell diameter was not measured for the cells harvested from the alginate slabs, a separate experiment where CHO cells were cultured for 4.5 days showed that the 13.9 \pm 0.5 (SD) μ m cell diameter in alginate slabs was significantly lower than the 17.4 \pm 0.3 (SD) μ m cell diameter of suspension controls. Floating cells that had exited the slab during the culture were also larger with a diameter of 15.6 \pm 0.6 (SD) μ m.

Compared to the suspension cultures, however, the apparent maximum specific growth rate was significantly decreased by 40~50% in both the alginate slabs and in the AHFBR (Table 2.3). The growth also appeared to be less efficient, as shown by the 30~40% decrease in cell yield per glucose consumed (Table 2.3), glutamine consumed, lactate or glutamate produced (data not show). Such changes have been reported for bacterial (Zhang et al. 1989), plant (Bodeutsch et al. 2001) and mammalian cells (Stabler et al. 2001), though part (~17% based on Figure 2.5A) of the decrease in the cell yield could be explained by the incomplete recovery of immobilized cells. Also of note, the cells were smaller in alginate

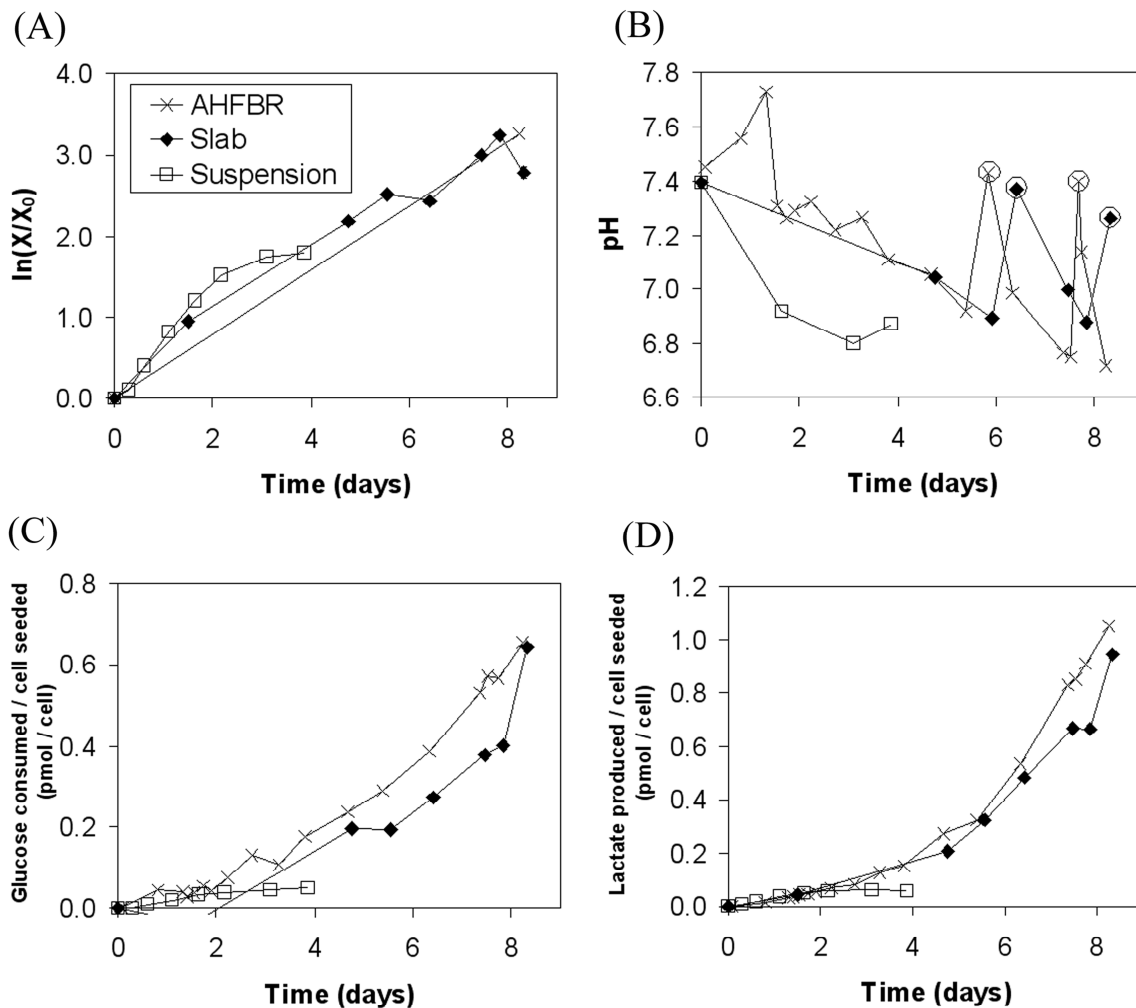


Figure 2.6. CHO cell concentration, pH and metabolite profiles in the AHFBR compared to slab and suspension cultures.

The representative data of one of three suspension cultures is plotted. A) Cell concentrations measured after degelling the AHFBR, separate alginate slabs (3 slabs were degelled at day 8.3) or from aliquots taken from the suspension culture. B) pH profiles obtained by CO₂ buffering and medium exchange (circled points represent data after medium exchange). C, D) Total amount of glucose consumed (C) or lactate (D) produced per cell seeded, based on a mass balance. Note that the initial total culture volume/cell seeded was 2.1 mL/10⁵ cells for the AHFBR, 1.6 mL/10⁵ cells for the alginate slabs 0.25 mL/10⁵ cells for suspension cultures.

than suspension (Table 2.3). It is unlikely that reduced cell volumes resulted from the colloid osmotic pressure of alginate (Woods et al. 1999) since cell volume would be expected to return to normal 30-40 s after liberation from alginate and cell volumes were only measured after washing with medium. A more plausible hypothesis is that specific maintenance

requirements are higher in alginate where cells must counter pressure from the matrix to expand. This hypothesis agrees with the negative correlation that has been found between alginate network strength as measured by the relative number of calcium cross-links and the growth rate of immobilized β TC3 cells (Simpson et al. 2004). The impact of alginate immobilization on cell metabolism, particularly pertaining to islet function, should be studied in more detail.

After 5 degelling passes, the cell concentration recovered at the end of the second AHFBR culture was $1.5 \pm 0.1 \times 10^7$ cells/mL alginate, corresponding to a 25 ± 2 fold increase in cell number. The actual production is likely even higher since the total cell recovery is expected to be $\sim 83\%$ (Figure 2.5A) and since a plateau in the number of cells recovered was not completely reached by the 5th degelling pass (Figure 2.5B). Faster growth may occur locally near the fibers in regions from which alginate was incompletely retrieved. In the alginate slabs, the final expansion was 16-fold but actually higher one day prior to the end of the culture, at 22-fold. Thus the cell expansion in the AHFBR process was comparable or superior to the slab system.

2.2.7 AHFBR capacity to produce islet-sized CHO cell aggregates

To determine if the AHFBR system could produce islet-sized cell aggregates, the AHFBR run was continued until the slab control aggregates (166 ± 34 μm diameter) reached approximately the size of an islet equivalent (150 μm diameter). At that time, the volume-weighted diameter of cell aggregates in the suspension controls was 56 ± 1 (SEM) μm (Table 2.3), or on average ~ 26 aggregated CHO cells based on the measured CHO cell volume and neglecting interstitial space. The volume-weighted diameter of aggregates recovered from the AHFBR was 142 ± 101 (SD) μm , corresponding to a 15-fold greater volume per aggregate compared to the suspension cell controls. The mean cell diameter decreased from 19.0 ± 0.3 (SD) μm to 11.7 ± 0.8 (SD) μm in the AHFBR. The AHFBR mean increase in the cell number per aggregate was calculated to be 70-fold. That this is greater than the aforementioned 25-fold recovery of cells compared to the inoculum indicates that only a fraction of the cells seeded proliferated to form aggregates. The spherical aggregates (circularity of 0.75 ± 0.17)

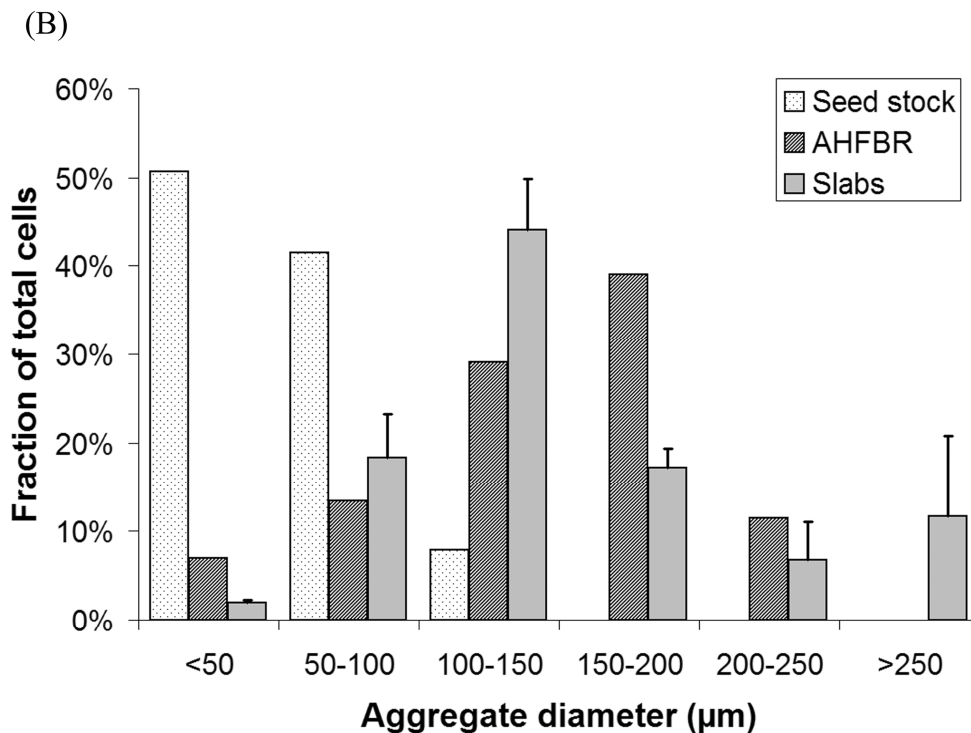


Figure 2.7. Aggregate formation by CHO cells in the AHFBR and the control slabs.

A) Representative bright field microphotographs of the suspension cells used to seed the AHFBR and slabs, of the aggregates after 8 days of culture observed in slabs or obtained after degelling the AHFBR. B) Aggregate size distributions obtained based on such microphotographs. The 200 mm scale bar applies to all three images.

were of strikingly uniform size (Figure 2.7A), with aggregates of 100 – 200 μm diameter accounting for 68% of the cells (Figure 2.7B). Aggregates in alginate displayed smooth edges, but adopted more irregular shapes after degelling (Figure 2.7A), suggesting that aggregates were under opposing pressure from the surrounding alginate matrix, perhaps in

a manner similar to *in vivo* pancreatic islets. The total number of cells produced in the AHFBR would correspond to 1.1×10^6 islet equivalents.

2.2.8 AHFBR immobilized culture of NPCCs

The potential of the AHFBR for primary cell culture was then assessed in a proof-of-concept experiment by evaluating the survival and maturation of NPCCs in 0.75% MVG alginate. The NPCCs were first cultured in suspension for 8 days to eliminate debris and factors from the mainly exocrine cells that undergo apoptosis during this phase of culture (Humphrey et al. 2001). The tissue was then transferred to alginate, loaded in the AHFBR and cultured for 10 more days. Due to the limited supply of these neonatal cells, the seeding density of NPCCs in the AHFBR was ~10-fold lower than the standard protocol but an extra control was performed in a small-scale slab at 5 times higher seeding density to test for any

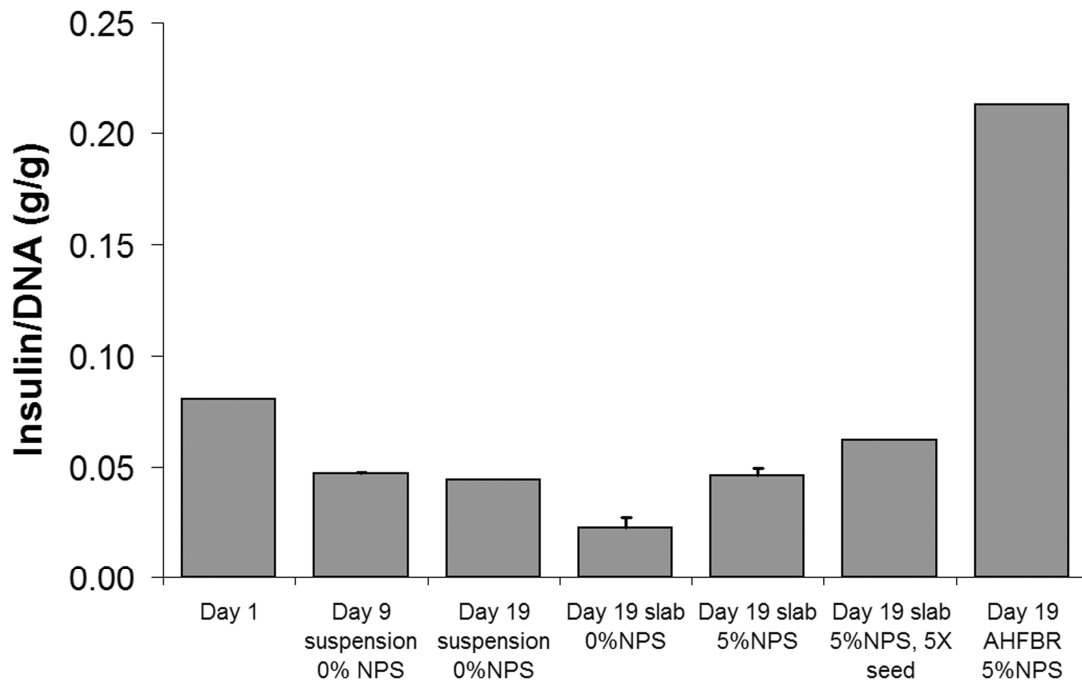


Figure 2.8. Insulin content of NPCCs during suspension or alginate-immobilized culture.

NPCCs were maintained in suspension 9 days to eliminate debris from apoptotic cells, followed by 10 days of continued suspension or alginate culture. Error bars represent the SEM of 2 separate cultures (from the same pooled 1.5 pancreata).

cell concentration effects. The insulin/DNA ratio of this control fell within the 95% confidence interval of the insulin/DNA values of alginate slabs with 10-fold reduced seeding density (Figure 2.8). During this experiment, the insulin content of cells in the small-scale alginate slabs failed to increase, with or without serum, contrary to the ~2.5 fold increase expected from the literature for alginate culture in the presence of autologous serum (Tatarkiewicz et al. 2001). Pancreas-to-pancreas variability or shipment effects can explain the poor performance this batch of NPCCs. Deleterious effects related to the shear stress experienced while pumping the cells and alginate are ruled out due to the equally poor performance of the cells in control suspensions and in the alginate slab with higher seeding density that did not undergo pumping. If unlimited amounts of tissue were available, an ideal control would have been suspension NPCC culture without alginate in a parallel AHFBR cartridge, which may better mimic the conditions cells experience in the AHFBR apart from matrix-induced signals. Also, the alginate concentration could be varied to determine the effect on gel strength on insulin expression by NPCCs. Nonetheless, most important for this study, the AHFBR had a 4.5-fold increased insulin content compared to the day 9 AHFBR inoculum cells (Figure 2.8). The final insulin/DNA ratio of 0.21 g/g achieved was of the same order of magnitude as the ~0.4 g/g obtained by Tatarkiewicz *et al.* (2001). This increase was likely due to an increase in insulin protein expression per cell rather than a significant increase in the fraction of insulin+ cells (Figure B1 in Appendix B). These observations suggest that alginate promotes progenitor differentiation rather than expansion, consistent with the reduction in growth rate observed for cell lines (see Figure 2.3, Figure 3.9, and Stabler et al., 2001) in alginate. A two-step protocol consisting of (1) progenitor expansion followed by (2) progenitor differentiation in alginate can be envisioned for the production of insulin+ cells.

2.2.9 Potential applications

The AHFBR is a novel process for practical immobilized mammalian cell culture with cell recovery, either at the one patient-scale (one AHFBR culture to treat one patient) or at the donor-scale (one AHFBR culture of the cells from one donor to generate cells to treat several patients). Potential applications of this system include the *in vitro* culture of islet-like

clusters for use in islet transplantation starting from xenografts (MacKenzie et al. 2003), embryonic stem cells or allogeneic grafts generated from adult stem or progenitor cells (Street et al. 2004b). In the latter case, it can be expected that the cells from each donated pancreas would be processed separately and expanded then differentiated or re-differentiated into islet-like clusters. This donor-scale would correspond to an estimated target of 100×10^6 islet-like clusters generated per pancreas. The AHFBR process developed in this study was able to generate $>10^6$ islet-equivalent sized CHO cell aggregates (with higher nutrient consumption rates than those of islets). One 120 mL AHFBR can therefore accommodate at least enough islets to treat one diabetic patient (Ryan et al. 2005). To achieve the anticipated cell numbers required for 100 patients, hopefully starting from a single donated organ, the cell concentration could be increased. Even with CHO cells, there was no evidence of increased nutrient limitation with time, suggesting that the highest cell density capacity of the AHFBR was not reached, especially if β -cells with lower nutrient consumption rates were cultured in the unit. The cell density would nonetheless be limited by the need to maintain and harvest separate islet-sized cell aggregates. Alternatively, rather than increasing the cell density, the hollow fiber density could be decreased. This could have the benefit of facilitating alginate and cell recovery, for example by facilitating mixing and flow of the citrate solution in the ECS. Also, the cartridge size could be increased by at least 1 or 2 orders of magnitude, such as has been done for other applications (Brindle and Stephenson 1996).

To further adapt the AHFBR process for cell production, the ECS manifolds could be reduced since ECS flow is not required during culture. Given that this was the last volume to gel, this could decrease the required gelling time and should ensure a more uniform nutrient distribution in the AHFBR. Non-adherent cells tend to settle in non-alginate containing HFBRs, reducing viable cell numbers and productivity. Alginate immobilization should insure a more uniform cell distribution, although alginate-hindered protein mass transport could become an issue (Koska et al. 1997).

Stirred suspension is usually the most readily scalable configuration for bioreactors and these systems are increasingly being developed for cellular therapy applications (King

and Miller 2007). This has included production of insulin+ cells from NPCC aggregates cultured in suspension (Chawla et al. 2006). Many other bioreactor configurations are also being considered for cellular therapy products (Godara et al. 2008). Bioreactors allowing gel-immobilized culture of pancreatic progenitors will likely be required since many small-scale differentiation protocols for the generation of islet-like cell clusters require immobilized culture in matrices (Beattie et al. 2002; Bonner-Weir et al. 2000; Gao et al. 2003).

Small (<1 mm) alginate beads are commonly generated by a vibrating nozzle, coaxial gas flow or cutting of a laminar jet by rotating blades (JetCutter) (Koch et al. 2003). The JetCutter (Schwinger et al. 2002), one of the highest throughput laboratory-scale mammalian cell encapsulators described in the literature, would take >20 h to produce 10 L of alginate beads from a single nozzle. Lengthy and variable residence times of cells in the non-ideal conditions of the gelling bath could be detrimental to cell health and lead to bead-to-bead variability. Processing the cells in smaller batches instead could introduce batch-to-batch variability. The 120 mL AHFBR process described here requires ~40 min cell processing time. Unlike the JetCutter, however, the 100-fold anticipated scale-up of the AHFBR would not require 100 additional processing units and/or prolonged processing times. For the case of primary islet encapsulation, these would likely be damaged by the nozzle tip shear at the maximum 330 mL/h JetCutter alginate flow rates. Islets have been reported to be sensitive to energy dissipation rates below 10^3 W/m³ for water – which is much less viscous than alginate – passing through a 500 µm tube (Mollet et al. 2004) at 330 mL/min. Mesenchymal stem cell biosynthetic activity and differentiation are particularly sensitive to shear stress and strain and hollow fiber systems were hence suggested for the production of mesenchymal-derived cell products (Godara et al. 2008). Another advantage of the AHFBR is that cells cannot migrate outside of the alginate, contrary to beads, allowing immobilized culture to higher cell densities. Moreover, gel stability in long-term cultures could be increased in AHFBRs by eliminating the abrasive shear present in stirred systems (Vogelsang et al. 2000). Following *in vitro* culture and differentiation, the alginate could be degelled and the alginate and cell mixture could be sent to a bead generator or injected into

an immunoprotective device. The alginate could also be removed by chelation, dilution and centrifugation prior to transplantation.

Alginate was chosen as the immobilization matrix in this study due to its reversible gelling at physiological pH, temperature and osmolarity. In addition, alginate encapsulation, with or without a poly-cationic membrane, has been extensively studied as a means to protect islets from immune rejection in xenogeneic (Dufrane et al. 2006b; Elliott et al. 2005; Lanza et al. 1999b; Schneider et al. 2005) or allogeneic (Duvivier-Kali et al. 2001; Lim and Sun 1980; Soon-Shiong et al. 1993) islet transplantations, including ongoing human clinical trials (Calafiore et al. 2006b). However, alternative reversible gels could be used in an AHFBR-type process. The ion concentration, pH and reducing potential of the ICS solution could be varied to manipulate the gelled state of protein block co-polymers (Xu et al. 2005) or disulfide hydrogels (Hisano et al. 1998). Temperature control could allow immobilization and recovery of cells in thermo-reversible synthetic (Jeong et al. 2002) or karrageenan gels. Advances in alginate matrix engineering could improve the characteristics of the gel, including mechanical (Boonthekul et al. 2005; Donati et al. 2005), cell signalling (Perets et al. 2003) or adhesion (Rowley et al. 1999) properties, and thereby lead to other applications of gel-filled HFBRs.

2.3 CONCLUSIONS

This paper describes a novel HFBR bioprocess for the alginate-immobilized production of mammalian cells that require a three-dimensional support as well as cell recovery. Key processing issues were investigated, including (1) ICS flow obstruction due to alginate gelling in the ICS, (2) the degree of alginate gelling, and (3) recovery of cells from the ECS. ICS fiber obstruction by alginate was eliminated by using higher ICS flow rates (300 mL/min) during alginate gelling while keeping the ECS ports closed. Alginate gelling was complete within 30 min of gelling solution circulation through the ICS. CHO cell recoveries were improved from 37% to 83% by adding degelling solution directly to the ECS after an initial ICS circulation. When CHO cells were grown in the bioreactor and in parallel small-scale alginate slabs, cell growth and metabolite profiles were similar. At the end of 8

days of culture and 25-fold cell expansion from single cells, uniformly sized aggregates of $142 \pm 101 \mu\text{m}$ (SD) average diameter were obtained. Therefore, one AHFBR could be used on a per-patient basis for the potential treatment of diabetes using islet-like clusters produced *in vitro*. The HFBR volume and the maximum cell density could be scaled-up for use on a per-donor basis, generating islet-like clusters for ~100 patients. To test whether this system is appropriate for primary tissue culture, NPCCs were cultured in alginate in the presence of autologous serum, a combination reported to lead to NPCC maturation. Indeed, the NPCC insulin/DNA ratio rose by 4.5-fold after 10 days of culture in the AHFBR. The AHFBR constitutes an alternative to bead generation that could be adapted to a wide range of *ex vivo* stem cell differentiation protocols.

3 PANCREATIC CELL IMMOBILIZATION IN ALGINATE BEADS GENERATED BY EMULSION AND INTERNAL GELATION²

The AHFBR may allow the generation of up to 100~200L alginate gel/h, but an even more scalable method that may also have potential for transplantation applications is bead generation by emulsion and internal gelation. However, this process had not yet been reported for use with mammalian cells and it was expected that some cell losses would occur during the emulsion and/or the acidification steps required for the process. After optimization, the emulsion process yielded $87 \pm 4\%$ mouse insulinoma 6 (MIN6) cell survival, similar to the $84 \pm 2\%$ measured for immobilization in 2% alginate beads generated by a conventional vibrating nozzle extrusion device. During 16 days of *in vitro* culture, the MIN6 cells expanded at the same rate in both bead types to form pseudo-islets with increased glucose stimulation index compared to cells in suspension. The emulsion process was also suitable for primary pancreatic exocrine cell immobilization, leading to a 67 ± 32 fold increased insulin expression after 10 days of immobilized culture.

3.1 INTRODUCTION

For the last three decades, microencapsulation has been investigated as a means to protect transplanted cells from the host immune system without the use of anti-rejection drugs by providing a size exclusion barrier between the graft and host immune cells and some of their secreted proteins (Lim and Sun 1980). More recently, gel-immobilized cell culture in microbeads has been shown to provide additional control over stem cell fate and survival. For instance, alginate-immobilized culture enhances the differentiation of embryonic stem (ES) cells into definitive endoderm (Chayosumrit et al. 2010) and

² An abbreviated version of this chapter has been published: Pancreatic Cell Immobilization in Alginate Beads Produced by Emulsion and Internal Gelation, Hoesli CA, Raghuram K, Kiang RLJ, Mocinecová D, Xiaoke H, Johnson JD, Lacík I, Kieffer TJ, Piret JM, Biotechnology & Bioengineering published online ahead of print on November 17, Copyright © 2010 by Wiley-Blackwell. Link to the article: <http://onlinelibrary.wiley.com/doi/10.1002/bit.22959/abstract>.

downstream lineages such as hepatocytes (Maguire et al. 2006) and insulin-expressing cells (Wang et al. 2009). The production of cellular therapeutics could, therefore, make use of alginate beads both during the *in vitro* generation of desired cell types and/or as part of the final product to protect the graft after transplantation.

Islet transplantation is being studied as a treatment for type 1 diabetes in clinical trials (Hirshberg 2007; Kaddis et al.), including trials involving encapsulated islets without immune suppression (Living Cell Technologies 2010; Tuch et al. 2009). However, widespread access to this treatment would require ~100-fold increase in tissue availability (Ricordi 2003). To satisfy this demand, glucose-responsive insulin-producing cells could be procured from differentiated ES cells (D'Amour et al. 2006), differentiated adult pancreatic progenitor cells (Xu et al. 2008), expanded β -cells (Efrat 2008) or xenogeneic tissue (Living Cell Technologies 2010; Tatarkiewicz et al. 2001). All of these options could benefit from larger-scale cell immobilization in a reversible hydrogel matrix such as alginate. Commonly used alginate bead generators rely on droplet formation by extrusion of an alginate and cell mixture through a nozzle and external gelation upon contact of the falling droplet with a calcium or barium solution, herein referred to as “extrusion” processes. However, the throughput of these devices is limited by the requirement for drop formation at the nozzle tip and by the shear stress experienced by the cells in the nozzle. Increasing the number of nozzles increases the throughput of these devices but complicates process control in particular for solutions of viscosity higher than ~0.2 Pa·s (Brandenberger and Widmer 1998; DeVos et al. 1997).

One attractive alternative, due to its scalability and the low shear experienced by the encapsulated material, is the production of alginate beads in a stirred system by emulsion and internal gelation (Poncelet et al. 1992), herein referred to as the “emulsion” process. The immobilization processing steps consist of (1) mixing with oil to obtain an emulsified aqueous dispersed phase containing the cells, the alginate and a calcium salt with low solubility at the initial pH (e.g. CaCO_3), (2) acidification by an oil-soluble acid that transits into the aqueous phase, leading to calcium release and alginate cross-linking to form gelled beads and (3) phase separation. To date, this emulsion process has been used to encapsulate

biological molecules, bacteria, yeast and plant cells (Reis et al. 2006), but to our knowledge had not yet been used to immobilize mammalian cells.

Chapter 3 describes the adaptation of this highly scalable emulsion process to mammalian cell immobilization and culture using the MIN6 cell line and primary pancreatic cells as model systems. First, time course measurements of cell viability during the process and omitting various processing steps were used to determine the main causes of cell losses. Then, the duration of the processing steps and the pH shift during internal gelation were modified to minimize these losses. MIN6 cell expansion and function in beads generated by this optimized process were compared to standard beads generated by vibrating nozzle extrusion. Lastly, primary human islet-depleted pancreatic cells were immobilized and cultured in the emulsion-generated beads to assess the effects of the process and immobilized cell culture on cell survival and insulin expression.

3.2 MATERIALS AND METHODS

3.2.1 Alginate and cells

MIN6 cells, an immortalized pancreatic β -cell line, were a kind gift of Dr. Jun-Ichi Miyazaki (University of Osaka, Osaka, Japan) (Miyazaki et al. 1990). Adherent and alginate-immobilized cells were cultured in DMEM medium supplemented with 10% fetal bovine serum (FBS), 6 mM glutamine, 100 units/mL penicillin and 100 μ g/mL streptomycin (all from Invitrogen, Carlsbad, CA), referred to as “DMEM + 10% FBS medium”. Unless otherwise mentioned, this medium was also used in all other instances where medium was required during processing or for immobilized MIN6 cell culture. Adherent cultures were maintained at 37°C and 5% in a humidified incubator in tissue culture treated T-flasks (Sarstedt) seeded at 4×10^4 cells/cm². Unless otherwise stated, the alginate used was Sigma A0682 lots 123K01181 and 076K01431, with 250 Pa·s viscosity for a 2% solution at 25°C, molecular weight between 12 and 80 kDa and 39%:61% mannuronic:guluronic acid content (Sigma technical support). A HEPES buffered saline solution consisting of 10 mM HEPES (Sigma) and 170 mM NaCl (Thermo Fisher Scientific) at pH 7.4 was initially used to dissolve

the alginate and suspend the CaCO_3 , until this was replaced by a MOPS buffered saline solution consisting of 60 mM MOPS (Sigma) and 127 mM NaCl at pH 7.6.

3.2.2 Emulsion process

The emulsion process was adapted from the Poncelet *et al.* method (1992) by changing the buffer system and processing times, as well as by adding repeated washes and centrifugations to accelerate and improve phase separation (Figure 3.1). The “HEPES emulsion” refers to the initial non-optimized process using 10 mM HEPES buffering with 12 min emulsification and 8 min acidification, while “MOPS emulsion” refers to the optimized process using 60 mM MOPS buffered saline solution, 3 min emulsification and 1 min acidification. MIN6 cells from trypsinized adherent cultures were washed in medium and re-suspended in medium as a 10.5-fold concentrated cell stock. One volume of this stock was added to 9 volumes alginate and 0.5 volumes of 500 mM CaCO_3 (Mallinckrodt Baker, Phillipsburg, NJ) to obtain 1.5% to 2% final alginate concentration and 1×10^6 to 2.5×10^6 cells per mL alginate depending on the experiment. When the process was performed in the absence of cells, the same volume of medium replaced the cell stock to achieve the same

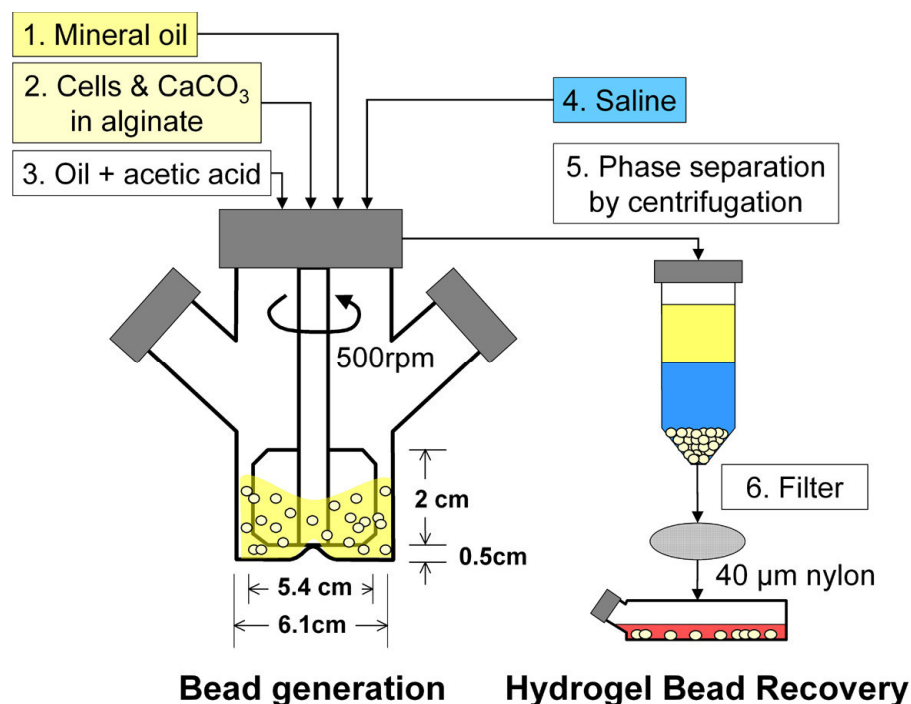


Figure 3.1. Schematic of the emulsion process adapted to mammalian cell immobilization.

process pH. The presence of medium reduced the amount of oil at the bead surface as well as bead agglutination, presumably because some medium components such as globular proteins could act as surfactants (Denkov 2006).

First, 20 mL of light mineral oil (O121-4, NF/FCC grade, Thermo Fisher Scientific) was agitated at 500 rpm (unless otherwise specified) for 2 min in a 100 mL microcarrier spinner flask (Bellco, NJ, impeller configuration shown in Figure 3.1) to establish a stable fluid flow (Figure 3.1, Step 1). The 10.5 mL of the alginate, cell and CaCO₃ mixture was then added and emulsified for 12 min (non-optimized) or 3 min (optimized) (Step 2). Internal Ca²⁺ release and bead gelling was triggered by adding 40 µL glacial acetic acid dissolved in 10 mL mineral oil (Step 3). After 8 min (non-optimized) or 1 min acidification (optimized), a higher pH was re-established by adding 40 mL of HEPES buffered saline solution mixed with 10% medium (Step 4), which led to phase inversion. The agitation was ceased 1 min later and the mixture was transferred to 50 mL centrifuge tubes, along with an additional 20 mL medium used to rinse the flask. The tubes were centrifuged for 3 min at 630 x g to accelerate bead settling and phase separation (Step 5). The oil and excess HEPES-buffered saline solution were removed by aspiration, followed by two washes with 30 mL medium, centrifugation and aspiration. The beads were filtered (Step 6) on a 40 µm nylon cell strainer (BD Biosciences, San Jose, CA) and transferred into the desired solution with a spatula. Bead volumes were measured by volume displacement, which included any liquid entrained in the bead interstitial space. Typically, beads were filtered on a 40 µm nylon cell strainer, the liquid remaining in the strainer was removed by suction applied on a Pasteur pipette, then ~1 mL were transferred into ~4 mL HEPES-buffered saline solution with the spatula. The total volume was then measured with a 5 mL pipette. The amounts of CaCO₃ and acetic acid required for the process were based on the original process by Poncelet et al. (Poncelet et al. 1992) and were close to calculated amounts allowing complete guluronic acid cross-linking of 1.5% alginate in the absence of buffer (refer to Section A1 in Appendix A).

3.2.3 Extrusion process using a vibrating nozzle bead generator

For the generation of alginate beads by extrusion and external gelation, the alginate and cell mixture was prepared as above using the same alginate stock solution dissolved in MOPS

buffered saline solution. Instead of the CaCO₃ suspension, the same volume of MOPS buffered saline solution was added to the mixture. Beads were generated by extrusion at 360 mL/h through a 250 µm diameter nozzle using an Inotech encapsulator (IE-50 R, Reppischhof, Switzerland) following the manufacturer's instructions. The beads were agitated 10 min in gelling solution (75 mM CaCl₂, 10 mM HEPES, 75 mM NaCl, pH 7.4), followed by 5 min in HEPES buffered saline solution. The beads were then transferred to a biological safety cabinet and washed twice with medium.

3.2.4 Alginate bead size distribution

Alginate beads (1 mL) were transferred into 4 mL HEPES-buffered saline solution and stained by adding 100 µL of 5 g/L toluidine blue-O solution (Sigma), which binds the COO-groups of alginate. The beads were incubated in this solution for 1 h at room temperature at 50 rpm on a rotary shaker. The mixture was transferred into a 10 cm Petri dish containing 5 mL HEPES-buffered saline solution and a picture was taken with a Powershot A630 camera (Canon). Image processing was performed using the CellProfiler (Carpenter et al. 2006) freeware (cellprofiler.org). The volume moment mean diameter (D_{43}) of >1000 beads and the corresponding volume weighted standard deviation (s_{D43}) were calculated as described (but for cell aggregates) in Section 2.1.10 (page 43) using Equations 2.1 and 2.2. The circularity was also calculated as previously described by Equation 2.3. The surface area moment mean diameter (D_{32}) and the surface area weighed standard deviation (s_{D32}) were calculated from Equations 3.1 and 3.2. The individual diameters D_i were based on the diameter of a circle occupying the same area as the bead in the 2D photograph.

$$D_{32} = \frac{\sum_{i=1}^N D_i^3}{\sum_{i=1}^N D_i^2} \quad (\text{Equation 3.1})$$

$$s_{D32} = \sqrt{\frac{\sum_{i=1}^N D_i^2 (D_i - \bar{D})}{(N-1) \sum_{i=1}^N D_i^2}} \quad (\text{Equation 3.2})$$

There were no significant differences between the average bead diameters and standard deviations obtained by this method (D_{32} of $626 \pm 20 \mu\text{m}$) and the standard method of measuring ~30 bead diameters on photomicrographs (D_{32} of $668 \pm 11 \mu\text{m}$) using extrusion-generated beads as a test. The bead identification by the toluidine blue method is illustrated in Figure B2 (Appendix B).

3.2.5 Bead liquefaction and cell enumeration

To retrieve cells from gelled beads, 1 volume of beads was added to 4 volumes of degelling solution (90% of 55 mM citrate, 10 mM HEPES, 90 mM NaCl, pH 7.4) mixed with 10% medium and left for 15 min on ice and a rotary shaker at 75 rpm. Single cells released from the beads were counted using trypan blue exclusion by a Cedex automated cell counter. For MIN6 cell growth curves, the packed cell volume (PCV) was used because MIN6 cell aggregates remained after liquefaction for most time points. The PCV was measured after centrifuging cells for 5 min at $250 \times g$ and then for 1 min at $2500 \times g$ in PCV tubes (Techno Plastic Product AG, Trasadingen, Switzerland). The PCV/cell ratio was constant at $7.5 \pm 0.5 \times 10^5$ total MIN6 cells/ μL PCV for trypsinized MIN6 cells at all culture times.

3.2.6 Testing the effect of alginate, oil, CaCO_3 , and acetic acid on MIN6 cell survival

To test the effect of the different processing components on MIN6 cells, the HEPES emulsion process was performed omitting various process components. Sampling was performed every 4 min and at the 13 min time point to collect 1 mL of the aqueous phase (plus 2 to 4 mL oil for some samples). The conditions tested were as follows: (1) "Process" – the complete HEPES emulsion process as described in Section 2.2, (2) "No CaCO_3 " – the process omitting CaCO_3 , (3) "No oil, no acid" – the process omitting oil and acetic acid, (4) "No acid" – the process omitting acetic acid, (5) "No alginate, no CaCO_3 , no oil, no acid" – a positive control of cell survival. For the "Process" condition, the emulsion process was carried out. However, since part of the mixture was removed during sampling, the amount of acidified oil and HEPES buffered saline solution mixed with 10% medium were scaled proportionally to the amount of alginate left in the emulsion. In the "No CaCO_3 " condition, the CaCO_3 suspension was replaced by HEPES buffered saline solution alone. In the "No

acid" condition, non-acidified mineral oil was added at the 12 min time point. In the "No oil, no acid" condition, the mixture of alginate, cells and CaCO₃ was kept at room temperature at 75 rpm on a rotary shaker. In the "No alginate, no oil, no acid" condition, the cells were kept in medium at 37°C and 5% CO₂ in an Infors (Bottmingen, Switzerland) shaking incubator. The samples were transferred directly into tubes containing 4 mL citrate solution followed by tube inversion mixing and centrifugation at 400 x g for 3 min. The oil, if present, was removed by aspiration. The aqueous volume was then measured before placing the mixtures on ice on a rotary shaker at 75 rpm for 20 min followed by CEDEX cell enumeration.

3.2.7 Measurement of the initial and final process pH

Direct measurements of the pH at the beginning of the process were taken 1 min after adding the CaCO₃ suspension to the alginate and medium (replacing the cells) mixture on a Symphony pH meter (VWR, West Chester, PA). The pH inside 1.5% alginate beads at the end of the acidification step was approximated by the pH measured in a solution at equilibrium with a concentrated alginate slab at ambient temperature and CO₂ partial pressure. The concentrated 2.5% alginate slab was prepared by mixing 5 mL of 3% alginate in process buffer (saline solution with 10 mM HEPES or various concentrations of MOPS) with 0.476 mL 500 mM CaCO₃ in the same buffer and 0.556 mL medium. This mixture was pipetted into a 6 cm Petri dish, then covered with a gelling solution consisting of 3.57 mL process buffer mixed with 0.397 mL medium and 40 µL glacial acetic acid. The slab was left to gel for 1 h at room temperature on a rotary shaker at 200 rpm. The pH of the solution remained constant for 24 h.

3.2.8 Bead mechanical properties

The HEPES emulsion, MOPS emulsion or the extrusion processes were used to generate 2% alginate beads without cells using three different alginate batches for each process. These batches were generated (1) from alginate lot 123K01181, (2) from lot 076K01431 or (3) from a 50:50 mix of both alginate lots. Although the manufacturer specifications were the same for both lots, this strategy was chosen to test lot-to-lot variation and so verify process

robustness. To render the beads generated from the three processes as comparable as possible, the volume-weighted average bead diameter D_{43} of the emulsion-generated beads was matched to the D_{43} of $714 \pm 15 \mu\text{m}$ obtained for the extrusion process by adjusting the agitation rate. For the HEPES emulsion process, an agitation rate of 522 rpm resulted in a D_{43} of $738 \pm 58 \mu\text{m}$ and for the MOPS emulsion process, an agitation rate of 522 rpm resulted in a D_{43} of $700 \pm 70 \mu\text{m}$. The bursting force and bead deformation was determined in compression mode by a Texture Analyzer TA-XT2i (Stable Micro Systems, Godalming, UK) equipped with mobile probe and software Texture Expert Exceed 2.64. The analysis was carried out on hand-picked emulsion-generated beads of approximately the same diameter as the extrusion-generated beads. Beads were placed on a glass slide in medium with 100 ppm sodium azide. One bead was carefully positioned under the mobile probe and the excess medium gently removed. The compression measurement was performed up to ~95% bead deformation at a compression speed of 0.5 mm/s on 30 beads from each batch of alginate. This speed was sufficiently high to avoid the loss of liquid during the compression.

The resistance of the beads to low but sustained hydrodynamic stress was assessed by placing 2.5 mL beads into 37.5 mL medium in 50 mL shake flasks. The flasks were kept for 21 days at 136 rpm at 37°C in a shaking incubator (Minitron Infors, Switzerland). The resistance to acute hydrodynamic stress was examined by placing 4 mL beads in 250 mL in a 250 mL microcarrier spinner flask (Bellco, NJ) agitated at 750 rpm for 24 h. The dimensions of the flask and impeller were the same as those reported by Venkat *et al.* (1996) but included an air-liquid interface. At the end of each test, the beads were recovered by 40 μm sieving. The recovery was defined as the bead volume measured at the end of the 24 h or 21 days, divided by the volume measured when the same amount of beads was placed into medium and immediately recovered. The beads were examined visually under a microscope and by toluidine blue measurement of the bead size distribution.

3.2.9 MIN6 alginate-immobilized culture and growth parameters

MIN6 cells were immobilized in 2% alginate beads according to either the MOPS emulsion or extrusion processes. The D_{43} was matched between the two bead types as described in Section 2.8. The cells were immobilized at 1×10^6 cells/mL alginate with each 1 mL alginate

transferred into 9 mL medium and placed in a 25 cm² suspension T-flask (Sarstedt). Half medium exchanges and medium sampling (before and after medium exchange) were performed at days 1, 4, 7 and then every second day. At the same time, 0.5 to 1 mL of beads were recovered and liquefied to monitor the cell concentration by PCV. Adherent controls were seeded at a density of 2 × 10⁴ cells/cm² (1 × 10⁵ cells/mL) in 6-well plates. Full medium changes were performed every second day. Each day, one well was used for medium sampling and cell enumeration after trypsinization by PCV or by trypan blue counts. The maximum specific growth rate (μ_{\max}) was calculated from the slope of $\ln(\text{PCV}(t)/\text{PCV}(0))$ versus time during exponential growth. Metabolite concentrations (glucose, lactate, glutamine, glutamate) were analyzed using a YSI 7100 MBS bioanalyzer (Yellow Springs, OH). The total amount of metabolites consumed or produced was used to calculate specific glutamine consumption (q_{glu}) or glutamate production rates (q_{glu}) over each time interval. The total cell yield per mol glutamine utilized was highly linear during exponential growth ($R^2 > 0.95$).

3.2.10 Live/dead staining of MIN6 cells in alginate beads

Alginate beads containing cells were washed twice with HEPES-buffered saline solution before adding ethidium homodimer and calcein AM (L3224 Live/Dead kit, Invitrogen, Carlsbad, CA) to obtain a final concentration of 5.33 μM each. Stacks of 26 images were acquired on an inverted Olympus IX81 microscope (Olympus, Center Valley, PA) or on a Zeiss LSM 510 Meta confocal microscope (Carl Zeiss International, Oberkochen, Germany). The images were processed using Slidebook (Olympus, Center Valley, PA) or the Zeiss LSM Image Browser 4.2.0.121 (Carl Zeiss International).

3.2.11 Perifusion of immobilized or trypsinized non-immobilized MIN6 cells

After 15 days of culture in 2% alginate beads produced by the MOPS emulsion or extrusion processes, the insulin secretion of MIN6 cells was assessed by perifusion as previously described (Johnson et al. 2009). Beads containing cells were transferred to 300 μL perifusion chambers at 2 μL PCV/chamber (corresponding to ~ 100 μL beads/chamber) containing ~100 μL medium. The perifusion system consisted of 6 parallel chambers exposed to 5% CO₂ and

37°C temperature control (Endotronics Acusyst-s Cell Culture Instrumentation). Also, cells from adherent cultures were trypsinized, washed twice in medium and the same total cell number was placed (2 μ L PCV/ chamber) in 100 μ L medium. In order to avoid clogging of the perfusion filter membrane by cells, 100 μ L of a sterile Cytodex 1 bead suspension was also added to chambers without alginate beads. The remaining space in the chambers was filled with Krebs Ringer buffer (KRB, 129 mM NaCl, 4.8 mM KCl, 1.2 mM MgSO₄, 1.2 mM KH₂PO₄, 2.5 mM CaCl₂, 5 mM NaHCO₃, 10 mM HEPES and 0.5% BSA) with 3 mM glucose (3G-KRB). The chambers were perfused at 0.35 mL/min/chamber for 1 h with 3G-KRB before starting the experiment. The perfusion assay consisted of perfusing for 25 min with 3G-KRB, 30 min with KRB with 20 mM glucose (20G-KRB), 30 min with 3G-KRB, 20 min with KRB containing 30 mM KCl and finally 15 min with 3G-KRB. The flowthrough was pooled every 5 min by a fraction collector (Spectrum Chromatography, Houston TX) and analyzed for insulin by a radioimmunoassay according to the manufacturer's instructions (rat insulin RIA, Millipore, Billerica, MA). The glucose stimulation index was defined as the average insulin concentration in fractions collected during the first 25 min of 20G-KRB perfusion, divided by the average insulin concentration during the first 25 min of 3G-KRB perfusion.

3.2.12 Immobilized culture of human pancreatic exocrine tissue and quantitative PCR

Islet-depleted cell aggregates derived as a by-product of human islet isolation from four pancreatic tissue donors (ages 18, 22, 50, 56) were kindly provided by Dr. Garth Warnock and the Ike Barber Human Islet Transplant Laboratory (Vancouver General Hospital, Vancouver, British Columbia, Canada). The tissue was procured with informed consent of all donors and institutional review board approval for all procedures. The cell aggregates received on day 0 were placed in T-flasks (Sarstedt) at 1 μ L PCV/cm² in CMRL medium with 10% FBS (CMRL with 2 mM glutamine, 10% FBS, 100 units/mL penicillin, 100 μ g/mL streptomycin, all Invitrogen, Carlsbad, CA). Full medium changes were performed on days 1, 3 and 5. By day 7, the cell culture consisted mainly of vimentin+ cells (54%) or CK19+ cells (40%) with rare amylase+ cells. These cells were trypsinized and split into adherent and suspension cultures, as well as immobilized in 1.5% alginate beads generated by the MOPS emulsion process, during which CMRL with 10% FBS was used as the medium. The beads

were then washed twice with serum-free CMRL medium (CMRL supplemented with 5 mg/L insulin + 5 mg/L transferrin + 5 µg/L selenite I-1884 from Sigma, 10 mM nicotinamide and 0.2% BSA from STEMCELL Technologies, Vancouver, Canada). All cells and beads were cultured for a further ten days in serum-free CMRL medium with the exception of the adherent culture where the cells were initially grown in CMRL-10FBS medium for one day before replacement with the serum-free medium. The seeding density was 2×10^5 cells/mL total culture volume (corresponding to $9 \pm 1 \times 10^5$ cells/mL alginate for the immobilized cultures). On culture days 0, day 7 and 17, 1 µL PCV from liquefied beads, trypsinized adherent cultures or suspension cultures were washed in PBS and re-suspended in 350 µL buffer RLT⁺ (Qiagen) and stored at -80°C until analysis. Samples were analyzed for insulin, PDX-1, as well as aldolase A expression by q-PCR. The mRNA isolation and cDNA synthesis were performed using commercially available kits according to the manufacturer's instructions (respectively RNeasy Plus Mini Kit, Qiagen, Hilden, Germany and SuperScript® III First-Strand Synthesis System for RT-PCR, Invitrogen, CA). The quantitative PCR (q-PCR) was performed using the SYBR Green Universal Supermix (Invitrogen, CA) on a 7300 Thermocycler (Applied Biosystems, Foster City, CA). The q-PCR primers are provided in Table B2. The insulin and pdx-1 expression levels were normalized to aldolase while taking into account the PCR efficiency, which was > 1.9 for all primer sets.

3.2.13 Statistical analysis.

Statistical comparison was based on a 2-tailed Student's t-test and errors represent the standard error of the mean (SEM) for three replicate experiments, unless otherwise noted. Results were considered to be statistically significant for $p < 0.05$. For the comparison of MIN6 growth parameters, paired t-tests were performed because the same cell stock was used to initiate three cultures in parallel (adherent controls, MOPS emulsion beads, MOPS extrusion beads). The Van der Waerden non-parametric t-test was implemented for comparisons involving primary pancreatic tissue due to the high pancreas-to-pancreas variability using JMP Statistics (SAS Institute, Cary, NC). JMP was also used to fit the normal distribution to the bead diameter data.

3.3 RESULTS

3.3.1 Bead size distribution and control of the average bead diameter

Figure 3.2A shows typical beads obtained by the HEPES emulsion process at an emulsification agitation rate of 500 rpm. These beads were highly spherical over the entire range of agitation rates, with a circularity of 0.918 ± 0.004 at 500 rpm. At 500 rpm, the bead diameter distribution was close to a normal distribution, with an average bead diameter of $757 \pm 20 \mu\text{m}$ (Figure 3.2B). The corresponding surface area (D_{32}) and volume (D_{43}) moment

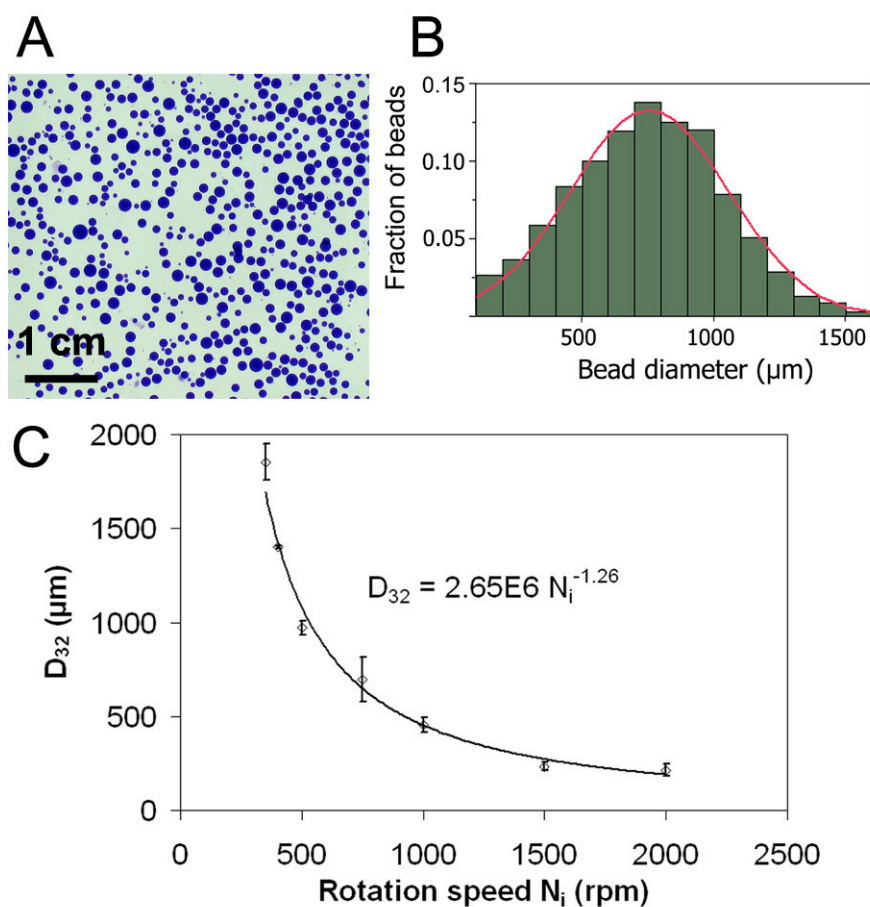


Figure 3.2. Size distribution of HEPES emulsion alginate beads.

A) Light micrograph after toluidine blue-O staining (bar = 1 cm). B) Size distribution quantified by the CellProfiler image analysis software and fitted to a normal distribution with JMP statistics. C) Area weighted average diameter D_{32} as a function of the impeller agitation rate (N_i). Error bars represent the SEM. The standard deviation of the bead size distribution represented $56 \pm 8\%$ of D_{32} , which was constant over the range of agitation rates tested.

mean diameters were $972 \pm 38 \mu\text{m}$ and $1136 \pm 82 \mu\text{m}$ respectively. The D_{32} is considered more relevant to the emulsion properties since the interfacial tension forces are proportional to the bead surface area while the D_{43} is considered more relevant to the conditions experienced by the cells, assumed to be homogeneously distributed throughout the alginate volume. The standard deviations were proportional to the average bead diameters, with $SD_{D_{32}}$ representing $56 \pm 10\%$ of the value of D_{32} , and this was constant over the range of agitation rates tested. Figure 3.2C shows that the D_{32} could be controlled between $\sim 200 \mu\text{m}$ and $2000 \mu\text{m}$ by adjusting the agitation rate N_i . In addition, D_{32} was found to be proportional to $N_i^{-1.26}$, indicating that the main retentive force governing the maximum stable droplet size in the emulsion was related to the oil/alginate interfacial tension (in which case D_{32} should theoretically be proportional to $N_i^{-1.2}$) rather than viscous forces within the dispersed alginate phase (D_{32} theoretically proportional to $N_i^{-0.75}$) (Kolmogorov 1949; Lagisetty et al. 1986; Steiner et al. 2006; Vankova et al. 2007).

3.3.2 The effect of alginate, oil, CaCO₃, and acetic acid on MIN6 survival.

The initial HEPES emulsion process resulted in $83 \pm 2\%$ MIN6 cell survival at the end of the 20 min process (Figure 3.3). The citrate solution used to liquefy the beads and recover the cells prior to viability measurements had little influence on the cells with cell survival remaining $>98\%$ after 1 h of incubation (data not shown). To determine which step(s) led to the decreased cell viability, various process components were omitted and MIN6 survival was assessed. Figure 3.3 shows that cell survival was not significantly affected by cell suspension in alginate with CaCO₃ in the “No oil, no acid” condition. Emulsification alone had small negative effect in the “No acid” condition, while there was a greater and significant drop in cell survival immediately after the acidification step in the HEPES emulsion process, with additional viable cell losses in the “No CaCO₃” condition ($<70\%$ MIN6 survival). Thus, the MIN6 cells were most sensitive to the acidification step. Therefore, efforts to increase cell survival first focused on operating within a less extreme pH range and second on reducing the process duration.

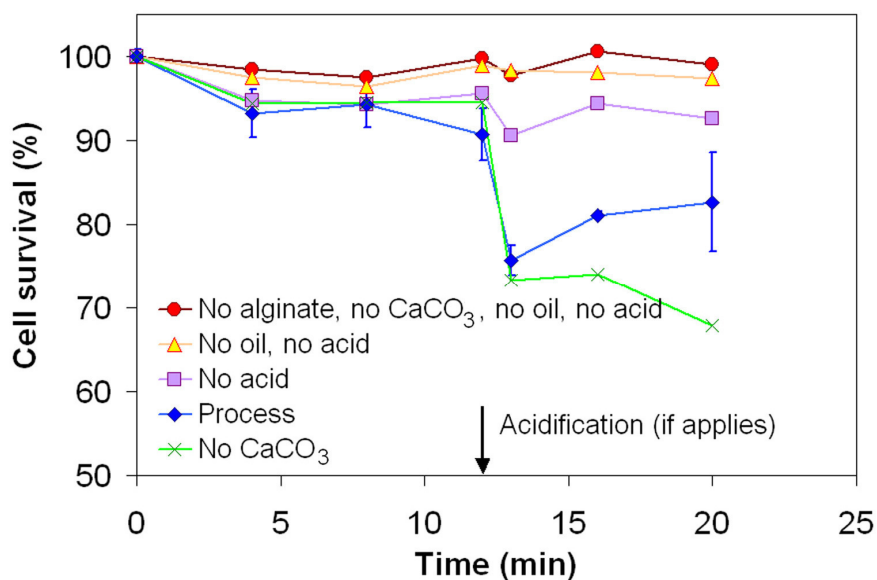


Figure 3.3. Cell survival as a function of time for the HEPES emulsion process and omitting various process components (alginate, CaCO₃, oil and/or acid).

Cell survival was defined as the cell viability determined by trypan blue after liquefying the beads with citrate normalized to the initial cell viability. The initial cell density was 2.5×10^6 cells/mL alginate.

3.3.3 Process optimization

Initial attempts to optimize the emulsion process focused on minimizing the exposure of the MIN6 cells to extremes of pH. In the non-optimized HEPES emulsion process, the alginate was dissolved in 10 mM HEPES buffer, with the bicarbonate medium providing additional buffering capacity. In these conditions, the pH shifted from 7.9 after addition of CaCO_3 to 5.0 after acidification. To examine the pH effects on cell survival, MIN6 cells with an initial viability of $94.7 \pm 0.7\%$ were incubated for 5 to 90 min in HEPES-citrate solutions at a range of pH conditions between pH 4.0 and pH 8.5 (Figure 3.4A). At $\text{pH} < 6.5$, the cell viability decreased to 80~85% within the first 5 min of incubation and then decreased linearly with time, resulting in 63% viability after 90 min at pH 5.0 compared to $87 \pm 2\%$ viability after 90 min at pH 7.4. The zero order death rates calculated over the 90 min exposure were similarly influenced by low pH, but indicated that $\text{pH} > 8.0$ was also undesirable. Based on these observations, the target pH shift was set to pH 7.5 for the initial alginate, cell and CaCO_3 mixture and pH 6.5 after acidification. Optimal buffering was particularly important at the end of the process, since MIN6 cells were more sensitive to acidic conditions than basic conditions, suggesting that a buffer with a lower pKa than HEPES (pKa 7.55) such as MOPS (pKa 7.21) could better suit this process. A 70 mM MOPS buffer was initially chosen because it led to the desired pH change during emulsion acidification (Figure 3.4B). Unfortunately, the resulting pH of 7.48 ± 0.01 of the alginate, medium and CaCO_3 mixture was too low, triggering calcium release from CaCO_3 and partial gelling leading to increased viscosity of the alginate solution before the mixture could be emulsified. To avoid this problem, the target pH of the alginate, medium and CaCO_3 mixture was increased to pH 7.7, such that no premature gelling was observed even after overnight incubation. To achieve the new target shift of pH 7.7 to pH 6.5, the MOPS concentration was decreased to 60 mM and the pH of the buffer was adjusted to 7.6 prior to alginate addition and dissolution.

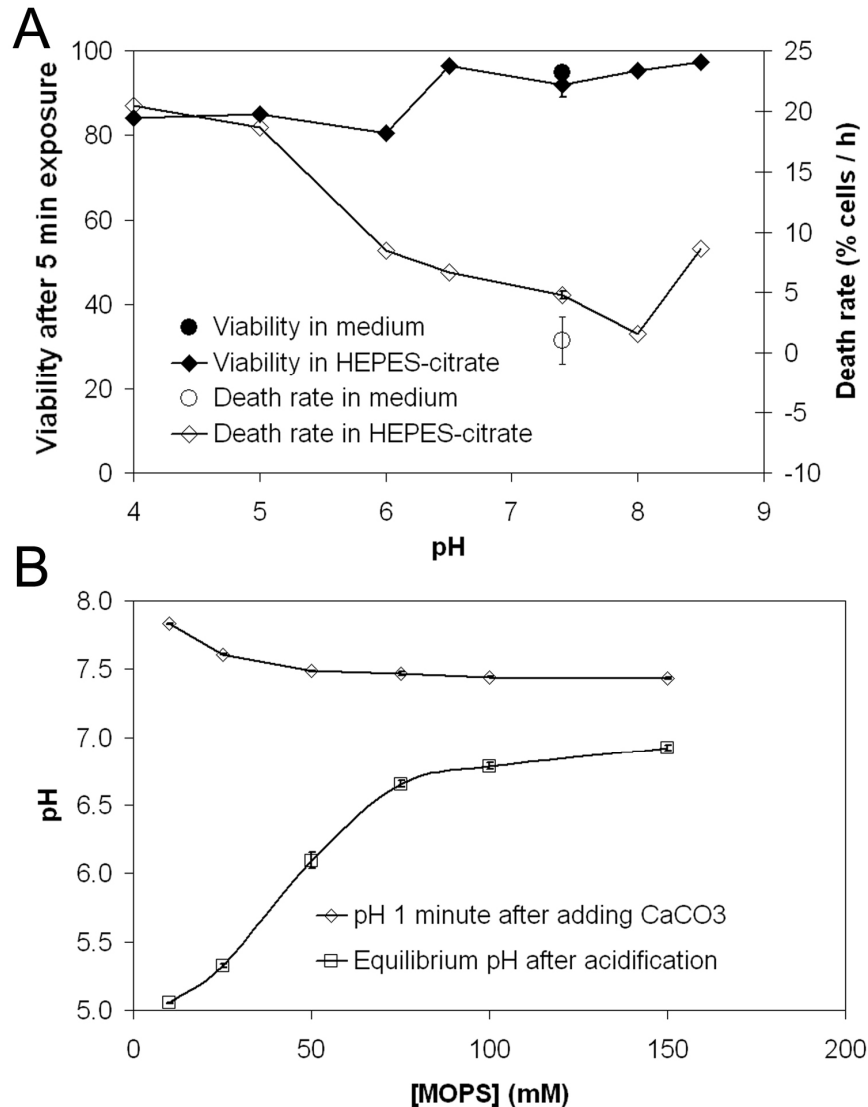


Figure 3.4. Process pH operating range.

A) Short-term effects of pH on MIN6 zero order death rate during 90 min exposure and viability after 5 min exposure. B) pH of the alginate solution as a function of MOPS concentration 1 min after adding CaCO₃ (before acidification) and at equilibrium 24 h after acidification.

Further efforts to improve MIN6 cell survival focused on reducing oil and acid exposure times. The emulsification occurs rapidly after adding the alginate and cell mixture to the mineral oil. Thus, the emulsification time could be reduced from the 12 min used in the non-optimized process, which allowed the emulsion to reach equilibrium between droplet break-up and coalescence (Figure 3.5A). However, if the emulsification was ended too quickly after the initial alginate addition, small changes in the method of alginate

addition could lead to important changes in bead size distribution, and that could in turn impact the degree of bead cross-linking and the cell behavior. The minimum acceptable emulsification time was selected based on the time required to reach a D_{43} that was not significantly different from D_{43} at 12 min for N=3 replicates using a 1-tailed t-test. This condition was met after ~3 min of emulsification.

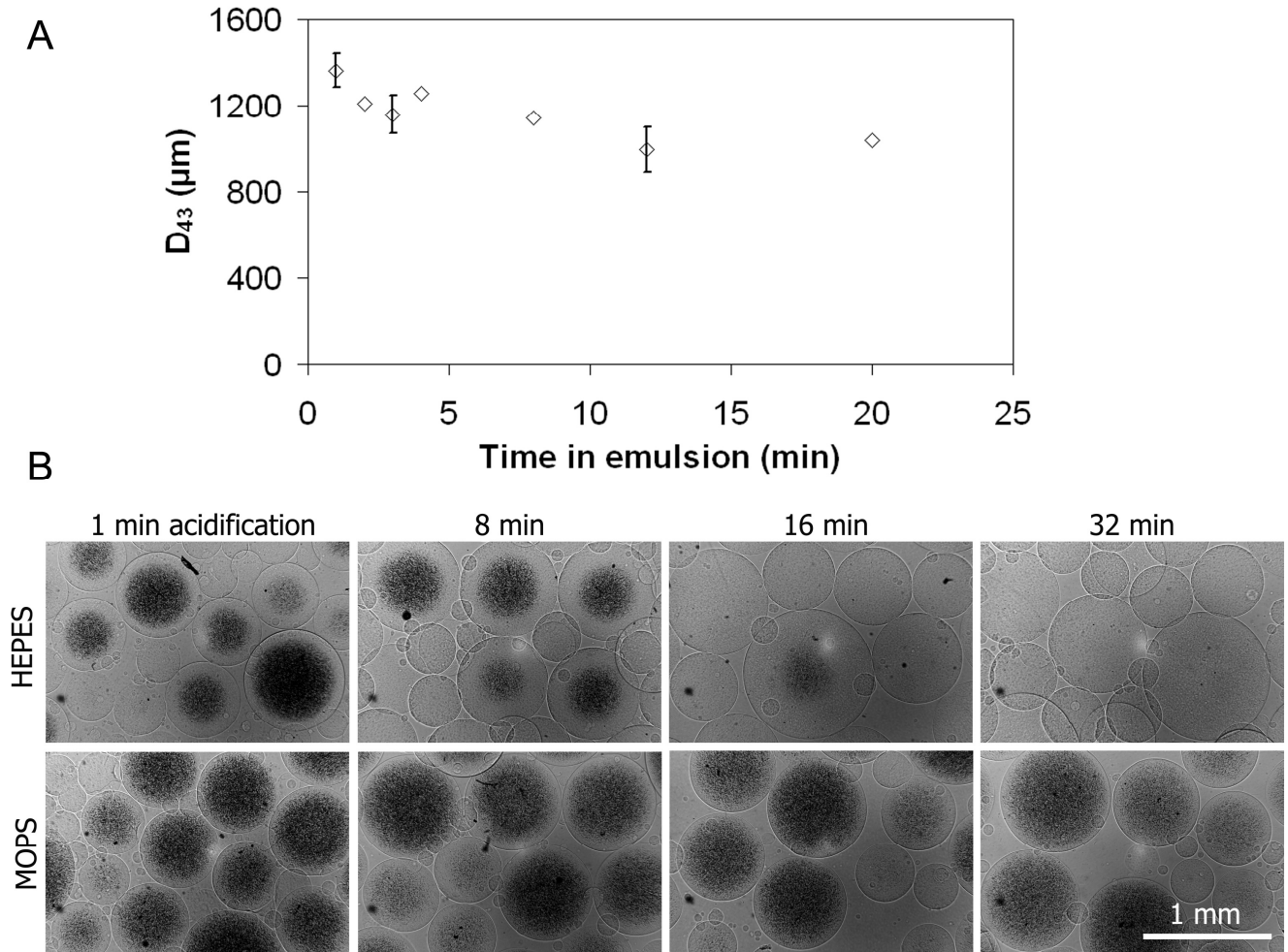


Figure 3.5. Effects of changes in process time on bead diameter and CaCO_3 dissolution.

A) Effect of emulsification mixing time on the volume-weighted average bead diameter. The acidification was kept constant at 8 min. B) Effect of the duration of acidification on the amount of visible unreacted CaCO_3 in the beads. The emulsification time was kept constant at 3 min.

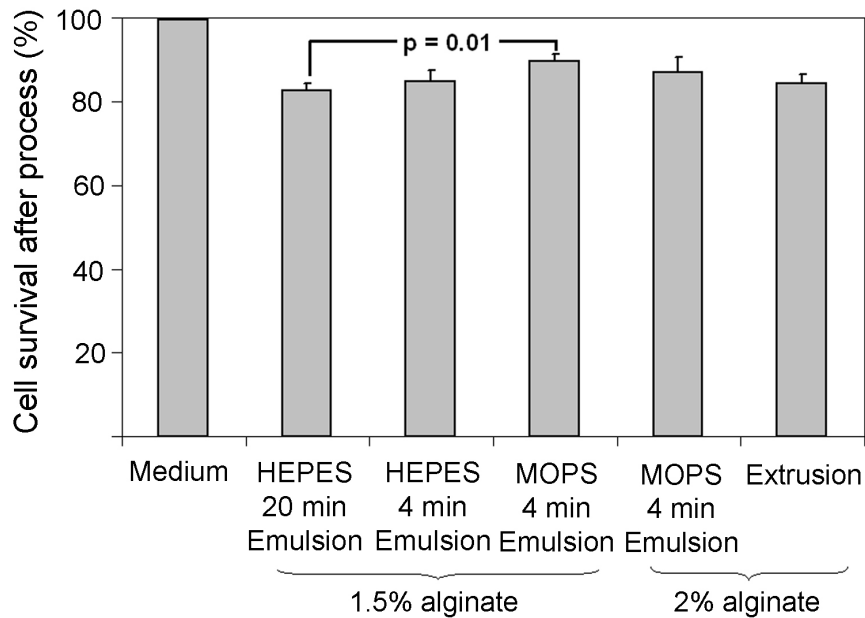


Figure 3.6. Effect of process modifications on MIN6 cell survival.

The HEPES process with 12 min emulsion and 8 min acidification (HEPES 20 min) was compared to a shortened process using HEPES buffering but 3 min emulsion and 1 min acidification (HEPES 4 min), as well as the fully optimized shortened and MOPS buffered process (MOPS 4 min). These experiments were performed using 1.5% alginate and a cell density of 2.5×10^6 cells/mL. The alginate concentration was increased to 2% to compare the MOPS (4 min) emulsion process to the extrusion process. For the 2% alginate beads, the seeding density was 1×10^6 cells/mL since these were then used for the MIN6 cell growth experiments. The number of replicates was $N = 9$ for HEPES 20 min emulsion, $N = 4$ for HEPES 4 min emulsion, $N = 7$ for MOPS 4 min emulsion at 1.5% alginate and $N = 3$ for the other conditions.

The effect of acidification time on bead generation and on the amount of non-reacted CaCO_3 was assessed by visual inspection (Figure 3.5B). A visible shrinking core of non-reacted CaCO_3 grains was observed with HEPES-buffered alginate that required up to 32 min acidification time for complete reaction in the largest ~1 mm diameter beads. In the case of MOPS buffering, CaCO_3 grains were visible in beads larger than ~500 μm even after 32 min acidification. Nevertheless, spherical beads gelled enough for handling by pipetting without bead rupture or changes in bead shape were generated even after 1 min acidification for both HEPES and MOPS-buffered beads. This was selected to be acidification time because the addition of acidified oil took 20 s.

As a result of changing the 10 mM HEPES buffer to 60 mM MOPS and reducing the processing time from 20 to 4 min (3 min emulsification, 1 min acidification), the final MIN6 cell survival in the alginate bead was significantly increased from $83 \pm 2\%$ to $90 \pm 2\%$ (Figure 3.6). The effect of changing the HEPES to a MOPS buffer appeared to be greater than the effect of reducing the process time. However the individual effects did not reach statistical significance. The total cell recovery calculated by multiplying the total bead volume by the viable cell density obtained after liquefying the beads was $84 \pm 7\%$ for the MOPS emulsion process. There were no apparent differences in MIN6 cell survival in beads of $> 500 \mu\text{m}$ diameter between the HEPES and the MOPS processes based on Calcein AM and Ethidium homodimer staining (Figure 3.7). However, a higher fraction of dead cells was qualitatively observed in smaller beads with the 20 min and 4 min HEPES processes but not with the MOPS 4 min process (Figure 3.7). Cells recovered by liquefying the beads from the HEPES and the MOPS emulsion processes were re-seeded in adherent cultures and compared to

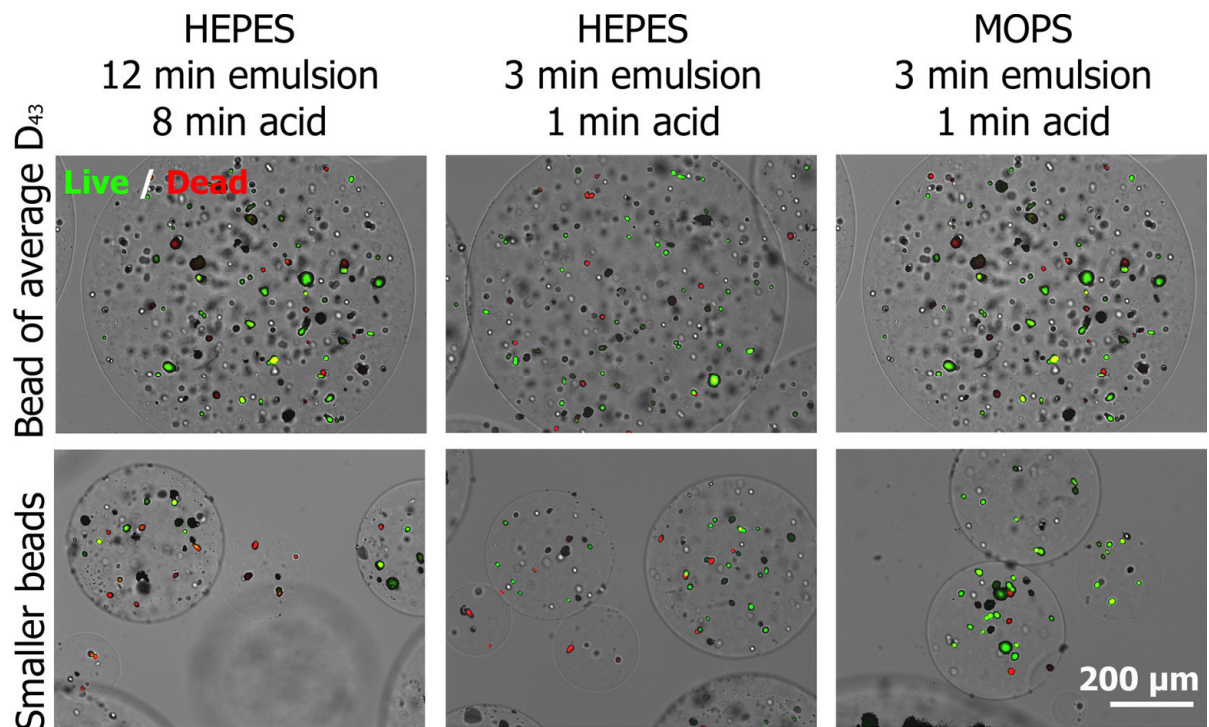


Figure 3.7. Cell survival dependence on bead diameter, process buffer and process time.

Cells were visualized by Calcein AM (live)/Ethidium homodimer (dead) staining. The cell density used was 2.5×10^6 cells/mL alginate.

passaged non-immobilized cells. There was no significant difference in the cell concentration after 1 or 7 days between the three groups, suggesting that the HEPES and MOPS emulsion processes did not have a negative influence on the seeding efficiency or the expansion of the surviving cells (data not shown).

3.3.4 Comparison of the emulsion processes with the extrusion process

The performances of the emulsion processes were compared to conventional nozzle-based extrusion bead generation. For this purpose, the alginate concentration was increased from 1.5% to 2% to avoid teardrop-shaped bead formation with the extrusion device. These resulted from insufficient viscous and surface tension forces for drop rounding in the time before contacting the CaCl₂ gelling solution.

3.3.5 Bead strength

The mechanical properties of beads generated by the HEPES emulsion and MOPS emulsion processes were compared with the extrusion process under compression and hydrodynamic stress (Figure 3.8). Compression experiments consisted of monitoring bead

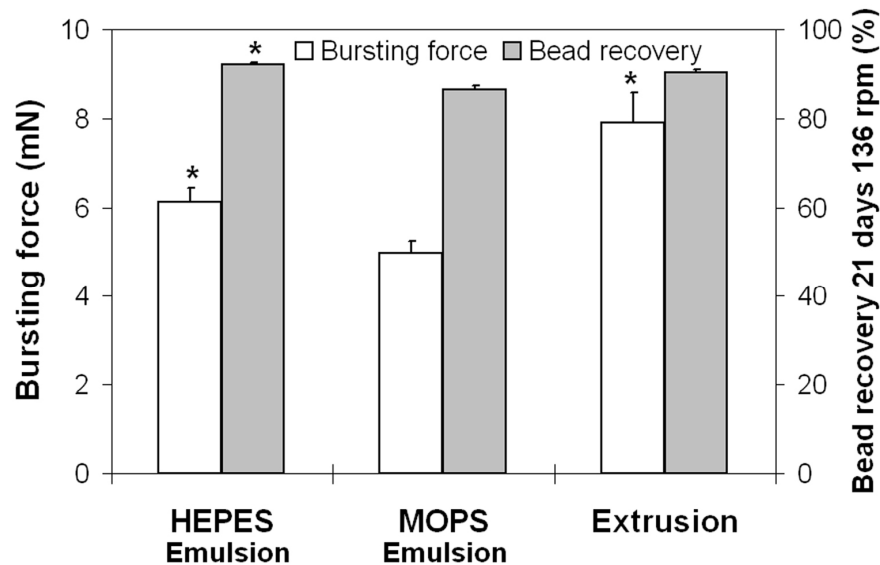


Figure 3.8. Initial bead bursting force and bead recovery after 21 days agitation at 136 rpm.

Error bars are the SEM of 3 batches of alginate. For compression tests, 30 beads were measured for each batch. *p<0.05 compared to the MOPS emulsion beads, 2 tailed t-test paired by alginate batch.

deformation and bursting under an increasing compressive load. The bursting force of the MOPS emulsion beads was 5.0 ± 0.3 mN (average \pm SEM of 3 alginate batches), which was $19 \pm 4\%$ lower than that of the HEPES emulsion beads. This was consistent with the incomplete CaCO_3 dissolution observed in Figure 3.5B, suggesting that the calcium release during the MOPS emulsion process reduced the alginate cross-linking. In addition, the bursting force of the HEPES emulsion beads was $21 \pm 9\%$ less than that of the extrusion-generated beads, although this difference was not significant. Bursting occurred for all beads at approximately the same bead deformation ($60 \pm 10\%$). There were no significant differences in the average bead bursting force between the 3 alginate batches.

Hydrodynamic testing was performed in 50 mL shake flasks at 136 rpm for 21 days. The bead recoveries were similar for all processes, but slightly lower for MOPS emulsion beads at $86 \pm 1\%$ compared to $92 \pm 1\%$ for HEPES emulsion beads and $90 \pm 1\%$ for extrusion-generated beads. There was no significant difference in the bead circularity or D_{43} after 21 days for any of the bead types. The MOPS emulsion beads were also subjected to extreme hydrodynamic stress during overnight agitation at 750 rpm in a 250 mL microcarrier spinner flask. The maximum energy dissipation for a flask of the same dimensions, including the impeller geometry, was reported to be 1.6×10^3 W/m³ at 210 rpm by Venkat *et al.* (1996). Since the maximum energy dissipation rate is proportional to N_i^3 , its value was estimated to be $\sim 7 \times 10^4$ W/m³ under the conditions tested. There were no significant changes in bead visual appearance, circularity or D_{43} (data not shown).

3.3.6 MIN6 cell survival and alginate-immobilized growth

MIN6 cell survival after immobilization, as well as growth and morphology were compared in beads generated by the emulsion and the extrusion processes. As can be seen from Figure 3.6, the $87 \pm 4\%$ MIN6 cell survival at the end of the MOPS emulsion process was not significantly different from the $84 \pm 2\%$ measured for the MOPS extrusion process. In addition, MIN6 cell survival was also not significantly affected by changing the alginate concentration from 1.5% to 2% ($90 \pm 2\%$ vs $87 \pm 4\%$).

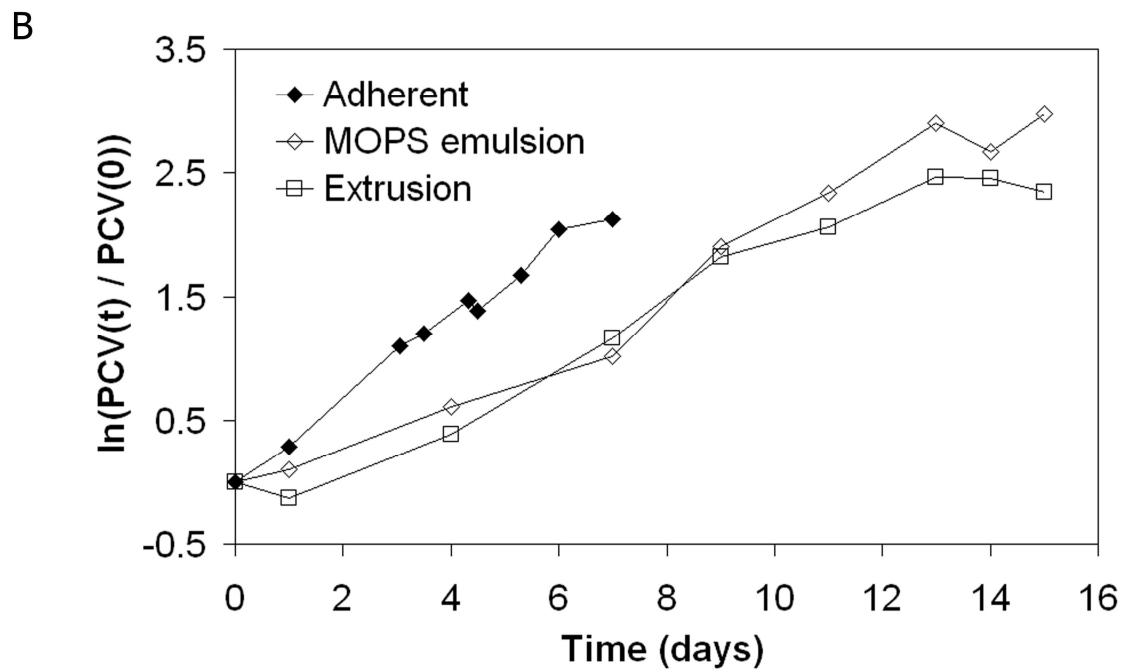
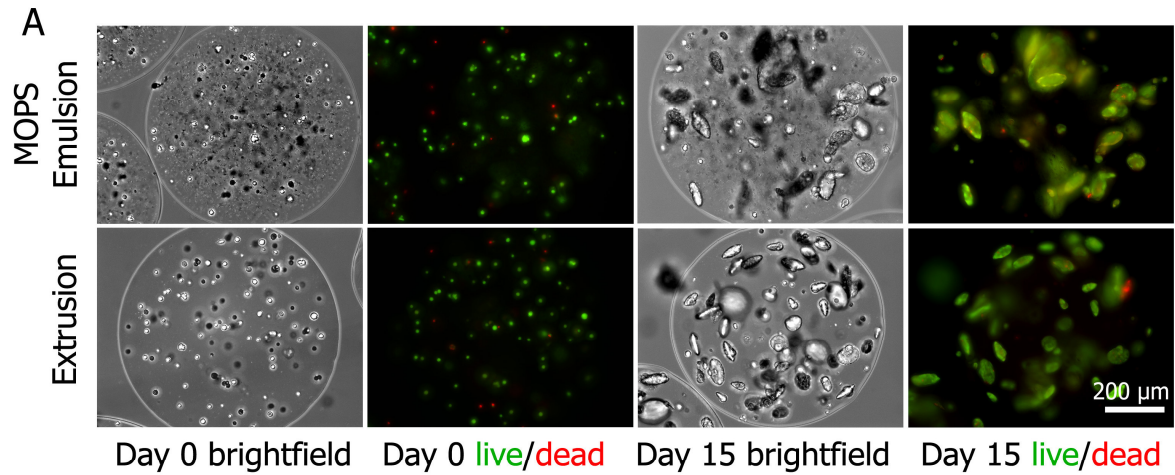


Figure 3.9. MIN6 cell expansion in MOPS emulsion-generated 2% alginate beads, MOPS extrusion-generated 2% alginate beads and control adherent cultures.

A) MIN6 cell growth from single cells into $\sim 100 \mu\text{m}$ diameter cell aggregates after 15 days and staining with Calcein AM (live)/Ethidium homodimer (dead). B) The seeding density was 1×10^6 cells/mL alginate with 1 mL alginate / 10 mL total culture volume. Growth curves were based on PCV.

After 15 days of culture, the MIN6 cells had expanded from mostly single cells into aggregates of $\sim 100\ \mu\text{m}$ diameter with little morphological difference between cells in the MOPS emulsion-generated and the extrusion-generated beads (Figure 3.9A). The total amount of MIN6 cells growing outside of the beads at the end of the culture period accounted for $<2\%$ of the total PCV and was deemed negligible when calculating growth and glutamine consumption rates. For both bead types, MIN6 cells grew exponentially from day 1 until day 13~14 (representative growth curves shown in Figure 3.9B). The maximum specific growth rate of $0.19 \pm 0.02\ \text{day}^{-1}$ in the emulsion-generated beads was not significantly different from the $0.15 \pm 0.02\ \text{day}^{-1}$ growth rate in extrusion-generated beads, but both were reduced by ~ 2 -fold compared to the $0.39 \pm 0.03\ \text{day}^{-1}$ growth rate of adherent controls. During exponential growth of all cultures including adherent controls, glutamine was consumed at a higher rate than glucose ($6 \pm 3\ \text{mol glutamine/mole glucose consumed}$). The specific glutamine consumption rate followed similar trends to the growth rate. There was no significant difference between the glutamine consumption rates in emulsion-

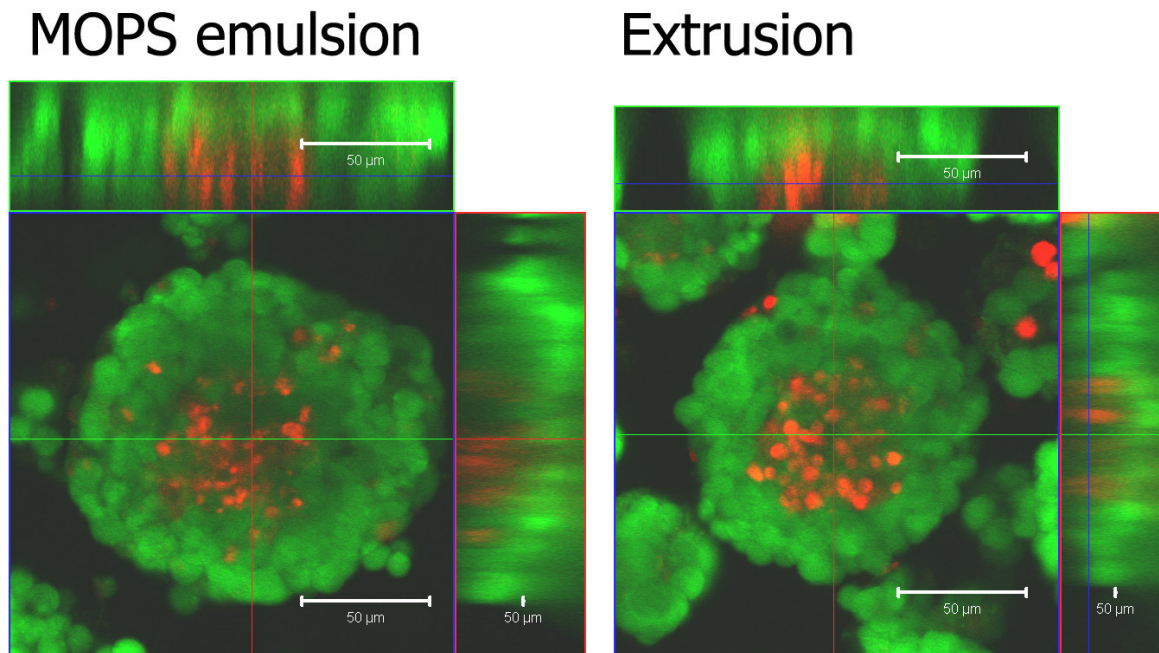


Figure 3.10. Live/dead stained MIN6 aggregates after of 2 weeks of expansion.

Projection image of islet-sized MIN6 aggregates obtained after 2 weeks of expansion in beads produced by the MOPS emulsion or extrusion processes stained by Calcein AM (live) / Ethidium homodimer (dead). The views in the center, top and right respectively show the x-y, x-z and y-z cross-section of the same image stack acquired for one cell aggregate.

generated beads and extrusion-generated bead, respectively $0.22 \pm 0.02 \times 10^{-8}$ mol cells⁻¹ day⁻¹ and $0.14 \pm 0.03 \times 10^{-8}$ mol cells⁻¹ day⁻¹, but both were significantly lower than the $0.43 \pm 0.09 \times 10^{-8}$ mol cells⁻¹ day⁻¹ glutamine consumption of adherent controls. The reduced growth rate and glutamine consumption of the immobilized cells can be explained by the presence of a dead cell core developed by the aggregates in both bead types (Figure 3.10). However, nutrient limitations were not the sole cause for the reduced growth rate and cell death of the alginate cultures, since the growth rate was constant and hence independent of the MIN6 aggregate size for most of the culture period. Overall, the growth characteristics of the cells in the emulsion-generated beads were similar to the extrusion-generated beads.

3.3.7 MIN6 cell glucose-stimulated insulin secretion after immobilized growth

The insulin secretion of the cell aggregates obtained after 15 days of immobilized culture in MOPS emulsion-generated or extrusion-generated alginate beads in response to elevated glucose or KCl depolarization was examined by perfusion. The results were

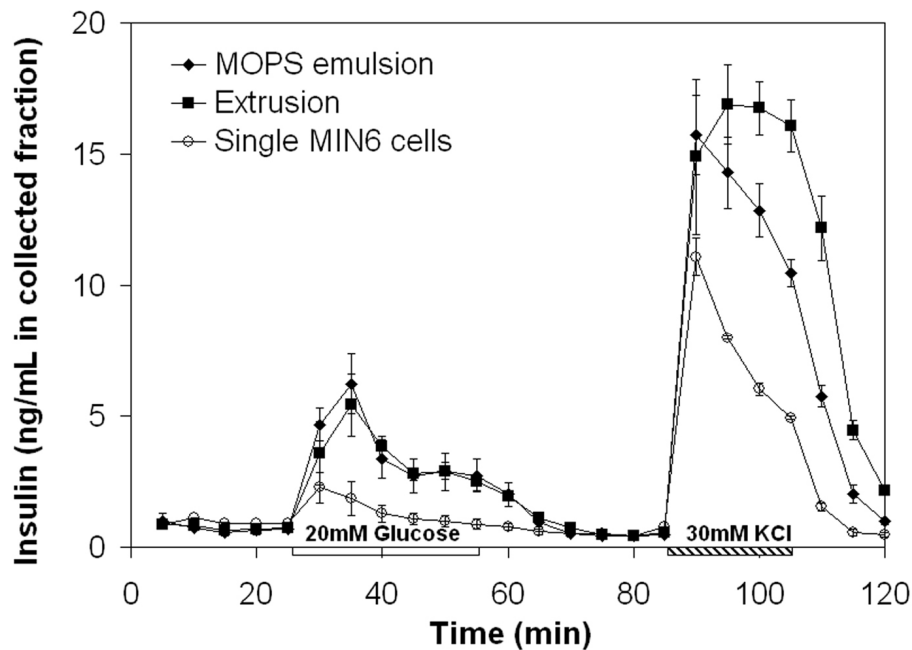


Figure 3.11. Insulin secretion of MIN6 cell aggregates in emulsion-generated beads.

The MIN6 cell aggregates obtained after 15 days of culture (initially seeded at 1×10^6 cells/mL alginate) in MOPS emulsion 2% alginate beads were compared to the aggregates obtained in 2% alginate extrusion beads and non-immobilized single MIN6 cells. The basal glucose concentration is 3 mM.

compared to single MIN6 cells in suspension derived from trypsinized adherent cultures (Figure 3.11). After a step change in glucose concentration from 3 mM to 20 mM, MIN6 cells responded with the expected biphasic insulin secretion. The peak insulin secretion from the immobilized cell aggregates occurred in the fraction collected between 5 min and 10 min after 20 mM glucose exposure, while the peak insulin secretion of non-immobilized single MIN6 cells occurred within the first 5 min. This ~5 min delay could be explained by changes in the insulin secretion kinetics by the immobilized cell aggregates or by hindered insulin diffusion in the gel matrix. The insulin secretion by cells immobilized in either the extrusion or the emulsion beads was significantly higher than for non-immobilized cells within 10 minutes and up to 40 min after starting glucose stimulation. This was reflected by the glucose stimulation index of 6.0 ± 1.9 for MIN6 cells in the emulsion-generated beads, which was not significantly different from the stimulation index of 6.0 ± 1.6 for MIN6 cells in the extrusion-generated beads, which in turn was significantly higher than the stimulation index of 1.5 ± 0.5 for the single MIN6 cells. Immobilized MIN6 cells also showed a robust response to depolarization with 30 mM KCl. The insulin secreted during the 20 min following KCl depolarization appeared to be reduced for the MIN6 cells immobilized in the emulsion-generated beads compared to the extrusion-generated beads, but this difference was not significant. The normalized insulin concentrations in the fractions collected during high glucose or KCl exposure were significantly higher for MIN6 cells in MOPS emulsion or extrusion-generated beads than for single MIN6 cells. Together, these data demonstrate that immobilized growth improved β -cell glucose responsiveness without significant differences between beads generated by the MOPS emulsion and the MOPS extrusion processes.

3.3.8 Culture of primary islet-depleted pancreatic cells in emulsion-generated beads

The potential of the emulsion process for immobilized culture of primary cells was assessed using islet-depleted human pancreatic tissue generated as a by-product of islet isolations for clinical transplantation. Islet-depleted cell aggregates were placed in adherent culture in CMRL medium with 10% FBS. After the first day, the cell aggregates had adhered to the culture surface and by 7 days, a confluent monolayer of cells had been established. As expected for adherent cultures promoting non-islet cell expansion, the insulin/aldolase A

expression of these mixed cultures decreased to $3.3 \pm 0.5\%$ of their initial expression (Figure 3.12). Similarly, amylase and PDX-1 expression decreased, while CK19 and vimentin expression progressively increased (Figure B3 in Appendix B). On day 7, the adherent cells were trypsinized and split into adherent and suspension cultures as well as immobilized in 2% MOPS emulsion alginate beads and cultured for a further ten days in serum-free CMRL medium. The cell survival from the emulsion process was $71 \pm 4\%$. Over the 10 days of serum-free culture, the viable cell concentration of the immobilized cells progressively decreased to $35 \pm 6\%$ of the initial viable cell concentration (Figure B4 in Appendix B).

Insulin expression increased significantly for all conditions over the 10 days of serum-free culture by 4 ± 2 fold for adherent cultures, 21 ± 5 fold for suspension cultures and 67 ± 32 fold for the immobilized cultures in emulsion-generated alginate beads. This increase was much greater than the < 2 -fold increase in insulin expression measured for cell clusters formed by Matrigel overlay as described by Bonner-Weir et al. (2000) and Gao et al. (2003) (see the methods described in Section A2 in Appendix A and the results in Figure B5 in Appendix B). The increase observed was higher in serum-free medium than in the presence of 10% FBS (Figure B7). A similar increase in insulin expression was also observed using alginate-poly-L-lysine-alginate (APA) beads generated by coating the emulsion-generated beads with poly-L-lysine and alginate, and then degelling the bead core (Figure B7 in Appendix B). No significant changes in gapdh/aldolase A expression were observed in any of the culture conditions (Figure B7 in Appendix B). Since APA beads did not lead to higher insulin expression than simple ungelled emulsion-generated beads, the use of these beads was not further pursued. The final insulin/aldolase A expression achieved in gelled emulsion-generated beads corresponded to $3.5 \pm 0.9\%$ of the expression measured for the transplanted islet-rich fractions for the same pancreata. The islet purity of these islet-rich fractions was $70 \pm 6\%$ based on dithizone staining at the Ike Barber Human Islet Transplant Laboratory. PDX-1/aldolase A gene expression also increased by 5 ± 2 fold during serum-free immobilized culture in the emulsion-generated beads (Figure B6 in Appendix B).

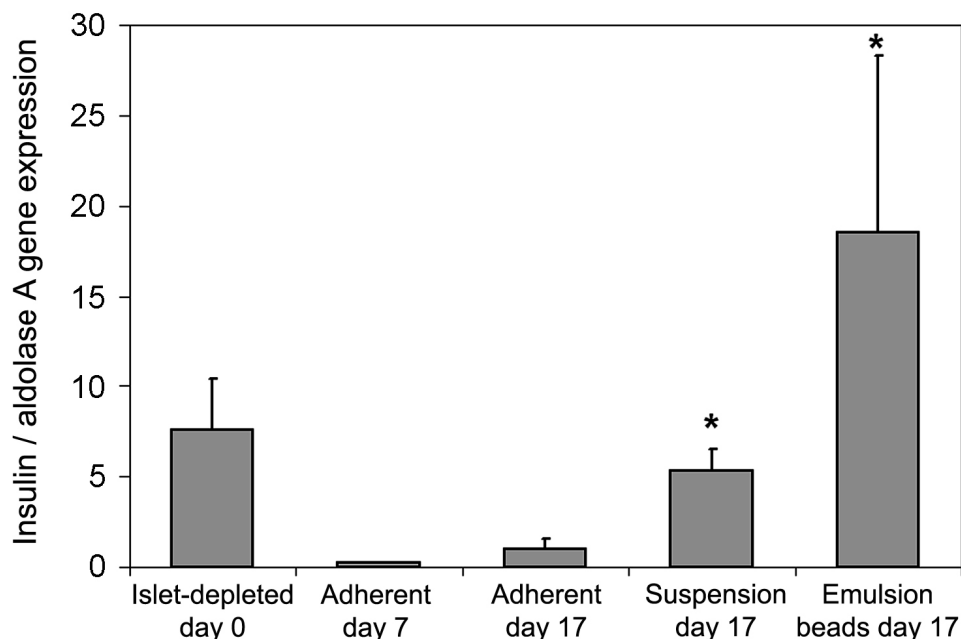


Figure 3.12. Insulin gene expression of islet-depleted human pancreatic tissue before and after 10 days of immobilized culture in emulsion-generated alginate beads.

Insulin gene expression was quantified by q-PCR and normalized to the aldolase A housekeeping gene. Islet-depleted pancreatic tissue aggregates were first cultured under adherent conditions for 7 days and then split into adherent, suspension and MOPS emulsion immobilized serum-free cultures for 10 days. Results averaged from N = 4 pancreata. * $p < 0.05$ compared to the day 7 adherent cells using the Van der Waerden non-parametric test.

3.4 DISCUSSION

The alginate emulsion and internal gelation process was developed as an industrially scalable (Poncellet et al. 1992) alternative to extrusion and external gelation methods for the encapsulation of materials sensitive to pH or temperature, such as certain natural compounds (Lee et al. 2009), DNA (Alexakis et al. 1995) or proteins (Liu et al. 2007) including insulin (Reis et al. 2007a; Silva et al. 2006). The process was also used to encapsulate *Lactococcus lactis* (Larisch et al. 1994b) and live attenuated *Mycobacterium bovis* respectively for applications in the dairy and vaccine production industries. An emulsion-based process has been described for mammalian cell immobilization relying on external (Choi et al. 2007; Sugiura et al. 2005) or internal (Huang et al. 2007) gelation in a microfluidic

device, but the highest throughput reported is 54 mL/h. Chapter 3 describes the novel immobilization of mammalian cells in alginate beads generated by emulsion and internal gelation in a stirred vessel.

Alginate could be used as an immobilization matrix promoting the differentiation of adult human pancreatic progenitors into islet-like clusters useful for islet transplantation. Immobilization of cells expanded from human islets in alginate-PLL-alginate beads increased the insulin expression of these cells (Tsang et al. 2007). Alginate-immobilized culture also increased the insulin content of neonatal pancreatic porcine tissue (Korbitt et al. 1997a; Tatarikiewicz et al. 2001). We have previously developed a hollow fiber bioreactor system providing 120 mL alginate immobilized culture volumes sufficient to accommodate the ~1 million islet-like cell clusters required to treat one diabetic patient (Hoesli et al. 2009). As a minimum target, the culture volumes would be scaled up to ~10 L to allow the single batch production of enough islet-like clusters to treat ~100 patients using the cells from a single donor. Even larger scales would be desirable for progenitors derived from ES cells, since these can be readily expanded and since the validation burden for each batch is very important. In the commercialization model of the only human clinical trial with ES cells that had been approved by the FDA, the cells used for the treatment of all the patients were produced in one large batch that was thoroughly validated and cryopreserved (Alper 2009). A similar model could be used with an encapsulated cell product, particularly if the cells and/or beads could be cryopreserved (Hardikar et al. 2000; Mahler et al. 2003; Malpique et al. 2009; Murua et al. 2009; Riolland et al. 2000). The throughput for mammalian cell immobilization by single nozzle extrusion bead generators varies between ~10 mL/h and ~600 mL/h (Koch et al. 2003; Schwinger et al. 2002), requiring more than 15 hours to generate 10 L of beads. The emulsion and internal gelation process using a simple stirred vessel could allow pancreatic progenitor cell immobilization at larger scales than either hollow fiber bioreactors or nozzle extrusion encapsulators. Compared to the hollow fiber system, the emulsion process allows easier sampling of the immobilized cells. Also, the emulsion process does not require recovery of the cells from the gel prior to transplantation, since the beads could improve cell survival or contribute to immune protection. However, the effects

of the emulsion process steps (i.e. contact with CaCO_3 , emulsification, acidification, etc.) on mammalian cell survival were unknown.

Using MIN6 cells as a model, we first determined that mammalian cells can withstand the processing conditions associated with cell immobilization using the emulsion process. However, the initial non-optimized HEPES emulsion process with 10 mM HEPES buffering led to a significant decrease in cell survival to $83 \pm 2\%$ due a pH of 5.0 at the end of the process. It was then determined that $\text{pH} < 6.5$ or > 8.0 should be avoided during the process. Although mammalian cell proliferation and function can be affected by pH shifts as low as 0.2~0.4 (Chaudhry et al. 2009; Gunawardana and Sharp 2002), a fraction of the MIN6 cells tolerated up to 90 min exposure to acidic conditions surprisingly well. The cells maintained $>70\%$ viability after 90 min at pH 4.0. MIN6 cells also showed no reduction in plating efficiency or adherent cell expansion compared to maintenance cultures after being recovered from HEPES emulsion-generated beads, in which the pH after acidification was of 5.0. Hence, mammalian cells that survive the initial viability loss can be resilient to 8 min exposure to pH 5.0. However, to minimize the initial drop in viability at such an extreme pH (Figure 3.3 and Figure 3.4A), the process buffer was changed to 60 mM MOPS, which led to a pH shift from 7.7 (initial pH) to 6.5 (final pH) during acidification, allowing sufficient calcium release for bead gelling. To further reduce the cell exposure to non-optimal conditions, the emulsification time was shortened from 12 min to 3 min and the acidification time from 8 min to 1 min without significantly affecting the bead size distribution, appearance or handling. Implementation of this optimized MOPS emulsion process using 1.5% alginate increased cell survival to $90 \pm 2\%$. Most of the cell losses and hence most of the improvement was observed in smaller ($< 500 \mu\text{m}$) alginate beads, although the qualitative observations in Figure 3.7 should be verified quantitatively. This could be explained by a greater pH drop experienced in the smaller alginate beads, due to their higher surface/volume ratios, and hence to the higher rate of acetic acid delivery compared to larger beads. The increased buffering provided by 60 mM MOPS compared to 10 mM HEPES may have avoided harmful pH drops in these small beads, consistent with the unreacted CaCO_3 seen even in some of the small beads with the MOPS process Figure 3.5B).

Next, the emulsion-generated beads were compared to beads generated by the more traditional extrusion process. The resistance of the emulsion-generated beads to compressive and hydrodynamic stress was studied to determine if their mechanical properties would limit their use in various applications. For transplantation purposes, alginate beads should be able to withstand compressive forces during intra-peritoneal injection (Lacík 2006). The peak bursting force of capsules currently being used in human clinical trials has been reported to be as low as 8.8 mN (Thanos et al. 2007). The bursting force of the MOPS emulsion-generated beads was of the same order at 5.0 ± 0.3 mN, although the HEPES emulsion and the extrusion-generated beads were significantly stronger, by respectively $19 \pm 4\%$ and $37 \pm 5\%$. For the same calcium saturation, extrusion-generated beads are expected to be more resistant to compressive stress than emulsion-generated beads due to the higher alginate gel gradients resulting from an inward-moving gelling zone (Thu et al. 1997). Nevertheless, emulsion-generated beads withstood 21 days of suspension culture in 125 mL shake flasks at 136 rpm with little or no change in bead shape or size distribution. No differences were noted even after subjecting the beads to extreme hydrodynamic stress of 750 rpm for 24 h in a 250 mL microcarrier spinner flask, corresponding to $\sim 7 \times 10^4$ W/m³ maximum energy dissipation in the vessel. This energy dissipation rate approaches the maximum rate of $\sim 10^5$ W/m³ found in 22 000 L industrial bioreactors agitated at 140 rpm (Godoy-Silva et al. 2009; Wernersson and Tragardh 1999). Thus, the mechanical strength of the emulsion-generated beads was sufficient for most *in vitro* applications.

Visual examination of CaCO₃ particle dissolution gave a qualitative understanding of the emulsion and internal gelation kinetics. A shrinking core of non-dissolved CaCO₃ was observed in the beads (Figure 3.5B), suggesting that the gelling reaction is at least partially limited by the rate of H⁺ diffusion. While a pH gradient is maintained within the beads, alginate would diffuse towards an inward-moving gelling zone, similar to that observed in the formation of externally gelled extrusion-generated beads (Thu et al. 2000). This could explain the presence of the slight alginate concentration gradients near the surface of emulsion-generated beads (Quong et al. 1998). The reaction rate at the CaCO₃ crystal

surface, the rate of Ca^{2+} diffusion and/or the rate of alginate cross-linking may then eventually become rate-limiting (Morse and Arvidson 2002; Thu et al. 2000). The 24 mM CaCO_3 concentration used in the emulsion processes is slightly lower than what would be required to reach 1:2 stoichiometric equivalence (Morris et al. 1978) with the concentration of guluronic acid (~70 mM for 2% alginate). Complete CaCO_3 dissolution should therefore be reached with sufficient reaction time, which was clearly not the case (i.e. CaCO_3 granules remained visible, Figure 3.5) after 1 min acidification, especially with MOPS buffering. If the mechanical stability of the beads is a priority with cell survival less of a concern, longer reaction times and/or decreased buffering should be considered. A mathematical model of these rates could be useful for such optimization (Xiu-Dong et al. 2007). Alternatively, finer CaCO_3 grains could reduce the time required to reach equilibrium. Excess CaCO_3 may even be desirable, acting as a calcium reservoir stabilizing the beads in the presence of chelating molecules.

The emulsion and extrusion processes were further compared based on the survival, growth and nutrient consumption of immobilized MIN6 cells. Glutamine, which significantly contributes to anaplerosis in islets (Malaisse et al. 1983) and other β -cell lines (Cline et al. 2004), served as the primary carbon source for immobilized cultures as well as adherent controls. As expected (Constantinidis et al. 1999; Hoesli et al. 2009), the MIN6 growth rate in alginate was significantly reduced compared to adherent culture controls, which was reflected by a lower cell-specific glutamine consumption rate. The growth rate reduction commonly observed for immobilized cultures can be explained by nutrient limitations (Buchwald 2009) and/or by the requirement for growing cells to counter opposing gel forces (Simpson et al. 2004; Stabler et al. 2001). Importantly for this study, there were no significant differences in the cell survival, growth rate and glutamine consumption rate of cells immobilized in alginate beads generated by either the emulsion or the extrusion processes. The goal of the current work was not to minimize nutrient limitations of the emulsion-generated beads, since these issues could be irrelevant with slower-dividing primary cells. If nutrient limitations are problematic for certain applications, the bead size could be decreased using faster emulsion agitation rates to decrease the bead diameter.

There was no significant difference between the glucose-stimulated insulin secretion of MIN6 cells immobilized in the emulsion-generated and the extrusion-generated beads. For both bead types, the peak insulin secretion was observed 5 min later than for non-immobilized cells. This could be due to decreased insulin diffusivity in the beads (Tziampazis and Sambanis 1995). However, a 5 min delay in insulin secretion from grafted cells would still provide clinically acceptable glycemic control *in vivo*. In addition, alginate-immobilized growth significantly increased the glucose stimulation index of MIN6 cells by 4-fold compared to single MIN6 cells in suspension. A similar phenomenon has been reported for MIN6 aggregates obtained upon expansion on gelatin-coated tissue flasks (Hauge-Evans et al. 1999; Luther et al. 2006). Cell aggregation and proximity can have a profound effect on β -cell function (Bavamian et al. 2007; Jain and Lammert 2009). It is also possible that immobilized growth promoted cell differentiation, increasing the insulin content of the cells. A higher insulin content of the alginate-immobilized cells compared to single cells grown in adherent cultures is suggested by their higher KCl-induced insulin release. These hypotheses could be investigated by quantifying the insulin content of the cells, as well as the fraction of PDX-1+/insulin- and PDX1+/insulin+ cells in the MIN6 population using a dual reporter system developed in the Piret laboratory (Szabat et al. 2010). Thus, MIN6 pseudo-islets could serve as a closer islet model system than MIN6 cells grown in adherent cultures. The emulsion process could enable the production of large amounts of these pseudo-islets in scalable suspension cultures for use in high throughput screening and pharmacological testing of drug toxicity to pancreatic β -cells.

Human islet-depleted pancreatic tissue was cultured in emulsion-generated alginate beads to determine the applicability of this process to primary cell immobilization. Cell aggregates consisting mainly of exocrine and duct cells were first cultured under adherent conditions for 1 week. During the first week of adherent culture, the insulin expression of the tissue decreased 30-fold, as is normally observed due to selective adhesion of non-islet cells and/or β -cell dedifferentiation (Efrat 2008). The cells were then trypsinized and immobilized using the MOPS emulsion process with slightly lower survival ($71 \pm 4\%$) than for the MIN6 cell line. After 10 days of immobilized cultures, the viable cell density in the

beads had decreased to $35 \pm 6\%$ of the initial viable cells seeded. This level of long-term cell survival was comparable or superior to our previous experience with neonatal pancreatic porcine cells (Hoesli et al. 2009) and other reports of 20~30% primary cell survival after 10 days of alginate-immobilized culture (Tatarkiewicz et al. 2001; Yang et al. 2002). Immobilized culture resulted in a 67 ± 32 fold (ranging between 11-fold and 159-fold) increase in insulin/aldolase A gene expression that could not be solely explained by the selective death of insulin-negative cells, based on the aforementioned cell survival. The final insulin/aldolase A expression level corresponded to $3.5 \pm 0.9\%$ the expression measured for the transplanted islet-rich fraction. This result is comparable to the 1~5% of the insulin mRNA of islets previously reported for islet-depleted human pancreatic cells cultured in Matrigel (Bonner-Weir et al. 2000; Gao et al. 2007). However, Matrigel is an ill-characterized animal-derived matrix that would not be suitable for human transplantation application. In addition, these results could not be replicated by the author of this thesis, with only $0.004 \pm 0.003\%$ of the insulin expression of the islet-rich fraction measured after 4 weeks of culture in Matrigel (Figure B5 in Appendix B). In addition to a contribution by selective β -cell survival, the increased insulin gene expression observed during alginate-immobilized culture could be a result of β -cell proliferation, β -cell re-differentiation, differentiation of a progenitor cell and/or transdifferentiation of exocrine (Minami et al. 2005), ductal (Todorov et al. 2006) or mesenchymal cells (Seeberger et al. 2006). The presence of the gel may have impacted the expression profile of the cells by, for example, promoting cell clustering (Boretti and Gooch 2006) and altering the physical cues received by the cells (Engler et al. 2006). Based on the yields of the different processing steps, this differentiation protocol only yielded an increase by ~50% of the insulin-expressing cell mass per pancreas (calculation in Table B4). Therefore, further optimization and a better understanding of the mechanisms involved in the differentiation would be required to achieve the target of 100X increased islet mass per donor pancreas. Currently, ES cell-derived islet progenitors may therefore be a more promising source of tissue for the cellular therapy of diabetes. Nevertheless, these results served as a proof-of-concept for using the emulsion process to immobilize and potentially influence the cell fate of primary cells.

The main advantages of the emulsion process over conventional nozzle-based extrusion processes are the scalability and robustness of the process. Emulsion processes are broadly used in the food, cosmetic and pharmaceutical industries. Improvement and scale-up of the emulsion process would draw from the experience gained in these industries. Emulsion characteristics and reaction kinetics could be monitored over time by on-line turbidity, conductivity, FT-IR or Raman spectroscopy measurements (Reis et al. 2007b). In this study it was noted that the emulsion process was less prone to failure. For example, the vibrating nozzle extrusion process was at times interrupted (~1 out of 4 times) by nozzle blockages, which was not a problem with the emulsion process. In addition, 1.5% alginate could not be used with a 250 μm nozzle due to insufficient droplet flight time, leading to tear-drop shaped beads with drag marks. Another advantage of the emulsion process is that the cost of the equipment is negligible compared to commercially available extrusion-based bead generators. Laboratories that do not have access to expensive encapsulators could use the alternative emulsion process. The emulsion process equipment described here allows the average bead diameter to be controlled over a wide range (<250 μm to >1.5 mm) suitable for mammalian cell immobilization by simply adjusting the agitation rate, contrary to nozzle-based extrusion processes where changes in the nozzle diameter and several process parameters would typically be required. Finally, since the gel stiffness can affect the fate of differentiating cells (Engler et al. 2006), the increased gel homogeneity of the internally gelled emulsion beads (Quong et al. 1998) could allow the production of a less heterogeneous cell progeny from an initial stem cell population.

A potential drawback of the emulsion process, particularly for transplantation purposes, resides in the polydispersity of the bead sizes. For islet encapsulation, the fraction of inadequately encapsulated islets increases as the bead size decreases (de Vos et al. 1996), while larger beads exacerbate oxygen limitations, especially for transplantation sites with low oxygen tension such as the peritoneal cavity (Dulong and Legallais 2007; Gross et al. 2007). For the emulsion process, the encapsulation efficiency for cell aggregates such as islets along with the fraction of islets found in beads larger than ~ 1 mm needs to be examined. If loss of the encapsulated cells is not an issue, sieving or settling strategies could be

considered to eliminate small or large beads prior to transplantation to avoid cell death which could exacerbate graft immunogenicity. Alternatively, increased bead homogeneity could be obtained by optimizing the impeller geometry (Giapos et al. 2005; Pacek et al. 1999; Sechremeli et al. 2006) or, if needed, by replacing the stirred system by a membrane emulsion process. The relative uniformity of the gel distribution in internally gelled beads obtained by the emulsion process could also be problematic for *in vivo* immune isolation. For these applications, higher gel density near the bead surface can be a desirable feature due to the resulting increase in the elastic modulus (Moe et al. 1994). Also, if bead coating is found to be required to reduce the bead permeability, higher surface gel density would be preferable because this increases the ionic interactions between the gel and polymer coatings (Thu et al. 1996a).

The emulsion process is an attractive option for the immobilization of mammalian cells that can be readily expanded, such as cell lines, mesenchymal stem cells or ES cells. Immobilized culture of ES cells in alginate beads has been proposed as a means to efficiently scale-up embryoid body formation, the first step in several differentiation protocols (Magyar et al. 2001). Alginate-immobilized culture was conducive to vascular (Gerecht-Nir et al. 2004) and hepatic (Maguire et al. 2006) differentiation of ES cells. The gel concentration and cell seeding density greatly impacted the ES cell progeny. Adjustment of the gel properties could therefore increase the number of parameters that can be modified to control ES cell progeny compared to 2D cultures. Alginate-immobilized culture also promoted chondrogenic differentiation of mesenchymal stem cells (Ma et al. 2003). Finally, peptides, extra-cellular matrix components or growth factors could be tethered to the alginate matrix for added control over stem cell fate or to improve cell survival (Augst et al. 2006).

The potential for use of emulsion-generated alginate beads in transplantation applications should be investigated. The bead biocompatibility, *in vivo* stability and immune isolation properties should be optimized building on the abundant literature related to extrusion-generated beads (de Vos et al. 2006) and the past experiences gained from human clinical trials. For example, CaCO_3 could be replaced by BaCO_3 to increase gel stability.

3.5 CONCLUSIONS

This study demonstrates the feasibility of mammalian cell alginate immobilization using a scalable emulsion and internal gelation process. The process yielded MIN6 cell line survival, growth and function similar to beads generated by extrusion. Primary human pancreatic exocrine cell immobilization was also successful and led to ~70 fold increased insulin expression. The emulsion process is simpler and less expensive than conventional nozzle-based extrusion processes while not compromising the bead performance. This process is suitable for *in vitro* immobilized mammalian cell culture studies and potentially for cell therapy and transplantation purposes.

4 TRANSPLANTATION OF β -CELLS IN ALGINATE BEADS GENERATED BY EMULSION AND INTERNAL GELATION

Having demonstrated that the emulsion and internal gelation process can be used to immobilize and culture a β -cell line *in vitro* in Chapter 3, the goal in Chapter 4 was to assess the potential of the emulsion process for *in vivo* applications. Higher alginate concentrations (10% alginate solution, 112 Pa·s viscosity) could be achieved by the emulsion process than reports for extrusion processes in the literature. Compared to 1.5% alginate beads generated by a standard extrusion process, 5% alginate beads generated by the emulsion process were more stable when perfused with medium *in vitro*. The fraction of the liquid volume of the beads from which antibody-sized molecules were excluded increased from $49 \pm 7\%$ in the 1.5% alginate extrusion-generated beads to 82% in the 5% alginate emulsion-generated beads. When β TC3 cells were transplanted into streptozotocin-induced allogeneic diabetic mice, a significant decrease in the blood glucose levels was seen after 2 days with the 5% emulsion beads but not until >16 days with the 1.5% extrusion beads. This was correlated with higher *in vivo* / *in vitro* DNA yields for the 5% emulsion beads and lower graft-specific plasma immunoglobulin (IgG) levels. These results suggest that the 5% alginate beads produced by emulsion and internal gelation could provide improved protection against allorejection.

4.1 INTRODUCTION

Islet transplantation has emerged as a potential treatment for type 1 diabetes. However, its widespread application remains limited by the requirement for long-term immune suppression to protect the graft from autoimmune (Huurman et al. 2008) and allogeneic (Roelen et al. 2009) rejection, as well as the limited donor tissue supply (Ricordi 2003). Encapsulation of insulin-producing cells in alginate beads has been investigated as a means to avoid the need for immune suppression since the 1980s (Lim and Sun 1980) and has led to several clinical trials of allogeneic (Calafiore et al. 2006b; Scharp et al. 1994; Soon-

Shiong 1999; Tuch et al. 2009) and xenogeneic (Elliott et al. 2007; Living Cell Technologies 2010) encapsulated islet transplantation. The purpose of immune isolation devices such as alginate beads is to provide a physical barrier between the islets and immune cells and their secreted effectors. Ideally, the surface pore size of the beads would be precisely controlled to exclude harmful molecules involved in graft rejection such as IgGs (~150 kDa MW) and certain cytokines (e.g. TNF- α homotrimers, 51 kDa) while allowing access of nutrients, growth factors and the counter-diffusion of waste products and insulin (5.8 kDa). However, alginate beads generated by extrusion and external gelation are permeable to IgG (Kulseng et al. 1997; Nurdin et al. 2000; Strand et al. 2002). The pore sizes range between 5 nm and 200 nm for 2% calcium alginate (Smidsrod and Skjakbraek 1990), which, based on their viscous radius, corresponds to the size of globular proteins ranging between 158 kDa and >1000 kDa (Brissova et al. 1996).

To reduce the bead permeability and also increase the bead strength and stability, various coating strategies have been pursued, mainly using cationic polymers such as poly-L-lysine (Lanza et al. 1999b; Robitaille et al. 2000; Strand et al. 2002), poly-L-ornithine (Calafiore et al. 2004; Calafiore et al. 2006b; De Castro et al. 2005; Luca et al. 2001), polyethyleneimine (Schneider et al. 2001b), chitosan (Gaserod et al. 1998), polymethylene-co-guanidine (Renken and Hunkeler 2007a) or polyvinylamine (Renken and Hunkeler 2007b). Unfortunately, the cationic polymers used for coating lead to complement (Darquy et al. 1994) and macrophage activation (Juste et al. 2005; Pueyo et al. 1993; Strand et al. 2001), and have been associated with fibrotic overgrowth of the beads (Duvivier-Kali et al. 2001; King et al. 2003a; King et al. 2001). To shield the cationic polymers from the immune system and reduce fibrotic overgrowth, additional non-immunogenic coating layers such as alginate (King et al. 2003b) or polyacrylic acid (Bunger et al. 2003) have been added. This leads to decreased bead surface charge (Hunt et al. 1996; Schneider et al. 2004) and hence reduced zeta potential (de Vos et al. 2007) and this is correlated with reduced fibrotic overgrowth of the beads. Nevertheless, complete shielding of the cationic polymer by additional coatings has not yet been achieved, limiting the biocompatibility of these coated beads (Juste et al. 2005; Orive et al. 2006; Tam et al. 2005).

Alternatively, uncoated alginate beads have allowed the survival of allogeneic or xenogeneic islets in rodents (Cui et al. 2009; Duvivier-Kali et al. 2001; Lanza et al. 1999b; Omer et al. 2005) and larger mammals (Dufrane et al. 2006b; Lanza et al. 1999a; Soonshiong et al. 1992; Sun et al. 1996) for > 14 weeks. For example, uncoated barium alginate beads with MWCO values of 600 kDa (Omer et al. 2005) provided blood glucose normalization of non-obese diabetic mice for >1 year using allogeneic islets (Duvivier-Kali et al. 2001). Since uncoated alginate beads have a broad pore size distribution (Smidsrod and Skjakbraek 1990), the volumetric fraction of the beads from which antibodies or cytokines are excluded may be a more relevant measurement that is usually not provided. This volumetric fraction can be determined by size exclusion chromatography at low flow rates using molecules of known size that do not bind to the beads. The %volume exclusion from the bead liquid volume is then equivalent to $1-K_{SEC}$, where K_{SEC} is the partition coefficient in the beads (Brissova et al. 1996). The relationship between the MWCO and $1-K_{SEC}$ values for molecules of various sizes depends on the bead pore size distribution. To provide one comparison, the value of $1-K_{SEC}$ for uncoated alginate/cellulose sulfate beads with a MWCO of 750 kDa was 0.5 (50% exclusion from the bead pore volume) for antibody-sized (150 kDa protein) molecules (Brissova et al. 1998). The protection offered by uncoated beads despite antibody penetration underlines the importance of events unrelated to the antibody-dependent response to the graft. Foremost, shielding the donor cells from direct contact with host T-cells should avoid the acute rejection of human leukocyte antigen-mismatched grafts (Bharat and Mohanakumar 2007; Gray 1997). In addition, the uncoated beads may offer some protection from the innate response triggered by the transplantation surgery (de Vos et al. 2002; Lai et al. 2009). The beads may also reduce stress to islets by dampening islet environmental changes and this in turn may reduce the secretion of pro-inflammatory molecules by the islets (de Vos et al. 2003a). Lastly, the beads may retain some of the cell fragments and antigens released by apoptotic or necrotic graft cells, and this could reduce the subsequent adaptive response to the graft.

Because of the immune reaction to cationic polymers, new strategies to reduce the alginate bead pore size should be pursued. Chapter 3 described the novel adaptation of an

emulsion and internal gelation process to pancreatic cell immobilization and *in vitro* culture. The emulsion process is more scalable than the traditional method of bead generation by extrusion and external gelation.

Chapter 4 describes the novel application of these beads for immune isolation *in vivo*. It was hypothesized that the emulsion process could allow the production of high-density alginate beads with reduced permeability to antibodies and improved immunoprotection than the lower-density beads produced with extrusion-based cell encapsulators used in most transplantation trials (Table 1.1). First, the alginate solution concentrations and viscosities that allowed bead generation by the emulsion process were determined. The bead strength, stability and size exclusion profiles were compared between 1.5% alginate extrusion-generated beads and 1.5% as well as 5% alginate emulsion-generated beads. Next, β TC3 insulinoma cells (derived from mice with H2 haplotype b/d) were encapsulated in the three bead types and transplanted into allogeneic (H2 haplotype b) streptozocin-treated diabetic mice. Encapsulated β TC3 were also cultured *in vitro* to determine cell growth in the absence of *in vivo* nutrient limitations or immune rejection. The performance of the beads *in vivo* was assessed by monitoring blood glucose levels, body weight and insulin concentration in serum. In addition, the beads were retrieved from the animals to assess cell expansion, insulin expression and bead overgrowth by host cells. Finally, the host immune reaction was investigated by quantifying immune cells present at the site of the transplant (in the peritoneal cavity), as well as plasma levels of antibodies raised against the graft cells.

4.2 MATERIALS AND METHODS

4.2.1 Cell culture

β TC3 cells were cultured in DMEM medium supplemented with 10% fetal bovine serum (FBS), 6 mM glutamine, 100 units/mL penicillin and 100 μ g/mL streptomycin (all from Invitrogen). Adherent cultures were maintained at 37°C and 5% in a humidified incubator and tissue culture treated T-flasks (Sarstedt). Alginate-immobilized cultures in beads were maintained in the same medium, with 1 mL beads for 10 mL total culture volumes in 25 cm²

suspension T-flasks (Sarstedt). Half of the medium was exchanged every 2~3 days by placing the flasks with the vent facing upward, letting the beads settle to the bottom of the flasks, removing the medium in excess of 5 mL and adding 5 mL of fresh medium.

4.2.2 Alginate

Unless otherwise indicated, the alginate used was a 50:50 mixture of transplant-grade LVM alginate and MVG alginate (Novamatrix). The viscosity provided by the manufacturer for a 1% solution of LVM alginate at 25°C was 0.024 Pa·s and the mannuronic:guluronic acid content was 60%:40% (Novamatrix Product Information). The viscosity of a 1% MVG alginate solution was 0.33 Pa·s and the mannuronic:guluronic acid content was 27%:72%. Initial experiments to develop the high-concentration beads also made use of Sigma A0682 alginate. For the 5% alginate beads, 5.83% LVM:MVG (50:50) alginate (i.e. 2.92% of each alginate type) was dissolved in HEPES-buffered saline solution (described in Section 3.2.1). For the 1.5% alginate beads, 1.75% LVM:MVG alginate was dissolved in MOPS-buffered saline solution (described in Section 3.2.1). All alginate solutions were sterilized by autoclaving for 30 min at 101 kPa and 122°C.

4.2.3 Microencapsulation by emulsion and internal gelation

Alginate bead generation by emulsion and internal gelation was performed as described in Section 3.2.2 except for different alginate types, concentrations and agitation rates. Also, at alginate concentrations of 5% and above, the alginate solutions were heated to 37°C to allow flow through syringes, which was precluded by their high viscosity at room temperature. The viable cell concentration in the alginate + cells + CaCO₃ mixture prior to emulsification was 6 × 10⁶ cells/mL for the 1.5% alginate beads or 10.8 × 10⁶ cells/mL for the 5% alginate beads. A higher initial cell concentration was used for the 5% beads with the HEPES-buffered process because the cell survival was expected to be ~50% compared to ~90% for the MOPS-buffered process based on a preliminary experiment. The cell survival was higher than expected in the 5% beads, at 76 ± 2%. The 500 mM CaCO₃ suspension used was prepared in HEPES-buffered saline for 5% alginate beads and in MOPS-buffered saline for

1.5% alginate beads. After bead generation, the beads were filtered on a 40 μm cell strainer, transferred into medium and quantified by volume displacement (see also Section 3.2.2).

4.2.4 Microencapsulation by extrusion and external gelation

The extrusion process was performed using 1.5% LVM:MVG alginate dissolved in MOPS-buffered saline solution as described in Section 3.2.3.

4.2.5 Alginate bead size distribution

The toluidine blue imaging technique described in Section 3.2.4. was used to determine the alginate bead size distribution and the value of the surface area moment average bead diameter (D_{32}).

4.2.6 Alginate viscosity

Rheological measurements of dynamic viscosity of autoclaved alginate samples were performed using a stress-strain controlled Rheometer AR2000 (TA Instruments, DE) with plate-plate geometry (steel plate, diameter 40mm, gap 0,5 mm). The dynamic viscosity was measured over a shear stress range 0.01 – 1000 Pa at 25°C. The samples were equilibrated for 5 min in the rheometer after loading prior to testing. A steady flow ramp was applied to alginate solutions with $\geq 3\%$ alginate and a steady flow was applied for lower concentrations. The zero-shear viscosities were determined from the dynamic viscosity profiles as a function of shear stress based on the Cross model (Equation 1.2). A Huggins-type equation (1942) with combined higher order terms (Kulicke et al. 1990; Storz et al. 2009; Storz et al. 2010) was used to model the relationship between the zero-shear viscosities and the alginate concentration (Equation 1.3). The data shown represents the average \pm SEM of 3 batches prepared separately, with the value for one batch representing the average of 2 to 3 analytical replicates.

4.2.7 Cryo-scanning electron microscopy (cryo-SEM)

Samples of alginate beads were stored in HEPES-buffered saline solution at 4°C until analysis by cryo-SEM. The beads and solution were transferred onto filter paper, the solution was removed by suction and a piece of the filter with beads was glued onto a metal holder that was immediately plunge-frozen in liquid nitrogen. In some cases, a razor blade

was used to section beads a few seconds prior to freezing. The samples were transferred using a Leica EM VCT Cryo-Transfer System into a Hitachi S-2600N Variable Pressure Scanning Electron Microscope at -120°C under vacuum. Surface water was sublimated for 5 min at -105°C before acquiring images at 2000-fold magnification with an accelerating voltage of 3kV.

4.2.8 Inverse size exclusion chromatography and data analysis

Two batches of alginate beads were generated for each of the processes compared: 1.5% alginate beads generated by the extrusion process, 1.5% alginate beads generated by emulsion process and 5% alginate beads generated by the emulsion process. The beads were generated without cells by replacing the cell stock with MOPS-buffered saline solution in the case of the extrusion process or medium in the case of the emulsion processes. The beads were used to pack chromatography columns (0.785 mL, OMNIFIT, Cambridge, England) for inverse size exclusion chromatography measurements as previously described (Brissova et al. 1996). Pullulan standards of 0.667 kDa to 404 kDa molecular weight (Varian, Palo Alto, CA) were injected into the column at 3 mg/mL concentration and 0.2 mL/min flow rate using CMRL medium with 100 ppm sodium azide (AFT Bratislava s.r.o., Slovakia) as the mobile phase. This flow rate was low enough for pullulans to reach equilibrium between the mobile and stationary phases, allowing permeability measurements that were not affected by diffusion rates, based on the linear relationship between K_{SEC} and the distribution coefficient in static equilibrium experiments (Brissova et al. 1996). The elution volume (V_e) was defined as the volume at which 50% of the pullulan standard was eluted, as measured by a refractive index detector (ERC-7515A by Varian) and analyzed by the PGF Unity software (Polymer Standards Services GmbH, Mainz, Germany). The void volume (V_0) was determined by the elution of a 805 kDa pullulan standard assumed to be completely excluded from the beads and the total permeable volume (V_t) was determined by the elution volume of saccharose. The partition coefficient (K_{SEC}) for each standard was calculated by the $(V_e - V_0)/(V_t - V_0)$ ratio (see Section 1.3.1., Equation 1.3). The values of $1 - K_{SEC}$ were plotted as a function of the log value of the pullulan molecular weight fitted to the sigmoidal

function $Y = k_1 + \frac{k_2}{1 + \exp(k_3 - k_4 \log(MW))}$, where the k_i values are empirical constants and

MW is the molecular weight (Brissova et al. 1998). The chromatography testing of each batch of beads lasted for 7 days, during which the beads were continuously perfused.

4.2.9 Bead mechanical properties

For each batch of beads generated for porosity measurements, a sample of 0.2 mL beads was kept for mechanical testing. Emulsion-generated beads were hand-picked to be similar to the average bead diameter measured for the extrusion-generated beads, $652 \pm 30 \mu\text{m}$. After hand-picking, the average bead diameter of the 1.5% alginate emulsion-generated beads was $706 \pm 171 \mu\text{m}$ and $862 \pm 239 \mu\text{m}$ for the 5% alginate beads. The bursting force and bead deformation were determined in compression mode as described in Section 3.2.8. The bead mechanical properties were assessed for each batch of beads before and after the 7 days of continuous CMRL perfusion required for the size exclusion chromatography measurements.

4.2.10 Transplantation, animal monitoring and sampling

Male C57BL/6 mice (Jackson Labs) were injected intravenously with $0.03 \text{ mg}/\mu\text{L}$ freshly prepared streptozotocin (Sigma) dissolved in 0.1M sodium citrate buffer, pH 4.5, at a dosage of 200 mg/kg to induce diabetes (or buffer alone for non-diabetic controls) 7-9 days prior to transplantation. Diabetic animals were selected based on two consecutive fasting blood glucose readings above 20 mM. The experimental groups consisted of 3×10^6 βTC3 cells transplanted (1) without encapsulation, (2) in 1.5% alginate extrusion-generated beads and (3) in 5% alginate emulsion-generated beads, in addition to (4) non-diabetic mice that did not receive streptozotocin or cells. Each experimental group consisted of 4 mice, except for 5 mice transplanted with the 1.5% extrusion-generated beads and 8 mice transplanted with the 5% emulsion-generated beads. On the transplantation day, to have similar viable cell numbers in all transplants, the bead volume required per mouse was determined to be 0.493 mL beads for the 1.5% alginate beads generated by extrusion and 0.765 mL beads for the 5% alginate beads generated by emulsion. The beads were washed 5 times with phenol red-free DMEM medium containing 5.6 mM glucose and 2 mM glutamine (Invitrogen) without serum. The beads were then filtered on a $40 \mu\text{m}$ nylon cell strainer and transferred

into the same phenol red-free serum-free medium to transplant 1.5 mL total volume per mouse. By this method, no visible residual oil remained on bead or culture medium surfaces. The beads and medium were injected into the abdominal cavity of Isoflurane-anaesthetized mice through a small midline incision using non-pyrogenic pipette tips cut to create an opening larger than the beads, flame sterilized to remove sharp edges, then autoclaved. The transplant site was closed with sutures, then covered by Lidocaine salve and then wound clips for 7 days. The blood glucose (One Touch Glucometer, Lifescan) and the body weight of mice were monitored after a 4 h morning fast 3 times per week. Plasma samples were collected weekly by centrifuging 75 μ L blood for 9 min at 4000 x g in tubes containing 5 U/mL heparin (Fisher Scientific). Four mice per experimental group were sacrificed 20 days after the transplantation by cervical dislocation after Isoflurane anaesthesia. A large incision was made in the abdomen and the beads were retrieved by peritoneal lavage using 50 mL HEPES-buffered saline solution containing 100 units/mL penicillin and 100 μ g/mL streptomycin, 0.06% bovine serum albumin (StemCell Technologies, Vancouver, BC) and 5 U/mL heparin. The collected solution and beads were filtered on a 40 μ m nylon sieve. The first 10 mL of flow-through were used to quantify peritoneal lymphocytes. The beads were transferred with a spatula into medium to obtain a 1:10 beads:total volume ratio. Images were acquired on a Motic microscope with a 2X objective and fibrotic overgrowth was scored based on the bead surface area covered, assessed visually. Some of the beads (0.15 mL/mouse) were kept overnight for live/dead staining, bead liquefaction as well as DNA quantification. The rest were used for histology. The pancreata of 2 mice per group were also collected for histology after overnight fixation in 4% paraformaldehyde. The UBC Animal Care Committee approved all animal procedures (**Error! Reference source not found.**).

4.2.11 Bead liquefaction and cell enumeration

Bead liquefaction and cell enumeration before transplantation was performed as described in Section 3.2.5. However, after transplantation, the method was modified because fewer beads were available and the beads retrieved from the animals required a higher amount of citrate solution to achieve complete degelling. One day after sacrificing the mice from the

transplantation study, 10 μ L beads from each mouse were settled, the medium was removed to leave 200 μ L total volume (10 μ L beads + 190 μ L medium) and 800 μ L of citrate solution (without medium, described in Section 3.2.5) were added. After 15 min on ice and a rotary shaker at 75 rpm, the cells in 250 μ L of this solution were washed twice with 15 mM citrate, 3 mM EDTA and 150 mM NaCl (pH 7.4) solution before freezing the cell pellet in ~50 μ L of this solution for DNA analysis. DNA was quantified by the Picogreen method described in Section 2.1.14.

4.2.12 Live/dead staining of cells in alginate beads

Live/dead staining was performed by incubation with Calcein AM/Ethidium homodimer (Invitrogen) as described in Section 3.2.10.

4.2.13 Peritoneal lymphocyte quantification

The peritoneal cells in the first 10 mL of the peritoneal lavage were labelled and analyzed by flow cytometry based on the method described by Safley et al. (2005). Briefly, the cells were centrifuged 7 min at 250 \times g and then re-suspended in phosphate-buffered saline solution (PBS, Ca²⁺ and Mg²⁺ free, Invitrogen) containing 1% bovine serum albumin (BSA, StemCell). After trypan blue enumeration using a hemocytometer, two samples of 0.26 \times 10⁶ cells/mouse were centrifuged and re-suspended in 50 μ L PBS + 1% BSA. Then, 1 μ L anti-mouse CD16/32 Fc γ III/II receptor (Stem Cell Technologies) was added to block non-specific binding to the Fc region and the cells were incubated for 5 min on ice. The cells were labelled by adding 50 μ L antibodies diluted 1:400 (except for anti-CD3, diluted 1:30) in PBS + 1% BSA. For each mouse, the first sample was labelled with FITC-conjugated anti-MAC-1 (CD11b), APC-conjugated anti-CD45 and PE-conjugated Ly6G (Gr-1). The second sample was labelled with FITC-conjugated anti-CD3, APC-conjugated anti-CD8 and PE-conjugated anti-CD4. The cells were incubated 30 min in the dark on ice at 75 rpm orbital shaking. Then, 10 μ g/mL of propidium iodide (Sigma, prepared in PBS) were added and the cells were washed twice in PBS + 1% BSA after which the cells were analyzed on a FACS Calibur flow cytometer (BD Biosciences). For each series of stains, single stained controls were also

included. Data analysis including compensation was performed with Flowjo 7.2.5 software (Tree Star, Ashland, OR).

4.2.14 Quantification of graft-reactive antibodies in mouse serum

After being trypsinized and filtered through a 40 µm nylon sieve, 0.25×10^6 βTC3 cells per sample were added drop-wise to 100% ethanol at -20°C and fixed for 30 min on ice with 75 rpm rotary shaking. The cells were then re-suspended in PBS + 1% BSA + 0.5% Tween 20 (Sigma) and incubated on ice for 10 min on a rotary shaker at 75 rpm to permeabilize the cells. The cells were centrifuged, washed in PBS + 1% BSA and then incubated in 1:200 mouse sera diluted in PBS + 1% BSA for 1 h on ice at 75 rpm rotary shaking. The cells were washed once with PBS + 1% BSA before staining with 1:200 diluted Alexa 647-conjugated goat anti-mouse IgG antibody for 1 h on ice at 75 rpm in the dark. After two washes with PBS + 1% BSA, the cells were analyzed on a FACS Calibur flow cytometer. All samples were analyzed in a single run.

4.2.15 Histology

The remaining beads from all mice of each experimental group were pooled, washed with HEPES-buffered saline solution and then 1 mL saline containing 300 to 500 µL beads were fixed with 9 mL Bouin's solution (8.8% formaldehyde from 37% formaldehyde and 5% glacial acetic acid, Fisher Scientific). After 15 min of fixing on ice at 50 rpm on a rotary shaker, the beads were washed twice with HEPES-buffered saline solution and kept overnight before agarose and paraffin embedding by Waxit© histological services (Vancouver, BC). Pancreata were fixed by overnight incubation in 4% paraformaldehyde prepared in PBS and directly embedded in paraffin. Paraffin sections of 5 µm thickness were exposed for 5 min/incubation to 3 incubations in xylene, 2 incubations in 100% ethanol, an incubation in 95% ethanol and an incubation in 70% ethanol. The sections were washed in PBS and microwaved for 3 x 5 min at 700 Watts in 10 mM citrate buffer with 0.05% Tween 20 at pH 6.0 for proliferating cell nuclear antigen (PCNA) antigen retrieval. After washing with tap water, distilled deionized water (ddH₂O) and PBS, Serum-Free Protein Block (Dako) was added for 10 min at room temperature in a humid chamber. The blocking

solution was removed and primary antibodies were added for overnight incubation at 4°C in a humid chamber. Primary antibodies consisted of guinea pig anti-human insulin (1:1000 dilution, Linco) mixed with mouse anti-PCNA (1:200 dilution, BD Biosciences) diluted in Antibody Diluent (Dako). For pancreas samples, sections were alternatively stained with guinea pig anti-human insulin (1:1000 dilution) mixed with mouse anti-glucagon (1:1000 dilution, Sigma). The next day, the sections were washed with PBS and incubated for 1 h at room temperature and 75 rpm orbital shaking in the presence of secondary antibodies. These consisted of Alexa 488 labelled goat anti-guinea pig and Alexa 568 labelled goat anti-mouse antibodies (both at 1:250 dilution, Invitrogen) diluted in Antibody Diluent. The slides were washed with PBS, then ddH₂O, followed by 15 min staining with 1 µg/mL 4',6-diamidino-2-phenylindole (DAPI, Invitrogen) diluted in ddH₂O. The slides were washed in PBS before mounting with #1.5 coverslips using Vectasield mounting medium (Vector Labs, Burlingame, CA). Fluorescent images were acquired on a LSM 510 Meta confocal microscope (Carl Zeiss International, Oberkochen, Germany) using the LSM Image Browser 4.2.0.121 software.

4.2.16 Statistical analysis

Statistical comparison was based on 2-tailed Student's t-tests and the reported errors represent the standard error of the mean (SEM) for three replicate experiments, unless otherwise noted. Results were considered to be statistically significant for $p < 0.05$.

4.3 RESULTS

4.3.1 Emulsion process alginate concentration and viscosity operating range

Sigma alginate solutions of 0.5% - 10% with zero-shear viscosities ranging between 0.004 Pa·s and 112 Pa·s allowed bead generation by the emulsion and internal gelation process. The pH was controlled by a 10 mM HEPES buffer and the duration of the emulsification and acidification were respectively 12 min and 8 min. This overall 20 min HEPES process was used rather than the 4 min MOPS-buffered process optimized for *in vitro* applications in Chapter 3 because more complete CaCO₃ dissolution and maximal

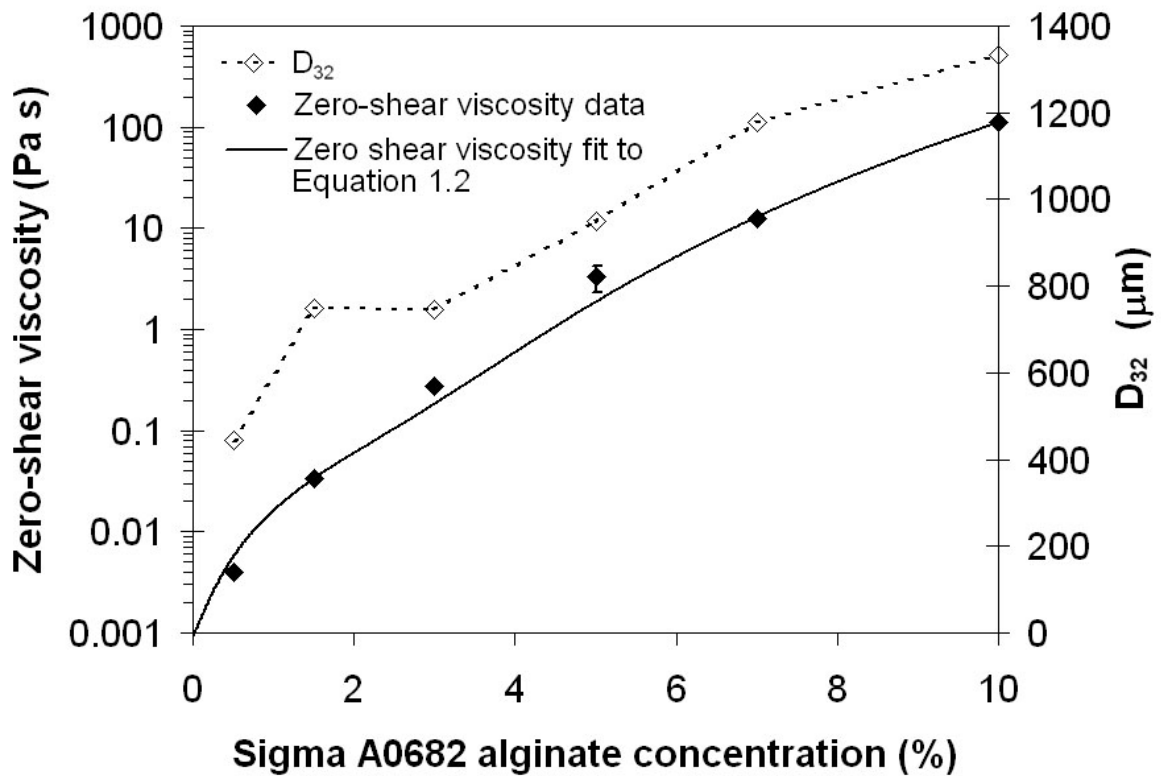


Figure 4.1. Effect of alginate concentration on the solution zero-shear viscosity and on the surface area moment emulsion bead diameter.

The zero shear viscosity was determined from measurements of the dynamic viscosity as a function of shear stress using the Cross model (Equation 1.1) based on the raw data shown in Figure B9. The curve fitting between the zero-shear viscosity data and the alginate concentration shown here was based on a Huggins-type equation with lumped higher order terms (Equation 1.2). Refer also to for the raw images used to calculate the area moment emulsion bead diameter (D_{32}). Each data point represents the average of 2 to 3 analytical replicates. The point with error bars represents the average \pm SEM of 3 replicate alginate preparations.

alginate cross-linking were desired for *in vivo* applications. The beads generated by the 20 min HEPES process had been shown to be more resistant to compression than the beads generated by the 4 min MOPS process (Figure 3.8 in Chapter 3), which is desirable to avoid bead damage during the surgery and *in vivo*. Moreover, the process optimization in Chapter 3 was performed with 1.5% alginate, but the conclusions may not hold for high-concentration beads, where complete alginate cross-linking may require longer reaction times. Figure 4.1 shows the zero-shear viscosity of the Sigma alginate solution and the surface area moment average bead diameter (D_{32} , defined by Equation 3.1 in Section 3.2.4) as a function of alginate concentration. At 500 rpm, the beads generated from 0.5% to 7%

alginate were highly spherical, with a circularity of 0.97 ± 0.01 . The circularity of the 10% beads was somewhat reduced, at 0.91 ± 0.01 . The distance between the bottom of the impeller blades and the spinner flask was 5 mm (see Section 3.2.2), which is close to the 2.8 mm diameter of the largest 10% alginate beads measured. The value of D_{32} was approximately proportional to the log-value of the viscosity (Figure B10 in Appendix B). This confirms the observation made in Section 3.4 that surface tension rather than viscous forces mainly governs bead size. In the opposite case, based on Equation 1.4, the value of $D_{32}^{4/3}$ would be expected to be proportional to the viscosity, not the log-value of the viscosity. Equation 1.4 is based on dynamic viscosities, but even at 1000 Pa shear stress, these are not orders of magnitude lower than the zero-shear viscosities (Figure B9 in Appendix B). Lastly, the zero-shear viscosities of the LVM:MVG alginate solutions used for the transplantation experiments were 0.05 Pa·s for 1.5% alginate and 3.3 Pa·s for 5% alginate.

4.3.2 Bead porosity, surface topography and strength

The bead porosity, surface topography and strength were analyzed. Figure 4.2 shows the bead permeability to pullulan standards measured by size exclusion chromatography, with the pullulan molecular weights converted to equivalent protein molecular weights based on their viscosity radius (Brissova et al. 1996). The value of $1-K_{SEC}$ corresponds to the volumetric fraction of the liquid volume in the beads from which the pullulan standards are excluded. A value of 1 therefore represents complete exclusion from the beads. The change between exclusion and permeation occurred between molecular weights of 10 kDa to 2500 kDa for both the emulsion and the extrusion-generated 1.5% alginate beads, with a higher rate of change for the emulsion beads. The values of $1-K_{SEC}$ of the 5% beads was significantly lower than both 1.5% alginate bead types between pullulan molecular weights of ~1 kDa to 113 kDa, corresponding to equivalent protein molecular weights of ~1 kDa to 884 kDa. The value of $1-K_{SEC}$ for antibody-sized molecules (150 kDa proteins) was 0.82 for the 5% emulsion beads compared to 0.49 ± 0.07 for the 1.5% extrusion beads and 0.26 for the 1.5% emulsion beads. Thus, ~80% of the 5% emulsion bead volume can be expected to exclude antibody sized molecules. This also was reflected in the pore size distribution curves estimated from the derivative of the $1-K_{SEC}$ versus the pullulan molecular weight: the peak of

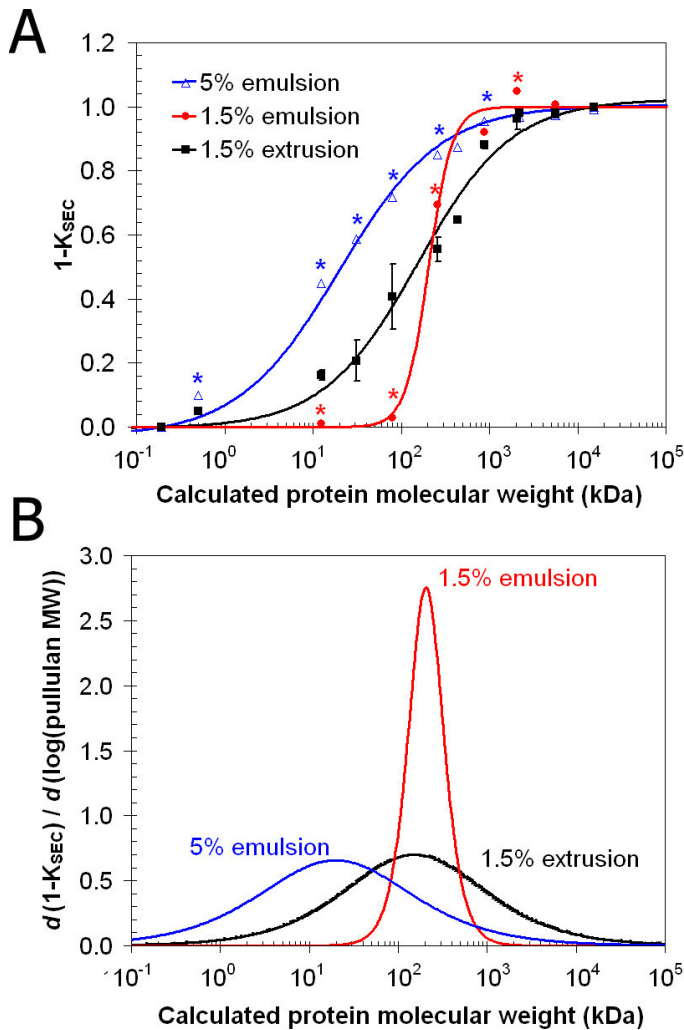


Figure 4.2. Bead permeability measured by size exclusion chromatography.

(A) Volumetric fraction of the beads from which the pullulan standards are excluded ($1-K_{SEC}$) as a function of pullulan molecular weight converted to equivalent protein molecular weight. (B) Slope of the curve shown in (A) as a function of the protein molecular weight. The shape of this curve provides an estimate of the pore size distribution. The maxima of the distributions occur at 20 kDa (2 nm viscous radius) for the 5% emulsion beads, 153 kDa (4.6 nm viscous radius) for the 1.5% extrusion beads and 207 kDa (5 nm viscous radius) for the 1.5% emulsion beads. *Values higher or lower than the 95% confidence interval of the 1.5% extrusion beads, determined from 3 preparations of 1.5% alginate extrusion beads.

the pore size distribution for the 5% beads occurred at ~ 20 kDa (protein equivalent molecular weight) compared to >150 kDa for both of the 1.5% alginate bead types (Figure 3B).

Figure 4.3 shows that the alginate gel networks at the surface of the 1.5% extrusion-generated beads (Figure 4.3A) and the 5% emulsion-generated beads (Figure 4.3D) were denser than for the 1.5% emulsion-generated beads (Figure 4.3B). The alginate structures at the surface of the 5% emulsion-generated beads formed alveolar cavities of $0.5\text{--}1.5$ μm diameter with internal gel interstitial spaces as small as $20\text{--}50$ nm. The internal gel structure of the 5% emulsion bead (Figure 4.3E) seemed as dense or denser than the surface.

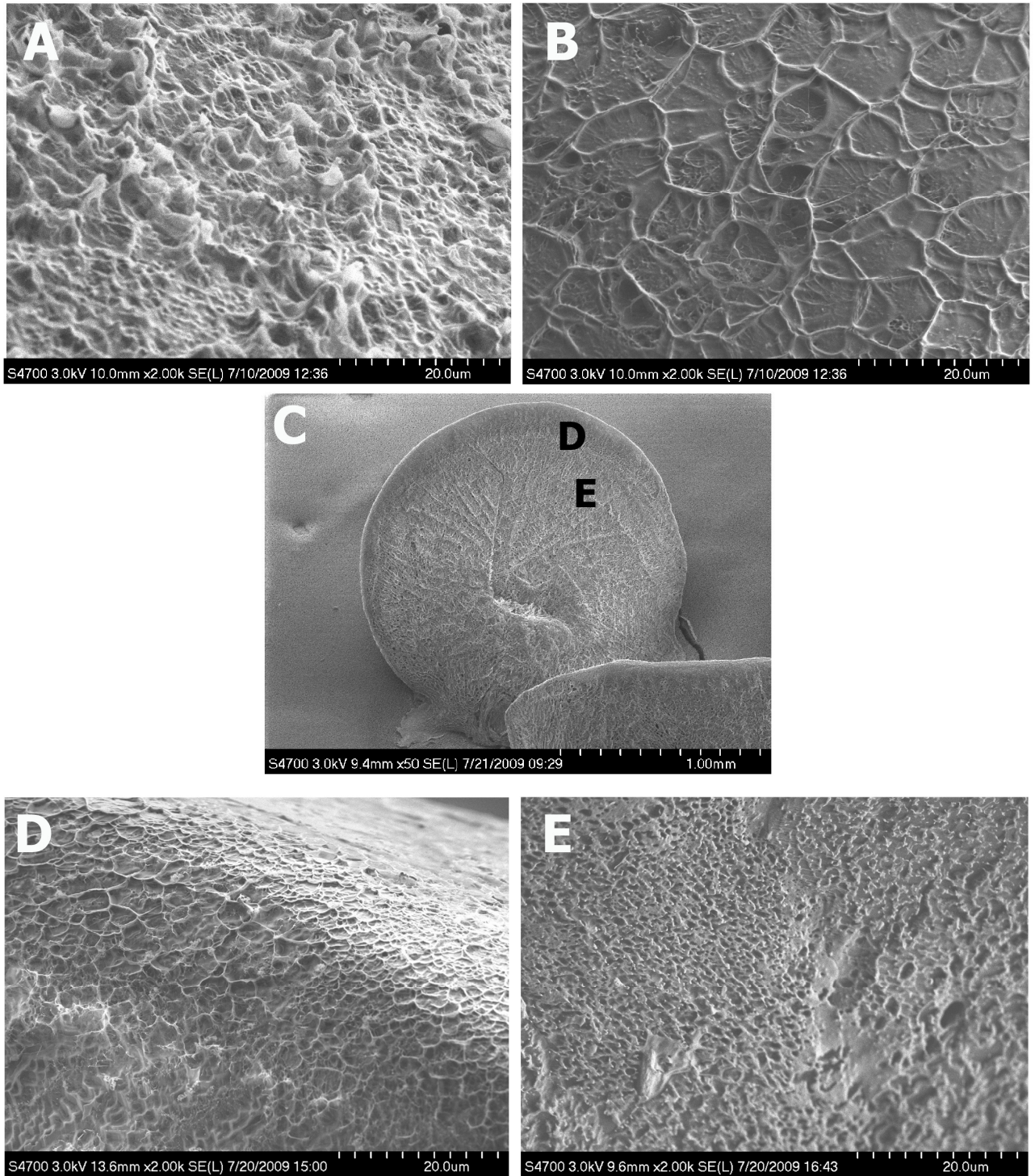


Figure 4.3. Cryo-scanning electron micrographs of the alginate bead surface.

A) 2% extrusion alginate bead generated with the Inotech encapsulator; B) 2% alginate emulsion bead generated with the 4 min MOPS process; C) Two halves of a cut 5% emulsion bead with the cut surface of one half facing the camera. The approximate locations where the D and E images were acquired is indicated. D) Surface of the bead + cut surface facing the camera. E) Cut surface further from the edge towards the inside of the bead.

Figure 4.4 shows the compressive load that could be applied before bead rupture was measured before and after 7 days of perfusion with CMRL medium during the chromatography measurements. Prior to perfusion, the bead rupture load was 31.2 ± 0.2 mN for the 1.5% extrusion-generated beads, which was significantly higher than the 4 ± 1 mN rupture load of the 1.5% emulsion-generated beads but not significantly different from the rupture load of 30.2 ± 0.9 mN of the 5% emulsion-generated beads. However, the rupture

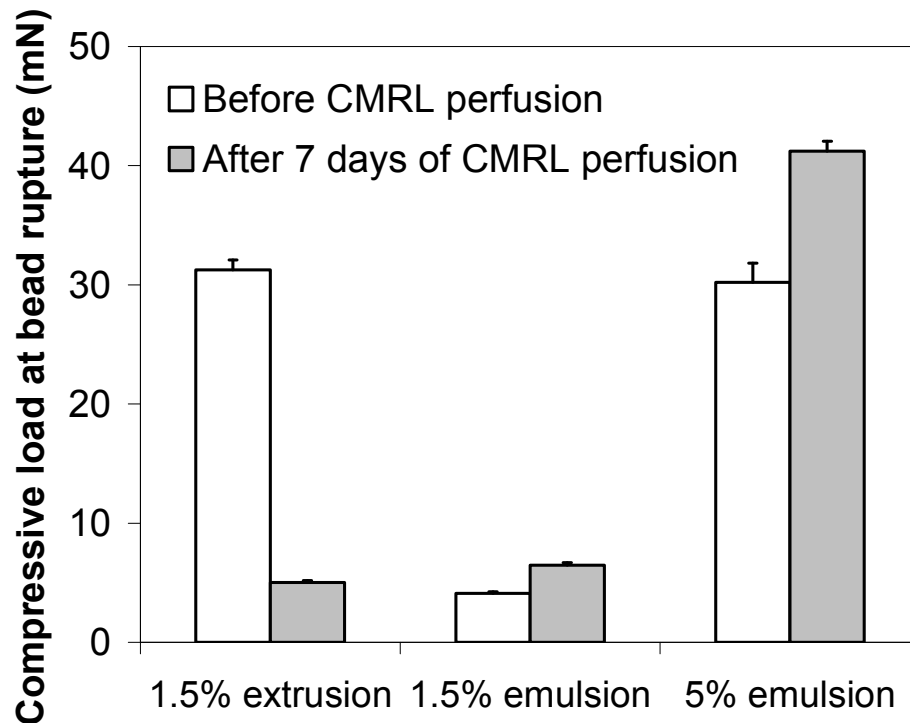


Figure 4.4. Bead rupture strength before and after size exclusion chromatography.

load of the beads generated by extrusion significantly decreased during the chromatography to 5 ± 3 mN. The decrease in the gel strength of these externally gelled beads may be a result of chelation by the CMRL medium used for the chromatography. CMRL contains 1 mM phosphate buffer that could chelate calcium and 150 mM monovalent cations that could be exchanged with calcium. If significant chelation occurred during the chromatography, this may have led to an under-estimation of $1-K_{SEC}$ of the initial beads, but this would better reflect *in vivo* conditions (Smidsrod and Skjakbraek 1990). On the other

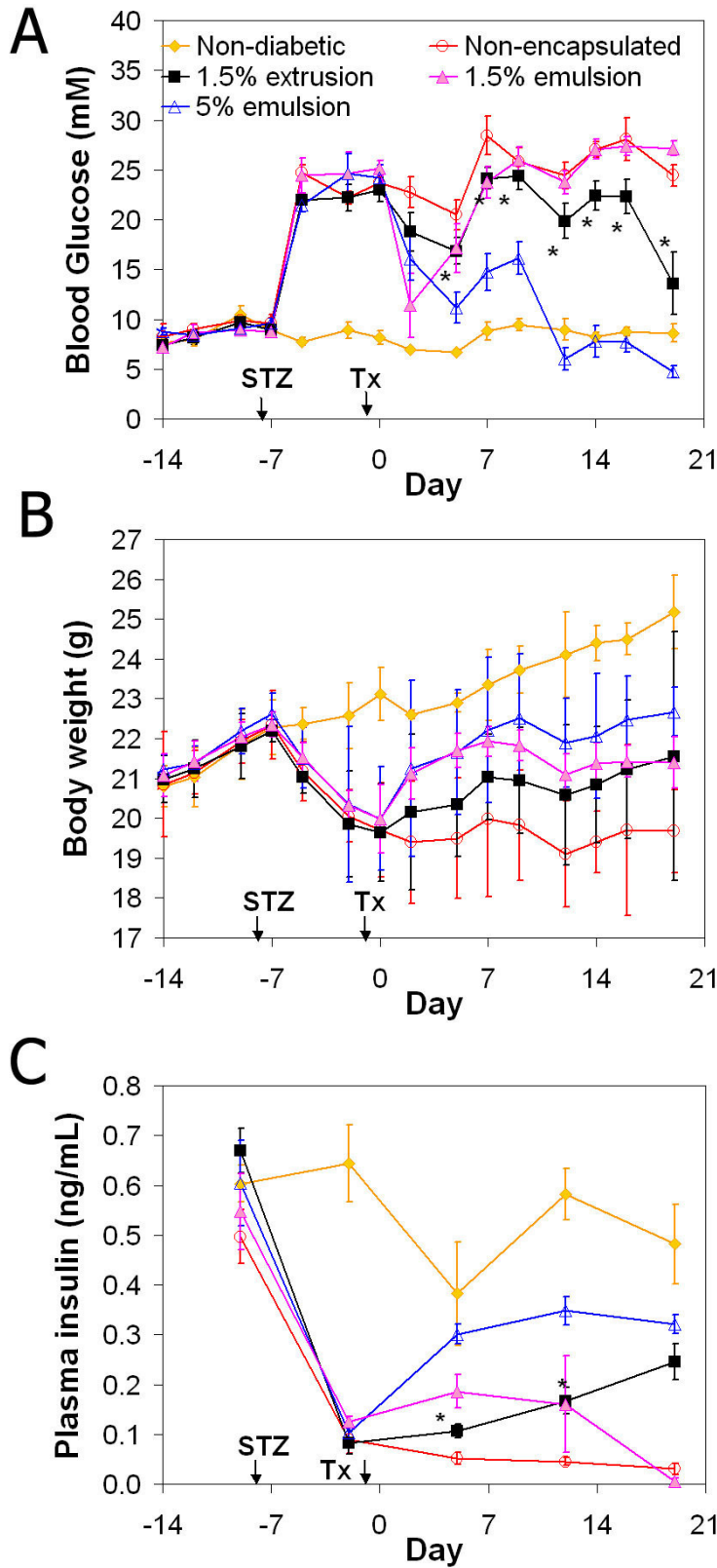


Figure 4.5. (A) Blood glucose (B) body weight and (C) plasma insulin profiles of C57BL/6 mice transplanted with encapsulated β TC3 cells.

The experimental groups included cells encapsulated in 1.5% alginate beads generated by extrusion and external gelation (N = 5, black) or 1.5% (N = 4, purple) and 5% (N = 8, blue) alginate beads generated by emulsion and internal gelation. Controls were non-diabetic mice with sham surgery (N = 4, yellow) or mice transplanted with the same number of non-encapsulated cells (N = 4, red). STZ: day of the streptozotocin treatment to induce diabetes. Tx: day of the transplantation. * $p < 0.05$ for 1.5% extrusion compared to 5% emulsion beads.

hand, the rupture load was not significantly changed after the chromatography experiment for the beads generated by the emulsion processes. In sum, the bead rupture strength of the 5% emulsion-generated beads was comparable to the strength of the 1.5% extrusion-generated beads, with the advantage for the emulsion-generated beads that they were more stable when exposed to CMRL for 7 days than the extrusion-generated beads.

4.3.3 *In vivo* function of β TC3 cells in emulsion-generated beads

β TC3 cells were transplanted into streptozotocin-induced diabetic allogeneic C57BL/6 mice in 1.5% or 5% alginate beads generated by the emulsion process, and compared to 1.5% alginate beads generated by the conventional extrusion process. The blood glucose levels (Figure 4.5A), body weight (Figure 4.5B) and plasma insulin concentrations (Figure 4.5C) of mice transplanted with control non-encapsulated cells failed to normalize in the 19 days following the transplantation until the mice were sacrificed. The mice transplanted with 1.5% emulsion-generated beads remained diabetic during the 19 days of monitoring, without significant increase in body weight or plasma insulin concentrations. However, the blood glucose levels of mice transplanted with the 5% emulsion-generated beads significantly decreased within 2 days after the transplantation and were not significantly elevated compared to non-diabetic controls 12 days after the transplantation and onward (Figure 4.5A). In contrast, the blood glucose levels of animals implanted with extrusion-generated beads did not significantly decrease until 19 days after the transplantation and were significantly higher than for the 5% emulsion-generated beads throughout the study. The animal body weight and plasma insulin concentrations were consistent with these observations. The body weight of mice transplanted with 5% emulsion-generated beads recovered to pre-streptozotocin treatment levels 9 days after the transplantation (2 tailed paired t-test), while 16 days were required for the mice transplanted with 1.5% extrusion-generated beads to reach these levels. The plasma insulin concentrations measured for the mice transplanted with 5% emulsion-generated beads were also significantly higher than for mice transplanted with 1.5% extrusion-generated beads 5 days and 12 days after the transplantation. The contribution of endogenous pancreatic β -cells to these results was assumed to be negligible based on (1) the lack of recovery in

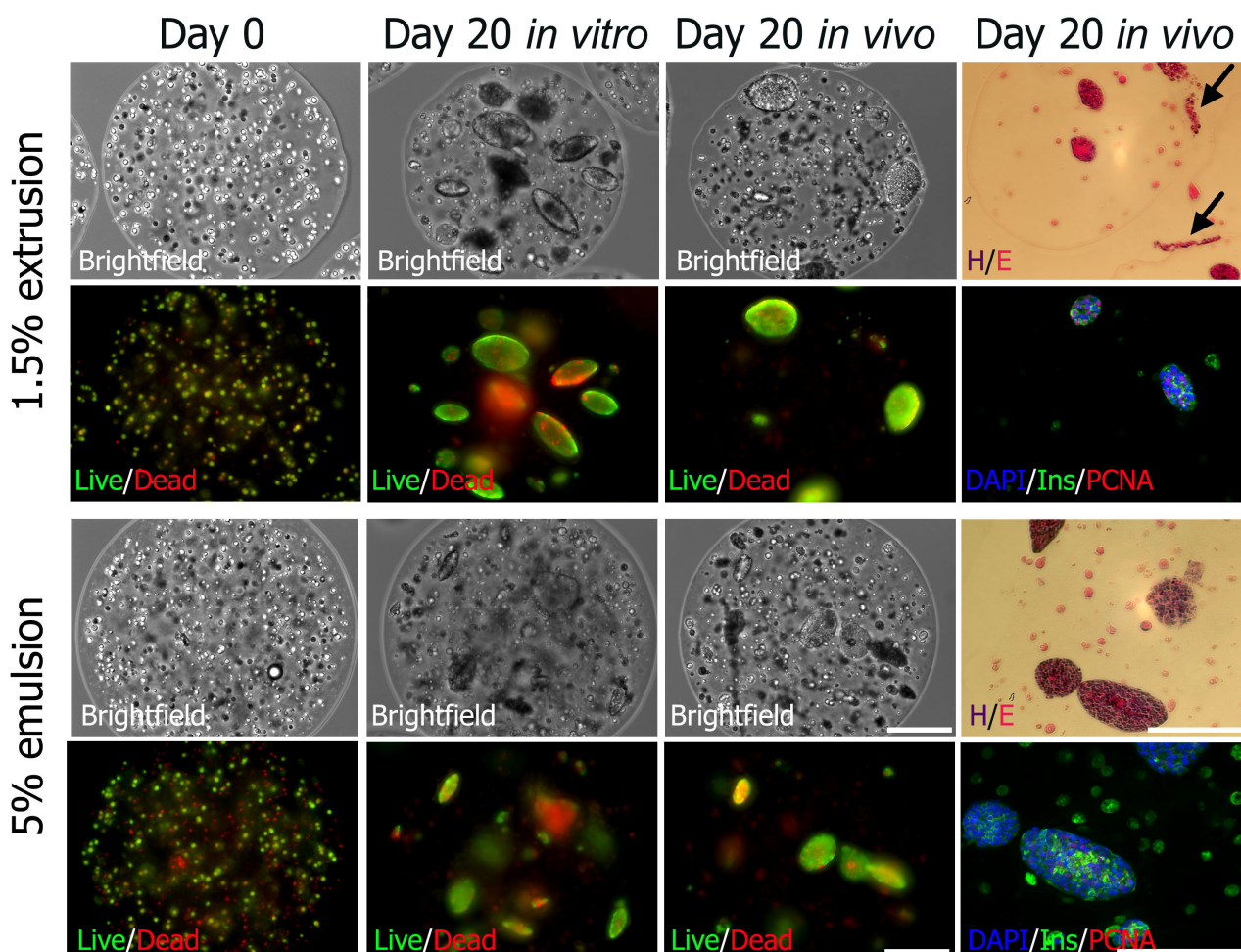


Figure 4.6. Staining of β TC3 cells in alginate beads before and after 20 days *in vitro* or *in vivo*.

For Live/Dead staining, live cells are shown in green due to cleavage of Calcein AM by intracellular esterases while dead cells appear red due to binding of Ethidium homodimer to cellular DNA. Live/dead staining was in fact performed on day 21 for practical reasons. DAPI/insulin (Ins) and proliferating cell nuclear antigen (PCNA) staining used beads fixed immediately after sacrificing the mice on day 20. The arrow points to fibrosis on the surface of an extrusion bead. Note: the same bead is shown in neighbouring H&E and insulin/PCNA stained sections for the 5% emulsion beads, but not the 1.5% extrusion beads. Scale bars (200 μ m) are the same for each type of image (e.g. same scale for all Live/Dead images).

plasma insulin levels for mice transplanted with non-encapsulated β TC3 cells (Figure 4.5C) and (2) on the rarity of β -cells identified in pancreas sections of mice in the experimental groups on day 20 (Figure B11 in Appendix B).

The volumetric bead recovery rate was not significantly different between the three groups, at $45 \pm 11\%$ for the 1.5% extrusion-generated beads, $47 \pm 7\%$ for the 1.5% emulsion-

generated beads and $47 \pm 9\%$ for the 5% emulsion-generated beads. At day 19, the beads recovered from the mice remained spherical for the three bead types (Figure 4.6). Rare beads (<1%) with fibrotic overgrowth were only observed on the 1.5% extrusion-generated beads and <5% of the bead surface was covered (Figure 4.6). Although most animals were sacrificed at day 19 post-transplantation, 4 mice transplanted with the 5% emulsion-generated beads and 1 mouse transplanted with the extrusion-generated beads were kept alive until day 56 post-transplantation. When these mice were sacrificed, fibrotic overgrowth was clearly observed on 32% of the 1.5% extrusion-generated beads (out of 184 beads counted), but on none (out of >200) of the 5% emulsion-generated beads (Figure 4.7).

The beads retrieved from the mice on day 20 were compared by live/dead and insulin/PCNA staining to the initial beads transplanted on day 0 and to beads kept *in vitro* (Figure 4.6). On day 0, the trypan-blue measured viability of the cells encapsulated was $87 \pm 2\%$ in the 1.5% alginate extrusion beads and $75 \pm 2\%$ in the 5% alginate emulsion beads. The live/dead staining observations concurred with these results. For both the extrusion and the emulsion beads, live cell aggregates of 30~150 μm diameter had expanded from the single cells seeded after 20 days of *in vitro* culture. Similar spheroids were also observed in the beads recovered from the mice at day 20, although at a much lower frequency than *in vitro*. For both bead types, the spheroids in the beads recovered from the mice were insulin+ and

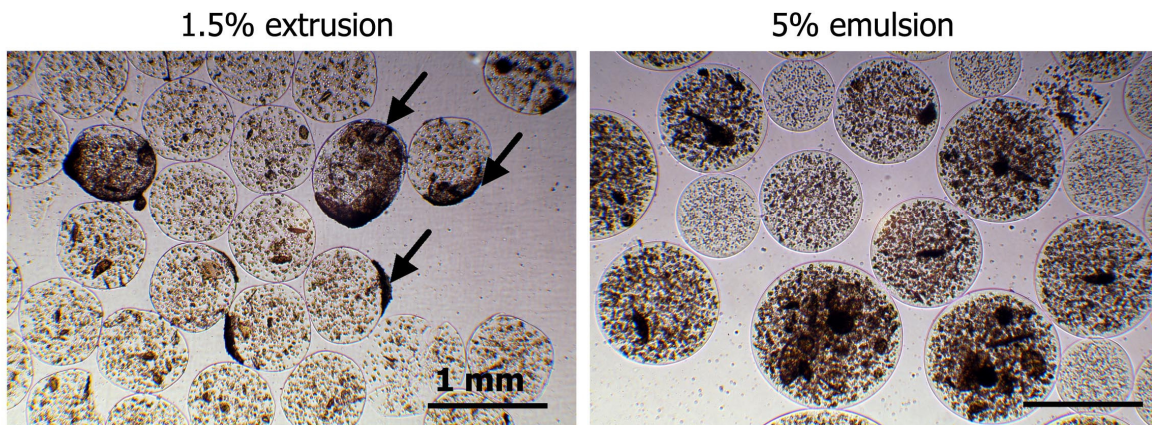


Figure 4.7. Beads retrieved from animals 56 days after transplantation.

Bead fibrotic overgrowth (exemplified by arrows) was observed on the 1.5% extrusion beads (N=1 mouse at day 56). No overgrowth was observed on any of the 5% emulsion beads (N=4 mice).

contained subsets of proliferating cells (PCNA+).

Figure 4.8 shows the total β TC3 cell yield *in vitro* and *in vivo* based on the DNA concentration measured in the beads. *In vitro*, the cell expansion in the 1.5% extrusion bead was significantly higher than in the 5% emulsion beads, with a doubling time of 5.9 ± 0.01 days in the 1.5% extrusion beads and 7.4 ± 0.4 days in the 5% emulsion beads. However, *in vivo* there was no significant increase in the DNA concentration in the beads, even though cell spheroids had formed, suggesting that cell growth was compensated by cell losses. The contribution of DNA from host cells was assumed to be negligible since the cells in the beads were insulin+ (Figure 4.6) and since >99% of the beads were free of fibrotic overgrowth at day 20. Whereas the *in vitro* growth rate of the 5% emulsion beads was lower than for the 1.5% extrusion beads, the DNA concentration had increased by $54 \pm 37\%$ in the 5% emulsion beads and decreased by $28 \pm 26\%$ in the 1.5% extrusion beads after 20 days *in vivo*. Although the difference was not significant, a 2-fold higher cell number in the 5% emulsion beads at day 20 is consistent with the lower blood glucose levels observed in the

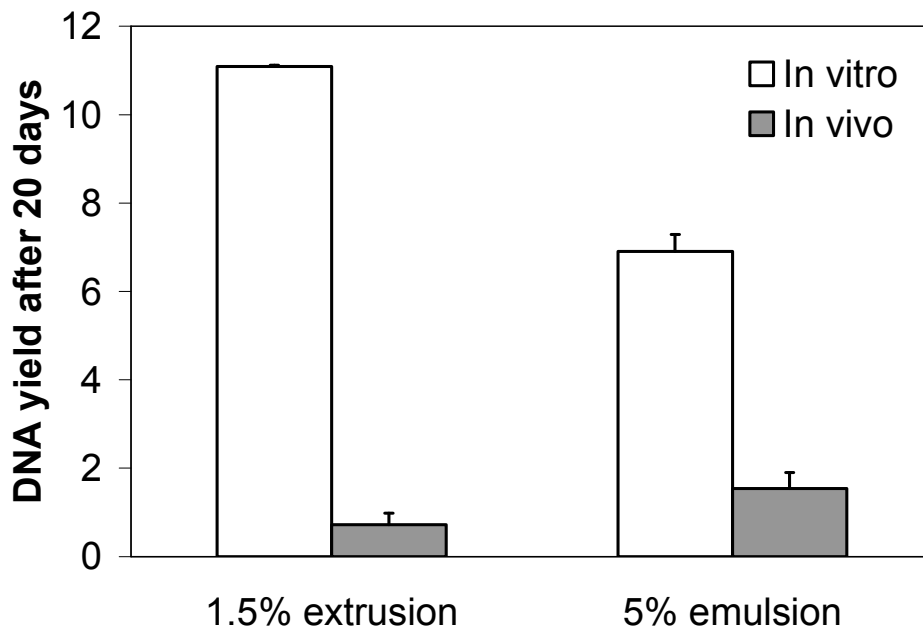


Figure 4.8. DNA yield in the alginate beads after 20 days *in vivo* or *in vitro*.

The DNA yield was determined from the ratio of the DNA concentration (DNA per mL beads) on day 20 to the DNA concentration on day 0.

mice from this group (Figure 4.5A). The blood glucose, body weight, insulin concentration (Figure 4.5), staining (Figure 4.6) and DNA results (Figure 4.8) all indicate that β TC3 cell *in vivo* survival was improved in the 5% emulsion beads compared to the 1.5% extrusion beads.

4.3.4 Adaptive immune response to the grafts

To assess the adaptive immune response elicited by the grafts and beads during the

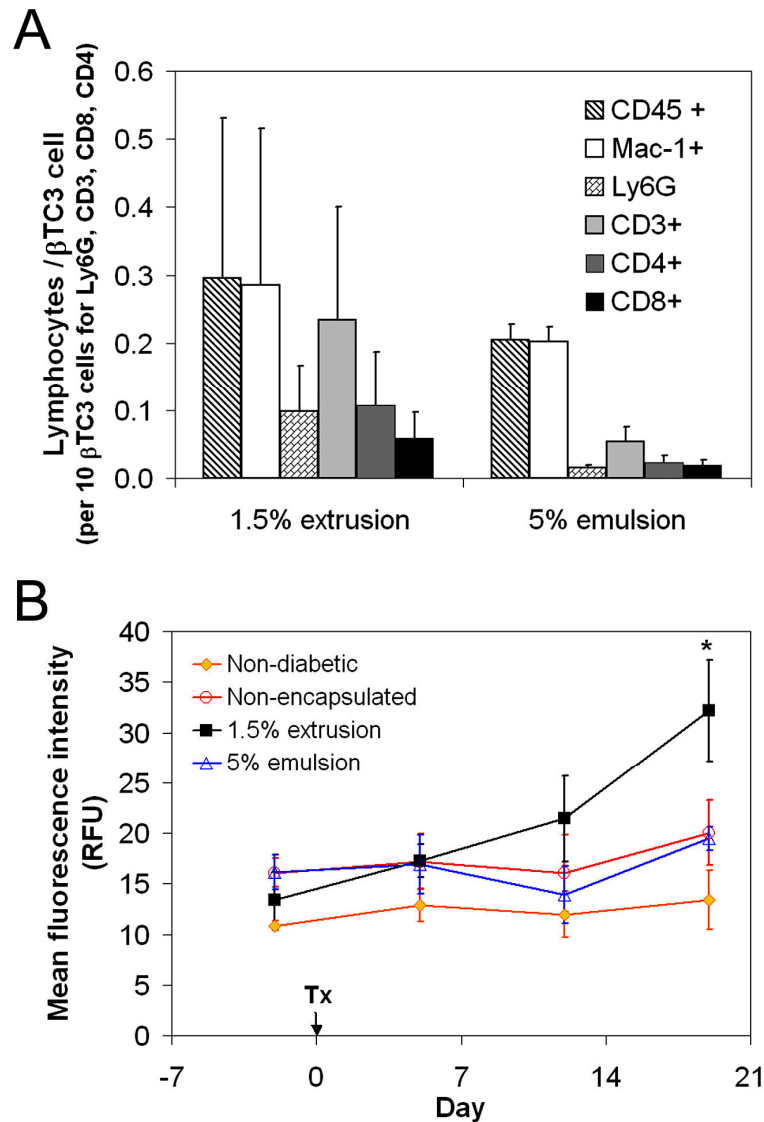


Figure 4.9. Adaptive immune response to the β TC3 graft.

(A) Quantification of peritoneal lymphocytes at day 20. The lymphocyte cell numbers are normalized to the total amount of DNA quantified in the beads collected from the peritoneal cavity. (B) Graft-specific IgG antibody levels in the plasma of the mice. * $p < 0.05$ compared to the 5% emulsion beads. Tx: day of the transplantation.

20 days *in vivo*, peritoneal infiltrating immune cells and antibodies raised against the grafts were examined. Figure 4.9A shows the number of peritoneal lymphocytes (CD45+ cells) recovered from the mice normalized to the total amount of DNA quantified in the beads recovered from each mouse at day 20. There were no significant differences in the lymphocyte/graft cell ratio between the 1.5% extrusion beads and the 5% emulsion beads. However, for all cell types quantified – i.e. lymphocytes via CD45, macrophages via Mac-1, subsets of T cells via CD4 or CD8 – the lymphocyte/graft cell ratio was lower for the 5% emulsion beads.

In Figure 4.9B, flow cytometry of fixed β TC3 cells was used to compare the plasma concentrations of IgGs raised against the graft using diluted mouse plasma for primary labelling and Alexa 647 labelled goat anti-mouse IgG for secondary labelling. There were no significant differences in the fluorescent intensity between non-diabetic non-transplanted controls and mice transplanted with 5% emulsion beads. There was also no significant increase in the fluorescent intensity for plasma collected from mice transplanted with non-encapsulated β TC3 cells. Conversely, the fluorescent intensity measured for plasma collected from mice transplanted with the 1.5% extrusion beads was significantly higher than the 5% emulsion bead and non-diabetic groups by day 19. The fluorescent intensity measured did not significantly increase until day 54 for the mice transplanted with 5% emulsion beads kept alive until day 56, while the signal measured for the mouse transplanted with 1.5% extrusion beads steadily increased to reach 39 RFU by day 54 (data not shown). To determine whether the mouse anti-graft IgG antibodies were able to penetrate the beads and bind to the cells inside, Alexa 568-labeled goat anti-mouse IgG was added directly to the beads for 1 h (Figure B12 in Appendix B). During this incubation time, if the beads were permeable, the goat IgG should diffuse to a certain distance into the beads and strongly bind mouse IgG molecules encountered. Based on the background staining in Figure B12, goat IgG could indeed diffuse into the beads and equilibrium was not reached within 1 h. The non-cell associated Alexa 568 background labelling was lower in the 5% emulsion beads than in the 1.5% extrusion beads (Figure B12 in Appendix B), consistent with the higher $1-K_{SEC}$ values of these beads. The mouse IgGs detected were concentrated on

single cells within the beads. Since single cells were mainly found to be dead cells in Figure 4.6, this suggested that most of the mouse IgGs detected were raised against intracellular antigens.

4.4 DISCUSSION

The goal of this study was to determine whether alginate beads produced by emulsion and internal gelation were biocompatible, stable *in vivo* and could improve the survival of allogeneic grafts. The high-density alginate beads produced by the emulsion process were of particular interest because beads with higher alginate concentration are predicted to have reduced pore sizes and increased strength (Smidsrod et al. 1972), but this is problematic with nozzle extrusion processes where the alginate concentration operating range is limited. The highest alginate concentration reported for extrusion beads in transplantation experiments is 3.3% (Cui et al. 2009) with most transplantation studies conducted at 1~2% alginate (Table 1.1 in Section 1.3.3.3). The highest reported alginate solution viscosity used for nozzle-based bead generation is 11 Pa·s, with the vibrating nozzle technology limited to <1.5 Pa·s (Prusse et al. 2008). For instance, with the vibrating nozzle system used in this work, adequate bead formation was obtained with 1.5% alginate for the LVM:MVG mixture (0.053 Pa·s), with tear-drop shaped beads at 1% alginate and no droplet formation at the nozzle for 2% alginate. The scale-up of extrusion processes is also more challenging at high alginate concentrations, since process control of multi-nozzle devices is problematic for alginate solutions of viscosities higher than ~0.2 Pa·s (Brandenberger and Widmer 1998; DeVos et al. 1997). By contrast, solutions of 0.5% to 10% alginate with 0.004 to 112 Pa·s viscosities allowed bead generation by the emulsion process. Overall, the emulsion process has the combined advantages of providing smaller pore size high alginate concentration gels as well as a more scalable production process.

Next, the physical properties of the emulsion beads were examined to determine to what extent increasing the alginate concentration from 1.5% to 5% in the emulsion beads would impact the pore sizes and bead strength. IgG-sized pullulans molecules (with a 4.5 nm viscous radius corresponding to the size of 150 kDa globular proteins) were excluded

from 82% of the liquid volume of the 5% alginate emulsion-generated beads, much higher than the $49 \pm 7\%$ exclusion from the 1.5% alginate extrusion beads and the 26% exclusion from the 1.5% alginate emulsion beads. The actual permeability of alginate beads to proteins will depend on additional factors such as their charge interactions with the matrix, the real gyration radius of the protein and alginate pore size distributions (de Vos et al. 2006). The pore size distribution for the 5% emulsion beads was shifted towards smaller pores (maximum frequency at ~ 2 nm) than the 1.5% extrusion beads (maximum frequency at ~ 4.6 nm) or the 1.5% emulsion beads (maximum frequency at ~ 5 nm). These results were qualitatively confirmed by scanning electron microscopy, which showed a much denser gel network at the surface of the 5% emulsion beads than the 1.5% emulsion beads (Figure 4.3). The surface of the 1.5% extrusion beads was more similar to the 5% emulsion beads, which can be attributed to gel gradients in externally gelled beads. Indeed, ~ 3 fold higher concentrations near the bead surface compared to the bead average have been observed in externally gelled beads (Thu et al. 2000). Much lower gradients (~ 1.25 surface/bead average concentration) have been reported for internal gels (Quong et al. 1998). Further chromatography experiments using proteins instead of pullulans and other techniques such as confocal imaging of protein binding to antibodies cross-linked to Dynabeads entrapped alginate beads (Strand et al. 2003) should be performed to determine the permeability of beads to proteins. These experiments should guide the selection of alginate concentration to achieve the desired IgG exclusion. Although the alginate concentration could have been further increased in the emulsion beads, 5% alginate already exceeded the concentrations used for transplantation in the literature. The use of $>5\%$ may also have completely arrested β TC3 expansion and further complicated the interpretation of *in vivo* results. Lastly, further increasing the alginate concentration may have hindered insulin diffusion from the beads, since insulin was already excluded from $\sim 30\%$ of the pore volume of the 5% emulsion beads.

The strength of the beads was tested to determine if they were suited for *in vivo* applications. While it was expected that higher alginate concentrations would produce beads with higher rupture forces, these parameters were similar between the 5% emulsion and 1.5% extrusion beads. This can be explained by the higher strength of beads with higher

gel gradients (Moe et al. 1994). For transplantation purposes, alginate beads should be able to withstand compressive forces during intra-peritoneal injection (Lacík 2006). The peak bursting force of capsules currently being used in human clinical trials has been reported to be as low as 8.8 mN (Thanos et al. 2007). Based on the ~30 mN measurements, both the 1.5% extrusion and the 5% emulsion beads were sufficiently strong for *in vivo* testing. In addition, after 1 week exposure to the CMRL medium used for the size exclusion chromatography, the 5% emulsion beads were 8-fold stronger than the 1.5% extrusion beads, suggesting higher long-term bead stability. This greater bead stability may be due to higher total calcium concentration in the 5% alginate beads, since these contain 3.3 fold more guluronic acid residues than the 1.5% beads. The 1.5% alginate beads generated by emulsion were also stable after chromatography, suggesting that unreacted CaCO₃ could have an added effect by acting as a calcium reservoir. Indeed, surplus divalent ions have been purposely added to extrusion beads to increase their stability by caging the ions or adding them via the crystal gun method (Zimmermann et al. 2005). The use of excess CaCO₃ in the emulsion beads could therefore be desirable and should be examined as a strategy to increase bead stability *in vivo*.

The next step was to test *in vitro* βTC3 cell culture in the 5% emulsion beads. The yield of DNA/mL alginate was significantly lower after 20 days of culture in the 5% emulsion beads than in the 1.5% extrusion beads. This was expected, since the growth rate of βTC3 cells is reduced in gels with higher guluronic acid concentration (Stabler et al. 2001). The cell aggregates that expanded from single cells seeded in the beads were smaller in the 5% emulsion beads than in the 1.5% extrusion beads, suggesting that the growth rate of proliferating cell aggregates was reduced in the 5% beads, rather than the frequency of the initial cells that started to expand. In both cases, the aggregates generated consisted mainly of live cells, contrary to single cells that had not expanded.

Knowing that βTC3 cells survive the emulsion process and remain viable for >20 days in the 5% alginate beads, they were next used for transplantation studies. There was no difference between the 5% emulsion beads and the 1.5% extrusion beads in the fraction of the injected beads that could be retrieved from the animals after 20 days (~45% of the initial

bead volume). The bead retrieval rate is an indication of biocompatibility (Fritschy et al. 1994), suggesting that the emulsion process did not affect the bead biocompatibility or *in vivo* stability. The 5% emulsion bead recovery was unchanged after 56 days *in vivo*, further demonstrating their *in vivo* stability. No fibrotic overgrowth was observed for the 5% emulsion beads at day 20 or 56 (Figure 4.6 and Figure 4.7), while some overgrowth was seen on the 1.5% extrusion beads, starting as early as day 20 (arrows, Figure 4.6). Cell overgrowth has been associated with bead (Menard et al. 2010) and graft (Rokstad et al. 2001) immunogenicity. Since the same alginate was used for both bead types, this was a first indication of that graft immunogenicity may be decreased by encapsulation in the 5% emulsion beads. The increased fibrosis on the surface of 1.5% alginate extrusion-generated beads could be explained by higher β -cell stress and death in these beads, leading to higher cytokine secretion by β -cells and DNA leakage from these beads. This could lead to greater recruitment of phagocytic and other immune cells to the 1.5% extrusion-generated beads.

The β TC3 cells transplanted in the 5% emulsion beads significantly lowered the blood glucose of the mice below pre-transplant levels within 2 days compared to >16 days for the 1.5% extrusion beads. The improved performance of the 5% emulsion beads was also reflected by higher body weight and plasma insulin levels. A higher β TC3 cell survival in the 5% emulsion beads was apparent based on the more frequent live insulin+ cell aggregates and the higher yield of DNA in the beads recovered after 20 days *in vivo*. Most of the observations in the first 5 days after transplantation can be attributed to cell survival since the doubling times in both bead types *in vitro* was > 5 days. The advantage of the 5% emulsion beads over the 1.5% extrusion beads in such a short time frame suggests that this initial difference was unlikely due to an adaptive response to the graft, which requires several days to become fully effective (Janeway et al. 2001). In the first few days after transplantation, allogeneic cell losses have been associated with a lack of access to nutrients such as oxygen, with the innate immune response triggered by the surgery and potentially with the acute rejection triggered by direct cellular contact of MHC-mismatched cells with immune cells (de Vos et al. 2006). In particular, macrophage activation and secretion of cytokines plays a major role in the initial cell losses (de Vos et al. 2003a). Bead integrity and

the lack of graft cells exposed at the bead surface are also crucial to avoid graft rejection (DeVos et al. 1996).

It is unlikely that the 5% emulsion beads allowed better access to nutrients than the 1.5% extrusion beads. Diffusivities should be lower in the 5% emulsion beads due to the higher alginate concentration, even though internal gels have been shown to have higher diffusivities than external gels of the same concentration (Martinsen et al. 1992). The volume moment mean diameter (D_{43} , average bead diameter based on cell volumetric distribution, see Section 3.3.1) of 990 ± 192 (SD) μm measured for the 5% emulsion beads was larger than the volume moment mean diameter of 652 ± 30 (SD) μm of the 1.5% extrusion beads. Therefore, on average, the diffusion length was greater for the 5% emulsion beads than for the 1.5% extrusion beads. In addition, due to higher cell death in the smaller beads during the emulsion process (see Section 3.3.6, Figure 3.7), the live cell aggregates recovered from the 5% emulsion beads were more frequent in beads $> 750 \mu\text{m}$. Since it is unlikely that the 5% emulsion beads provided better access to nutrients, their performance *in vivo* could be due to the anticipated effect of their lower porosity to reduce access of cytotoxic molecules from the innate inflammatory response (Wilson and Chaikof 2008). The higher stability of these beads may also have reduced macrophage activation and acute rejection of the exposed cells. Interestingly, a cell-free layer was observed near the surface of the emulsion-generated beads (Figure 4.6). This could be due to the negative surface charge of the cells, leading to repulsion from the oil phase and bead surface during the emulsion step. The electrostatic phenomena occurring during the emulsion process should be further investigated using particles with various charges and sizes. At day 7, an increase in the blood glucose levels of all experimental groups was observed, which may be due to day-to-day experimental variation, but could also be indicative of the development of an adaptive response to the grafts.

To determine whether the 5% emulsion beads also reduced graft immunogenicity compared to the more permeable 1.5% extrusion beads, the peritoneal lymphocytes and graft-reactive IgGs were examined. The number of peritoneal lymphocytes, in particular macrophages and T cells, has been used as a time-dependent indicator of the cellular

immune response to the graft (Safley et al. 2005; Siebers et al. 1999). There was no significant difference in the number of peritoneal lymphocytes between the 1.5% extrusion beads and the 5% emulsion beads, however for all immune cell subtypes examined there were fewer immune cells in the case of the 5% emulsion beads. At day 19, there was no significant increase over non-diabetic control mice in the anti-graft antibody reactivity in the plasma of mice transplanted with 5% emulsion beads, contrary to the 1.5% extrusion beads. Therefore, the humoral response to the graft was reduced in the 5% emulsion beads although these beads contained ~twice the number of β TC3 cells on day 20 as in the 1.5% extrusion beads. Of note, there was no significant humoral response to the non-encapsulated β TC3 cells at day 19, likely because these cells were eliminated within 2~5 days, as suggested by the elevated blood glucose levels of these mice at day 2 (Figure 4.5A) and the lack of recovery in plasma insulin concentrations 5 days after transplantation (Figure 4.5C). These cells may have been destroyed by the innate immune system before a detectable adaptive response was raised and sustained. A lack of antibody generation in response to non-encapsulated islets has been previously reported (Kulseng et al. 1999). Lastly, mouse IgG was detected in both the 1.5% extrusion and the 5% emulsion beads recovered from the mice on day 20, but in far lesser amounts in the 5% emulsion beads, consistent with the size exclusion results in Figure 4.2. Taken together, these results suggest a reduced adaptive immune response to the β TC3 cells transplanted in the 5% emulsion beads compared to the 1.5% extrusion beads. The 5% emulsion beads could have reduced the adaptive response both directly by reducing antigen leakage, antibody permeability or immune cell access to the transplanted cells and indirectly by increasing cell survival during the environmental changes and innate response associated with the transplantation.

The results obtained with β TC3 cells should be confirmed with non-immortalized β -cells. The β TC3 cells were chosen as a model to allow direct comparison of mice transplanted with non-encapsulated cells, cells in emulsion-generated beads and cells in conventional extrusion-generated beads transplanted on the same day. This would not have been feasible using primary mouse islets, since ~1000 encapsulated islets from 3~6 donor mice (de Vos et al. 2003b; Zhang et al. 2010) are typically required to treat one mouse

(Duvivier-Kali et al. 2001; King 2001). An allogeneic mouse strain was chosen to elicit allogeneic responses to the graft, but it should be noted that tumor-specific antigens, including the simian virus 40 tumor antigen used to generate the β TC3 cell line (Efrat et al. 1988) could also contribute to graft immunogenicity. Based on the lack of blood glucose normalization of the non-encapsulated β TC3 cells in our experiments and other reports with a similar cell line, β TC6 cells (Zhou et al. 1998), the β TC3 line was an appropriate first model to test bead performance. In future experiments, β TC-tet cells, a conditionally immortalized β -cell line, could be used instead of the β TC3 cells to quantify *in vivo* cell survival without a significant contribution from cell proliferation (Black et al. 2006). However, both the β TC3 and β TC-tet cell lines have dysregulated insulin secretion, with maximal secretion at \sim 1.25 mM glucose for the β TC3 cells (Efrat et al. 1988) and \sim 9 mM glucose for the β TC-tet cells (Fleischer et al. 1998) rather than 15 mM as is the case with normal islets. Ultimately, the promising results obtained with the high-density alginate emulsion beads should be confirmed with primary islets. The use of primary cells would also enable month or year-long experiments to assess the long-term function of the high-density alginate emulsion beads. If needed, CaCO_3 could be replaced by BaCO_3 during the emulsion process to generate barium cross-linked beads with higher gel strength and stability (Morch et al. 2006), though this would likely require re-optimization of the process pH. Transplantation experiments with insulin+ cells derived from cell populations available in large numbers, such as trans-differentiated exocrine cells (Zhou et al. 2008) or embryonic stem cells (D'Amour et al. 2006) could take full advantage of the scalability of the emulsion process.

The mechanism by which the 5% emulsion beads increased allogeneic β -cell survival compared to the 1.5% extrusion beads should be further investigated. Animals with severe combined immunodeficiency in the innate immune system and cytokine secretion (Ito et al. 2002) transplanted with syngeneic cells could provide information about the cell death mainly associated with nutrient limitations. Comparison of these results with syngeneic transplants in immune competent mice could provide information about the graft cell death associated with the innate response. The adaptive response to allogeneic grafts in immune competent mice should be examined in more detail at different time points. For example, the

mixed host leukocyte reaction against donor cells could be quantified *in vitro* (Zekorn et al. 1995) or the adaptive response assessed by delayed type hypersensitivity assays (Orlowski et al. 2005). Transplantation experiments should be complemented by *in vitro* experiments to further assess bead performance. Leukocytes from non-obese diabetic mice could be co-cultured with encapsulated or non-encapsulated islets to determine whether the beads can protect the cells from autoimmunity (Duvivier-Kali et al. 2001). Co-cultures of macrophages with encapsulated or non-encapsulated allogeneic or xenogeneic islets could be used to assess macrophage activation and islet cytotoxicity (Basta et al. 2004). Cytokine effects could also be measured directly by incubating encapsulated or non-encapsulated islets with recombinant cytokines (Duvivier-Kali et al. 2001).

4.5 CONCLUSIONS

Contrary to traditional extrusion and external gelation bead generation, the emulsion and internal gelation process can be used to generate high-density (4 to at least 10% alginate) beads. The 5% alginate emulsion-generated beads had reduced porosity and were more stable than the 1.5% alginate beads generated by a vibrating nozzle extrusion device. Allogeneic β TC3 cell transplantation in the 5% emulsion beads resulted in faster blood glucose normalization, higher plasma insulin concentrations and lower graft-targeted antibody generation, as well as higher cell survival than the 1.5% extrusion beads. Contrary to the 1.5% extrusion beads, no fibrotic overgrowth was observed on the 5% emulsion beads, even after 56 days *in vivo*. Therefore, alginate beads produced by the emulsion and internal gelation process are suitable for transplantation applications. The high alginate concentrations that can be reached with this process may open new avenues for encapsulated islet transplantation without the need for additional coating of the beads.

5 OPTIMIZATION OF PRIMARY CK19+ CELL CULTURES

In Chapter 4, it was found that 10 days of alginate-immobilized culture significantly increased the insulin expression of cultured human pancreatic islet-depleted tissue. The further study of this phenomenon and similar observations in the literature is hindered by the lack of methods to expand purified populations from pancreatic tissue. Chapter 5 describes a method to remove the fibroblast-like CD90+ cells and obtain cultures with duct phenotype that proliferate in an optimized serum-free medium. CD90 depletion decreased CD90+ cell contamination of the cultures from $34 \pm 20\%$ to $1.3 \pm 0.6\%$, while the fraction of cells expressing the Ca19-9 duct marker increased from $59 \pm 27\%$ to $86 \pm 7\%$. Bromodeoxyuridine (BrdU) incorporation by CK19+ cells was developed as a high content screening assay for duct mitogens with signal:noise ratio of 25:1 using EGF as a positive control. This screening assay confirmed the expected mitogenic effects of bFGF, EGF, HGF and KGF on CK19+ cells and additionally revealed a negative interaction between bFGF and VEGF. The optimized serum-free medium yielded ~3.5 fold increased CK19+ cell proliferation (measured by incorporation of BrdU into the DNA) and ~2 fold increased CK19+ cell numbers after 6 days compared to the medium without additives.

5.1 INTRODUCTION

Primary human pancreatic duct or acinar cells are one of the potential sources for the production of insulin-secreting cells for the treatment of diabetes. Several different protocols have been published to obtain C-peptide and insulin positive cell clusters from human non-islet pancreatic tissue. Generally, these protocols involve an “expansion” step by adherent culture of non-dispersed islet-depleted pancreatic cell clusters in serum-containing medium for ~ 1 week. This is followed by a differentiation step by serum-free culture and cell aggregation in a matrix such as Matrigel (Bonner-Weir et al. 2000; Gao et al. 2003) or by suspension culture in medium containing high concentrations of divalent ions (Todorov et al. 2006). Two main cell populations are observed during the monolayer adherent culture step: CK19+ duct-like cells are more proliferative during the first ~4 days and then these

tend to be overgrown by vimentin+ cells (Gao et al. 2003). By labelling the cells with BrdU at day 3 or day 7 and then examining BrdU+ cells in the islet-like clusters generated after Matrigel overlay, Gao et al. (Gao et al. 2003) concluded that the CK19+ cells rather than the vimentin+ cells give rise to the insulin+ cells after differentiation. However, there was no overall total cell expansion during the adherent culture step and a <2-fold overall increase in the total insulin content of the tissue (Bonner-Weir et al. 2000). Also, the insulin/DNA content of the islet-like clusters was only ~6% of the value obtained for islets. Interestingly, islet-like clusters could also be generated by alginate immobilization of expanded islet-rich human pancreatic tissue (Tsang et al. 2007). During the expansion step, the cultured islet-rich fraction gave rise mainly to insulin-/CK19+ cells very similar to those described for human exocrine cell cultures. In this case, the adherent culture step did allow ~10 fold total cell expansion. Overall, 2.2 ± 2.1 islet-like clusters were generated for each original islet, but the insulin content and expression of the clusters was not reported.

The widespread access of type 1 diabetic patients to islet transplantation as a therapeutic option would require ~100 fold increase in the number of islets available. If primary pancreatic tissue is to be used, each currently available donor pancreas would need to produce enough islet-like cell clusters to treat approximately 100 patients, i.e. the equivalent of ~100 million islets. If duct cells, which constitute ~10% of pancreatic cells, were to be used to generate islet-like cell clusters for transplantation, much greater expansion of these cells and greater efficiency of the differentiation protocols would be required. A different method to obtain insulin+ cells from the more abundant exocrine cells may be provided by genetic re-programming (Zhou et al. 2008).

The development of an optimized serum-free medium adapted to non-mesenchymal pancreatic cell types would facilitate any clinical applications of these cells. The culture medium could be optimized to favour the net expansion of pancreatic acinar-derived or duct-derived CK19+ cells rather than vimentin+ mesenchymal cells. Serum-free culture of purified pancreatic duct or acinar cells would also allow to study the effects of soluble factors on these cells without interference by serum components.

For cellular therapy applications as well as for *in vitro* studies of human exocrine cell biology, improved methods to sort pancreatic exocrine cell subtypes are needed. A purified and well-characterized starting cell population would be important for transplantation process robustness, safety and validation. Even though insulin+ cells in the islet-like clusters appear to come from the CK19+ duct-like cells present in the monolayer cultures (Gao et al. 2003), these CK19+ cells are not necessarily derived solely from duct cells. Contaminating β -cells may have de-differentiated (Weinberg et al. 2007), expressed CK19, then simply re-expressed insulin upon aggregation and serum-free culture. Alternatively, amylase+ acinar cells could have trans-differentiated into CK19+ cells, as has been demonstrated by lineage tracing of villin-expressing (Means et al. 2005) or elastase-expressing (Minami et al. 2005) mouse pancreatic cells. Lastly, the vimentin+ mesenchymal cells dominate long-term cultures of both islet-rich (Gershengorn et al. 2004; Weinberg et al. 2007) and islet-depleted tissue (Seeberger et al. 2006), suggesting that maintenance and expansion of the other pancreatic cell types will require that the vimentin+ cell numbers be limited. These cells express mesenchymal stem cell markers, have similar differentiation potential as mesenchymal stem cells and their differentiation into insulin-expressing and secreting cells has required over-expression of the β -cell transcription factor PDX1 (Li et al. 2007; Seeberger et al. 2006).

Several studies have focused on the purification of islet cell subtypes by fluorescence-activated cell sorting (FACS) using β -cell surface markers such as the sialylated form of the neural cell adhesion molecule (Bernard-Kargar et al. 2001). Other studies in rodents have described the isolation of putative pancreatic stem or progenitor cells using the CD133 (Oshima et al. 2007), C-met (Oshima et al. 2007; Suzuki et al. 2004), platelet-derived growth factor receptor beta (Hori et al. 2008) and/or CD90.1 (Thy1.1) (Stevenson et al. 2009) surface markers. The CD90.1 sorting study demonstrated that rat pancreatic CD90.1+ cells adopt a fibroblast-like phenotype in culture and express much lower levels of duct markers than CD90.1- cells. Although CD90.1 cells were described as pancreatic progenitors, no positive insulin staining or secretion results were shown. One reported method to separate human exocrine cell subtypes was based on the expression of the carbohydrate antigen 19-9

(Ca19-9) duct surface marker (Gmyr et al. 2004). It was demonstrated that this antigen allows duct purification to 97% purity by FACS or 93% purity by magnetic-activated cell sorting (MACS). However, the cell phenotypes obtained after 7 days of culture have not been quantified and the Ca19-9 enriched cells expanded poorly, even in the presence of serum (Yatoh et al. 2007).

Chapter 5 describes a novel method for the adherent culture of purified primary pancreatic CK19+ cells using a platform suitable for high content screening applications. Depletion of CD90-expressing cells was used to successfully eliminate most fibroblast-like cells from the cultures. High content imaging of BrdU incorporation by the CD90-depleted cultures in 96-well plates allowed the multifactorial testing of the effects of five reported duct mitogens on duct-like cell apoptosis after 1 day, as well as expansion and proliferation after 5 days of culture. This led to the development of a preliminary serum-free medium adapted to pancreatic duct-like cell culture.

5.2 MATERIALS AND METHODS

5.2.1 Cell culture

Islet-depleted cell aggregates derived as a by-product of human islet isolation from nine (BC107 to BC130) pancreatic tissue donors (Table SI) were kindly provided by Dr. Garth Warnock and the Ike Barber Human Islet Transplant Laboratory (Vancouver General Hospital, Vancouver, BC). Human islet-depleted pancreatic cell clusters were washed twice in CMRL-10FBS medium (CMRL with 2 mM glutamine, 10% fetal bovine serum i.e. FBS, 100 units/mL penicillin, 100 µg/mL streptomycin, all from Invitrogen). The undispersed cells were quantified by packed cell volume (PCV, see Section 3.2.5) When needed, the cell aggregates were dispersed to generate “Day 0 unsorted” cells as described in the next section. Alternatively, the cell clusters to be used for magnetic-activated cell sorting (MACS) were plated at 1 µL PCV/cm² in 175 cm² tissue culture-treated T-flasks (Sarstedt). For most experiments, MACS was performed on day 1 after trypsinizing the cell clusters that had adhered to the T-flask surface. All cultures including the “unsorted day 0”, “unsorted day

1" and "sorted day 1" (CD90+, CD90-, Ca19-9+ and Ca19-9-) cells were seeded at 40 000 cells/ well (1.25×10^5 cells / cm^2) in CMRL-10FBS and cultured at 37°C and 5% CO₂ and 90% relative humidity. Live cells were enumerated based on trypan blue exclusion using a Cedex automated cell counter (Innovatis). Prior to seeding, 0.31 mL/ cm^2 of this medium was added for at least 1 h at 37°C and 5% CO₂ to the plates seeded. The concentration of the cell stocks used for seeding was adjusted to add 0.31 mL/ cm^2 of the cell stock to the medium already present. In one experiment, the wells were coated with 50 μL /well Matrigel (BD Biosciences) diluted 1:30 in DMEM/F12 (Invitrogen) for 2 h at 37°C and 5% CO₂ prior to rising with CMRL-10FBS and adding the cells. Medium was fully exchanged on days 2 and 5, while only 0.31 mL/ cm^2 was added after removing the medium on day 7. One h after the last medium exchange, 5 mL/100 mL culture volume of 5-Bromo-2'-deoxy-uridine (BrdU, from the Labelling and Detection Kit II, Roche, Basel, Switzerland) diluted in CMRL-0.1X ITS (CMRL with 0.5 mg/L insulin + 0.5 mg/L transferrin + 0.5 μg /L selenite, i.e. 0.1 times the usual concentration of I-1884 from Sigma, 10 mM nicotinamide and 0.2% BSA, both from Stem Cell Technologies) were added to obtain a final concentration of 10 μM BrdU. On day 8, the cultures were fixed for staining and Cellomics analysis (Section 2.6). During the series of experiments related to the development and application of a serum-free screening platform, the culture time was shortened to 6 days since some cultures with 10% FBS reached near confluency (~90%) by day 6. As a result, medium exchanges of 0.31 mL/ cm^2 of the test solutions were performed on days 2 and 5, BrdU was added on day 5 and the cultures were fixed on day 6 instead. The culture duration is indicated in the figure legends. The basal medium for all test solutions was CMRL-0.1XITS. The test solutions contained 0.1% FBS, 1% FBS, 10% FBS (Invitrogen), basic fibroblast growth factor (bFGF, Stem Cell Technologies), recombinant human epidermal growth factor (EGF, Stem Cell Technologies), hepatocyte growth factor (HGF, Sigma), recombinant human keratinocyte growth factor (KGF, Sigma), recombinant human vascular endothelial growth factor (VEGF, Sigma) and/or 50% pancreatic fibroblast-conditioned medium diluted in CMRL-0.1X ITS. Unless otherwise mentioned, the growth factor concentrations were 20 ng/mL.

5.2.2 Conditioned medium

The pancreatic fibroblast-like cells used to generate the conditioned medium were passaged CD90-enriched cells cultured in CMRL-10FBS that were treated with 10 µg/mL mitomycin c (Sigma) in CMRL-10FBS for 1 h. After this inactivation, the fibroblast-like cells were washed 3 times with CMRL-0.1X ITS and then incubated for 24 h in CMRL-0.1X ITS. This medium was filtered with 0.2 µm Steriflip filters (Millipore, Billerica, MA) and stored at -80°C until use. CMRL-0.1XITS medium from the same batch was also kept frozen and used in the controls that were compared to the 50% conditioned medium tests.

5.2.3 Cell dispersion

Human islet-depleted pancreatic cell clusters were washed twice with dispersion medium consisting of calcium and magnesium-free HBSS (Invitrogen) supplemented with 1 mM EDTA (Invitrogen), 10 mM HEPES (Sigma) and 0.5% bovine serum albumin (Stem Cell Technologies). The cell clusters were then re-suspended at 0.5 mL packed cell volume (PCV) in 10 mL dispersion medium placed in a 25 cm² suspension T-flask (Sarstedt) for 7 min at 37°C and 75 rpm on a rotary shaker. Concentrated stocks of trypsin and DNase (both from Sigma) were added to obtain a final concentration of 25 µg/mL and 4 µg/mL respectively. The cells were kept agitating at 75 rpm for another 10 min. The digestion was then immediately ceased by adding 20 mL of CMRL-10FBS medium. The cells were triturated and filtered through a 40 µm nylon sieve (BD Biosciences) into a tube containing an additional 10 mL of CMRL-10FBS. The cells were enumerated by trypan blue, centrifuged for 7 min at 200 x g and re-suspended at the desired stock concentration. The total cell yield based on PCV was 43 ± 7%, leading to 168 ± 39 million live dispersed cells per 1 mL PCV of initial tissue clusters.

5.2.4 Magnetic-activated cell sorting (MACS)

Adherent cells were rinsed once with 0.08 mL/cm² of MACS buffer (Ca²⁺ and Mg²⁺-free phosphate buffered saline with 1% FBS, 2 mM EDTA, 100 units/mL penicillin, 100 µg/mL streptomycin) and then trypsinized with 1 mL of 0.05% trypsin / 0.53 mM EDTA (Invitrogen) per 1 cm² culture surface for 10 min at 37°C. Then, 0.08 mL/cm² CMRL-10FBS

were added, followed by trituration until the cell suspension consisted mainly of single cells. This method yielded $30 \pm 9 \times 10^6$ cells/175 cm² flask, i.e. a yield of ~30% compared to the packed cell volume seeded (based on the ratio of cells/PCV determined in Figure B8) on day 0. The cell suspension was immediately passed through a 40 µm cell strainer (BD Biosciences), centrifuged at 200 x g for 7 min and re-suspended in ~1 mL MACS buffer / 10⁶ cells (“washed”), counted by trypan blue, centrifuged and re-suspended at 2×10^7 cells/mL in MACS buffer in a minimum volume of 50 µL. This cell stock was used to seed “unsorted day 1” cultures. To this volume of cell stock, an equal volume of 2-fold concentrated sterile filtered primary antibody was added. The final primary antibody concentrations were 1:100 mouse anti-Ca19-9 (Catalogue # NCL-L-CA19-9, Leica Microsystems, Germany) or 1:500 mouse anti-CD90 (Catalogue #555593, BD Pharmingen, CA). After 25 min of incubation on ice at 75 rpm agitation, the cells were washed twice with 1 mL MACS buffer per 10⁶ cells before re-suspending the cells at 2.5×10^8 cells/mL in a minimum volume of 80 µL. For each 80 µL of cells, 20 µL of microbead-labelled goat or rat anti-mouse IgG1 antibody (130-048-402 or 130-047-102, Miltenyi Biotec GmbH, Germany) was added. After 15 min incubation at 4°C and 75 rpm, the cells were washed once with 1 mL MACS buffer per 10⁶ cells and re-suspended at 4×10^6 cells/mL. A maximum of 10⁸ total cells were separated using the “possel” (for Ca19-9) or “depletes” (for CD90) program using an Automacs® (Miltenyi) cell separator. The positive and negative fractions were collected in 50 mL tubes containing 10 mL CMRL-10FBS to minimize the time without medium. The cells from the positive and negative cell fractions were enumerated by trypan blue, washed once with CMRL-10FBS and re-suspended at 4×10^5 cells/mL in CMRL-10FBS. The sorted cell populations were used to seed the “Ca19-9+ day 1”, “Ca19-9- day 1”, “CD90+ day 1” and “CD90- day 1” populations.

5.2.5 Flow cytometry

Adherent cells were washed with Ca²⁺ and Mg²⁺-free phosphate buffered saline (PBS), trypsinized for 10 min, after which 1 mL / cm² culture surface of FACS buffer (PBS + 10% FBS) was added, the cells were triturated and filtered through a 40 µm cell strainer (BD Biosciences). The cells were centrifuged at 200 x g for 7 min at 4°C and re-suspended in ~1

mL/10⁶ cells of FACS buffer, enumerated, distributed to obtain 2.5 x 10⁶ cells/FACS sample and kept on ice from here onward. After washing with 1 mL FACS buffer/sample, the cells were centrifuged at 250 x g for 2 min and the supernatant was removed to leave 50 µL/sample. The cells were gently re-suspended and 50 µL of 2-fold concentrated primary antibody (diluted in FACS buffer but at the same concentrations as for MACS) were added except for controls to which buffer was added instead. The cells were incubated on ice for 25 min at 75 rpm. The cells were washed twice in FACS buffer, with one wash consisting of adding 1 mL FACS buffer, 2 min centrifugation at 250 x g, removing the supernatant down to 50 µL, then gently re-suspending the cells. For all samples including controls, 50 µL of Alexa 647-labelled goat anti-mouse IgG (catalogue # A21450, Invitrogen) diluted 1:100 (to obtain a final concentration of 1:200) were added to each sample. After 15 min on ice in the dark at 75 rpm, 10 µL of propidium iodide stock solution at 100 µg/mL (Sigma, prepared in PBS) was added to all the samples except controls. The cells were washed twice in FACS buffer, re-suspended in 500 µL FACS buffer and analyzed on a BD FACSCalibur flow cytometer.

5.2.6 Staining of live cells in 96-well plates.

Cells were incubated for 1 h at 37°C, 5% CO₂ and 90% relative humidity in the presence of 2 µM YoPro-1 dye (Invitrogen) by adding 10 µL/well of YoPro at 42 µM in CMRL-0.1XITS. The solutions were removed by inverting the plate and gentle blotting on a tissue. The cells were washed once with 200 µL/well phenol red-free CMRL-0.1XITS (CMRL from Cellgro), followed by the addition of 50 µL/well mouse anti-Ca19-9 antibody diluted 1:200 with CMRL-0.1XITS. After 25 min incubation on ice with orbital shaking at 100 rpm, the cells were washed twice with 200 µL/well phenol-red free CMRL-0.1XITS. After the second wash, instead of removing the solution, 25 µL/well of Hoechst in phenol red-free CMRL-0.1X ITS was added to obtain a final Hoechst concentration of 16 ng/mL. The 96-well plates were incubated 30 min at 37°C, 5% CO₂ and 90% relative humidity prior to Cellomics imaging.

5.2.7 Immunocytochemistry and Cellomics

For staining of insulin, amylase, CK19, vimentin, and/or Ki67 without BrdU, the cells were fixed with Bouin's fixative (8.8% formaldehyde, 4.76% glacial acetic acid) for 15 min and stored in 70% ethanol until staining. In this case, prior to staining, antigen retrieval was performed by microwaving samples 6 times for 5 s at 1000 Watts in 10 mM citrate (Sigma) at pH 6.0. The solutions were then replaced by 100 mL/well 0.25% Triton X 100 (Sigma) dissolved in PBS and incubated for 10 min at room temperature and 100 rpm on an orbital shaker to further permeabilize the cells. For co-staining with BrdU, which used a commercial kit (BrdU Labelling and Detection Kit, Roche), fixing and staining were performed according to manufacturer's instructions. The cells were fixed for 45 min at -20°C with pre-cooled 70% ethanol mixed with 30% of 50 mM glycine (Invitrogen) at pH 2.0, which replaced glycine as described in the kit instructions. The cells were then stained sequentially for BrdU, followed by CK19 or vimentin. The primary (mouse anti-BrdU IgG) and secondary (fluorescein-labelled sheep anti-mouse IgG) antibodies from the kit were diluted 1:20. The unstained samples fixed with Bouin's or BrdU-stained samples were washed with PBS and incubated in blocking solution (Dakocytomation, Glostrup, Denmark) for 15 min at 100 rpm on an orbital shaker. The solution was removed primary antibodies in Antibody Diluent (Dako) were incubated at 4°C in a humidified environment and 100 rpm on an orbital shaker. The primary antibody dilutions were as follows: 1:200 guinea pig anti-human insulin (Dako A0564), 1:1000 rabbit anti-human amylase (Sigma A8273), 1:200 mouse anti-human CK19 (Dako M0888), 1:200 mouse anti-human vimentin (Dako M0725) and 1:50 rabbit anti-human Ki67 (Santa Cruz Biotech sc-15402, Santa Cruz, CA) or 1:200 mouse anti-human Ki67 (BD Biosciences 556003). The next day, the cells were washed with PBS before adding secondary antibodies diluted 1:200 in Antibody Diluent and incubating for 1 h in the dark at room temperature and 100 rpm on an orbital shaker. Secondary antibodies were Alexa 488-labelled goat anti-guinea pig IgG, Alexa 488 or 568-labelled goat anti-rabbit IgG and/or Alexa 568-labelled goat anti-mouse IgG (all from Invitrogen). The cells were washed with PBS and then with distilled deionized water (ddH₂O) prior to adding DAPI at 1 mg/mL in ddH₂O and incubating for 15 min in the dark at room temperature and 100 rpm on an

orbital shaker. The cells were washed 3 times with 200 mL/well ddH₂O, twice with PBS, followed by Cellomics imaging of 96-well plates or mounting the slides with Vectaschield mounting medium (Vector Labs, Burlingame, CA). The 96-well plates were imaged on a Cellomics ArrayScan VTI and the data was analyzed with the Cellomics software. The slides were imaged on a Zeiss Axioplan 2 (Carl Zeiss International, Oberkochen, Germany) microscope, with data analysis using a custom-programmed ImageJ plug-in (open-source freeware from the NIH). Further details on the Cellomics and the ImageJ data analysis are provided in Appendix A, Sections A3 and A4. The Cellomics analysis parameters are provided in Table B5 with sample images shown in Figure B13 (Appendix B).

5.2.8 Alginate immobilization

This method is described in Section 3.2.12 except for sorting the cells prior to alginate immobilization. Also, to immobilize CD90+ cells, the amounts of all processing solutions were scaled down by 1/5 without changing the vessel geometry but using an impeller with a lower bottom clearance of 1 mm. Briefly, unsorted non-dispersed islet-depleted pancreatic cells were cultured for 7 days in CMRL-10FBS. On day 7, the cells were sorted for CD90 by MACS. On the same day, unsorted, CD90-enriched and CD90-depleted cells were immobilized in separate batches of beads. The process used was the 4 min 60 mM MOPS process, using 1.5% alginate. The cells were then cultured for 10 days in serum-free medium similar to CMRL-0.1XITS except that the insulin+transferrin+selenium supplement was 10-fold more concentrated. Half of the medium was exchanged every 2nd day. On day 17, the beads were liquefied (see Section 3.2.5) and the cells were sampled for q-PCR (see Section 5.2.9).

5.2.9 Quantitative reverse transcription polymerase chain reaction

Cell samples (usually 10⁶ cells) were washed in PBS and re-suspended in 350 µL buffer RLT+ (Qiagen) and kept at -80°C until analysis. The mRNA extraction, cDNA generation and q-PCR methods are described in Section 3.2.12.

5.2.10 Design of experiments and statistical analysis

All results reported represent the average values obtained for 2 to 4 pancreata \pm the standard error of the mean. Apart from the full factorial model described below, p-values result from two-way comparisons using Student's t-test and pancreata replicates. Unless otherwise indicated, p-values <0.05 were considered significant. For the factorial effects, p-values <0.1 were considered significant because the number of replicate pancreata was low ($N=2$), in order to avoid falsely rejecting significant effects (type 2 error). In cases where test conditions are normalized to the basal condition, confidence intervals with an α level of 0.05 around the test condition read-out were used to determine significant differences between the test and basal conditions. The number of replicates is indicated for each figure. In cases where the data for 2 pancreata are provided, at least one replicate will be added before submission for publication.

For the 2^5 full factorial screening of the mitogenic effects of bFGF, EGF, HGF, KGF and VEGF, a two level design with 8 centre points with a total of 40 runs was chosen. The response measured (\hat{Y}) was the ratio of the BrdU incorporation by CK19+ in the given run divided by the BrdU incorporation by CK19+ cells without any growth factors added, measured on day 6. The low levels were defined as the absence of growth factor (0 ng/mL) and the high levels defined as 20 ng/mL. The centre points contained 10 ng/mL of all five factors. Each run was replicated three times on three 96 well plates. The test runs were randomized differently on each plate and placed in the centre of the plates in the rectangle delimited by wells C2 and F11. The average read-out from the three plate replicates was defined as the read-out for each run. This experiment was repeated for two pancreata (BC129 and BC130) and the results were combined to generate a linear mathematical model. The results were analyzed with JMP 7.0 or 8.0 statistics software (SAS, Cary, NC). The pancreas-to-pancreas variation was taken into account by including the "pancreas" categorical variable. This original full factorial scaled model was defined as:

$$\begin{aligned}
Y = & \beta_0 + \beta_F x_F + \beta_E x_E + \beta_H x_H + \beta_K x_K + \beta_V x_V \\
& + \beta_{FE} x_F x_E + \beta_{FH} x_F x_H + \beta_{FK} x_F x_K + \beta_{FV} x_F x_V + \beta_{EH} x_E x_H + \beta_{EK} x_E x_K + \beta_{EV} x_E x_V + \beta_{HK} x_H x_K + \beta_{HV} x_H x_V + \beta_{KV} x_K x_V \\
& + \beta_{FEH} x_F x_E x_H + \beta_{FEK} x_F x_E x_K + \beta_{FEV} x_F x_E x_V + \beta_{FHK} x_F x_H x_K + \beta_{FHV} x_F x_H x_V + \beta_{FKV} x_F x_K x_V + \beta_{EHK} x_E x_H x_K + \beta_{EHV} x_E x_H x_V + \beta_{HKV} x_H x_K x_V \\
& + \beta_{FEHK} x_F x_E x_H x_K + \beta_{FEHV} x_F x_E x_H x_V + \beta_{FEKV} x_F x_E x_K x_V + \beta_{FHKV} x_F x_H x_K x_V + \beta_{EHKV} x_E x_H x_K x_V \\
& + \beta_{FEHKV} x_F x_E x_H x_K x_V \\
& + \beta_{pancreas} x_{pancreas}
\end{aligned}$$

(Equation 5.1)

Where the dependent variable “Y” was the fold increase in CK19+ cell proliferation compared to the basal medium. The β_i values are the scaled model parameters determined by least squares fitting. The x_i independent variables represent the growth factor concentrations (C_i in ng/mL) converted to non-dimensional scaled variables ($x_i = \frac{C_i - 10}{10}$).

The subscripts F, E, H, K, V respectively represent the “i” factors bFGF, EGF, HGF, KGF and VEGF. In this case, the model intercept “ β_0 ” is the value expected for “Y” when all the growth factor concentrations are 10 ng/mL for the average of all pancreata tested. The model error was calculated from the centre point replicates and pancreas replicates. Finally, the model was reduced to include all main and interaction effects that had a p-value < 0.1 and re-written as a function of the non-scaled variables.

5.3 RESULTS

5.3.1 Characterization of the main cell types in adherent cultures of unsorted human islet-depleted pancreatic cells

The cell types found in the human islet-depleted tissue were quantified on day 0 after dispersing the cell clusters, as well as after 2 and 8 days of adherent cell culture in the presence of 10% FBS. The Cellomics algorithm adequately identified the cell nuclei, as well as the CK19+, BrdU+ (Figure B13 in Appendix B) and vimentin+ cells (data not shown). On day 0, the tissue consisted of $61 \pm 16\%$ amylase+ cells, $6 \pm 3\%$ CK19+ cells, $12 \pm 6\%$ vimentin+ cells and $0.04 \pm 0.01\%$ insulin+ cells (N = 3 pancreata). Due to the low fraction of insulin+ cells, these were not quantified at later time points.

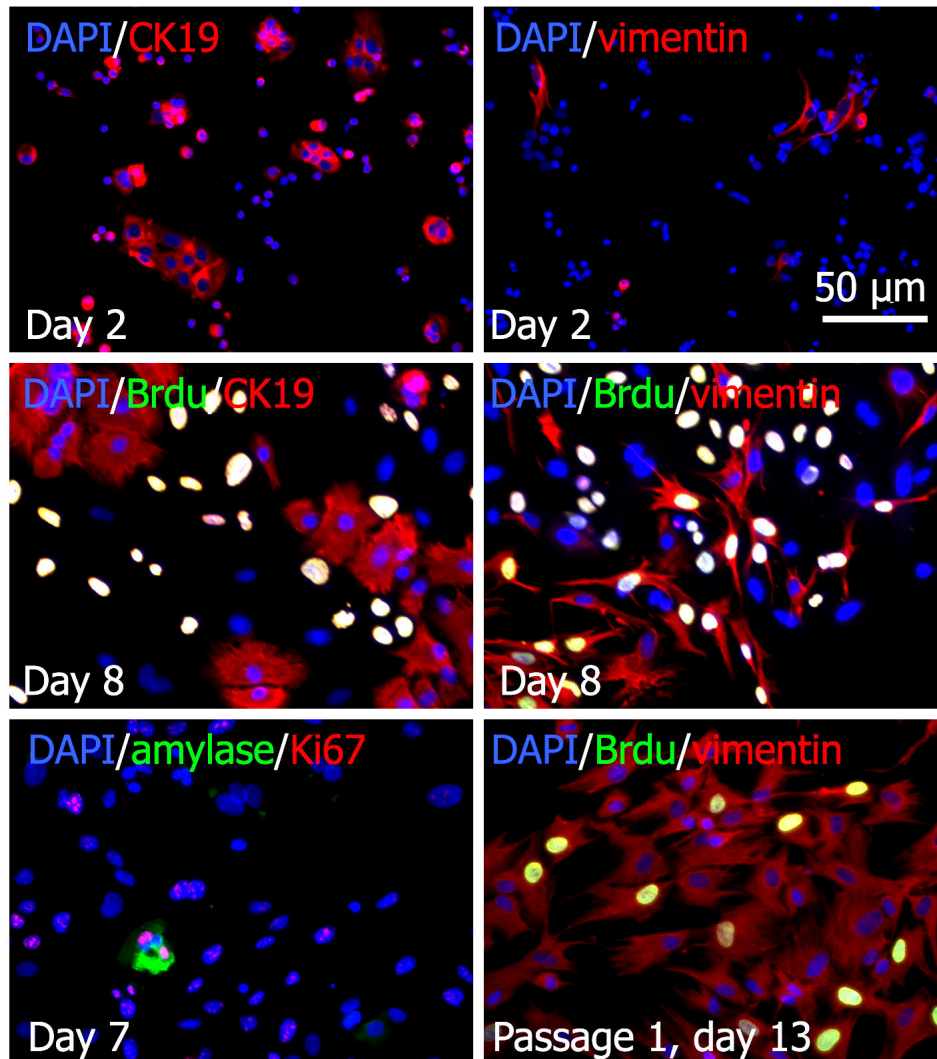


Figure 5.1. Phenotype of dispersed unsorted islet-depleted pancreatic cells.

Islet-depleted clusters were dispersed and seeded on day 0 and cultured in CMRL-10FBS for 7 days. Some of the cultures were passaged (trypsinized and re-seeded) at 1:8 dilution on day 7 and further cultured in CMRL-10FBS, generating cultures consisting mainly of vimentin+ cells by day 13.

After 2 days of adherent culture, the total adherent cell number was $27 \pm 16\%$ the number of cells seeded, as expected from the low plating efficiency and/or cell death reported for primary human acinar cells (Klein et al. 2009). This low plating efficiency was observed both for dispersed and non-dispersed cells seeded on day 0. However, the total cell yield on day 7 was increased by lower seeding densities of the non-dispersed clusters, but independent of the seeding density for dispersed clusters (Figure B15 in Appendix B).

On day 2, the fraction of amylase+ cells had decreased to $17 \pm 5\%$ while the fraction of CK19+ cells and vimentin+ cells had increased respectively to $25 \pm 10\%$ and $27 \pm 21\%$. Most of the CK19+ cells were in small clusters, suggesting that these cells proliferated within 2 days, were incompletely dispersed or re-aggregated selectively prior to adhering to the plastic surface. On the contrary, the vimentin+ cells were dispersed throughout the culture surface as single cells (Figure 5.1).

By day 7, the remaining amylase+ cells accounted for $< 1\%$ of the cells and appeared unhealthy based on punctate amylase staining and the irregular shape of their cytoplasm (Figure 5.1). The cultures mainly consisted of $39 \pm 5\%$ of CK19+ duct-like cells in rounded

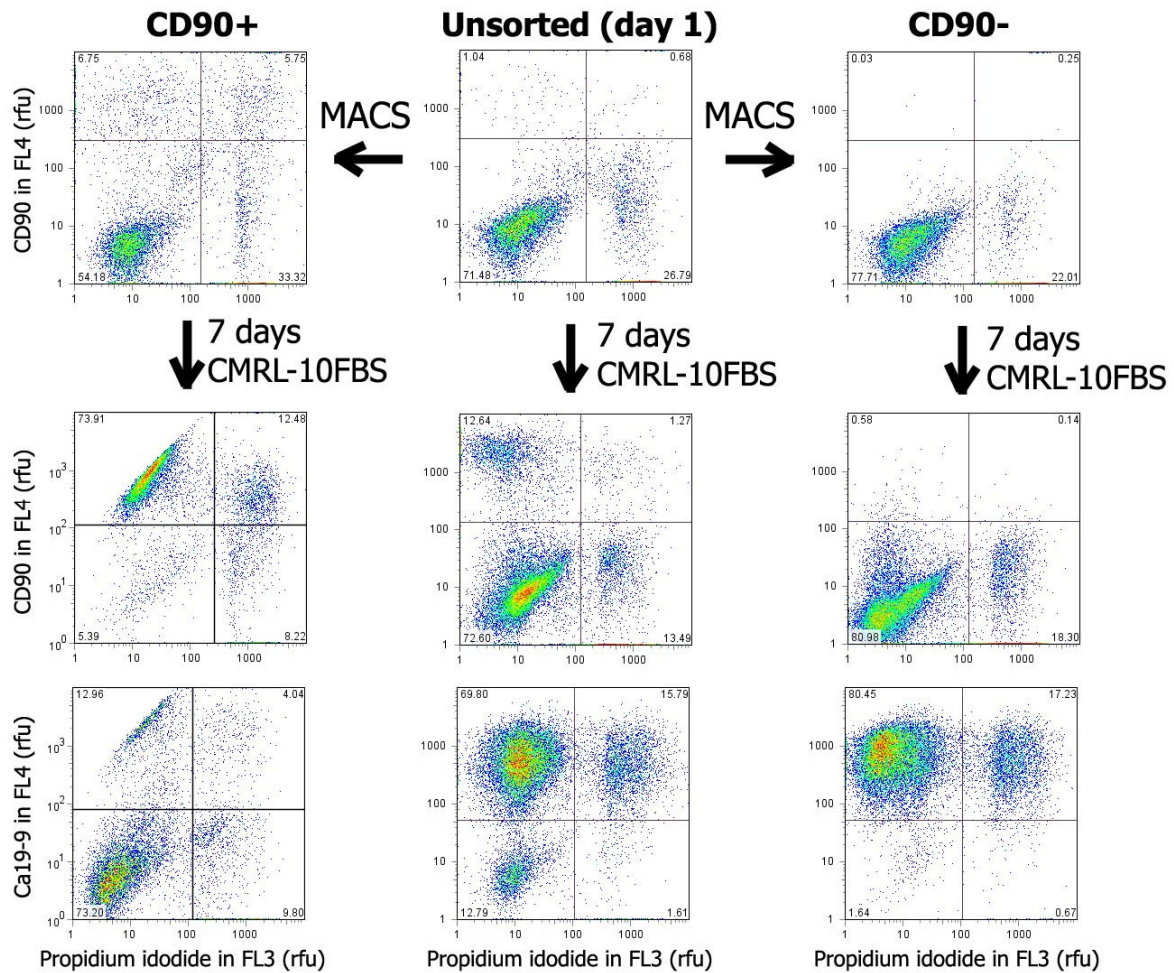


Figure 5.2. Depletion of CD90- cells on day 1 leads to CD90-/Ca19-9+ cell cultures on day 7 as shown by flow cytometry.

cobblestone patterns surrounded by $33 \pm 10\%$ fibroblast-like spindle-shaped cells (Figure 5.1). Cells from both of these populations were proliferative since $44 \pm 26\%$ of the CK19+ cells and $60 \pm 24\%$ of the vimentin + cells at day 8 had incorporated BrdU added at day 7. After a single passage, at day 13, the cultures consisted almost uniquely of vimentin+ cells (Figure 5.1) with very few CK19+ cells (data not shown). For all pancreata (N = 9), the proportion of vimentin+ cells was consistently increasing with culture time.

5.3.2 Effects of depleting CD90-expressing cells from pancreatic islet-depleted cultures

A negative cell selection strategy was developed to purify human pancreatic exocrine cell cultures by using the CD90 (Thy1) mesenchymal cell surface marker to selectively remove fibroblast-like cells. For dispersed unsorted islet-depleted pancreatic tissue after 7 days of adherent culture, the CD90 surface marker labelled $34 \pm 20\%$ of the cells (Figure 5.2), corresponding to the spindle-shaped fibroblast-like cells. When the CD90- cells were purified by MACS on day 7, these cells were enriched in CK19 mRNA and depleted in vimentin mRNA (Figure B16 in Appendix B), confirming that CD90 can be used to deplete the fibroblast-like cell population. Unfortunately, due to the limited notice of human tissue availability (< 24 h), it was impractical to sort the cells the day they were received (day 0). Therefore, the human islet-depleted cell clusters were plated and left to adhere overnight and the sorting was always done on day 1, while unsorted cells were plated both on day 0 and on day 1. Cell plating for 24 h also simplified the cell dispersion, since this could be achieved by trypsinizing the adherent cells for 7 min (leading to $85 \pm 4\%$ cell viability) rather than the more damaging ($71 \pm 4\%$ cell viability after dispersion) dispersion for 10 min with trypsin and DNase as was required on day 0, without any significant difference in the viable cell yield obtained (166 ± 72 million cells/mL packed cell volume dispersed or seeded on day 0). The composition of the cell populations (amylase+, CK19+, vimentin+, insulin+ fractions) obtained by this 24 h plating strategy was not significantly different from the composition obtained by cell dispersion on day 0 (Table 5.1, unsorted cells seeded day 0 versus day 1), although the fraction of CK19+ tended to increase at the expense of the amylase+ cells.

Table 5.1. Fractions of cells obtained at different culture times before and after sorting on day 1

Cell population	Day seeded	Day analyzed	% of positive cells by immunocytochemistry			% of positive cells FACS	
			Amylase	CK19	Vimentin	CD90	Ca19-9
Unsorted	0	0	61 ± 16*	6 ± 3	11.9 ± 6	N/A	N/A
Unsorted	0	1	46 ± 29*	20 ± 7	13 ± 6	0.6 ± 0.2	55
CD90-	0	1	33 ± 10*	15 ± 8	9 ± 3	0.12 ± 0.04	N/A
CD90+	0	1	15 ± 3*	7 ± 3	36 ± 25	23 ± 8	N/A
Ca19-9+	0	1	12 ± 11*	38 ± 22	3 ± 3	N/A	97
Ca19-9-	0	1	71 ± 25*	5 ± 2	26 ± 12	N/A	0.7
Unsorted	0	8	0.6	39 ± 5*	33 ± 10	34 ± 20*	59 ± 27
Unsorted	1	8	0.5	36 ± 10	36 ± 10	20 ± 5	70 ± 9
CD90-	1	8	2.3	55 ± 4	8.22 ± 0.04	1.3 ± 0.6	86 ± 7
CD90+	1	8	7.4	17 ± 5	48 ± 13	62 ± 19*	15
Ca19-9+	1	8	0.6	64 ± 6*	8 ± 2*	0.4	97
Ca19-9-	1	8	0.5	24 ± 17*	36 ± 25*	76.4	5

*N=2. For all others, N is between 3 and 5 pancreata, except where no SEM is provided, in which case N=1. N/A = non-available (experiment not done).

Prior to sorting on day 1, only $0.6 \pm 0.2\%$ of the cells were CD90+ (Table 5.1). Magnetic-activated cell sorting efficiently removed this cell population, reducing the fraction of CD90-expressing cells to $0.12 \pm 0.04\%$ in the CD90-depleted cultures and enriching them to $23 \pm 8\%$ in the CD90-enriched cultures. This >4 fold depletion was higher than what could be achieved by removing the fibroblast-like cells by a simple pre-plating step (Figure B17 in Appendix B). The live cell yield from MACS based on the sum of the live cells in the CD90+ and CD90- fractions was $60 \pm 3\%$, with a throughput of >50 million cells/h, including equipment start-up and shut-down. After 7 days, the progeny of the sorted populations developed significant differences in their expression of the CD90 fibroblast/mesenchymal marker and of the Ca19-9 duct/epithelial cell surface marker. While the unsorted cells consisted of a mixture of Ca19-9+ ($34 \pm 20\%$) and CD90+ ($59 \pm 27\%$) cells, the CD90-enriched cultures consisted of >60% CD90+ cells, while the CD90-depleted cultures consisted of >85% Ca19-9+ cells. The separation of duct-like cells from fibroblast-like cells was also evidenced by immunocytochemistry for CK19 and vimentin (Table 5.1).

Ca19-9 sorting to select duct cells but not acinar cells was also performed. Immediately after sorting on day 1, the fraction of amylase+ cells was significantly higher in

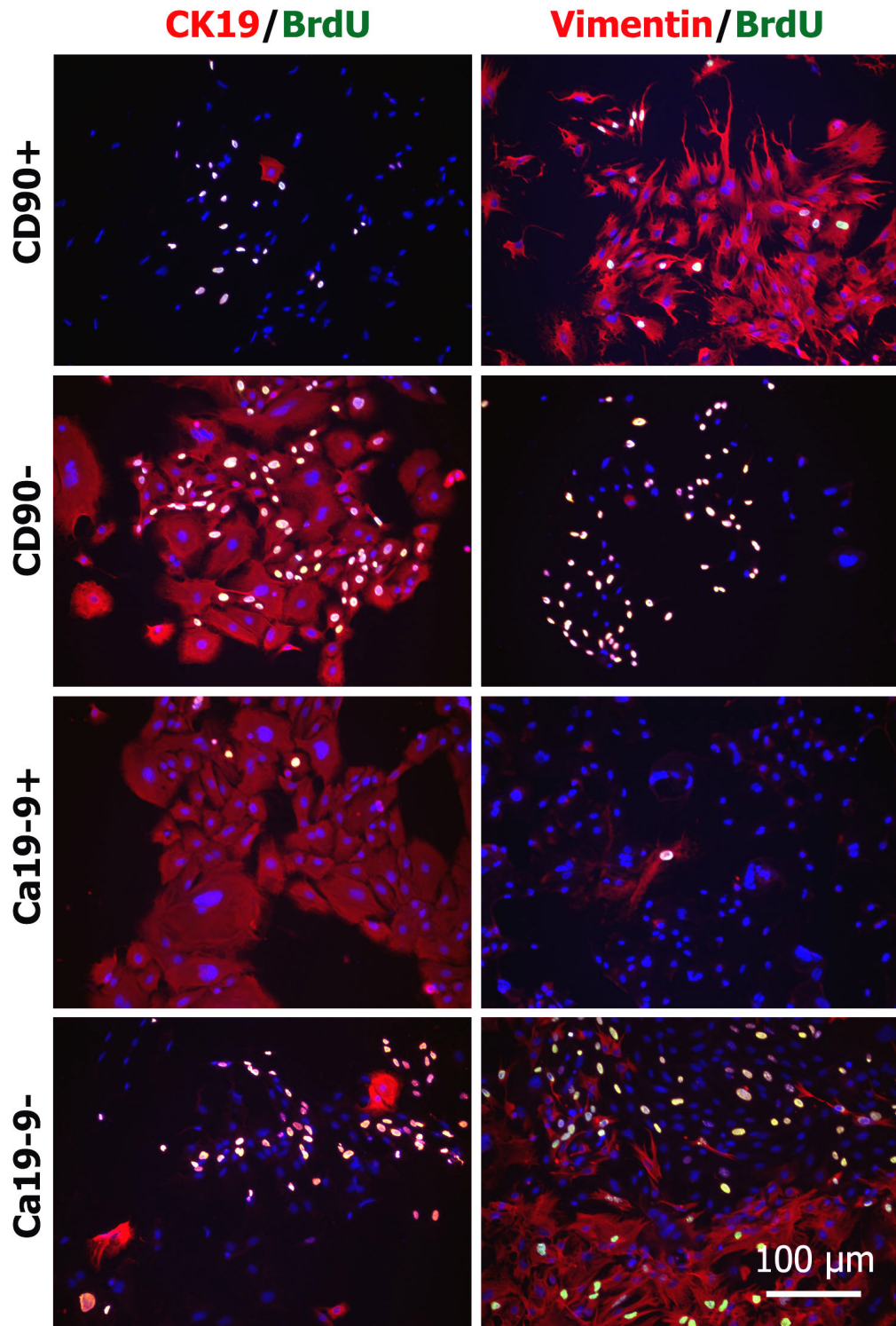


Figure 5.3. Morphology of cultures generated by CD90 sorted cells compared to Ca19-9 sorted cells

MACS sorting based on CD90 expression generates cultures of spindle-shaped vimentin+ cells for the CD90+ sorted cells and cobblestone-pattern CK19+ cells for the CD90- sorted fraction after 7 days of adherent culture in CMRL-10FBS. The cells were sorted on day 1 and fixed on day 8.

the CD90-depleted population ($33 \pm 10\%$) than in the Ca19-9 enriched population ($11 \pm 11\%$). As a result, the proportion of CK19+ cells was lower in the CD90-enriched population than in the Ca19-9 enriched population, leading to a lower seeding density of the CK19+ cells. Yet, after 7 days of culture, the cell morphology, CD90, Ca19-9, CK19 and vimentin expression were not significantly different between the CD90-depleted and the Ca19-9 enriched cell progenies (Figure 5.3 and Table 5.1). This was not due to higher plating efficiency of the CK19+ cells from the CD90-depleted sort, which was not significantly different between the two sorting strategies ($11 \pm 8\%$ for the CD90-depleted cultures and $15 \pm 5\%$ for the Ca19-9-enriched cultures). Rather, this could be attributed to a higher net expansion of the CK19+ cells in the CD-90 depleted cultures (2.6 ± 1.0 fold for the CD90-depleted cultures versus no significant expansion for the Ca19-9-enriched cultures). Indeed, the fraction of the CK19+ cells that were BrdU+ was more elevated in the CD90-depleted cultures ($40 \pm 14\%$) than in the Ca19-9-enriched cultures ($17 \pm 15\%$).

5.3.3 Development of a screening platform to optimize CK19+ cell proliferation

To identify factors promoting human CK19+ cell proliferation and develop a serum-free medium for CK19+ cell culture, the responses of cultured cells to multiple factors were measured and compared. The serum-free basal CMRL-0.1XITS served as a negative control for platform development. Positive controls included adding FBS concentrations of up to 10% or the reported duct mitogen EGF to the serum-free basal medium. Basal medium conditioned by passaged mitomycin-treated CD90-enriched cultures was also included at 1:2 dilution in basal medium to determine whether soluble factors from the fibroblast-like cells can impact the proliferation of the CK19+ cells. The first response that was considered was the number of CK19+ cells obtained at the end of the cultures compared to the number obtained in basal medium. In the absence of any additives, unsorted cells did not expand in this basal medium (Figure B18 in Appendix B). Figure 5.4A shows that for the unsorted cells seeded on day 0, FBS and EGF significantly increased the number of CK19+ cells in unsorted cultures compared to basal medium alone, with similar trends for the CD90-depleted cells. Conditioned medium from passaged fibroblast-like cells also increased the number of CK19+ cells. This complicates the interpretation of the results for unsorted cells, which

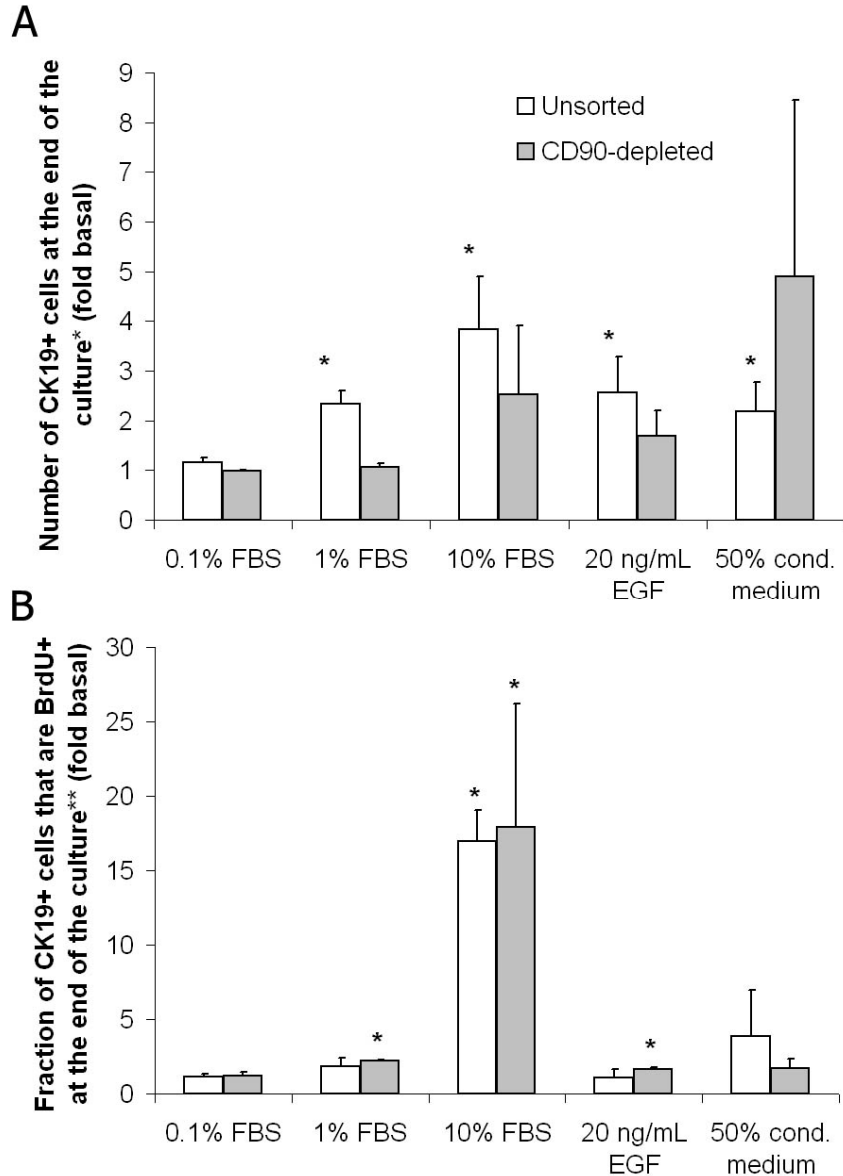


Figure 5.4. Validation of a screening platform to identify CK19+ cell mitogens

The basal medium was CMRL supplemented with 0.1X ITS (insulin, transferrin, selenium). Positive controls included 10% FBS or 20 ng/mL EGF. Unsorted cells were seeded on day 0 while CD90-depleted cells were sorted and seeded on day 1. * $p < 0.05$. **Data pooled from cultures ended at day 8 (N=3 pancreata) or day 6 (N=2 pancreata).

contain $33 \pm 10\%$ vimentin+ fibroblast-like cells, because any effects on the CK19+ cells may be indirectly due to the vimentin+ cells. Therefore, CD90-depleted cells were considered to provide a more reliable source material to screen CK19+ cell mitogens. The signal:noise ratio of the assay was defined as the ratio between the response measured, divided by the standard error of the mean of the response. For the CD90-depleted cells, the signal:noise

ratio was 3.3:1 using the number of CK19+ cells obtained in the presence of 20 ng/mL EGF normalized to the basal medium control. One factor responsible for lowering the range of this assay was that confluency (~5000 cells/well) was reached for 2 pancreata (BC127 and BC129) out of the 8 assayed, even after decreasing the culture duration to end the assay on day 6.

To solve this problem, BrdU incorporation was investigated as a read-out that could be less affected by confluency. In the presence of 20 ng/mL EGF, the fraction of CK19+ cells that had incorporated BrdU was 1.67 ± 0.07 fold the value obtained with basal medium alone (Figure 5.4B), corresponding to a signal:noise ratio of 25:1. Increased BrdU incorporation was observed even when the cultures were confluent on day 6. For instance, the BrdU incorporation by CK19+ cells was 10 ± 3 fold higher than the basal medium control when 10% FBS was added for the BC129 pancreas, even though the cultures were confluent at 5000 ± 230 cells/well. In the presence of 10% FBS, the fraction of CK19+ cells that had incorporated BrdU was $29 \pm 9\%$ in the CD90-depleted cultures. The proliferation of CK19-cells was significantly higher, at $60 \pm 8\%$, as can also be observed in Figure B14 (Appendix B). These results are consistent with the previous observation (Passage 1 cells in Figure 5.1) that the vimentin+ fibroblast-like cells overtake primary human pancreatic cell cultures due to their higher proliferation rate. In summary, BrdU incorporation by CK19+ cells analyzed by Cellomics provided a sensitive platform to screen CK19+ cell mitogens.

5.3.4 Multifactorial screening of the effects of bFGF, EGF, HGF, KGF and VEGF

The methodology developed to identify CK19+ cell mitogens based on BrdU incorporation was then applied to test the effects of five growth factors: bFGF, EGF, HGF, KGF and VEGF. A 2^5 full factorial design of experiments was used to quantify and determine the significance of main effects, as well as up to fifth order interactions between these factors. The two levels chosen for all factors were 0 ng/mL (low level) and 20 ng/mL (high level) based on doses used to promote duct proliferation in the literature (reviewed by Luu 2004). Centre points using 10 ng/mL of all factors were also included, providing some information on the dose response to the factors. Dose response experiments were not initially conducted since factorial design is used in screening experiments, typically

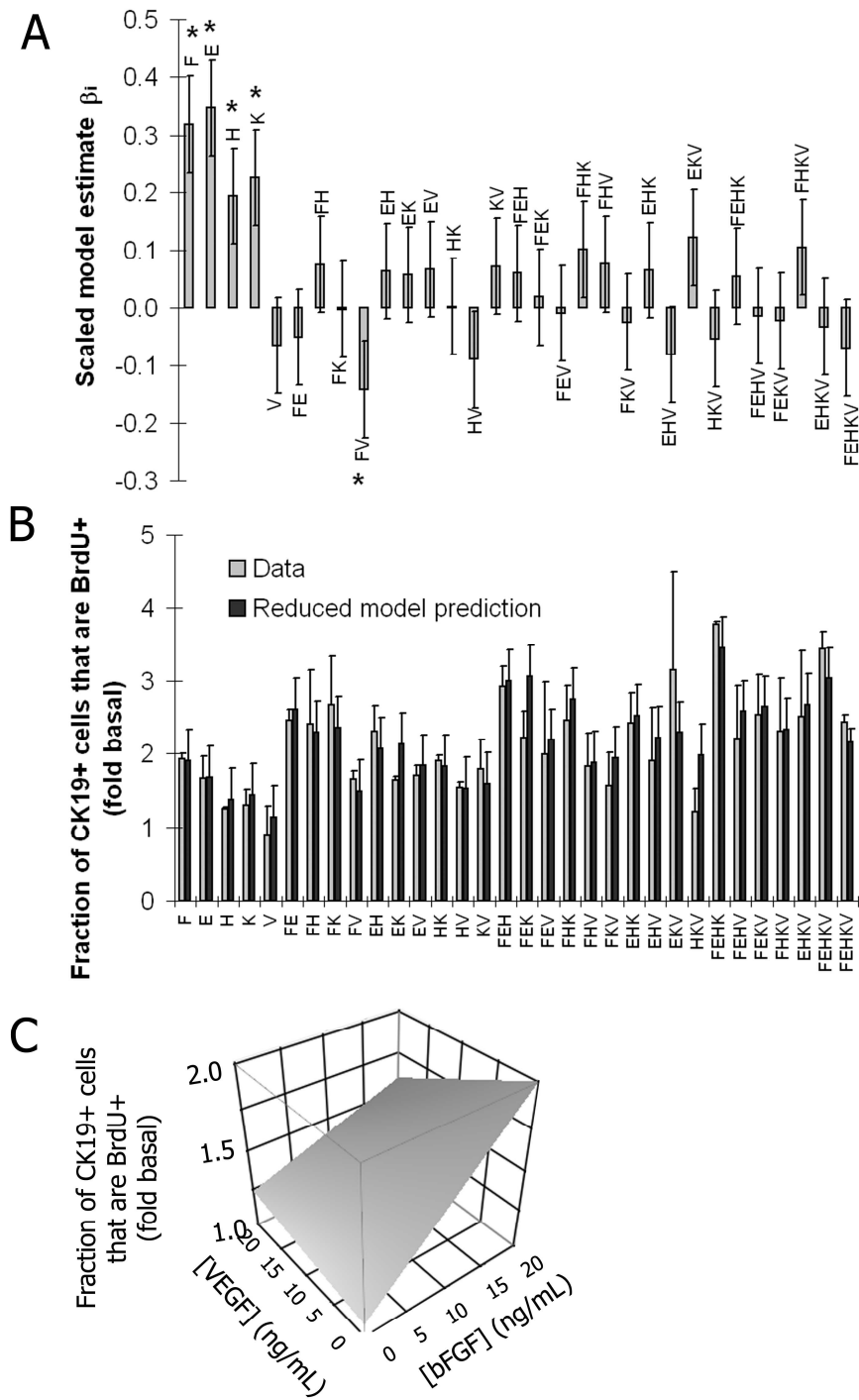


Figure 5.5. 2^5 full factorial effects of bFGF (F), EGF (E), HGF (H), KGF (K) and VEGF (V) on the BrdU incorporation by CD90- purified CK19+ cells.

(A) Scaled parameter estimates of the full factorial model. The response Y was the fraction of CK19+ cells that are BrdU+ on day 6 normalized to the read-out in basal medium for each pancreas. The legend refers to the main effects (e.g. the effect of bFGF alone as "F") and the interaction effects (e.g. the bFGF and EGF interaction effect as "FE"). (B) Raw data compared to the prediction of the reduced model (Equation 5.2). (C) Response surface predicted by the reduced model illustrating the negative interaction between bFGF and VEGF. The concentrations of EGF, HGF and KGF were assumed to be 0 ng/mL. * $p < 0.1$. Note: the p-value for the bFGF*VEGF interaction was 0.09 for the full factorial model and 0.07 for the reduced model. For raw data, the values represent the average of 2 pancreata \pm SEM. For the model prediction, the values represent the predicted value \pm standard error of the model. The model was generated 8 replicate centre points and 32 factorial runs per plate, with triplicate plates for each pancreas (N = 2 pancreata).

followed by central composite designs to determine non-linear effects. However, one dose response experiment conducted later with a single pancreas (BC 130, results shown in Figure B20 in Appendix B) showed that the doses of KGF and bFGF may have been insufficient to detect some of their effects, particularly with older pancreata (the BC130 donor was 58 years old). The response measured (\hat{Y}) was the fraction of CK19+ cells that were BrdU+ on day 6 normalized to the value obtained in the absence of growth factors. Cell apoptosis on day 2 was also examined, but did not yield any significant effects except for a reduction in apoptosis by KGF (Figure B21 in Appendix B). For the CK19+ cell proliferation response, Figure 5.5A shows the values of all the scaled model parameters β_i except for the model intercept β_0 . For the scaled model, the units of all parameters are dimensionless since the independent (Y) and the dependent (x_i) variables are dimensionless. As expected, the model prediction Y when all growth factor concentrations were set to 0 ng/mL (scaled values of x_i of -1) averaged close to 1.0 for both BC129 (1.16 ± 0.96) and BC130 (0.97 ± 0.96), since the response was normalized to the “no growth factor” condition for each pancreas. The model intercept (β_0) was 2.15 ± 0.07 , which signifies that the BrdU incorporation by CK19+ cells was ~ 2.15 fold higher in the presence of 10 ng/mL of all five growth factors vs. in the absence of growth factors. This provided a first indication that at least one of the growth factors significantly increased CK19+ cell proliferation. Based on the p-values associated with each of the model parameters, all of the growth factors tested except for VEGF had a significant ($p < 0.05$) positive main effect on CK19+ cell proliferation. Among these, the effect of EGF was among the greatest, at 0.35 ± 0.8 . This means that increasing the concentration of EGF to 20 ng/mL from 10 ng/mL while keeping all the other concentrations at 10 ng/mL led to an average Y value of 2.50 compared to 2.15. However, if all growth factor concentrations are 0 ng/mL (or scaled x_i value of -1) with only EGF at 20 ng/mL, the Y value predicted by the model is 1.83 ± 0.95 . In other words, adding EGF alone leads to ~ 1.8 fold increase in the BrdU incorporation by CK19+ cells compared to the no growth factor condition. Even though scaled models are useful to directly compare lower order to higher order effects, mental calculation of model predictions based simply on the scaled model parameters is more arduous.

A simplified reduced model was thus derived by removing any parameters with $p > 0.1$ from the scaled model. After removing variable scaling to obtain a model of the same form as Equation 5.1, the reduced model equation (Equation 5.2) was found to be:

$$Y = 1.13 + 0.0318[bFGF] + 0.0347[EGF] + 0.0194[HGF] + 0.0226[KGF] - 0.0066[VEGF] + -0.00142[bFGF] \cdot [VEGF]$$

(Equation 5.2)

Where the standard error of the intercept was 0.19, the standard error of all main effects was 0.078 and the standard error of the bFGF*VEGF interaction effect was 0.00078. Most parameters were clearly significant ($p < 0.02$) while the VEGF main effect was not significant ($p = 0.4$) and the bFGF*VEGF interaction effect had p values closer to the statistical significance cut-off ($p = 0.07$). Although the reduced model was relatively simple, the trends found in the fold increase in BrdU incorporation by CK19+ cells in the presence of various growth factor combinations were well reflected by the model (Figure 5.5B). Both the raw data and the model indicate that the best combination of factors to promote CK19+ cell proliferation is the

addition of bFGF, EGF, HGF and KGF (denoted as FEHK in the graph) without adding VEGF. The negative interaction between bFGF and VEGF that was included in the reduced model is derived from, for instance, how the “FV” condition gives a lower result than “F” alone, or how the “FKV” condition gives a lower result than “FK”.

Figure 5.5C further illustrates the negative interaction between bFGF and VEGF on BrdU incorporation by CK19+ cells as predicted by the reduced model. For this simulation, the EGF, HGF and KGF concentrations were assumed to be 0 ng/mL. When the VEGF concentration is at 0 ng/mL, bFGF exerts a large positive effect on the normalized BrdU incorporation by CK19+ cells. There is also a small (though non-significant) positive trend in CK19+ cell proliferation with increasing VEGF concentration when the bFGF is kept constant at 0 ng/mL. However, when the VEGF concentration is 20 ng/mL, the magnitude of the positive effect of bFGF is reduced to ~40% of its magnitude in the absence of VEGF.

Figure 5.6 shows the fold expansion of CK19+ cells or vimentin- cells for the BC130 pancreas in basal screening medium or with basal medium and the addition of the optimal bFGF, EGF, HGF and KGF growth factor combination. The vimentin- cells expanded 2.72 ± 0.06 fold during 4 days in the presence of this growth factor combination, which was significantly higher than 1.61 ± 0.02 fold expansion in basal medium. The increase in the expansion of the CK19+ cells was not significantly higher in the presence of the growth factors, but the trends were the same as for the vimentin- cells.

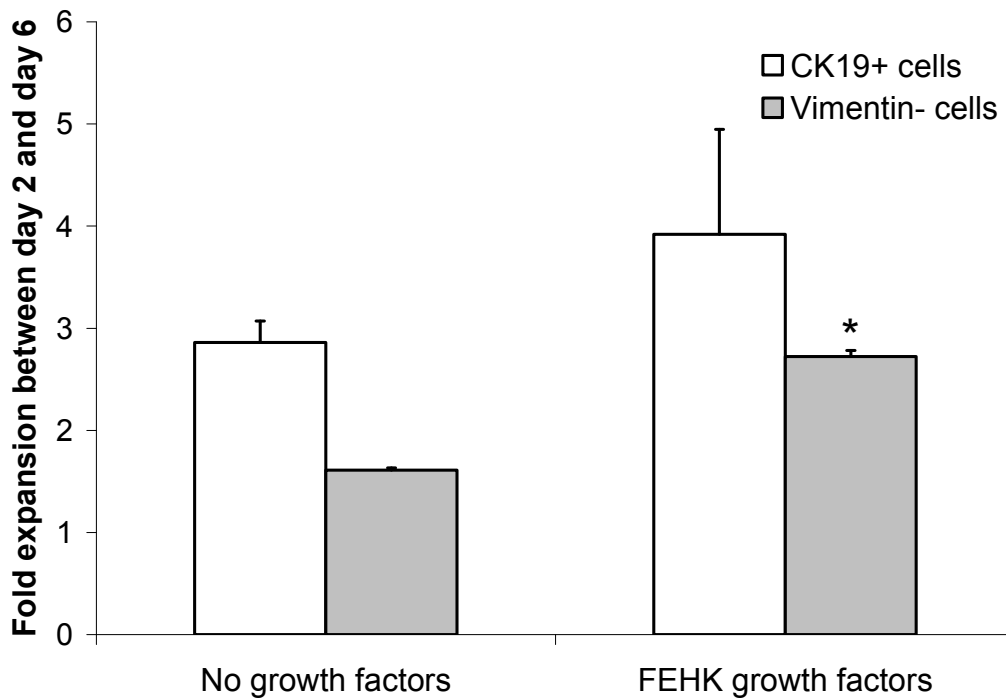


Figure 5.6. Fold expansion of CD90-depleted CK19+ cells or vimentin- cells in basal medium or basal medium + bFGF, EGF, HGF and KGF, all at 20 ng/mL.

The initial number of CK19+ cell seeded was 402 cells/well and the number of CK19+ cells counted in the wells at day 2 after overnight plating in CMRL-10FBS was 318 ± 29 cells/well. The initial number of vimentin- cells seeded was 3.4×10^4 cells/well and the number of vimentin- cells counted on day 2 was 659 ± 154 cells/well. Cellomics was used to enumerate the cells on days 2 and 6. The data represent the average of triplicate wells in triplicate 96-well plates for the BC130 pancreas.

5.3.5 Effect of alginate immobilization of CD90 sorted cells on insulin expression

After 7 days of adherent culture of unsorted cells, CD90-enriched and CD90-depleted cells were immobilized separately in alginate beads generated by emulsion and internal gelation (Figure 5.7). As expected from the results in Chapter 3 (Figure 3.12), the

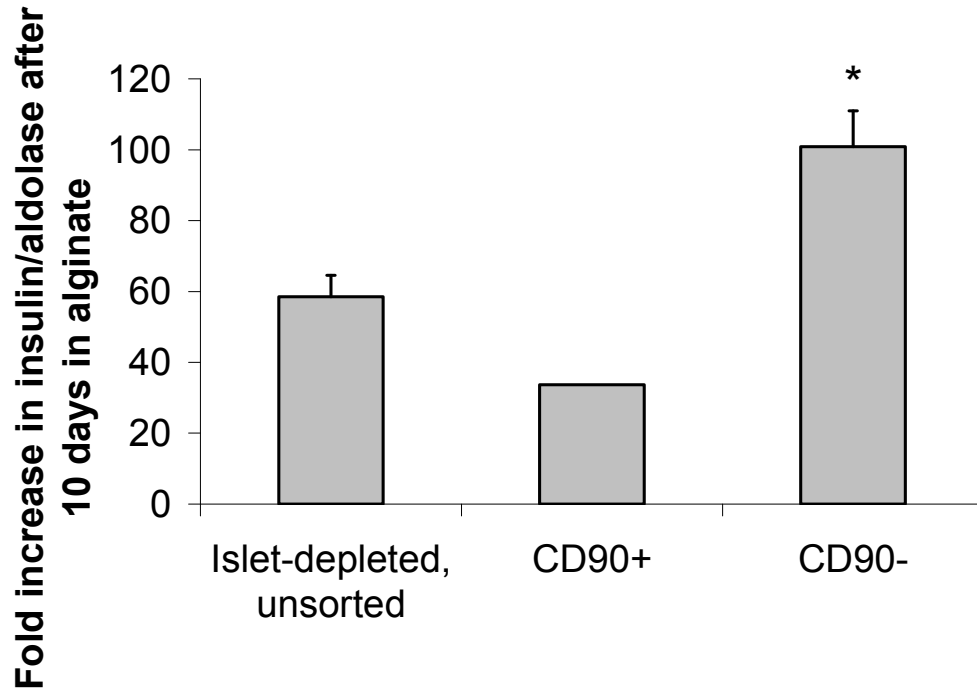


Figure 5.7. Insulin expression of alginate-immobilized CD90 sorted cells

Non-dispersed islet-depleted human pancreatic cell aggregates were kept in serum-containing adherent cultures for 7 days. On day 7, the cells were MACS sorted and immobilized in emulsion-generated 1.5% alginate beads. The cells were kept in serum-free immobilized culture until day 17. The fold increase in insulin/aldolase represent the expression levels at day 17 divided by the expression at day 7. Each bar represents the average \pm SEM of 3 independent cultures (immobilized in separate process batches) performed for N=1 pancreas. The CD90+ cells do not have an error bar because the number of cells available was insufficient to generate more than one batch of emulsion beads. *p < 0.05 compared to the increase measured for unsorted tissue. Note that the increase measured for the CD90+, although not replicated, was not included within the confidence interval determined for the unsorted tissue.

insulin expression of unsorted cells significantly increased during 10 days of serum-free alginate immobilized culture by 58 ± 6 fold. The increase observed for the CD90-depleted cells (100 ± 6 fold) was ~triple the increase observed for the CD90-enriched cells (33 fold).

5.4 DISCUSSION

Duct-like CK19+/Ca19-9+ cells derived from human pancreatic islet-depleted cells could be differentiated, trans-differentiated or reprogrammed to express insulin and serve as an alternative source of tissue for islet transplantation. In addition, the study of these cells could provide more insight into the normal function and plasticity of human duct and/or

exocrine pancreatic cells. The islet-depleted by-product generated during islet transplantation procedures is a convenient source of human duct and acinar pancreatic cells. Two main cell populations arise in adherent cultures of this tissue: (1) fibroblast-like cells with spindle-shaped morphology that express vimentin, CD90 and other mesenchymal cell markers and (2) duct-like cells that grow in cobblestone patterns and express CK19, carbonic anhydrase and other pancreatic duct markers. However, the study of the duct-like cells derived from this mixed tissue is hampered by fibroblast-like cell overgrowth, the small overall expansion of the duct-like cells in culture and the lack of a serum-free medium to study these cells without interference from unknown components found in serum. Since the fibroblast-like cells are fast-cycling and have high plating efficiency, the duct-like cells derived from this mixed tissue are generally not passaged prior to being studied (Bonner-Weir et al. 2000; Gao et al. 2007; Gao et al. 2005; Gao et al. 2003; Lipsett et al. 2007; Todorov et al. 2006).

Several strategies have been used to reduce or eliminate the fibroblast-like cells. Pancreatic duct dissection coupled with digestion protocols optimized for duct cell survival and adhesion obtained >90% pure duct-like epithelial cell cultures from rodents (Chen et al. 2009a) and humans (Trautmann et al. 1993). The human duct-like cells can be maintained in culture for up to 5 weeks if fibroblast overgrowth is avoided by selective cell scraping (Trautmann et al. 1993). However, this requires human pancreatic duct dissection rather than the simpler use of the more commonly tissue discarded after islet transplantation. Pre-plating reduces but does not completely eliminate contaminating fibroblast-like cells (Bonner-Weir et al. 2000). Treatment with G418 leads to highly purified endothelial cell cultures (Zhao et al. 2005), but this non-specifically affects any cycling cells in cultures. Fluorescence or magnetic-activated cell sorting of CA19-9 expressing cells generates highly purified duct cell cultures without contribution from acinar cells (Gmyr et al. 2004). However, positive cell sorting strategies using magnetic beads can affect cell survival and function (Berry et al. 2004; Pisanic et al. 2007). One aim of Chapter 5 was to obtain fibroblast-depleted pancreatic exocrine cell cultures using scalable methods while avoiding the presence of magnetic beads on the cells of interest. Another aim was to avoid removing

acinar cells, since the CK19+/Ca19-9+ cells arising from acino-ductal transdifferentiation likely contribute to the generation of insulin+ cells (Minami et al. 2005; Okuno et al. 2007) from pancreatic exocrine tissue and may be of interest for studies related to pancreatic cancer progression (Means et al. 2005). Fibroblast/mesenchymal cell surface markers that could allow the selective elimination of these cells were therefore considered as candidates for the development of a negative cell sorting strategy. Pancreatic fibroblast-like cells express several mesenchymal stem cell markers, with >98% expressing CD90 and CD105, 94% expressing CD44, and <60% expressing CD49b or CD54 (Seeberger et al. 2006). As expected, we identified a distinct CD90+ cell population representing $34 \pm 20\%$ of the adherent cells after 7 days of culture, corresponding to the $33 \pm 10\%$ vimentin+ cells enumerated in the cultures. When the CD90+ cells were removed by magnetic-activated cell sorting after 1 day adhesion, the reseeded CD90+ cells generated fibroblast-like vimentin+ cells, while the reseeded CD90- cells generated CK19+ ($54 \pm 4\%$) and Ca19-9+ ($86 \pm 7\%$) cells with epithelial morphology (Figure 5.3). The lower CK19+ cell fraction compared to Ca19-9 likely results from an under-estimation of the CK19+ cells by Cellomics analysis compared to FACS. Setting thresholds using Cellomics data, where the fluorescence is quantified in a small region surrounding each nucleus, is more problematic than with FACS, where the whole cell fluorescence is quantified. Also, the Cellomics thresholds needed to be conservatively high due to crossover of the BrdU green signal into the CK19 red channel. The addition of compensation algorithms to the Cellomics software or the use of more distinct fluorophores could reduce the under-estimation of CK19+ cell numbers in future experiments. Most important, even though only a small fraction ($0.61 \pm 0.23\%$) of the cells expressed CD90 on day 1, removal of this population led to cultures with <2% CD90+ cells at day 8, compared to between 15% and 54% CD90+ cells in the unsorted cultures.

The CD90-depletion strategy to remove fibroblast-like cells was compared to the established Ca19-9+ cell sorting method, since the two main populations present in unsorted cultures were duct-like (Ca19-9+) cells and fibroblast-like (CD90+) cells. Cultures obtained at day 8 from the CD90-depleted cells were very similar to the cultures obtained from the Ca19-9-enriched cultures in terms of cell phenotype and number. Yet, the initial CK19+ cell

number seeded was 2.5 fold lower for the CD90- sorted cells compared to the Ca19-9+ sorted cells due to the presence of acinar cells in the CD90- sorted population. It is possible that the additional CK19+ cells in the CD90- sorted populations arise from acino-ductal transdifferentiation (Means et al. 2005; Minami et al. 2005; Rooman et al. 2000). However, higher CK19+ cell proliferation for the CD90- sorted cells than for the Ca19-9+ sorted cells could also explain these results. Indeed, the fraction of the CK19+ cells that had incorporated BrdU between days 7 and 8 was >2 fold higher for the CD90-depleted cultures cells than for the Ca19-9-enriched cultures. It is possible that molecules released by lysing amylase+ cells (Nguyen et al. 1999) or contaminating endocrine cells (Gao et al. 2005) increased the CK19+ cell proliferation in the CD90-depleted cultures by mechanisms similar to those occurring after pancreas injury (Sakaguchi et al. 2006). The presence of antibodies and MACS beads on the surface of the Ca19-9+ cells may have decreased their subsequent proliferation or survival. Another indication that additional CK19+ cells did not come from trans-differentiated acinar cells arises from one experiment (pancreas BC148) where CD90 and Ca19-9 cells were co-depleted. After 7 days of culture, very few CK19+ cells (~25 cells/well) were found in Ca19-9 and CD90 co-depleted cultures, compared to CD90-depleted cultures (~1900 CK19+ cells/well).

The sum of the CK19+ and the vimentin+ cells did not account for 100% of the cells present at day 8. However, less than 1% amylase+ and no insulin+ cells were found in any of the cultures on day 8. Part of the missing population may be due to cells that did express these markers but were not identified as positive by the Cellomics algorithm which relies on the pixel intensity in a small region surrounding the cell nucleus. However, analysis of the cells by FACS on day 8 also identified a population of $6 \pm 7\%$ of the cells in the cultured unsorted cells and $13 \pm 7\%$ in the CD90-depleted cultures that were not labelled by either CD90 or Ca19-9. These observations suggest that vimentin, CD90, CK19, Ca19-9, amylase or insulin staining failed to label a population present in the cultured cells. This population may represent other pancreatic endocrine cell types, endothelial cells or de-differentiated pancreatic (e.g. acinar) cells with undetectable levels of the aforementioned markers. Similar to other reports of selective human pancreatic acinar cell death (Klein et al. 2009; Street

2004), we did not observe any amylase+ cells co-stained with CK19 and the amylase+ cells observed were of irregular shape, with condensed nuclei characteristic of apoptotic cells (Wyllie et al. 1984). Lineage tracing studies with primary human pancreatic tissue could help determine the fate of acinar cells in these culture conditions.

CD90 depletion could be combined with other sorting strategies to separate the main cell populations in adult human pancreatic tissue. The contribution of acino-ductal transdifferentiation to the CK19+ cells could be verified by separating CD90-/Ca19-9+ cells, which should be mainly duct cells, from CD90-/Ca19-9- cells, which should mainly represent acinar cells. This would constitute a novel strategy to purify human pancreatic acinar cells. This sorting strategy to separate duct and acinar cells could also help elucidate the mechanisms and cell types involved in pancreatic cancer progression. For example, the purified duct-like cells could be infected with the K-ras oncogen, one of the initial events in the development of pre-cancerous lesions (Qian et al. 2005). This could be followed by co-infection with other oncogenes to determine which combinations lead to neoplastic conversion, and which pathways are activated during these events. Then, drug screening may allow the discovery of compounds that inhibit this conversion. CD90-depletion could also be useful to purify dispersed human islets. For instance, the anti-CD90 and anti-Ca19-9 antibodies could be mixed to remove duct and fibroblast-like cells in a single step prior to NCAM+ sorting (Banerjee and Otonkoski 2009).

Next, a Cellomics-based imaging method was developed to screen CK19+ cell mitogens. CD90-depleted cells were used rather than unsorted populations to avoid measuring indirect effects exerted by vimentin+ cells on the CK19+ cells. Indeed, serum-free basal medium conditioned by CK19-/vimentin+ cells generated by passaging the CD90-enriched cells significantly increased CK19+ cell expansion. The use of the CK19+ cell expansion as a read-out for optimization was problematic due to the broad range in cell yield depending on the pancreas. For 40 000 unsorted total cells seeded per well, the final cell number after 7 days of culture in the presence of 10% FBS varied between 75 ± 24 cells/well (BC123 Pancreas) and 5231 ± 395 cells/well (BC127 pancreas). However, the BrdU incorporation by CK19+ cells was increased in the presence of positive control media even

for pancreata that reached confluency at the end of the cultures. In addition, the magnitude of the effect of 20 ng/mL EGF used as a positive control was higher for BrdU incorporation than for CK19+ cell number. To further minimize the effects of premature cell confluency, the cultures were terminated on day 6 instead of day 8.

This screening platform for BrdU incorporation by CK19+ cells was then used to quantify the main and interaction effects of five reported pancreatic duct mitogens – bFGF, EGF, HGF, KGF and VEGF – on primary pancreatic CD90-depleted cells. Factorial design, still an under-utilized tool for stem/progenitor cell culture optimization (Audet et al. 2002; Chen et al. 2009b; Fan et al. 2009; Szabat et al.), increases the statistical power of experiments and reduces the number of runs required compared to two-way comparisons (Yang et al. 2009). The results from factorial analysis and model reduction showed that bFGF, EGF, HGF and KGF had a significant positive main effect on CK19+ cell proliferation. The addition of 20 ng/mL of each individual factor resulted in ≥ 1.5 fold higher BrdU incorporation than in the absence of growth factors, based on the reduced factorial model. On the other hand, VEGF did not increase CK19+ cell proliferation and instead counteracted the mitogenic effects of bFGF when the two factors were added together.

The main effects of bFGF, EGF, HGF and KGF were consistent with the effects reported in the literature. Growth factors secreted by the mesenchyme play an important role in the expansion of early pancreatic epithelial progenitors during development (Scharfmann 2000). For example, KGF is expressed in the developing pancreatic mesenchyme and its receptor is expressed in the proliferating developing pancreatic epithelium, which responds to endogenous (Pulkkinen et al. 2003) or exogenous KGF (Elghazi et al. 2002; Ye et al. 2005) by increased growth. bFGF appears to be the more important for postnatal proliferation of pancreatic duct cells (Inchovska et al. 2006; Ogneva and Martinova 2002). The EGF receptors are expressed in the pancreatic epithelium during development and EGF treatment increases the proliferation of embryonic pancreatic epithelial cells *in vitro* (Miettinen et al. 2008). However, knock-down of the EGF receptor mainly affected pancreatic β -cell delamination from the ductal tree (Miettinen et al. 2000) and reduced postnatal β -cell growth (Miettinen et al. 2006), rather than affecting the

epithelium. Over-expression of heparin-binding EGF-like growth factor in the mouse pancreas led to pancreatic duct metaplasia (Means et al. 2003) and systemic EGF administration in adult pigs caused pancreatic duct hyperplasia (Vinter-Jensen et al. 1997). Similar to FGFs, HGF is likely involved in signalling between the developing pancreas, expressing the HGF receptor c-Met, and the surrounding mesenchyme, expressing HGF (Sonnenberg et al. 1993). HGF increased the expansion of tissue derived from fetal (Beattie et al. 1996) and adult (Beattie et al. 2002) human islets. Most of the proliferating cells in these cultures were CK19+ and insulin-. The c-Met receptor has been suggested as a marker of multipotent pancreatic progenitor cells (Oshima et al. 2007; Suzuki et al. 2004) that may reside in terminal ducts or centroacinar cells (Rovira et al. 2010). In addition, bFGF (Abraham et al. 2002; Zulewski et al. 2001), EGF (Abraham et al. 2002; Lechner et al. 2005; Lipsett et al. 2007; Rescan et al. 2005; Tsang et al. 2007; Zulewski et al. 2001), HGF (Gao et al. 2005) and KGF (Bonner-Weir et al. 2000; Gao et al. 2003; Hao et al. 2006) have been added to adult human pancreatic cultures to increase the yield or purity of CK19+ cells. Human pancreatic epithelial cells or subsets thereof have been shown to express the respective receptors for these factors (Ishiwata et al. 1998; Itakura et al. 2000; Kobrin et al. 1993; Liu et al. 1998; Rescan et al. 2005; Tomioka et al. 1995). However, the current study represents the first side-to-side comparison of the mitogenic effects of all four of these factors on human pancreatic tissue, demonstrating that their effects are additive (Figure 5.5).

The lack of effect of VEGF alone on adult human pancreatic CK19+ cells contradicts its reported mitogenic effect on fetal (Obergh-Welsh et al. 1997) and adult (Rooman et al. 1997) rat pancreatic endothelial cells *in vitro*. VEGF had no significant effect on the proliferation of duct or acinar cells in serum-free suspension cultures of islet-depleted human pancreatic tissue (Klein et al. 2009). Signals from blood vessels including VEGF signalling are thought to be crucial for pancreas specification of the developing foregut endoderm (Lammert et al. 2001). VEGF pancreatic over-expression leads to high pancreas vascularization and islet hyperplasia. Culturing fetal pancreatic tissue in the presence of VEGF increased the insulin secretion and content, without increasing islet proliferation. VEGF may therefore be more important for pancreas and β -cell differentiation rather than

duct cell expansion. Some confusion over the effects of VEGF on duct cells *in vitro* may arise from indirect effects of VEGF on mesenchymal cells (Jacquemin et al. 2006), underlining the importance of the CD90-depletion cell sorting strategy described in this study. The negative interaction between VEGF and bFGF uncovered by the factorial experiment could explain the contradicting *in vitro* results with VEGF, which may depend on the other factors present in the culture medium. This negative interaction could also explain the poor prognosis of pancreatic cancers with low expression of the VEGF receptor Flt-1 (Chung et al. 2006), since most of these cancers over-express bFGF and its receptors (Kornmann et al. 1998). The finding that bFGF and VEGF have a negative interaction on pancreatic CK19+ cell proliferation underlines the importance of quantifying interaction effects before combining growth factors in culture, even if they were individually reported to exert a desired effect.

The high content screening platform using CD90-depleted human pancreatic tissue could be used to further optimize pancreatic CK19+ cell culture conditions by testing other growth factors, basal media, media additives or coating of the culture surface with extracellular matrix components. Although the screening results presented in this work served mainly as a proof-of-concept, the results provide interesting leads for future investigation. The effect of conditioned medium from CD90-enriched cells on the CD90-depleted cells has already been described for Ca19-9 sorted cells (Yatoh et al. 2007). However, the secreted factors responsible for this effect are unknown. The conditioned medium could be fractionated and analyzed by mass spectrometry to identify active fractions or molecules. Also, the molecular mechanisms of the negative interaction between VEGF and bFGF should be investigated. Lastly, even though the growth factor concentrations could be further optimized, the bFGF, EGF, HGF and KGF-supplemented serum-free medium could be used in protocols requiring the expansion of pancreatic CK19+ cells.

The CD90-depleted cell culture platform could be used in high content screening experiments to discover molecules that promote or hinder pancreatic cancer development using primary human tissue. Most *in vitro* studies are currently performed on exocrine tissue explants consisting of mixed non-islet pancreatic cells from transgenic mice pre-

disposed to develop pancreatic duct adenocarcinoma (Means et al. 2003; Wagner et al. 2001). These explant cultures can form CK19+ tubular complexes *in vitro* that are similar to pre-cancerous cysts observed during adenocarcinoma progression *in vivo* (Furukawa et al. 2006). Studies in humans largely rely on tissue biopsies or *in vitro* experiments using pancreatic adenocarcinoma-derived cell lines (Deer et al. 2010). The culture method described in Chapter 5 provides an additional system to study normal human pancreatic exocrine cell biology and the mechanisms that can lead to their neoplastic conversion. For example, the effect of small molecules or antibodies on the apoptosis, yield and proliferation of normal pancreatic CK19+ cells obtained from CD90-depleted cultures could be compared to pancreatic cancer cell lines in an effort to uncover therapeutic targets for pancreatic cancer.

Lastly, to test a potential application of the cells generated by CD90 depletion, the cells were immobilized in emulsion-generated alginate beads. The results suggested that CD90- rather than CD90+ cells were responsible for the increased insulin expression that had been observed during alginate-immobilized culture in Chapter 3 (Figure 3.12). The CD90+ cells also showed an increased insulin expression during immobilized culture, but this could be due to the lack of purity obtained in the CD90-enriched fraction immediately after MACS (see the CD90+ panel on day 1 FACS plot in Figure 5.2). The CD90-depleted cells should be further sub-fractionated to refine the identity of the cells responsible for this increase (i.e. duct cells, acinar cells, contaminating β -cells or others).

5.5 CONCLUSIONS

In conclusion, Chapter 5 describes a novel negative cell sorting strategy to remove CD90+ fibroblast-like cells from human pancreatic exocrine cell cultures, as well as a high content imaging method to identify soluble factors that increase CK19+ cell proliferation in the cultures. CD90-depletion by magnetic-activated cell sorting decreased CD90+ cell contamination after 7 days of culture from $34 \pm 20\%$ to $1.3 \pm 0.6\%$, yielding cultures of epithelial CK19+ cell phenotype. The fraction of BrdU+ cells among CK19+ cells after overnight incubation between days 5 and 6 was a robust method to detect the mitogenic effects of growth factors on these cells. This method confirmed the positive effects of bFGF,

EGF, HGF and KGF on CK19+ cell proliferation, but not VEGF. Full factorial analysis of the effects of combinations of these factors demonstrated that the positive effects of bFGF, EGF, HGF and KGF are additive at 20 ng/mL concentrations. A negative interaction was identified between VEGF and bFGF, exemplifying the importance of assessing interaction effects before using combinations of growth factors to expand desired cell types. The CK19+ cells obtained after CD90-depletion and expansion in the optimized serum-free medium could be used as a source of cells to generate islet-like clusters by various differentiation protocols or by genetic reprogramming. High content imaging of BrdU incorporation primary purified CK19+ cells could accelerate studies of normal pancreatic duct proliferation and cancer progression.

6 CONCLUSIONS AND FUTURE DIRECTIONS

Significant advances in clinical islet transplantation, in particular the development of the Edmonton protocol, have provided a new approach to treat type 1 diabetes that could greatly diminish the long-term complications of the disease. Further advances depend on making available more therapeutic cells for transplantation and prolonging their efficacy. Surrogate sources of tissue include β -cell progenitors derived from embryonic stem cells or from adult human pancreatic tissue. Alginate immobilization has been used both as a tool to differentiate these progenitors into β -cells and to protect cells from immune rejection. However, there is a need for improved scalable and robust protocols for the clinical expansion and/or alginate immobilization of these progenitors. This thesis discusses the development of an expansion protocol for primary cells that could be differentiated or re-programmed into insulin-producing cells, as well as two novel alginate immobilization bioprocesses. Specifically, this work has shown that:

1. An alginate-filled hollow fiber bioreactor can be used to expand mammalian cells into islet-sized cell aggregates at the same rate as in small-scale alginate slab cultures. Neonatal porcine pancreatic cell clusters were successfully cultured and their insulin content increased in the bioreactor.
2. An emulsion and internal gelation process was adapted to be suitable for mammalian cell encapsulation with 90% process survival for mouse insulinoma cell lines, as long as the pH during internal gelation was maintained within pH 6.5 to 8.0. The growth rate and glucose-stimulated insulin secretion of MIN6 cells immobilized by this process were not altered compared to the “standard” beads generated by extrusion and external gelation. Alginate-immobilized culture for 10 days increased the insulin expression of human islet-depleted pancreatic tissue by 10- to 160-fold, depending on the pancreas.
3. The emulsion and internal gelation process allows bead generation over a wide range (0.004 Pa·s to 112 Pa·s) of alginate viscosities. In particular, this allowed the generation of high-concentration alginate beads with greater exclusion of antibody-sized molecules from the bead volume (e.g. ~80% for the 5% emulsion alginate beads

compared to ~50% for the 1.5% extrusion alginate beads). The high-concentration beads improved the survival of β TC3 cells transplanted into streptozotocin-induced diabetic allogeneic mice. This improvement may be due to higher bead stability and/or to lower bead permeability, leading to improved isolation from both innate and adaptive immune cells and molecules. A further optimized emulsion and internal gelation process may therefore allow the generation of beads suitable for immune isolation, without the need for cationic polymer coating.

4. Removing CD90-expressing fibroblast-like cells from primary cultures of islet-depleted human pancreatic cells generates purified cultures with duct phenotype. The BrdU incorporation by proliferating CD90-depleted cells in serum-free medium allows the high content screening of duct mitogens. Using statistical design of experiments, bFGF, EGF, HGF and KGF were found to promote the proliferation of duct-like cells, while VEGF counter-acted the effects of bFGF. For this application, these two factors should not be used in combination. In addition, it was shown by quantitative PCR that insulin expression by the CD90-depleted cells increased ~100 fold after 10 days in alginate compared to ~30 fold increase for the CD90-enriched cells, suggesting that the CD90- cells were responsible for this change in expression.

The novel processes presented in this work represent significant advances compared to currently available methods. The culture of purified duct-like cells described in Chapter 5 is a step forward relative to the previous use of mixed islet-depleted pancreatic tissue cultures to generate insulin+ cells (Bonner-Weir et al. 2000; Gao et al. 2005; Gao et al. 2003; Lipsett et al. 2007; Todorov et al. 2005; Todorov et al. 2006; Zhao et al. 2005 and see also Table B1). In most of these studies, the use of mixed cultures made questionable the cell type responsible for the differentiation. In Chapter 5, the CD90-depletion method led to the purification of the cell population responsible for the alginate-induced increase in insulin expression. The sorting method used (MACS) is also clinically scaleable, an advantage over manual scraping of fibroblast-like cells (Trautmann et al. 1993). Even after 7 days of culture, the CD90+ cell contamination remained <2%, contrary to the pre-plating method (Bonner-

Weir et al. 2000; Kerr-Conte et al. 1996). The culture of the cells purified by a negative sorting strategy in the optimized serum-free medium described in Chapter 5 would be useful clinically, since both animal proteins and magnetic beads on transplanted cells would be undesirable. The broader use of optimized serum-free media could improve the reproducibility of the results between laboratories. Lastly, duct-like cells were shown to proliferate and expand 3~4 fold in the serum-free medium, compared to the <2 fold total cell expansion, and in some cases no net cell expansion, reported by other groups in serum-containing medium (Table B1).

The hollow fiber or the emulsion and internal gelation bioprocesses distinguish themselves from currently available cell encapsulators because the immobilization is performed in a single batch instead of bead-by-bead. This avoids the proportional increase in processing time with the batch volume that is associated with nozzle extrusion encapsulators. Furthermore, this should contribute to improving process reproducibility by making the cellular exposure to process conditions more consistent. The hollow fiber bioreactor imparts relatively low shear stress on the cells since it does not require droplet generation. However, representative and regular cell sampling during culture in the hollow fiber unit is problematic. Monitoring instead depends on medium sampling that would allow, for example, the regular monitoring of glucose-responsive insulin secretion of the differentiating cells. The stirred tank emulsion and internal gelation process is highly scalable: the food industry uses emulsions at m³ scales. The cell survival during cell immobilization by the adapted MOPS-based emulsion process developed in Chapter 3 was similar to the cell survival after cell immobilization in alginate beads generated by a conventional cell encapsulator. The emulsion and internal gelation process is much more flexible, allowing the generation of beads with a broad range of average bead diameters (200 to 2000 μm) by simply adjusting the agitation rate. The alginate solutions can be of a much broader range of viscosities (0.004 to 112 Pa·s) than has been demonstrated by any of the currently available bead generators. Nozzle-based encapsulators are limited to solutions above a certain viscosity to avoid bead deformation upon contacting the gelling bath, as well as to solutions below a certain viscosity beyond which droplet formation at a desired

flow rate and maximum pressure drop becomes difficult. The characteristics of these two novel bioprocesses are compared to commonly used alginate encapsulation technologies in Table 6.1.

Table 6.1. Characteristics of alginate immobilization bioprocesses

Process	Potential production rate (approx.) (mL/h)	Range of alginate viscosities (Pa·s)	Equipment cost of commercial units* (\$)	Tested <i>in vivo</i> ?	Tested with pancreatic cells?	Sample references
Emulsion & internal gelation	>30 000	0.004 – 112	<10 000	√	√	This work
Hollow fiber bioreactor	>2 000	At least 0.02 – 0.3	<10 000		√	This work, (Hoesli et al. 2009)
Spinning disk	15 000	Not tested; 2 – 3% alg.	>3200			(Senuma et al. 2000)
Multiple vibrating nozzles	4 000	0.05 – 0.09	~150 000	√	√	(Brandenberger and Widmer 1998)
Multiple electrostatic nozzles	700	0.03 – 11	~150 000	√	√	(Lewinska et al. 2008; Poncelet et al. 1994)
Vibrating nozzle	600	0.05 – 0.09	15 000~40 000	√	√	(Dufrane et al. 2006b; Koch et al. 2003)
JetCutter®	330	0.15 – 11	>10 000	√		(Koch et al. 2003; Schwinger et al. 2002)
Alginate slabs	<100	Not reported but broad	<1000	√	√	(Storrs et al. 2001; Tatarikiewicz et al. 2001)
Electrostatic bead generator	16	0.03 – 11	~15 000	√	√	(Cui et al. 2004; Poncelet et al. 1994)
Air jet	10	0.03 – 5	~15 000	√	√	(Koch et al. 2003; Prusse et al. 2008; Schneider et al. 2003)

* Pricing of a stirred 30L agitator (T50 unit) for emulsion generation was provided by IKA® Works, Inc. Pricing of vibrating nozzle encapsulators (EBS-BT-1 unit) was provided by EncapBiosystems Inc. (Greifensee, Switzerland) and Nisco Engineering AG (Zürich, Switzerland). The price of a non-aseptic spinning disk atomizer was provided by Northern Industrial Distributing®. The pricing of hollow fiber and JetCutter units were estimated. Pricing of all other units was provided by Nisco.

There are many potential applications of the pancreatic cell culture methods presented in this work, as well as several avenues to further improve their performance. The

duct mitogens screening method developed in Chapter 5 should provide an improved cell source for the discovery of molecules that either promote or hinder the proliferation of these cells. Cells uniformly differentiated or re-programmed into insulin-producing cells, with further optimization of culture conditions, could be maintained in long-term cultures and cryopreserved for the treatment of HLA-matched diabetic patients. Conversely, the discovery of molecules that arrest the growth of pancreatic duct adenocarcinoma cells without affecting normal duct cells could lead to a treatment for pancreatic cancer. The interesting observation that alginate increased insulin mRNA in these cells should be confirmed by C-peptide and insulin staining, as well as functional assays. The cell type responsible for the increase could be further purified and the mechanism involved should be investigated. To optimize the differentiation cues provided by alginate, different types and concentrations of alginate could be tested, cell adhesion peptides could be grafted onto alginate or the alginate could be mixed with extracellular matrix components or chitosan. One enticing possibility would be the transplantation of expanded CD90-depleted cells in high concentration alginate beads generated by emulsion and internal gelation. *In vivo* factors could promote the more complete differentiation of these cells as has been reported for islet-like cell clusters obtained from the same tissue without CD90 sorting (Todorov et al. 2006) or for embryonic-derived progenitors (Kroon et al. 2008).

The alginate-filled hollow fiber bioreactor process could be tested with various types of alginates, including much higher or lower alginate concentrations. The alginate-filled hollow fiber bioreactor could be applied for the maturation of NPCCs for trials in non-human primates. In Chapter 2, the seeding density was 5-fold lower than the usual density used for NPCC maturation due to a limited supply of cells. The lack of cell density effects should be confirmed. If the NPCC seeding density is not important or if high densities are in fact desirable, then a single hollow fiber bioreactor unit could be used to transplant many animals to avoid confounding the alginate batch-to-batch variability with the animal-to-animal variability. The hollow fiber process could also be used to produce islet-sized MIN6 aggregates in one batch that, after recovering the aggregates, could be used as an islet model for drug discovery.

The most enticing future direction of this work is the use of alginate beads generated by emulsion and internal gelation for immune isolation, for example of islets or islet-like cell clusters derived from progenitors. However, the process has not yet been optimized for *in vivo* applications or for the immobilization of cell clusters. Cell aggregation may be required for the differentiation of progenitors (as discussed in Section 1.3.2) and islets are usually transplanted without dispersion. A potential issue with encapsulating aggregated cells is that the encapsulation efficiency could be lower for larger particles (aggregates) than for smaller particles (dispersed cells). Another issue is the access of islets to nutrients, particularly if high concentrations of alginate are used and in the larger beads generated during the process. Lastly, the same type of process optimization as was performed in Chapter 3 for 1.5% alginate should be repeated to minimize cell losses for the higher concentration alginate beads. The optimization function for transplantation will be more complex than for *in vitro* applications, because bead strength and porosity, as well as the encapsulation efficiency and survival of cell aggregates should be taken into account.

A first step towards addressing these issues would be to further determine the current limitations of the 5% alginate beads used in Chapter 5 in the context of islet transplantation. The use insulin-secreting cell aggregates generated from conditionally immortalized insulinoma cell lines such as β TC-tet cells could reduce the experimental burden imposed by the use of primary cells. The uncontrolled proliferation of the β TC-tet cells can be arrested using tetracycline, allowing to more closely model islet cells in longer-term *in vivo* experiments (Black et al. 2006; Fleischer et al. 1998). Using β TC-tet aggregates and then islets to confirm the results, the encapsulation efficiency, *in vitro* cell survival and function could be optimized. To determine the general cause of cell losses *in vivo*, encapsulated and non-encapsulated islets could be transplanted into syngeneic or allogeneic streptozotocin-induced diabetic mice. The comparison of syngeneic non-encapsulated and encapsulated islets would give an indication of environmental limitations to islet survival (e.g. due to hypoxia, anoikis or the innate immune response). The comparison between syngeneic and allogeneic encapsulated islets would assess the impact of the adaptive immune rejection. The comparison between non-encapsulated and encapsulated allogeneic

islets would show the sum and inter-actions between the environmental factors and the adaptive response. If cell encapsulation is optimized to minimize the non-specific cell death shortly after transplantation, this should greatly reduce allogeneic antigen presentation and reduce the adaptive responses. Autoimmune diabetic mice could be used as an ultimate model where challenges to cell survival include environmental factors, allogeneic rejection and the primed immune rejection of β -cells.

If the cell survival is low in syngeneic transplants, this may be an indication of nutrient limitations and/or anoikis. Nutrient limitations could be assessed *in vitro* by comparing the cell death of different sized non-encapsulated islets, or of encapsulated islets in beads of various diameters. The polydisperse bead size distributions of the emulsion process would be an advantage for these studies, since beads of different sizes are produced in one batch. The islets should be cultured at low densities to avoid limitations due to the presence of neighbouring islets. Different oxygen tensions could be tested as a model of the varied conditions at different transplantation sites. The effect of the bead size and alginate concentration on insulin secretion kinetics should also be examined. One strategy to minimize diffusion limitations would be to increase the alginate concentration gradients in the beads. Higher gel concentrations near the surface have typically been associated with external gelation but gel gradients have also been observed for internally gelled beads (Quong et al. 1998). This could be accomplished by reducing the alginate molecular weight, reducing the concentrations of non-gelling ions (e.g. Na^+) in the alginate formulation (Skjakbraek et al. 1989) or by neutralizing the emulsion shortly after initiating the internal gelation, potentially leading to less complete CaCO_3 dissolution towards the surface (Figure 3.5).

Having determined the desirable range of bead sizes, the emulsion methodology should be adjusted accordingly, using other vessel (e.g. baffling) and impeller geometries (Pacek et al. 1999) that may provide more uniform shear to obtain more uniform bead size distributions. Next, the fraction of pseudo-islets that are viable and not protruding from the beads should be optimized. The variables to consider include the agitation rate and surfactant concentration. In the current process, serum likely acted as a surfactant but other

surfactants including FDA-approved synthetic surfactants (Lanigan and Expert 2000) or globular proteins (Denkov 2006) such as casein or human serum albumin could be tested. Since mammalian cells are hydrophilic solid particles, their presence at the alginate-oil interface could be avoided if sufficient amounts of surfactant are included in the alginate formulation, depending on the importance of viscous vs. surface tension forces. The optimization could be conducted with β TC-tet aggregates of different sizes and different concentrations in alginate, providing optimal process parameters that may depend on these variables. If beads sufficiently small to avoid diffusion limitations cannot be obtained without significant damage to the cells, other strategies to reduce bead size such as changes in temperature (decreasing the interfacial tension and reducing the viscosity) could be pursued. Settling or sieving could also be used to remove large beads. Some cell losses from removing a minimized fraction of inadequate beads may be acceptable if this reduces graft rejection. Any remaining limitations to the commercial and clinical translation of this technology due to bead polydispersity could be addressed by using membrane emulsion (Liu et al. 2003), which produces more uniform droplets than stirred emulsions.

The lack of protein adsorption and cell interactions with alginate has the major advantage of limiting fibrosis and immune cell attachment (King et al. 2001), but this inertness of the gel can also be detrimental to islet survival and function (Pinkse et al. 2006). If anoikis is a significant issue, cell adhesion peptides could be added to the alginate as has been done for externally gelled beads (Weber et al. 2007). An alternative approach would be to pre-coat the islets with RGD-functionalised alginate (Lee et al. 2008), followed by the usual encapsulation process with non-functionalised alginate. Instead of RGD-functionalised alginate, a cationic polymer could also be used to coat the islets. This type of layer-by-layer polymer self-assembly has been used for conformal coating of islets using cationic polymers such as poly(L-lysine)-g-poly(ethylene glycol) (Wilson et al. 2008) or chitosan (Zhi et al. 2010). Upon contact with an alginate solution, ionic interactions between alginate and the cationic polymer leads to the formation of a membrane near the islet surface. By alternating the cationic polymer and alginate solutions, the membrane thickness and MWCO can be adjusted. Islets coated with RGD-alginate, poly(L-lysine)-g-

poly(ethylene glycol), chitosan or another polymer could then be immobilized in non-functionalised alginate, aiming to obtain an outer layer thick enough to avoid any exposure of the added positive charges to the host cells. In addition to reducing anoikis, these strategies could lead to the formation of a perm-selective membrane near the islets while avoiding the associated fibrotic overgrowth.

If cell losses appear to be associated with the innate or adaptive immune response, decreasing the porosity of the beads or increasing their stability could improve transplantation outcomes. This could be achieved by further increasing the alginate concentration, since the viscosity of the transplanted 5% beads was ~3 Pa·s, while >100 Pa·s solutions can be used with the emulsion process. The production of higher concentration alginate beads may require higher concentrations of CaCO₃, longer emulsification and/or changes in the mixing apparatus (different impeller, added baffles). Increasing the temperature to 37°C (from ambient temperature) may facilitate alginate dispersion and handling, but then the duration of the cell exposures to these solutions may need to be reduced further to maintain high viability. Another method to increase bead stability would be to generate barium cross-linked beads (Smidsrod and Skjakbraek 1990). Uncoated externally gelled barium-alginate beads have led to long-term immune protection in rodents (Duvivier-Kali et al. 2001; Omer et al. 2005) and these beads are being applied in human clinical trials (Tuch et al. 2009). The effect of replacing CaCO₃ by BaCO₃ or another barium salt on the physical properties (strength, stability, porosity) and *in vivo* bead performance of internally gelled beads should be examined. To optimize the immune protection offered by the beads, β -cell rejection could be assessed using an *in vitro* model, for example macrophage- or splenocyte-islet co-cultures (Basta et al. 2004; Mojibian et al. 2009).

Several reports, including the present thesis, have shown that alginate immobilization can be used for the differentiation and/or the immune isolation of β -cell progenitors derived from adult human pancreatic tissue, embryonic stem cells or other sources. The hollow fiber bioreactor and the emulsion processes could enable the clinical-scale generation of insulin+ cells from any of these cell sources. The adaptation of the emulsion process to mammalian cell immobilization opens new avenues, such as the

generation of high-concentration alginate beads, to further increase cell differentiation or immune protection. Since stirred vessels are widely available, the emulsion process also could accelerate research on pancreatic cell immobilization and mammalian cell immobilization in general. The bioprocesses described in this thesis provide new tools for the clinical application of novel cellular therapies that could revolutionize the treatment of devastating diseases such as diabetes.

REFERENCES

- Abouna S, Old RW, Pelengaris S, Epstein D, Ifandi V, Sweeney I, Khan M. 2010. Non-beta-cell progenitors of beta-cells in pregnant mice. *Organogenesis* 6(2):125-33.
- Abraham EJ, Leech CA, Lin JC, Zulewski H, Habener JF. 2002. Insulinotropic hormone glucagon-like peptide-1 differentiation of human pancreatic islet-derived progenitor cells into insulin-producing cells. *Endocrinology* 143(8):3152-61.
- Agbunag C, Bar-Sagi D. 2004. Oncogenic K-ras drives cell cycle progression and phenotypic conversion of primary pancreatic duct epithelial cells. *Cancer Res* 64(16):5659-63.
- Ahmad Z, Khuller GK. 2008. Alginate-based sustained release drug delivery systems for tuberculosis. *Expert Opinion on Drug Delivery* 5(12):1323-1334.
- Alexakis T, Boadi DK, Quong D, Groboillot A, O'Neill I, Poncelet D, Neufeld RJ. 1995. Microencapsulation of DNA within alginate microspheres and crosslinked chitosan membranes for in vivo application. *Appl Biochem Biotechnol* 50(1):93-106.
- Alper J. 2009. Geron gets green light for human trial of ES cell-derived product. *Nat Biotechnol* 27(3):213-4.
- Anderson JM, Rodriguez A, Chang DT. 2008. Foreign body reaction to biomaterials. *Seminars in Immunology* 20(2):86-100.
- Angepat S, Gorenflo VM, Piret JM. 2005. Accelerating perfusion process optimization by scanning non-steady-state responses. *Biotechnol Bioeng* 92(4):472-8.
- Anilkumar AV, Lacik I, Wang TG. 2001. A novel reactor for making uniform capsules. *Biotechnol Bioeng* 75(5):581-9.
- Association CD. 2010. Diabetes Facts.
- Atouf F, Choi Y, Fowler MJ, Poffenberger G, Vobecky J, Ta M, Chapman GB, Powers AC, Lumelsky NL. 2005. Generation of islet-like hormone-producing cells in vitro from adult human pancreas. *Cell Transplant* 14(10):735-48.
- Atouf F, Park CH, Pechhold K, Ta M, Choi Y, Lumelsky NL. 2007. No Evidence for Mouse Pancreatic beta-Cell Epithelial-Mesenchymal Transition In Vitro. *Diabetes* 56(3):699-702.
- Augst AD, Kong HJ, Mooney DJ. 2006. Alginate hydrogels as biomaterials. *Macromol Biosci* 6(8):623-33.
- Avgoustiniatos ES, Colton CK. 1997. Effect of external oxygen mass transfer resistances on viability of immunoisolated tissue. *Ann N Y Acad Sci* 831:145-67.
- Awad HA, Wickham MQ, Leddy HA, Gimble JM, Guilak F. 2004. Chondrogenic differentiation of adipose-derived adult stem cells in agarose, alginate, and gelatin scaffolds. *Biomaterials* 25(16):3211-22.
- Aye T, Block J, Buckingham B. 2010. Toward closing the loop: an update on insulin pumps and continuous glucose monitoring systems. *Endocrinol Metab Clin North Am* 39(3):609-24.
- Baeyens L, De Breuck S, Lardon J, Mfopou JK, Rooman I, Bouwens L. 2005. In vitro generation of insulin-producing beta cells from adult exocrine pancreatic cells. *Diabetologia* 48(1):49-57.

- Banerjee A, Arha M, Choudhary S, Ashton RS, Bhatia SR, Schaffer DV, Kane RS. 2009. The influence of hydrogel modulus on the proliferation and differentiation of encapsulated neural stem cells. *Biomaterials* 30(27):4695-4699.
- Banerjee M, Bhonde RR. 2003. Islet generation from intra islet precursor cells of diabetic pancreas: in vitro studies depicting in vivo differentiation. *Jop* 4(4):137-45.
- Basta G, Sarchielli P, Luca G, Racanicchi L, Nastruzzi C, Guido L, Mancuso F, Macchiarulo G, Calabrese G, Brunetti P and others. 2004. Optimized parameters for microencapsulation of pancreatic islet cells: an in vitro study clueing on islet graft immunoprotection in type 1 diabetes mellitus. *Transpl Immunol* 13(4):289-96.
- Bavamian S, Klee P, Britan A, Populaire C, Caille D, Cancela J, Charollais A, Meda P. 2007. Islet-cell-to-cell communication as basis for normal insulin secretion. *Diabetes Obesity & Metabolism* 9:118-132.
- Beattie GM, Itkin-Ansari P, Cirulli V, Leibowitz G, Lopez AD, Bossie S, Mally MI, Levine F, Hayek A. 1999. Sustained proliferation of PDX-1+ cells derived from human islets. *Diabetes* 48(5):1013-9.
- Beattie GM, Montgomery AM, Lopez AD, Hao E, Perez B, Just ML, Lakey JR, Hart ME, Hayek A. 2002. A novel approach to increase human islet cell mass while preserving beta-cell function. *Diabetes* 51(12):3435-9.
- Beith JL, Alejandro EU, Johnson JD. 2008. Insulin stimulates primary beta-cell proliferation via Raf-1 kinase. *Endocrinology* 149(5):2251-60.
- Berrocal T, Luque AA, Pinilla I, Lassaletta L. 2005. Pancreatic regeneration after near-total pancreatectomy in children with nesidioblastosis. *Pediatr Radiol* 35(11):1066-70.
- Bharat A, Mohanakumar T. 2007. Allopeptides and the alloimmune response. *Cell Immunol* 248(1):31-43.
- Black SP, Constantinidis I, Cui H, Tucker-Burden C, Weber CJ, Safley SA. 2006. Immune responses to an encapsulated allogeneic islet beta-cell line in diabetic NOD mice. *Biochem Biophys Res Commun* 340(1):236-43.
- Blandino-Rosano M, Perez-Arana G, Mellado-Gil JM, Segundo C, Aguilar-Diosdado M. 2008. Anti-proliferative effect of pro-inflammatory cytokines in cultured beta cells is associated with extracellular signal-regulated kinase 1/2 pathway inhibition: protective role of glucagon-like peptide -1. *J Mol Endocrinol* 41(1):35-44.
- Bockman DE, Guo J, Buchler P, Muller MW, Bergmann F, Friess H. 2003. Origin and development of the precursor lesions in experimental pancreatic cancer in rats. *Lab Invest* 83(6):853-9.
- Bodeutsch T, James EA, Lee JM. 2001. The effect of immobilization on recombinant protein production in plant cell culture. *Plant Cell Reports* 20(6):562-566.
- Bogdani M, Lefebvre V, Buelens N, Bock T, Pipeleers-Marichal M, In't Veld P, Pipeleers D. 2003. Formation of insulin-positive cells in implants of human pancreatic duct cell preparations from young donors. *Diabetologia* 46(6):830-8.
- Boland MJ, Hazen JL, Nazor KL, Rodriguez AR, Gifford W, Martin G, Kupriyanov S, Baldwin KK. 2009. Adult mice generated from induced pluripotent stem cells. *Nature* 461(7260):91-4.

- Bonner-Weir S, Baxter LA, Schuppin GT, Smith FE. 1993. A second pathway for regeneration of adult exocrine and endocrine pancreas. A possible recapitulation of embryonic development. *Diabetes* 42(12):1715-20.
- Bonner-Weir S, Sharma A. 2002. Pancreatic stem cells. *J Pathol* 197(4):519-26.
- Bonner-Weir S, Taneja M, Weir GC, Tatarkiewicz K, Song KH, Sharma A, O'Neil JJ. 2000. In vitro cultivation of human islets from expanded ductal tissue. *Proc Natl Acad Sci U S A* 97(14):7999-8004.
- Boonthekul T, Kong HJ, Mooney DJ. 2005. Controlling alginate gel degradation utilizing partial oxidation and bimodal molecular weight distribution. *Biomaterials* 26(15):2455-2465.
- Boretti MI, Gooch KJ. 2006. Induced cell clustering enhances islet beta cell formation from human cultures enriched for pancreatic ductal epithelial cells. *Tissue Eng* 12(4):939-48.
- Brandenberger H. 1999. Immobilisierung von Biokatalysatoren in monodispersen Alginatpartikeln mittels einer Eindüsen- und Mehrdüsenanlage. Zürich: Eidgenössische Technische Hochschule. 172 p.
- Brandenberger H, Widmer F. 1998. A new multinozzle encapsulation/immobilisation system to produce uniform beads of alginate. *Journal of Biotechnology* 63(1):73-80.
- Brennan K, Huangfu D, Melton D. 2007. All beta Cells Contribute Equally to Islet Growth and Maintenance. *PLoS Biol* 5(7):e163.
- Brindle K, Stephenson T. 1996. The application of membrane biological reactors for the treatment of wastewaters. *Biotechnology and Bioengineering* 49(6):601-610.
- Brissova M, Lacik I, Powers AC, Anilkumar AV, Wang T. 1998. Control and measurement of permeability for design of microcapsule cell delivery system. *J Biomed Mater Res* 39(1):61-70.
- Brissova M, Petro M, Lacik I, Powers AC, Wang T. 1996. Evaluation of microcapsule permeability via inverse size exclusion chromatography. *Anal Biochem* 242(1):104-11.
- Buchwald P. 2009. FEM-based oxygen consumption and cell viability models for avascular pancreatic islets. *Theoretical Biology and Medical Modelling* 6(5):13 pages.
- Bunger CM, Gerlach C, Freier T, Schmitz KP, Pilz M, Werner C, Jonas L, Schareck W, Hopt UT, de Vos P. 2003. Biocompatibility and surface structure of chemically modified immunisolating alginate-PLL capsules. *Journal of Biomedical Materials Research Part A* 67A(4):1219-1227.
- Butler AE, Cao-Minh L, Galasso R, Rizza RA, Corradin A, Cobelli C, Butler PC. 2010. Adaptive changes in pancreatic beta cell fractional area and beta cell turnover in human pregnancy. *Diabetologia*.
- Butler AE, Janson J, Bonner-Weir S, Ritzel R, Rizza RA, Butler PC. 2003. Beta-cell deficit and increased beta-cell apoptosis in humans with type 2 diabetes. *Diabetes* 52(1):102-10.
- Calafiore R, Basta G, Luca G, Calvitti M, Calabrese G, Racanicchi L, Macchiarulo G, Mancuso F, Guido L, Brunetti P. 2004. Grafts of microencapsulated pancreatic islet cells for the therapy of diabetes mellitus in non-immunosuppressed animals. *Biotechnol Appl Biochem* 39(Pt 2):159-64.
- Calafiore R, Basta G, Luca G, Lemmi A, Montanucci MP, Calabrese G, Racanicchi L, Mancuso F, Brunetti P. 2006a. Microencapsulated pancreatic islet allografts into

- nonimmunosuppressed patients with type 1 diabetes: first two cases. *Diabetes Care* 29(1):137-8.
- Calafiore R, Basta G, Luca G, Lemmi A, Racanicchi L, Mancuso F, Montanucci MP, Brunetti P. 2006b. Standard technical procedures for microencapsulation of human islets for graft into nonimmunosuppressed patients with type 1 diabetes mellitus. *Transplant Proc* 38(4):1156-7.
- Calafiore R, Calabrese G, Basta G, Racanicchi L, Luca G, Mancuso F, Lemmi A, Brunetti E, Montanucci MP. 2007. Microencapsulated Pancreatic Islet Allografts Into Nonimmunosuppressed Patients With Type 1 Diabetes. *Diabetes Care* 29(1):137-138.
- Campbell-Thompson M, Dixon LR, Wasserfall C, Monroe M, McGuigan JM, Schatz D, Crawford JM, Atkinson MA. 2009. Pancreatic adenocarcinoma patients with localised chronic severe pancreatitis show an increased number of single beta cells, without alterations in fractional insulin area. *Diabetologia* 52(2):262-70.
- Canada S. 2009. Diabetes, by sex, provinces and territories.
- Cardona K, Korbitt GS, Milas Z, Lyon J, Cano J, Jiang W, Bello-Laborn H, Hacquoil B, Strobert E, Gangappa S and others. 2006. Long-term survival of neonatal porcine islets in nonhuman primates by targeting costimulation pathways. *Nat Med* 12(3):304-6.
- Cardozo AK, Proost P, Gysemans C, Chen MC, Mathieu C, Eizirik DL. 2003. IL-1 beta and IFN-gamma induce the expression of diverse chemokines and IL-15 in human and rat pancreatic islet cells, and in islets from pre-diabetic NOD mice. *Diabetologia* 46(2):255-266.
- Carlsson PO, Palm F, Andersson A, Liss P. 2000. Chronically decreased oxygen tension in rat pancreatic islets transplanted under the kidney capsule. *Transplantation* 69(5):761-6.
- Carlsson PO, Palm F, Andersson A, Liss P. 2001. Markedly decreased oxygen tension in transplanted rat pancreatic islets irrespective of the implantation site. *Diabetes* 50(3):489-95.
- Carpenter AE, Jones TR, Lamprecht MR, Clarke C, Kang IH, Friman O, Guertin DA, Chang JH, Lindquist RA, Moffat J and others. 2006. CellProfiler: image analysis software for identifying and quantifying cell phenotypes. *Genome Biol* 7(10):R100.
- Chase LG, Ulloa-Montoya F, Kidder BL, Verfaillie CM. 2007. Islet-derived fibroblast-like cells are not derived via epithelial-mesenchymal transition from Pdx-1 or insulin-positive cells. *Diabetes* 56(1):3-7.
- Chaudhry MA, Bowen BD, Piret JM. 2009. Culture pH and osmolality influence proliferation and embryoid body yields of murine embryonic stem cells. *Biochemical Engineering Journal* 45(2):126-135.
- Chawla M, Bodnar CA, Sen A, Kallos MS, Behie LA. 2006. Production of islet-like structures from neonatal porcine pancreatic tissue in suspension bioreactors. *Biotechnol Prog* 22(2):561-7.
- Chayosumrit M, Tuch B, Sidhu K. 2010. Alginate microcapsule for propagation and directed differentiation of hESCs to definitive endoderm. *Biomaterials* 31(3):505-514.
- Chen KL, Zheng XL, Li Y, Yang L, Zhou ZG, Zhou XY, Zhou B, Wang R, Jiang JJ, Chen LH and others. 2009. An improved primary culture system of pancreatic duct epithelial cells from Wistar rats. *Cytotechnology*.

- Choi CH, Jung JH, Rhee YW, Kim DP, Shim SE, Lee CS. 2007. Generation of monodisperse alginate microbeads and in situ encapsulation of cell in microfluidic device. *Biomed Microdevices* 9(6):855-62.
- Choi Y, Ta M, Atouf F, Lumelsky N. 2004. Adult pancreas generates multipotent stem cells and pancreatic and nonpancreatic progeny. *Stem Cells* 22(6):1070-84.
- Clark WR, Macias WL, Molitoris BA, Wang NHL. 1995. Plasma-Protein Adsorption to Highly Permeable Hemodialysis Membranes. *Kidney International* 48(2):481-488.
- Cline GW, LePine RL, Papas KK, Kibbey RG, Shulman GI. 2004. C-13 NMR isotopomer analysis of anaplerotic pathways in INS-1 cells. *Journal of Biological Chemistry* 279(43):44370-44375.
- Cnop M, Hughes SJ, Igoillo-Estevé M, Hoppa MB, Sayyed F, van de Laar L, Gunter JH, de Koning EJ, Walls GV, Gray DW and others. 2010. The long lifespan and low turnover of human islet beta cells estimated by mathematical modelling of lipofuscin accumulation. *Diabetologia* 53(2):321-30.
- Constantinidis I, Rask I, Long RC, Jr., Sambanis A. 1999. Effects of alginate composition on the metabolic, secretory, and growth characteristics of entrapped beta TC3 mouse insulinoma cells. *Biomaterials* 20(21):2019-27.
- Cozzi E, Tallacchini M, Flanagan EB, Pierson RN, 3rd, Sykes M, Vanderpool HY. 2009. The International Xenotransplantation Association consensus statement on conditions for undertaking clinical trials of porcine islet products in type 1 diabetes--chapter 1: Key ethical requirements and progress toward the definition of an international regulatory framework. *Xenotransplantation* 16(4):203-14.
- Cravedi P, Ruggenti P, Remuzzi G. 2010. Sirolimus for calcineurin inhibitors in organ transplantation: contra. *Kidney Int.*
- Cui H, Tucker-Burden C, Cauffiel SMD, Barry AK, Iwakoshi NN, Weber CJ, Safley SA. 2009. Long-Term Metabolic Control of Autoimmune Diabetes in Spontaneously Diabetic Nonobese Diabetic Mice by Nonvascularized Microencapsulated Adult Porcine Islets. *Transplantation* 88(2):160-169.
- Cui W, Barr G, Faucher KM, Sun XL, Safley SA, Weber CJ, Chaikof EL. 2004. A membrane-mimetic barrier for islet encapsulation. *Transplant Proc* 36(4):1206-8.
- Dai C, Huh CG, Thorgeirsson SS, Liu Y. 2005. Beta-cell-specific ablation of the hepatocyte growth factor receptor results in reduced islet size, impaired insulin secretion, and glucose intolerance. *Am J Pathol* 167(2):429-36.
- D'Amour KA, Bang AG, Eliazar S, Kelly OG, Agulnick AD, Smart NG, Moorman MA, Kroon E, Carpenter MK, Baetge EE. 2006. Production of pancreatic hormone-expressing endocrine cells from human embryonic stem cells. *Nat Biotechnol* 24(11):1392-401.
- d'Apice AJ, Cowan PJ. 2009. Xenotransplantation: the next generation of engineered animals. *Transpl Immunol* 21(2):111-5.
- Darquy S, Pueyo ME, Capron F, Reach G. 1994. Complement Activation by Alginate-Polylysine Microcapsules Used for Islet Transplantation. *Artificial Organs* 18(12):898-903.
- Davalli AM, Bertuzzi F, Socci C, Scaglia L, Gavazzi F, Freschi M, DiCarlo V, Pontiroli AE, Pozza G. 1993. Paradoxical release of insulin by adult pig islets in vitro. Recovery after

culture in a defined tissue culture medium. *Transplantation* 56(1):148-54.

- Davies JT. 1985. Drop Sizes of Emulsions Related to Turbulent Energy-Dissipation Rates. *Chemical Engineering Science* 40(5):839-842.
- Davis TA, Volesky B, Mucci A. 2003. A review of the biochemistry of heavy metal biosorption by brown algae. *Water Research* 37(18):4311-4330.
- De Castro M, Orive G, Hernandez RM, Gascon AR, Pedraz JL. 2005. Comparative study of microcapsules elaborated with three polycations (PLL, PDL, PLO) for cell immobilization. *Journal of Microencapsulation* 22(3):303-315.
- De La O J, Emerson LL, Goodman JL, Froebe SC, Illum BE, Curtis AB, Murtaugh LC. 2008. Notch and Kras reprogram pancreatic acinar cells to ductal intraepithelial neoplasia. *Proc Natl Acad Sci U S A* 105(48):18907-12.
- de Vos P, de Haan B, Wolters GH, Van Schilfgaarde R. 1996. Factors influencing the adequacy of microencapsulation of rat pancreatic islets. *Transplantation* 62(7):888-93.
- de Vos P, de Haan BJ, Kamps JA, Faas MM, Kitano T. 2007. Zeta-potentials of alginate-PLL capsules: a predictive measure for biocompatibility? *J Biomed Mater Res A* 80(4):813-9.
- de Vos P, Faas MM, Strand B, Calafiore R. 2006. Alginate-based microcapsules for immunoisolation of pancreatic islets. *Biomaterials* 27(32):5603-5617.
- de Vos P, Smedema I, van Goor H, Moes H, van Zanten J, Netters S, de Leij LFM, de Haan A, de Haan BJ. 2003a. Association between macrophage activation and function of micro-encapsulated rat islets. *Diabetologia* 46(5):666-673.
- de Vos P, van Hoogmoed CG, de Haan BJ, Busscher HJ. 2002. Tissue responses against immunoisolating alginate-PLL capsules in the immediate posttransplant period. *Journal of Biomedical Materials Research* 62(3):430-437.
- de Vos P, van Hoogmoed CG, van Zanten J, Netter S, Strubbe JH, Busscher HJ. 2003b. Long-term biocompatibility, chemistry, and function of microencapsulated pancreatic islets. *Biomaterials* 24(2):305-12.
- Dean SK, Yulyana Y, Williams G, Sidhu KS, Tuch BE. 2006. Differentiation of encapsulated embryonic stem cells after transplantation. *Transplantation* 82(9):1175-84.
- Delacour A, Nepote V, Trumpp A, Herrera PL. 2004. Nestin expression in pancreatic exocrine cell lineages. *Mech Dev* 121(1):3-14.
- Denkov ND. Globular proteins as emulsion stabilizers - similarities and differences with surfactants and solid particles; 2006; Lyon, France.
- Desai BM, Oliver-Krasinski J, De Leon DD, Farzad C, Hong N, Leach SD, Stoffers DA. 2007. Preexisting pancreatic acinar cells contribute to acinar cell, but not islet beta cell, regeneration. *J Clin Invest* 117(4):971-7.
- DeVos P, DeHaan B, Pater J, VanSchilfgaarde R. 1996. Association between capsule diameter, adequacy of encapsulation, and survival of microencapsulated rat islet allografts. *Transplantation* 62(7):893-899.
- DeVos P, DeHaan BJ, VanSchilfgaarde R. 1997. Upscaling the production of microencapsulated pancreatic islets. *Biomaterials* 18(16):1085-1090.
- Dionne KE, Colton CK, Yarmush ML. 1989. Effect of oxygen on isolated pancreatic tissue. *ASAIO Trans* 35(3):739-41.

- Dionne KE, Colton CK, Yarmush ML. 1993. Effect of hypoxia on insulin secretion by isolated rat and canine islets of Langerhans. *Diabetes* 42(1):12-21.
- Discher DE, Janmey P, Wang YL. 2005. Tissue cells feel and respond to the stiffness of their substrate. *Science* 310(5751):1139-43.
- Donati I, Draget KI, Borgogna M, Paoletti S, Skjak-Braek G. 2005. Tailor-made alginate bearing galactose moieties on mannuronic residues: Selective modification achieved by a chemoenzymatic strategy. *Biomacromolecules* 6(1):88-98.
- Dor Y, Brown J, Martinez OI, Melton DA. 2004. Adult pancreatic beta-cells are formed by self-duplication rather than stem-cell differentiation. *Nature* 429(6987):41-6.
- Draget KI, Gaserod O, Aune I, Andersen PO, Storbakken B, Stokke BT, Smidsrod O. 2001. Effects of molecular weight and elastic segment flexibility on syneresis in Ca-alginate gels. *Food Hydrocolloids* 15(4-6):485-490.
- Draget KI, Ostgaard K, Smidsrod O. 1990. Homogeneous Alginate Gels - a Technical Approach. *Carbohydrate Polymers* 14(2):159-178.
- Draget KI, Simensen MK, Onsoyen E, Smidsrod O. 1993. Gel Strength of Ca-Limited Alginate Gels Made in-Situ. *Hydrobiologia* 261:563-569.
- Dufrane D, D'Hoore W, Goebbels RM, Saliez A, Guiot Y, Gianello P. 2006a. Parameters favouring successful adult pig islet isolations for xenotransplantation in pig-to-primate models. *Xenotransplantation* 13(3):204-14.
- Dufrane D, Gianello P. 2009. Pig islets for clinical islet xenotransplantation. *Curr Opin Nephrol Hypertens* 18(6):495-500.
- Dufrane D, Goebbels RM, Saliez A, Guiot Y, Gianello P. 2006b. Six-month survival of microencapsulated pig islets and alginate biocompatibility in primates: proof of concept. *Transplantation* 81(9):1345-53.
- Dulong JL, Legallais C. 2007. A theoretical study of oxygen transfer including cell necrosis for the design of a bioartificial pancreas. *Biotechnol Bioeng* 96(5):990-8.
- Dusseault J, Tam SK, Menard M, Polizu S, Jourdan G, Yahia L, Halle JP. 2006. Evaluation of alginate purification methods: effect on polyphenol, endotoxin, and protein contamination. *J Biomed Mater Res A* 76(2):243-51.
- Duvivier-Kali VF, Omer A, Parent RJ, O'Neil JJ, Weir GC. 2001. Complete protection of islets against allo rejection and autoimmunity by a simple barium-alginate membrane. *Diabetes* 50(8):1698-705.
- Efrat S. 2008. Ex-vivo Expansion of Adult Human Pancreatic Beta-Cells. *Rev Diabet Stud* 5(2):116-22.
- Efrat S, Linde S, Kofod H, Spector D, Delannoy M, Grant S, Hanahan D, Baekkeskov S. 1988. Beta-cell lines derived from transgenic mice expressing a hybrid insulin gene-oncogene. *Proc Natl Acad Sci U S A* 85(23):9037-41.
- Elliott RB, Escobar L, Tan PL, Garkavenko O, Calafiore R, Basta P, Vasconcellos AV, Emerich DF, Thanos C, Bambra C. 2005. Intraperitoneal alginate-encapsulated neonatal porcine islets in a placebo-controlled study with 16 diabetic cynomolgus primates. *Transplant Proc* 37(8):3505-8.

- Elliott RB, Escobar L, Tan PL, Muzina M, Zwain S, Buchanan C. 2007. Live encapsulated porcine islets from a type 1 diabetic patient 9.5 yr after xenotransplantation. *Xenotransplantation* 14(2):157-61.
- Elliott RBA, NZ), Calafiore, Riccardo (Perugia, IT), Basta, Gusseppe (Perugia, IT); DIABCELL PTY LTD (Parkside South, AU), assignee. 2008. Preparation and xenotransplantation of porcine islets. United States patent 20080279827.
- Engler AJ, Griffin MA, Sen S, Bonnemann CG, Sweeney HL, Discher DE. 2004. Myotubes differentiate optimally on substrates with tissue-like stiffness: pathological implications for soft or stiff microenvironments. *J Cell Biol* 166(6):877-87.
- Engler AJ, Sen S, Sweeney HL, Discher DE. 2006. Matrix elasticity directs stem cell lineage specification. *Cell* 126(4):677-689.
- Ertesvag H, Valla S. 1998. Biosynthesis and applications of alginates. *Polymer Degradation and Stability* 59(1-3):85-91.
- Espevik T, Otterlei M, Skjak-Braek G, Ryan L, Wright SD, Sundan A. 1993. The involvement of CD14 in stimulation of cytokine production by uronic acid polymers. *Eur J Immunol* 23(1):255-61.
- Fernandes A, King LC, Guz Y, Stein R, Wright CV, Teitelman G. 1997. Differentiation of new insulin-producing cells is induced by injury in adult pancreatic islets. *Endocrinology* 138(4):1750-62.
- Finegood DT, Scaglia L, Bonner-Weir S. 1995. Dynamics of beta-cell mass in the growing rat pancreas. Estimation with a simple mathematical model. *Diabetes* 44(3):249-56.
- Fleischer N, Chen C, Surana M, Leiser M, Rossetti L, Pralong W, Efrat S. 1998. Functional analysis of a conditionally transformed pancreatic beta-cell line. *Diabetes* 47(9):1419-25.
- Forte P, Lilienfeld BG, Baumann BC, Seebach JD. 2005. Human NK cytotoxicity against porcine cells is triggered by Nkp44 and NKG2D. *J Immunol* 175(8):5463-70.
- Fritschy WM, de Vos P, Groen H, Klatter FA, Pasma A, Wolters GH, van Schilfgaarde R. 1994. The capsular overgrowth on microencapsulated pancreatic islet grafts in streptozotocin and autoimmune diabetic rats. *Transpl Int* 7(4):264-71.
- Fritschy WM, Strubbe JH, Wolters GH, van Schilfgaarde R. 1991. Glucose tolerance and plasma insulin response to intravenous glucose infusion and test meal in rats with microencapsulated islet allografts. *Diabetologia* 34(8):542-7.
- Game DS, Lechler RI. 2002. Pathways of allorecognition: implications for transplantation tolerance. *Transpl Immunol* 10(2-3):101-8.
- Gao R, Ustinov J, Korsgren O, Mikkola M, Lundin K, Otonkoski T. 2007. Maturation of in vitro-generated human islets after transplantation in nude mice. *Mol Cell Endocrinol* 264(1-2):28-34.
- Gao R, Ustinov J, Korsgren O, Otonkoski T. 2005. In vitro neogenesis of human islets reflects the plasticity of differentiated human pancreatic cells. *Diabetologia* 48(11):2296-304.
- Gao R, Ustinov J, Pulkkinen MA, Lundin K, Korsgren O, Otonkoski T. 2003. Characterization of endocrine progenitor cells and critical factors for their differentiation in human adult pancreatic cell culture. *Diabetes* 52(8):2007-15.

- Gaserod O, Smidsrod O, Skjak-Braek G. 1998. Microcapsules of alginate-chitosan--I. A quantitative study of the interaction between alginate and chitosan. *Biomaterials* 19(20):1815-25.
- Gerecht-Nir S, Cohen S, Ziskind A, Itskovitz-Eldor J. 2004. Three-dimensional porous alginate scaffolds provide a conducive environment for generation of well-vascularized embryoid bodies from human embryonic stem cells. *Biotechnol Bioeng* 88(3):313-20.
- Gershengorn MC, Hardikar AA, Wei C, Geras-Raaka E, Marcus-Samuels B, Raaka BM. 2004. Epithelial-to-mesenchymal transition generates proliferative human islet precursor cells. *Science* 306(5705):2261-4.
- Ghosh K, Ingber DE. 2007. Micromechanical control of cell and tissue development: implications for tissue engineering. *Adv Drug Deliv Rev* 59(13):1306-18.
- Giancotti FG, Ruoslahti E. 1999. Integrin signaling. *Science* 285(5430):1028-32.
- Giapos A, Pachatouridis C, Stamatoudis M. 2005. Effect of the number of impeller blades on the drop sizes in agitated dispersions. *Chemical Engineering Research & Design* 83(A12):1425-1430.
- Gittes GK. 2009. Developmental biology of the pancreas: a comprehensive review. *Dev Biol* 326(1):4-35.
- Gmyr V, Kerr-Conte J, Belaich S, Vandewalle B, Leteurtre E, Vantuyghem MC, Lecomte-Houcke M, Proye C, Lefebvre J, Pattou F. 2000. Adult human cytokeratin 19-positive cells reexpress insulin promoter factor 1 in vitro - Further evidence for pluripotent pancreatic stem cells in humans. *Diabetes* 49(10):1671-1680.
- Gmyr V, Kerr-Conte J, Vandewalle B, Proye C, Lefebvre J, Pattou F. 2001. Human pancreatic ductal cells: large-scale isolation and expansion. *Cell Transplant* 10(1):109-21.
- Godara P, McFarland CD, Nordon RE. 2008. Design of bioreactors for mesenchymal stem cell tissue engineering. *Journal of Chemical Technology and Biotechnology* 83(4):408-420.
- Godoy-Silva R, Chalmers JJ, Casnocha SA, Bass LA, Ma NN. 2009. Physiological Responses of CHO Cells to Repetitive Hydrodynamic Stress. *Biotechnology and Bioengineering* 103(6):1103-1117.
- Gokmen MR, Lombardi G, Lechler RI. 2008. The importance of the indirect pathway of allorecognition in clinical transplantation. *Curr Opin Immunol* 20(5):568-74.
- Grant GT, Morris ER, Rees DA, Smith PJC, Thom D. 1973. Biological Interactions between Polysaccharides and Divalent Cations - Egg-Box Model. *Febs Letters* 32(1):195-198.
- Grapin-Botton A, Melton DA. 2000. Endoderm development: from patterning to organogenesis. *Trends Genet* 16(3):124-30.
- Gray DW. 1997. Encapsulated islet cells: the role of direct and indirect presentation and the relevance to xenotransplantation and autoimmune recurrence. *Br Med Bull* 53(4):777-88.
- Gray DW. 2001. An overview of the immune system with specific reference to membrane encapsulation and islet transplantation. *Ann N Y Acad Sci* 944:226-39.
- Griffith LG, Swartz MA. 2006. Capturing complex 3D tissue physiology in vitro. *Nat Rev Mol Cell Biol* 7(3):211-24.
- Gross JD, Constantinidis I, Sambanis A. 2007. Modeling of encapsulated cell systems. *J Theor Biol* 244(3):500-10.

- Group TDCaCTR. 1993. The effect of intensive treatment of diabetes on the development and progression of long-term complications in insulin-dependent diabetes mellitus. The Diabetes Control and Complications Trial Research Group. *N Engl J Med* 329(14):977-86.
- Guignard AP, Oberholzer J, Benhamou PY, Touzet S, Bucher P, Penfornis A, Bayle F, Kessler L, Thivolet C, Badet L and others. 2004. Cost analysis of human islet transplantation for the treatment of type 1 diabetes in the Swiss-French Consortium GRAGIL. *Diabetes Care* 27(4):895-900.
- Gunawardana SC, Sharp GW. 2002. Intracellular pH plays a critical role in glucose-induced time-dependent potentiation of insulin release in rat islets. *Diabetes* 51(1):105-13.
- Gutierrez-Dalmau A, Campistol JM. 2007. Immunosuppressive therapy and malignancy in organ transplant recipients: a systematic review. *Drugs* 67(8):1167-98.
- Haardt MJ, Selam JL, Slama G, Bethoux JP, Dorange C, Mace B, Ramaniche ML, Bruzzo F. 1994. A cost-benefit comparison of intensive diabetes management with implantable pumps versus multiple subcutaneous injections in patients with type I diabetes. *Diabetes Care* 17(8):847-51.
- Habbe N, Shi G, Meguid RA, Fendrich V, Esni F, Chen H, Feldmann G, Stoffers DA, Konieczny SF, Leach SD and others. 2008. Spontaneous induction of murine pancreatic intraepithelial neoplasia (mPanIN) by acinar cell targeting of oncogenic Kras in adult mice. *Proc Natl Acad Sci U S A* 105(48):18913-8.
- Hakeam HA, Al-Jedai AH, Raza SM, Hamawi K. 2008. Sirolimus induced dyslipidemia in tacrolimus based vs. tacrolimus free immunosuppressive regimens in renal transplant recipients. *Ann Transplant* 13(2):46-53.
- Hall PA, Lemoine NR. 1992. Rapid acinar to ductal transdifferentiation in cultured human exocrine pancreas. *J Pathol* 166(2):97-103.
- Hao E, Tyrberg B, Itkin-Ansari P, Lakey JR, Geron I, Monosov EZ, Barcova M, Mercola M, Levine F. 2006. Beta-cell differentiation from nonendocrine epithelial cells of the adult human pancreas. *Nat Med* 12(3):310-6.
- Hardikar AA, Karandikar MS, Bhonde RR. 1999. Effect of partial pancreatectomy on diabetic status in BALB/c mice. *J Endocrinol* 162(2):189-95.
- Hardikar AA, Marcus-Samuels B, Geras-Raaka E, Raaka BM, Gershengorn MC. 2003. Human pancreatic precursor cells secrete FGF2 to stimulate clustering into hormone-expressing islet-like cell aggregates. *Proc Natl Acad Sci U S A* 100(12):7117-22.
- Hardikar AA, Risbud MV, Bhonde RR. 2000. Improved post-cryopreservation recovery following encapsulation of islets in chitosan-alginate microcapsules. *Transplant Proc* 32(4):824-5.
- Hauge-Evans AC, Squires PE, Persaud SJ, Jones PM. 1999. Pancreatic beta-cell-to-beta-cell interactions are required for integrated responses to nutrient stimuli - Enhanced Ca²⁺ and insulin secretory responses of MIN6 pseudoislets. *Diabetes* 48(7):1402-1408.
- Haveman JW, Logtenberg SJ, Kleefstra N, Groenier KH, Bilo HJ, Blomme AM. 2010. Surgical aspects and complications of continuous intraperitoneal insulin infusion with an implantable pump. *Langenbecks Arch Surg* 395(1):65-71.

- Hayashi KY, Tamaki H, Handa K, Takahashi T, Kakita A, Yamashina S. 2003. Differentiation and proliferation of endocrine cells in the regenerating rat pancreas after 90% pancreatectomy. *Arch Histol Cytol* 66(2):163-74.
- Heinzen C, Marison I, Berger A, von Stockar U. 2002. Use of vibration technology for jet break-up for encapsulation of cells, microbes and liquids in monodisperse microcapsules. *Practical Aspects of Encapsulation Technologies*:19-25.
- Heremans Y, Van De Castele M, in't Veld P, Gradwohl G, Serup P, Madsen O, Pipeleers D, Heimberg H. 2002. Recapitulation of embryonic neuroendocrine differentiation in adult human pancreatic duct cells expressing neurogenin 3. *J Cell Biol* 159(2):303-12.
- Hering BJ, Wijkstrom M, Graham ML, Hardstedt M, Aasheim TC, Jie T, Ansite JD, Nakano M, Cheng J, Li W and others. 2006. Prolonged diabetes reversal after intraportal xenotransplantation of wild-type porcine islets in immunosuppressed nonhuman primates. *Nat Med* 12(3):301-3.
- Hilbrands R, Huurman VA, Gillard P, Velthuis JH, De Waele M, Mathieu C, Kaufman L, Pipeleers-Marichal M, Ling Z, Movahedi B and others. 2009. Differences in baseline lymphocyte counts and autoreactivity are associated with differences in outcome of islet cell transplantation in type 1 diabetic patients. *Diabetes* 58(10):2267-76.
- Hinze JO. 1955. Fundamentals of the hydrodynamic mechanism of splitting in dispersion processes. *American Institute of Chemical Engineering Journal* 1(3):289-295.
- Hirshberg B. 2007. Lessons learned from the international trial of the edmonton protocol for islet transplantation. *Curr Diab Rep* 7(4):301-3.
- Hisano N, Morikawa N, Iwata H, Ikada Y. 1998. Entrapment of islets into reversible disulfide hydrogels. *J Biomed Mater Res* 40(1):115-23.
- Hoesli CA, Luu M, Piret JM. 2009. A Novel Alginate Hollow Fiber Bioreactor Process for Cellular Therapy Applications. *Biotechnology Progress* 25(6):1740-1751.
- Huang KS, Lai TH, Lin YC. 2007. Using a microfluidic chip and internal gelation reaction for monodisperse calcium alginate microparticles generation. *Frontiers in Bioscience* 12:3061-3067.
- Huebsch N, Arany PR, Mao AS, Shvartsman D, Ali OA, Bencherif SA, Rivera-Feliciano J, Mooney DJ. 2010. Harnessing traction-mediated manipulation of the cell/matrix interface to control stem-cell fate. *Nat Mater* 9(6):518-26.
- Huggins ML. 1942. The viscosity of dilute solutions of long-chain molecules. IV. Dependence on concentration. *Journal of the American Chemical Society* 64:2716-2718.
- Hui H, Khoury N, Zhao X, Balkir L, D'Amico E, Bullotta A, Nguyen ED, Gambotto A, Perfetti R. 2005. Adenovirus-mediated XIAP gene transfer reverses the negative effects of immunosuppressive drugs on insulin secretion and cell viability of isolated human islets. *Diabetes* 54(2):424-33.
- Hui H, Wright C, Perfetti R. 2001. Glucagon-like peptide 1 induces differentiation of islet duodenal homeobox-1-positive pancreatic ductal cells into insulin-secreting cells. *Diabetes* 50(4):785-96.
- Humphrey RK, Smith MS, Kwok J, Si Z, Tuch BE, Simpson AM. 2001. In vitro dedifferentiation of fetal porcine pancreatic tissue prior to transplantation as islet-like cell clusters. *Cells Tissues Organs* 168(3):158-169.

- Hunt JA, Flanagan BF, McLaughlin PJ, Strickland I, Williams DF. 1996. Effect of biomaterial surface charge on the inflammatory response: Evaluation of cellular infiltration and TNF alpha production. *Journal of Biomedical Materials Research* 31(1):139-144.
- Huurman VAL, Hilbrands R, Pinkse GGM, Gillard P, Duinkerken G, van de Linde P, van der Meer-Prins PMW, Maarschalk MFJV, Verbeeck K, Alizadeh BZ and others. 2008. Cellular Islet Autoimmunity Associates with Clinical Outcome of Islet Cell Transplantation. *Plos One* 3(6):-.
- Inada A, Nienaber C, Katsuta H, Fujitani Y, Levine J, Morita R, Sharma A, Bonner-Weir S. 2008. Carbonic anhydrase II-positive pancreatic cells are progenitors for both endocrine and exocrine pancreas after birth. *Proc Natl Acad Sci U S A* 105(50):19915-9.
- Ito M, Hiramatsu H, Kobayashi K, Suzue K, Kawahata M, Hioki K, Ueyama Y, Koyanagi Y, Sugamura K, Tsuji K and others. 2002. NOD/SCID/gamma(c)(null) mouse: an excellent recipient mouse model for engraftment of human cells. *Blood* 100(9):3175-82.
- Jain R, Lammert E. 2009. Cell-cell interactions in the endocrine pancreas. *Diabetes Obesity & Metabolism* 11:159-167.
- Janeway CAJ, Travers P, Walport M, Shlomchik MJ. 2001. Chapter 10, The course of the adaptive response to infection. *Immunobiology*, 5th edition, The Immune System in Health and Disease: Garland Science.
- Jansson L, Carlsson PO. 2002. Graft vascular function after transplantation of pancreatic islets. *Diabetologia* 45(6):749-63.
- Jensen J. 2004. Gene regulatory factors in pancreatic development. *Dev Dyn* 229(1):176-200.
- Jeong B, Kim SW, Bae YH. 2002. Thermosensitive sol-gel reversible hydrogels. *Advanced Drug Delivery Reviews* 54(1):37-51.
- Jiang W, Shi Y, Zhao D, Chen S, Yong J, Zhang J, Qing T, Sun X, Zhang P, Ding M and others. 2007. In vitro derivation of functional insulin-producing cells from human embryonic stem cells. *Cell Res* 17(4):333-44.
- Johansen A, Flink JM. 1986. Immobilization of Yeast-Cells by Internal Gelation of Alginate. *Enzyme and Microbial Technology* 8(3):145-148.
- Johnson JD, Ao Z, Ao P, Li H, Dai LJ, He Z, Tee M, Potter KJ, Klimek AM, Meloche RM and others. 2009. Different effects of FK506, rapamycin, and mycophenolate mofetil on glucose-stimulated insulin release and apoptosis in human islets. *Cell Transplant* 18(8):833-45.
- Johnson JD, Bernal-Mizrachi E, Alejandro EU, Han Z, Kalynyak TB, Li H, Beith JL, Gross J, Warnock GL, Townsend RR and others. 2006. Insulin protects islets from apoptosis via Pdx1 and specific changes in the human islet proteome. *Proc Natl Acad Sci U S A* 103(51):19575-80.
- Jonsson J, Carlsson L, Edlund T, Edlund H. 1994. Insulin-promoter-factor 1 is required for pancreas development in mice. *Nature* 371(6498):606-9.
- Jorjani P, Ozturk SS. 1999. Effects of cell density and temperature on oxygen consumption rate for different mammalian cell lines. *Biotechnology and Bioengineering* 64(3):349-356.
- Juste S, Lessard M, Henley N, Menard M, Halle JP. 2005. Effect of poly-L-lysine coating on macrophage activation by alginate-based microcapsules: Assessment using a new in vitro method. *Journal of Biomedical Materials Research Part A* 72A(4):389-398.

- Kaddis JS, Danobeitia JS, Niland JC, Stiller T, Fernandez LA. 2010. Multicenter Analysis of Novel and Established Variables Associated with Successful Human Islet Isolation Outcomes. *Am J Transplant* 10(3):646-56.
- Kang L, Wang J, Zhang Y, Kou Z, Gao S. 2009. iPS cells can support full-term development of tetraploid blastocyst-complemented embryos. *Cell Stem Cell* 5(2):135-8.
- Katdare MR, Bhonde RR, Parab PB. 2004. Analysis of morphological and functional maturation of neoislets generated in vitro from pancreatic ductal cells and their suitability for islet banking and transplantation. *Journal of Endocrinology* 182(1):105-112.
- Kayali AG, Flores LE, Lopez AD, Kutlu B, Baetge E, Kitamura R, Hao E, Beattie GM, Hayek A. 2007. Limited Capacity of Human Adult Islets Expanded In Vitro to Redifferentiate Into Insulin-Producing beta-Cells. *Diabetes* 56(3):703-8.
- Kerr-Conte J, Pattou F, Lecomte-Houcke M, Xia Y, Boilly B, Proye C, Lefebvre J. 1996. Ductal cyst formation in collagen-embedded adult human islet preparations. A means to the reproduction of nesidioblastosis in vitro. *Diabetes* 45(8):1108-14.
- Kikugawa R, Katsuta H, Akashi T, Yatoh S, Weir GC, Sharma A, Bonner-Weir S. 2009. Differentiation of COPAS-sorted non-endocrine pancreatic cells into insulin-positive cells in the mouse. *Diabetologia* 52(4):645-52.
- Kim A, Miller K, Jo J, Kilimnik G, Wojcik P, Hara M. 2009. Islet architecture: A comparative study. *Islets* 1(2):129-36.
- King A. 2001. Evaluation of Alginate Microcapsules for Use in Transplantation Of Islets of Langerhans. Uppsala: University of Uppsala. 42 p.
- King A, Lau J, Nordin A, Sandler S, Andersson A. 2003a. The effect of capsule composition in the reversal of hyperglycemia in diabetic mice transplanted with microencapsulated allogeneic islets. *Diabetes Technol Ther* 5(4):653-63.
- King A, Sandler S, Andersson A. 2001. The effect of host factors and capsule composition on the cellular overgrowth on implanted alginate capsules. *J Biomed Mater Res* 57(3):374-83.
- King A, Strand B, Rokstad AM, Kulseng B, Andersson A, Skjak-Braek G, Sandler S. 2003b. Improvement of the biocompatibility of alginate/poly-L-lysine/alginate microcapsules by the use of epimerized alginate as a coating. *Journal of Biomedical Materials Research Part A* 64A(3):533-539.
- King JA, Miller WM. 2007. Bioreactor development for stem cell expansion and controlled differentiation. *Curr Opin Chem Biol* 11(4):394-8.
- Klokk TI, Melvik JE. 2002. Controlling the size of alginate gel beads by use of a high electrostatic potential. *Journal of Microencapsulation* 19(4):415-424.
- Klossner J, Kivisaari J, Niinikoski J. 1974. Oxygen and carbon dioxide tensions in the abdominal cavity and colonic wall of the rabbit. *Am J Surg* 127(6):711-5.
- Kobayashi T, Harb G, Rajotte RV, Korbitt GS, Mallett AG, Arefanian H, Mok D, Rayat GR. 2006. Immune mechanisms associated with the rejection of encapsulated neonatal porcine islet xenografts. *Xenotransplantation* 13(6):547-59.

- Koch S, Schwinger C, Kressler J, Heinzen C, Rainov NG. 2003. Alginate encapsulation of genetically engineered mammalian cells: comparison of production devices, methods and microcapsule characteristics. *Journal of Microencapsulation* 20(3):303-316.
- Kolmogorov AN. 1949. On the breaking of drops in turbulent flow. *Doklady Akademii Nauk* 66:825-828.
- Korbitt GS, Ao Z, Rayat GR. 1997a. Effect of microencapsulation and autologous serum on the growth and maturation of neonatal porcine islets in vitro. *Acta Diabetologica*(34):136.
- Korbitt GS, Elliott JF, Ao Z, Flashner M, Warnock GL, Rajotte RV. 1997b. Microencapsulation of neonatal porcine islets: long-term reversal of diabetes in nude mice and in vitro protection from human complement mediated cytolysis. *Transplant Proc* 29(4):2128.
- Korbitt GS, Elliott JF, Ao Z, Smith DK, Warnock GL, Rajotte RV. 1996. Large scale isolation, growth, and function of porcine neonatal islet cells. *J Clin Invest* 97(9):2119-29.
- Korbitt GS, Mallett AG, Ao Z, Flashner M, Rajotte RV. 2004. Improved survival of microencapsulated islets during in vitro culture and enhanced metabolic function following transplantation. *Diabetologia* 47(10):1810-8.
- Koska J, Bowen BD, Piret JM. 1997. Protein transport in packed bed ultrafiltration hollow-fibre bioreactors. *Chemical Engineering Science* 52(14):2251-2263.
- Koulmanda M, Qipo A, Smith RN, Auchincloss H, Jr. 2003. Pig islet xenografts are resistant to autoimmune destruction by non-obese diabetic recipients after anti-CD4 treatment. *Xenotransplantation* 10(2):178-84.
- Krassowska AG. 2010. News Release July 30, 2010, Geron to Proceed with First Human Clinical Trial of Embryonic Stem Cell-Based Therapy. *Geron*.
- Kritzik MR, Krahl T, Good A, Krakowski M, St-Onge L, Gruss P, Wright C, Sarvetnick N. 2000. Transcription factor expression during pancreatic islet regeneration. *Mol Cell Endocrinol* 164(1-2):99-107.
- Kroon E, Martinson LA, Kadoya K, Bang AG, Kelly OG, Eliazar S, Young H, Richardson M, Smart NG, Cunningham J and others. 2008. Pancreatic endoderm derived from human embryonic stem cells generates glucose-responsive insulin-secreting cells in vivo. *Nat Biotechnol* 26(4):443-52.
- Kulicke WM, Aggour YA, Elsabee MZ. 1990. Preparation, Characterization, and Rheological Behavior of Starch-Sodium Trimetaphosphate Hydrogels. *Starch-Starke* 42(4):134-141.
- Kulicke WM, Kniewske R. 1984. The Shear Viscosity Dependence on Concentration, Molecular-Weight, and Shear Rate of Polystyrene Solutions. *Rheologica Acta* 23(1):75-83.
- Kulseng B, Skjak-Braek G, Ryan L, Andersson A, King A, Faxvaag A, Espevik T. 1999. Transplantation of alginate microcapsules: generation of antibodies against alginates and encapsulated porcine islet-like cell clusters. *Transplantation* 67(7):978-84.
- Kulseng B, Thu B, Espevik T, Skjak-Braek G. 1997. Alginate polylysine microcapsules as immune barrier: Permeability of cytokines and immunoglobulins over the capsule membrane. *Cell Transplantation* 6(4):387-394.

- Labecki M, Bowen BD, Piret JM. 1996. Two-dimensional analysis of protein transport in the extracapillary space of hollow-fibre bioreactors. *Chemical Engineering Science* 51(17):4197-4213.
- Labecki M, Weber I, Dudal Y, Koska J, Piret JM, Bowen BD. 1998. Hindered transmembrane protein transport in hollow-fibre devices. *Journal of Membrane Science* 146(2):197-216.
- Lacik I. 2006. Polymer Chemistry in Diabetes Treatment by Encapsulated Islets of Langerhans: Review to 2006. *Australian Journal of Chemistry* 59(8):508-524.
- Lacy PE, Davie JM. 1984. Transplantation of pancreatic islets. *Annu Rev Immunol* 2:183-98.
- Lacy PE, Hegre OD, Gerasimidi-Vazeou A, Gentile FT, Dionne KE. 1991. Maintenance of normoglycemia in diabetic mice by subcutaneous xenografts of encapsulated islets. *Science* 254(5039):1782-4.
- Lagisetty JS, Das PK, Kumar R, Gandhi KS. 1986. Breakage of Viscous and Non-Newtonian Drops in Stirred Dispersions. *Chemical Engineering Science* 41(1):65-72.
- Lai Y, Chen C, Linn T. 2009. Innate immunity and heat shock response in islet transplantation. *Clinical and Experimental Immunology* 157(1):1-8.
- Langlois G, Dusseault J, Bilodeau S, Tam SK, Magassouba D, Halle JP. 2009. Direct effect of alginate purification on the survival of islets immobilized in alginate-based microcapsules. *Acta Biomater* 5(9):3433-40.
- Lanigan RS, Expert CIR. 2000. Final report on the safety assessment of PEG-20 sorbitan cocoate; PEG-40 sorbitan diisostearate; PEG-2,-5, and-20 sorbitan isostearate; PEG-40 and-75 sorbitan lanolate; PEG-10,-40,-44,-75, and-80 sorbitan laurate; PEG-3, and-6 sorbitan oleate; PEG-80 sorbitan palmitate; PEG-40 sorbitan perisostearate; PEG-40 sorbitan peroleate; PEG-3,-6,-40, and-60 sorbitan stearate; PEG-20,-30,-40, and-60 sorbitan tetraoleate; PEG-60 sorbitan tetrastearate; PEG-20 and-160 sorbitantriisostearate; PEG-18 sorbitan trioleate; PEG-40 and-50 sorbitol hexaoleate; PEG-30 sorbitol tetraoleate laurate; and PEG-60 sorbitol tetrastearate - Addendum to the final report on the safety assessment of polysorbates. *International Journal of Toxicology* 19:43-89.
- Lanza RP, Ecker DM, Kuhlreiber WM, Marsh JP, Ringeling J, Chick WL. 1999a. Transplantation of islets using microencapsulation: studies in diabetic rodents and dogs. *Journal of Molecular Medicine-Jmm* 77(1):206-210.
- Lanza RP, Jackson R, Sullivan A, Ringeling J, McGrath C, Kuhlreiber W, Chick WL. 1999b. Xenotransplantation of cells using biodegradable microcapsules. *Transplantation* 67(8):1105-11.
- Lanza RP, Kuhlreiber WM, Ecker D, Staruk JE, Chick WL. 1995. Xenotransplantation of Porcine and Bovine Islets without Immunosuppression Using Uncoated Alginate Microspheres. *Transplantation* 59(10):1377-1384.
- Larisch BC, Poncelet D, Champagne CP, Neufeld RJ. 1994a. Microencapsulation of *Lactococcus lactis* subsp. *cremoris*. *J Microencapsul* 11(2):189-95.
- Larisch BC, Poncelet D, Champagne CP, Neufeld RJ. 1994b. Microencapsulation of *Lactococcus-Lactis* Subsp *Cremoris*. *Journal of Microencapsulation* 11(2):189-195.
- Lau J, Carlsson PO. 2009. Low revascularization of human islets when experimentally transplanted into the liver. *Transplantation* 87(3):322-5.

- Lau J, Henriksnas J, Svensson J, Carlsson PO. 2009. Oxygenation of islets and its role in transplantation. *Curr Opin Organ Transplant* 14(6):688-93.
- Lechner A, Nolan AL, Blacken RA, Habener JF. 2005. Redifferentiation of insulin-secreting cells after in vitro expansion of adult human pancreatic islet tissue. *Biochem Biophys Res Commun* 327(2):581-8.
- Lee JS, Kim EJ, Chung D, Lee HG. 2009. Characteristics and antioxidant activity of catechin-loaded calcium pectinate gel beads prepared by internal gelation. *Colloids and Surfaces B-Biointerfaces* 74(1):17-22.
- Lee KY, Kong HJ, Mooney DJ. 2008. Quantifying interactions between cell receptors and adhesion ligand-modified polymers in solution. *Macromol Biosci* 8(2):140-5.
- Lefebvre VH, Otonkoski T, Ustinov J, Huotari MA, Pipeleers DG, Bouwens L. 1998. Culture of adult human islet preparations with hepatocyte growth factor and 804G matrix is mitogenic for duct cells but not for beta-cells. *Diabetes* 47(1):134-7.
- Lehmann R, Zuellig RA, Kugelmeier P, Baenninger PB, Moritz W, Perren A, Clavien PA, Weber M, Spinass GA. 2007. Superiority of small islets in human islet transplantation. *Diabetes* 56(3):594-603.
- Lencki R, Neufeld RJ, Spinney T; 1989. Method of producing microspheres. US Patent 4822534. US.
- Lewinska D, Bukowski J, Kozuchowski M, Kinasiewicz A, Werynski A. 2008. Electrostatic microencapsulation of living cells. *Biocybernetics and Biomedical Engineering* 28(2):69-85.
- Li M, Miyagawa J, Moriwaki M, Yuan M, Yang Q, Kozawa J, Yamamoto K, Imagawa A, Iwahashi H, Tochino Y and others. 2003. Analysis of expression profiles of islet-associated transcription and growth factors during beta-cell neogenesis from duct cells in partially duct-ligated mice. *Pancreas* 27(4):345-55.
- Li RH, Altreuter DH, Gentile FT. 1996. Transport characterization of hydrogel matrices for cell encapsulation. *Biotechnology and Bioengineering* 50(4):365-373.
- Li Y, Zhang R, Qiao H, Zhang H, Wang Y, Yuan H, Liu Q, Liu D, Chen L, Pei X. 2007. Generation of insulin-producing cells from PDX-1 gene-modified human mesenchymal stem cells. *J Cell Physiol* 211(1):36-44.
- Lim F, Sun AM. 1980. Microencapsulated islets as bioartificial endocrine pancreas. *Science* 210(4472):908-10.
- Lin HT, Chiou SH, Kao CL, Shyr YM, Hsu CJ, Tarng YW, Ho LL, Kwok CF, Ku HH. 2006. Characterization of pancreatic stem cells derived from adult human pancreas ducts by fluorescence activated cell sorting. *World J Gastroenterol* 12(28):4529-35.
- Linning KD, Tai MH, Madhukar BV, Chang CC, Reed DN, Ferber S, Trosko JE, Olson LK. 2004. Redox-mediated enrichment of self-renewing adult human pancreatic cells that possess endocrine differentiation potential. *Pancreas* 29(3):E64-E76.
- Lipsett MA, Castellarin ML, Rosenberg L. 2007. Acinar plasticity: development of a novel in vitro model to study human acinar-to-duct-to-islet differentiation. *Pancreas* 34(4):452-7.
- Liu H, Guz Y, Kedeas MH, Winkler J, Teitelman G. 2010. Precursor cells in mouse islets generate new beta-cells in vivo during aging and after islet injury. *Endocrinology* 151(2):520-8.

- Liu Q, Rauth AM, Wu XY. 2007. Immobilization and bioactivity of glucose oxidase in hydrogel microspheres formulated by an emulsification-internal gelation-adsorption-polyelectrolyte coating method. *International Journal of Pharmaceutics* 339(1-2):148-156.
- Liu XD, Bao DC, Xue WM, Xiong Y, Yu WT, Yu XJ, Ma XJ, Yuan Q. 2003. Preparation of uniform calcium alginate gel beads by membrane emulsification coupled with internal gelation. *Journal of Applied Polymer Science* 87(5):848-852.
- Living Cell Technologies. 2010. Open-label Investigation of the Safety and Effectiveness of DIABECCELL(R) in Patients With Type I Diabetes Mellitus.
- Logtenberg SJ, Kleefstra N, Houweling ST, Groenier KH, Gans RO, Bilo HJ. 2010. Health-related quality of life, treatment satisfaction, and costs associated with intraperitoneal versus subcutaneous insulin administration in type 1 diabetes: a randomized controlled trial. *Diabetes Care* 33(6):1169-72.
- Lopez S, Prieto M, Dijkstra J, Dhanoa MS, France J. 2004. Statistical evaluation of mathematical models for microbial growth. *Int J Food Microbiol* 96(3):289-300.
- Lopez-Avalos MD, Tatarkiewicz K, Sharma A, Bonner-Weir S, Weir GC. 2001. Enhanced maturation of porcine neonatal pancreatic cell clusters with growth factors fails to improve transplantation outcome. *Transplantation* 71(8):1154-62.
- Luca G, Calafiore R, Basta G, Ricci M, Calvitti M, Neri L, Nastruzzi C, Becchetti E, Capitani S, Brunetti P and others. 2001. Improved function of rat islets upon co-microencapsulation with Sertoli's cells in alginate/poly-L-ornithine. *AAPS PharmSciTech* 2(3):E15.
- Lucas-Clerc C, Massart C, Champion JP, Launois B, Nicol M. 1993. Long-term culture of human pancreatic islets in an extracellular matrix: morphological and metabolic effects. *Mol Cell Endocrinol* 94(1):9-20.
- Luo Z, Gotoh M, Grochowicki T, Tanaka T, Kimura F, Kawashima H, Yagita H, Okumura K, Miyasaka M. 2000. Anergic T cells generated in vitro suppress rejection response to islet allografts. *Transplantation* 69(10):2144-8.
- Luther MJ, Hauge-Evans A, Souza KLA, Jorns A, Lenzen S, Persaud SJ, Jones PM. 2006. MIN6 beta-cell-beta-cell interactions influence insulin secretory responses to nutrients and non-nutrients. *Biochemical and Biophysical Research Communications* 343(1):99-104.
- Luu M. 2004. Process Development for the Production of Pancreatic Islet Equivalents [Master's]. Vancouver: University of British Columbia.
- Ma HL, Hung SC, Lin SY, Chen YL, Lo WH. 2003. Chondrogenesis of human mesenchymal stem cells encapsulated in alginate beads. *J Biomed Mater Res A* 64(2):273-81.
- MacKenzie DA, Hullett DA, Sollinger HW. 2003. Xenogeneic transplantation of porcine islets: an overview. *Transplantation* 76(6):887-91.
- Maehr R, Chen S, Snitow M, Ludwig T, Yagasaki L, Goland R, Leibel RL, Melton DA. 2009. Generation of pluripotent stem cells from patients with type 1 diabetes. *Proc Natl Acad Sci U S A* 106(37):15768-73.
- Maguire T, Novik E, Schloss R, Yarmush M. 2006. Alginate-PLL microencapsulation: effect on the differentiation of embryonic stem cells into hepatocytes. *Biotechnol Bioeng* 93(3):581-91.

- Magyar JP, Nemir M, Ehler E, Suter N, Perriard JC, Eppenberger HM. 2001. Mass production of embryoid bodies in microbeads. *Bioartificial Organs Iii: Tissue Sourcing, Immunoisolation, and Clinical Trials* 944:135-143.
- Mahler S, Desille M, Fremond B, Chesne C, Guillouzo A, Campion JP, Clement B. 2003. Hypothermic storage and cryopreservation of hepatocytes: the protective effect of alginate gel against cell damages. *Cell Transplant* 12(6):579-92.
- Makhlouf L, Kishimoto K, Smith RN, Abdi R, Koulmanda M, Winn HJ, Auchincloss H, Jr., Sayegh MH. 2002. The role of autoimmunity in islet allograft destruction: major histocompatibility complex class II matching is necessary for autoimmune destruction of allogeneic islet transplants after T-cell costimulatory blockade. *Diabetes* 51(11):3202-10.
- Maki T, Lodge JPA, Carretta M, Ohzato H, Borland KM, Sullivan SJ, Staruk J, Muller TE, Solomon BA, Chick WL and others. 1993. Treatment of Severe Diabetes-Mellitus for More Than One-Year Using a Vascularized Hybrid Artificial Pancreas. *Transplantation* 55(4):713-718.
- Malaisse WJ, Best L, Kawazu S, Malaissegae F, Sener A. 1983. The Stimulus-Secretion Coupling of Glucose-Induced Insulin Release - Fuel Metabolism in Islets Deprived of Exogenous Nutrient. *Archives of Biochemistry and Biophysics* 224(1):102-110.
- Malpique R, Osorio LM, Ferreira DS, Ehrhart F, Brito C, Zimmermann H, Alves PM. 2009. Alginate Encapsulation as a Novel Strategy for the Cryopreservation of Neurospheres. *Tissue Eng Part C Methods*.
- Manesso E, Toffolo GM, Saisho Y, Butler AE, Matveyenko AV, Cobelli C, Butler PC. 2009. Dynamics of beta-cell turnover: evidence for beta-cell turnover and regeneration from sources of beta-cells other than beta-cell replication in the HIP rat. *Am J Physiol Endocrinol Metab* 297(2):E323-30.
- Marcen R. 2009. Immunosuppressive drugs in kidney transplantation: impact on patient survival, and incidence of cardiovascular disease, malignancy and infection. *Drugs* 69(16):2227-43.
- Maria-Engler SS, Correa-Giannella ML, Labriola L, Krogh K, Colin C, Lojudice FH, Aita CA, de Oliveira EM, Correa TC, da Silva IC and others. 2004. Co-localization of nestin and insulin and expression of islet cell markers in long-term human pancreatic nestin-positive cell cultures. *J Endocrinol* 183(3):455-67.
- Martinsen A, Skjakbraek G, Smidsrod O. 1989. Alginate as Immobilization Material .1. Correlation between Chemical and Physical-Properties of Alginate Gel Beads. *Biotechnology and Bioengineering* 33(1):79-89.
- Martinsen A, Storro I, Skjakbraek G. 1992. Alginate as Immobilization Material .3. Diffusional Properties. *Biotechnology and Bioengineering* 39(2):186-194.
- Mason MN, Arnold CA, Mahoney MJ. 2009. Entrapped collagen type 1 promotes differentiation of embryonic pancreatic precursor cells into glucose-responsive beta-cells when cultured in three-dimensional PEG hydrogels. *Tissue Eng Part A* 15(12):3799-808.
- Matis LA, Sorger SB, McElligott DL, Fink PJ, Hedrick SM. 1987. The molecular basis of alloreactivity in antigen-specific, major histocompatibility complex-restricted T cell clones. *Cell* 51(1):59-69.

- McKinnon CM, Docherty K. 2001. Pancreatic duodenal homeobox-1, PDX-1, a major regulator of beta cell identity and function. *Diabetologia* 44(10):1203-14.
- Means AL, Meszoely IM, Suzuki K, Miyamoto Y, Rustgi AK, Coffey RJ, Jr., Wright CV, Stoffers DA, Leach SD. 2005. Pancreatic epithelial plasticity mediated by acinar cell transdifferentiation and generation of nestin-positive intermediates. *Development* 132(16):3767-76.
- Menard M, Dusseault J, Langlois G, Baille WE, Tam SK, Yahia L, Zhu XX, Halle JP. 2010. Role of protein contaminants in the immunogenicity of alginates. *J Biomed Mater Res B Appl Biomater* 93(2):333-40.
- Merani S, Toso C, Emamaullee J, Shapiro AM. 2008. Optimal implantation site for pancreatic islet transplantation. *Br J Surg* 95(12):1449-61.
- Minami K, Okuno M, Miyawaki K, Okumachi A, Ishizaki K, Oyama K, Kawaguchi M, Ishizuka N, Iwanaga T, Seino S. 2005. Lineage tracing and characterization of insulin-secreting cells generated from adult pancreatic acinar cells. *Proc Natl Acad Sci U S A* 102(42):15116-21.
- Miyazaki J, Araki K, Yamato E, Ikegami H, Asano T, Shibasaki Y, Oka Y, Yamamura K. 1990. Establishment of a pancreatic beta cell line that retains glucose-inducible insulin secretion: special reference to expression of glucose transporter isoforms. *Endocrinology* 127(1):126-32.
- Moe S, Skjakbraek G, Smidsrod O, Ichijo H. 1994. Calcium Alginate Gel Fibers - Influence of Alginate Source and Gel Structure on Fiber Strength. *Journal of Applied Polymer Science* 51(10):1771-1775.
- Mojibian M, Chakir H, Lefebvre DE, Crookshank JA, Sonier B, Keely E, Scott FW. 2009. Diabetes-specific HLA-DR-restricted proinflammatory T-cell response to wheat polypeptides in tissue transglutaminase antibody-negative patients with type 1 diabetes. *Diabetes* 58(8):1789-96.
- Mollet M, Ma NN, Zhao Y, Brodkey R, Taticek R, Chalmers JJ. 2004. Bioprocess equipment: Characterization of energy dissipation rate and its potential to damage cells. *Biotechnology Progress* 20(5):1437-1448.
- Morch YA. 2008. *Novel Alginate Microcapsules for Cell Therapy*. Trondheim: Norwegian University of Science and Technology.
- Morch YA, Donati I, Strand BL, Skjak-Braek G. 2006. Effect of Ca²⁺, Ba²⁺, and Sr²⁺ on alginate microbeads. *Biomacromolecules* 7(5):1471-1480.
- Morch YA, Holtan S, Donati I, Strand BL, Skjak-Braek G. 2008. Mechanical properties of C-5 epimerized alginates. *Biomacromolecules* 9(9):2360-2368.
- Morris ER, Rees DA, Thom D, Boyd J. 1978. Chiroptical and Stoichiometric Evidence of a Specific, Primary Dimerization Process in Alginate Gelation. *Carbohydrate Research* 66(OCT):145-154.
- Morse JW, Arvidson RS. 2002. The dissolution kinetics of major sedimentary carbonate minerals. *Earth-Science Reviews* 58(1-2):51-84.
- Morton RA, Geras-Raaka E, Wilson LM, Raaka BM, Gershengorn MC. 2007. Endocrine precursor cells from mouse islets are not generated by epithelial-to-mesenchymal transition of mature beta cells. *Mol Cell Endocrinol*.

- Moss LG, Rhodes CJ. 2007. Beta-cell regeneration: epithelial mesenchymal transition pre-EMTpted by lineage tracing? *Diabetes* 56(1):281-2.
- Mouquet C, Aymard C, Guilbert S, Cuvelier G, Launay B. 1997. Influence of initial pH on gelation kinetics of texturized passion fruit pulp. *Food Science and Technology-Lebensmittel-Wissenschaft & Technologie* 30(2):129-134.
- Murua A, Orive G, Hernandez RM, Pedraz JL. 2009. Cryopreservation based on freezing protocols for the long-term storage of microencapsulated myoblasts. *Biomaterials* 30(20):3495-3501.
- Nagata NA, Inoue K, Tabata Y. 2002. Co-culture of extracellular matrix suppresses the cell death of rat pancreatic islets. *J Biomater Sci Polym Ed* 13(5):579-90.
- Nishioka T, Yokota M, Tsuda I, Tatsumi N. 2002. Flow cytometric analysis of platelet activation under calcium ion-chelating conditions. *Clin Lab Haematol* 24(2):115-9.
- Noth U, Grohn P, Jork A, Zimmermann U, Haase A, Lutz J. 1999. 19F-MRI in vivo determination of the partial oxygen pressure in perfluorocarbon-loaded alginate capsules implanted into the peritoneal cavity and different tissues. *Magn Reson Med* 42(6):1039-47.
- Nurdin N, Canaple L, Bartkowiak A, Desvergne B, Hunkeler D. 2000. Capsule permeability via polymer and protein ingress/egress. *Journal of Applied Polymer Science* 75(9):1165-1175.
- Ohgawara H, Hirotani S, Miyazaki J, Teraoka S. 1998. Membrane immunoisolation of a diffusion chamber for a bioartificial pancreas. *Artificial Organs* 22(9):788-794.
- Olsson R, Carlsson PO. 2006. The pancreatic islet endothelial cell: emerging roles in islet function and disease. *Int J Biochem Cell Biol* 38(5-6):710-4.
- Omer A, Duvivier-Kali V, Fernandes J, Tchipashvili V, Colton CK, Weir GC. 2005. Long-term normoglycemia in rats receiving transplants with encapsulated islets. *Transplantation* 79(1):52-8.
- Omer A, Duvivier-Kali VF, Trivedi N, Wilmot K, Bonner-Weir S, Weir GC. 2003. Survival and maturation of microencapsulated porcine neonatal pancreatic cell clusters transplanted into immunocompetent diabetic mice. *Diabetes* 52(1):69-75.
- Orive G, Tam SK, Pedraz JL, Halle JP. 2006. Biocompatibility of alginate-poly-L-lysine microcapsules for cell therapy. *Biomaterials* 27(20):3691-700.
- Orlowski T, Godlewska E, Tarchalska M, Kinasiwicz J, Antosiak M, Sabat M. 2005. The influence of immune system stimulation on encapsulated islet graft survival. *Archivum Immunologiae Et Therapiae Experimentalis* 53(2):180-184.
- O'Shea GM, Goosen MF, Sun AM. 1984. Prolonged survival of transplanted islets of Langerhans encapsulated in a biocompatible membrane. *Biochim Biophys Acta* 804(1):133-6.
- O'Shea GM, Sun AM. 1986. Encapsulation of rat islets of Langerhans prolongs xenograft survival in diabetic mice. *Diabetes* 35(8):943-6.
- Ouziel-Yahalom L, Zalzman M, Anker-Kitai L, Knoller S, Bar Y, Glandt M, Herold K, Efrat S. 2006. Expansion and redifferentiation of adult human pancreatic islet cells. *Biochem Biophys Res Commun* 341(2):291-8.

- Pacek AW, Chamsart S, Nienow AW, Bakker A. 1999. The influence of impeller type on mean drop size and drop size distribution in an agitated vessel. *Chemical Engineering Science* 54(19):4211-4222.
- Papas KK, Long RC, Constantinidis I, Sambanis A. 1996. Effects of oxygen on metabolic and secretory activities of beta TC3 cells. *Biochimica Et Biophysica Acta-General Subjects* 1291(2):163-166.
- Pelaez C, Karel M. 1981. Improved Method for Preparation of Fruit-Simulating Alginate Gels. *Journal of Food Processing and Preservation* 5(2):63-81.
- Perets A, Baruch Y, Weisbuch F, Shoshany G, Neufeld G, Cohen S. 2003. Enhancing the vascularization of three-dimensional porous alginate scaffolds by incorporating controlled release basic fibroblast growth factor microspheres. *J Biomed Mater Res A* 65(4):489-97.
- Perl S, Kushner JA, Buchholz BA, Meeker AK, Stein GM, Hsieh M, Kirby M, Pechhold S, Liu EH, Harlan DM and others. 2010. Significant Human beta-Cell Turnover Is Limited to the First Three Decades of Life as Determined by in Vivo Thymidine Analog Incorporation and Radiocarbon Dating. *J Clin Endocrinol Metab.*
- Pinkse GG, Bouwman WP, Jiawan-Lalai R, Terpstra OT, Bruijn JA, de Heer E. 2006. Integrin signaling via RGD peptides and anti-beta1 antibodies confers resistance to apoptosis in islets of Langerhans. *Diabetes* 55(2):312-7.
- Piper K, Brickwood S, Turnpenny LW, Cameron IT, Ball SG, Wilson DI, Hanley NA. 2004. Beta cell differentiation during early human pancreas development. *J Endocrinol* 181(1):11-23.
- Piret JM, Cooney CL. 1990. Mammalian-Cell and Protein Distributions in Ultrafiltration Hollow Fiber Bioreactors. *Biotechnology and Bioengineering* 36(9):902-910.
- Piret JM, Devens DA, Cooney CL. 1991. Nutrient and Metabolite Gradients in Mammalian Cell Hollow Fiber Bioreactors. *The Canadian Journal of Chemical Engineering* 69:421-428.
- Piro S, Lupi R, Dotta F, Patane G, Rabuazzo MA, Marselli L, Santangelo C, Realacci M, Del Guerra S, Purrello F and others. 2001. Bovine islets are less susceptible than human islets to damage by human cytokines. *Transplantation* 71(1):21-6.
- Ponce S, Orive G, Hernandez R, Gascon AR, Pedraz JL, de Haan BJ, Faas MM, Mathieu HJ, de Vos P. 2006. Chemistry and the biological response against immunisolating alginate-polycation capsules of different composition. *Biomaterials* 27(28):4831-9.
- Poncelet D, Bugarski B, Amsden BG, Zhu J, Neufeld R, Goosen MFA. 1994. A Parallel-Plate Electrostatic Droplet Generator - Parameters Affecting Microbead Size. *Applied Microbiology and Biotechnology* 42(2-3):251-255.
- Poncelet D, Desmet BP, Beaulieu C, Huguet ML, Fournier A, Neufeld RJ. 1995. Production of Alginate Beads by Emulsification Internal Gelation .2. Physicochemistry. *Applied Microbiology and Biotechnology* 43(4):644-650.
- Poncelet D, Lencki R, Beaulieu C, Halle JP, Neufeld RJ, Fournier A. 1992. Production of alginate beads by emulsification/internal gelation. I. Methodology. *Appl Microbiol Biotechnol* 38(1):39-45.

- Porrett PM, Yeh H, Frank A, Deng S, Kim JL, Barker CF, Markmann JF. 2007. Availability of suitable islet donors in the United States. *Transplantation* 84(2):280-2.
- Project CD. 2010. Patient testimonies.
- Prusse U, Bilancetti L, Bucko M, Bugarski B, Bukowski J, Gemeiner P, Lewinska D, Manojlovic V, Massart B, Nastruzzi C and others. 2008. Comparison of different technologies for alginate beads production. *Chemical Papers* 62(4):364-374.
- Prusse U, Dalluhn J, Breford J, Vorlop KD. 2000. Production of spherical beads by JetCutting. *Chemical Engineering & Technology* 23(12):1105-1110.
- Pueyo ME, Darquy S, Capron F, Reach G. 1993. In-Vitro Activation of Human Macrophages by Alginate Polylysine Microcapsules. *Journal of Biomaterials Science-Polymer Edition* 5(3):197-203.
- Quong D, Neufeld RJ, Skjak-Braek G, Poncellet D. 1998. External versus internal source of calcium during the gelation of alginate beads for DNA encapsulation. *Biotechnology and Bioengineering* 57(4):438-446.
- Rabinovitch A, Suarez-Pinzon WL. 1998. Cytokines and their roles in pancreatic islet beta-cell destruction and insulin-dependent diabetes mellitus. *Biochemical Pharmacology* 55(8):1139-1149.
- Ramirez JA, Goodman WG, Menezes C, Segre GV, Salusky IB. 1993. Disodium ethylenediaminetetraacetate: adverse effects in dialyzed children. *Pediatr Nephrol* 7(2):182-4.
- Ramiya VK, Maraist M, Arfors KE, Schatz DA, Peck AB, Cornelius JG. 2000. Reversal of insulin-dependent diabetes using islets generated in vitro from pancreatic stem cells. *Nat Med* 6(3):278-82.
- Rankin MM, Kushner JA. 2009. Adaptive beta-cell proliferation is severely restricted with advanced age. *Diabetes* 58(6):1365-72.
- Rayat GR, Rajotte RV, Ao Z, Korbitt GS. 2000. Microencapsulation of neonatal porcine islets: protection from human antibody/complement-mediated cytolysis in vitro and long-term reversal of diabetes in nude mice. *Transplantation* 69(6):1084-90.
- Rayat GR, Rajotte RV, Hering BJ, Binette TM, Korbitt GS. 2003. In vitro and in vivo expression of Galalpha-(1,3)Gal on porcine islet cells is age dependent. *J Endocrinol* 177(1):127-35.
- Rayat GR, Rajotte RV, Korbitt GS. 1999. Potential application of neonatal porcine islets as treatment for type 1 diabetes: a review. *Ann N Y Acad Sci* 875:175-88.
- Registry CIT. 2009. 2007 update on allogeneic islet transplantation from the Collaborative Islet Transplant Registry (CITR). *Cell Transplant* 18(7):753-67.
- Rehfeldt F, Engler AJ, Eckhardt A, Ahmed F, Discher DE. 2007. Cell responses to the mechanochemical microenvironment--implications for regenerative medicine and drug delivery. *Adv Drug Deliv Rev* 59(13):1329-39.
- Reinsel MA, Borkowski JJ, Sears JT. 1994. Partition-Coefficients for Acetic, Propionic, and Butyric Acids in a Crude-Oil Water-System. *Journal of Chemical and Engineering Data* 39(3):513-516.

- Reis CP, Neufeld RJ, Vilela S, Ribeiro AJ, Veiga F. 2006. Review and current status of emulsion/dispersion technology using an internal gelation process for the design of alginate particles. *J Microencapsul* 23(3):245-57.
- Reis CP, Ribeiro AJ, Neufeld RJ, Veiga F. 2007a. Alginate microparticles as novel carrier for oral insulin delivery. *Biotechnology and Bioengineering* 96(5):977-989.
- Reis MM, Araujo PHH, Sayer C, Giudici R. 2007b. Spectroscopic on-line monitoring of reactions in dispersed medium: Chemometric challenges. *Analytica Chimica Acta* 595(1-2):257-265.
- Renken A, Hunkeler D. 2007a. Polymethylene-co-guanidine based capsules: a mechanistic study of the formation using alginate and cellulose sulphate. *J Microencapsul* 24(1):20-39.
- Renken A, Hunkeler D. 2007b. Polyvinylamine-based capsules: a mechanistic study of the formation using alginate and cellulose sulphate. *J Microencapsul* 24(4):323-36.
- Rialland L, Guyomard C, Scotte M, Chesne C, Guillouzo A. 2000. Viability and drug metabolism capacity of alginate-entrapped hepatocytes after cryopreservation. *Cell Biol Toxicol* 16(2):105-16.
- Ricordi C. 2003. Islet transplantation: a brave new world. *Diabetes* 52(7):1595-603.
- Rieck S, Kaestner KH. 2010. Expansion of beta-cell mass in response to pregnancy. *Trends Endocrinol Metab* 21(3):151-8.
- Robitaille R, Leblond FA, Bourgeois Y, Henley N, Loignon M, Halle JP. 2000. Studies on small (< 350 μ m) alginate-poly-L-lysine microcapsules. V. Determination of carbohydrate and protein permeation through microcapsules by reverse-size exclusion chromatography. *Journal of Biomedical Materials Research* 50(3):420-427.
- Roelen DL, Huurman VAL, Hilbrands R, Gillard P, Duinkerken G, van der Meer-Prins PWM, Maarschalk MFJVV, Mathieu C, Keymeulen B, Pipeleers DG and others. 2009. Relevance of cytotoxic alloreactivity under different immunosuppressive regimens in clinical islet cell transplantation. *Clinical and Experimental Immunology* 156(1):141-148.
- Roep BO. 2003. The role of T-cells in the pathogenesis of Type 1 diabetes: from cause to cure. *Diabetologia* 46(3):305-21.
- Rokka S, Rantamaki P. 2010. Protecting probiotic bacteria by microencapsulation: challenges for industrial applications. *European Food Research and Technology* 231(1):1-12.
- Rokstad AM, Kulseng B, Strand BL, Skjak-Braek G, Espevik T. 2001. Transplantation of alginate microcapsules with proliferating cells in mice - Capsular overgrowth and survival of encapsulated cells of mice and human origin. *Bioartificial Organs* Iii: Tissue Sourcing, Immunoisolation, and Clinical Trials 944:216-225.
- Rooman I, Heremans Y, Heimberg H, Bouwens L. 2000. Modulation of rat pancreatic acinoductal transdifferentiation and expression of PDX-1 in vitro. *Diabetologia* 43(7):907-14.
- Rovira M, Scott SG, Liss AS, Jensen J, Thayer SP, Leach SD. 2010. Isolation and characterization of centroacinar/terminal ductal progenitor cells in adult mouse pancreas. *Proc Natl Acad Sci U S A* 107(1):75-80.
- Rowley JA, Madlambayan G, Mooney DJ. 1999. Alginate hydrogels as synthetic extracellular matrix materials. *Biomaterials* 20(1):45-53.

- Rozario T, DeSimone DW. 2010. The extracellular matrix in development and morphogenesis: a dynamic view. *Dev Biol* 341(1):126-40.
- Rush BT, Fraga DW, Kotb MY, Sabek OM, Lo A, Gaber LW, Halim AB, Gaber AO. 2004. Preservation of human pancreatic islet in vivo function after 6-month culture in serum-free media. *Transplantation* 77(8):1147-54.
- Ryan EA, Paty BW, Senior PA, Bigam D, Alfadhli E, Kneteman NM, Lakey JR, Shapiro AM. 2005. Five-year follow-up after clinical islet transplantation. *Diabetes* 54(7):2060-9.
- Safley SA, Kapp LM, Tucker-Burden C, Hering B, Kapp JA, Weber CJ. 2005. Inhibition of cellular immune responses to encapsulated porcine islet xenografts by simultaneous blockade of two different costimulatory pathways. *Transplantation* 79(4):409-18.
- Saha K, Keung AJ, Irwin EF, Li Y, Little L, Schaffer DV, Healy KE. 2008. Substrate modulus directs neural stem cell behavior. *Biophys J* 95(9):4426-38.
- Sanchez D, Gmyr V, Kerr-Conte J, Kloppel G, Zenilman ME, Guy-Crotte O, Pattou F, Figarella C. 2004. Implication of Reg I in human pancreatic duct-like cells in vivo in the pathological pancreas and in vitro during exocrine dedifferentiation. *Pancreas* 29(1):14-21.
- Sardonini CA, Dibiasio D. 1992. An Investigation of the Diffusion-Limited Growth of Animal-Cells around Single Hollow Fibers. *Biotechnology and Bioengineering* 40(10):1233-1242.
- Scharp DW, Swanson CJ, Olack BJ, Latta PP, Hegre OD, Doherty EJ, Gentile FT, Flavin KS, Ansara MF, Lacy PE. 1994. Protection of encapsulated human islets implanted without immunosuppression in patients with type I or type II diabetes and in nondiabetic control subjects. *Diabetes* 43(9):1167-70.
- Schmied BM, Ulrich A, Matsuzaki H, Ding X, Ricordi C, Weide L, Moyer MP, Batra SK, Adrian TE, Pour PM. 2001. Transdifferentiation of human islet cells in a long-term culture. *Pancreas* 23(2):157-71.
- Schneider GB, English A, Abraham M, Zaharias R, Stanford C, Keller J. 2004. The effect of hydrogel charge density on cell attachment. *Biomaterials* 25(15):3023-3028.
- Schneider MK, Forte P, Seebach JD. 2001a. Adhesive interactions between human NK cells and porcine endothelial cells. *Scand J Immunol* 54(1-2):70-5.
- Schneider S, Feilen P, Cramer H, Hillgartner M, Brunnenmeier F, Zimmermann H, Weber MM, Zimmermann U. 2003. Beneficial effects of human serum albumin on stability and functionality of alginate microcapsules fabricated in different ways. *J Microencapsul* 20(5):627-36.
- Schneider S, Feilen PJ, Brunnenmeier F, Minnemann T, Zimmermann H, Zimmermann U, Weber MM. 2005. Long-term graft function of adult rat and human islets encapsulated in novel alginate-based microcapsules after transplantation in immunocompetent diabetic mice. *Diabetes* 54(3):687-93.
- Schneider S, Feilen PJ, Sloty V, Kampfner D, Preuss S, Berger S, Beyer J, Pommersheim R. 2001b. Multilayer capsules: a promising microencapsulation system for transplantation of pancreatic islets. *Biomaterials* 22(14):1961-70.

- Schonau E, Deeg KH, Huemmer HP, Akcetin YZ, Bohles HJ. 1991. Pancreatic growth and function following surgical treatment of nesidioblastosis in infancy. *Eur J Pediatr* 150(8):550-3.
- Schuurman HJ. 2009. The International Xenotransplantation Association consensus statement on conditions for undertaking clinical trials of porcine islet products in type 1 diabetes--chapter 2: Source pigs. *Xenotransplantation* 16(4):215-22.
- Schwinger C, Koch S, Jahnz U, Wittlich P, Rainov NG, Kressler J. 2002. High throughput encapsulation of murine fibroblasts in alginate using the JetCutter technology. *J Microencapsul* 19(3):273-80.
- Seaberg RM, Smukler SR, Kieffer TJ, Enikolopov G, Asghar Z, Wheeler MB, Korbitt G, van der Kooy D. 2004. Clonal identification of multipotent precursors from adult mouse pancreas that generate neural and pancreatic lineages. *Nat Biotechnol* 22(9):1115-24.
- Sechremeli D, Stampouli A, Stamatoudis M. 2006. Comparison of mean drop sizes and drop size distributions in agitated liquid-liquid dispersions produced by disk and open type impellers. *Chemical Engineering Journal* 117(2):117-122.
- Seeberger KL, Dufour JM, Shapiro AM, Lakey JR, Rajotte RV, Korbitt GS. 2006. Expansion of mesenchymal stem cells from human pancreatic ductal epithelium. *Lab Invest* 86(2):141-53.
- Seifert DB, Phillips JA. 1997. Porous alginate--poly(ethylene glycol) entrapment system for the cultivation of mammalian cells. *Biotechnol Prog* 13(5):569-76.
- Senuma Y, Lowe C, Zweifel Y, Hilborn JG, Marison I. 2000. Alginate hydrogel microspheres and microcapsules prepared by spinning disk atomization. *Biotechnology and Bioengineering* 67(5):616-622.
- Serp D, Cantana E, Heinzen C, von Stockar U, Marison IW. 2000. Characterization of an encapsulation device for the production of monodisperse alginate beads for cell immobilization. *Biotechnology and Bioengineering* 70(1):41-53.
- Shapiro A, Modai Y, Kohn A. 1967. Efficacies of vaccines containing alginate adjuvant. *J Appl Bacteriol* 30(2):304-11.
- Shapiro AM, Lakey JR, Ryan EA, Korbitt GS, Toth E, Warnock GL, Kneteman NM, Rajotte RV. 2000. Islet transplantation in seven patients with type 1 diabetes mellitus using a glucocorticoid-free immunosuppressive regimen. *N Engl J Med* 343(4):230-8.
- Shapiro AM, Ricordi C, Hering BJ, Auchincloss H, Lindblad R, Robertson RP, Secchi A, Brendel MD, Berney T, Brennan DC and others. 2006. International trial of the Edmonton protocol for islet transplantation. *N Engl J Med* 355(13):1318-30.
- Sharland A, Patel A, Lee JH, Cestra AE, Saidman S, Waneck GL. 2002. Genetically modified HLA class I molecules able to inhibit human NK cells without provoking alloreactive CD8+ CTLs. *J Immunol* 168(7):3266-74.
- Sharma A, Zangen DH, Reitz P, Taneja M, Lissauer ME, Miller CP, Weir GC, Habener JF, Bonner-Weir S. 1999. The homeodomain protein IDX-1 increases after an early burst of proliferation during pancreatic regeneration. *Diabetes* 48(3):507-13.
- Siebers U, Horcher A, Brandhorst H, Brandhorst D, Hering B, Federlin K, Bretzel RG, Zekorn T. 1999. Analysis of the cellular reaction towards microencapsulated xenogeneic islets after intraperitoneal transplantation. *J Mol Med* 77(1):215-8.

- Sikorski P, Mo F, Skjak-Braek G, Stokke BT. 2007. Evidence for egg-box-compatible interactions in calcium-alginate gels from fiber X-ray diffraction. *Biomacromolecules* 8(7):2098-2103.
- Silva CM, Ribeiro AJ, Figueiredo IV, Goncalves AR, Veiga F. 2006. Alginate microspheres prepared by internal gelation: Development and effect on insulin stability. *International Journal of Pharmaceutics* 311(1-2):1-10.
- Simpson NE, Stabler CL, Simpson CP, Sambanis A, Constantinidis I. 2004. The role of the CaCl₂-guluronic acid interaction on alginate encapsulated betaTC3 cells. *Biomaterials* 25(13):2603-10.
- Skjakbraek G, Grasdalen H, Smidsrod O. 1989. Inhomogeneous Polysaccharide Ionic Gels. *Carbohydrate Polymers* 10(1):31-54.
- Skjakbraek G, Smidsrod O, Larsen B. 1986. Tailoring of Alginates by Enzymatic Modification In vitro. *International Journal of Biological Macromolecules* 8(6):330-336.
- Smidsrod O, Haug A, Lian B. 1972. Properties of Poly(1,4-Hexuronates) in Gel State .1. Evaluation of a Method for Determination of Stiffness. *Acta Chemica Scandinavica* 26(1):71-&.
- Smidsrod O, Skjakbraek G. 1990. Alginate as Immobilization Matrix for Cells. *Trends in Biotechnology* 8(3):71-78.
- Solar M, Cardalda C, Houbracken I, Martin M, Maestro MA, De Medts N, Xu X, Grau V, Heimberg H, Bouwens L and others. 2009. Pancreatic exocrine duct cells give rise to insulin-producing beta cells during embryogenesis but not after birth. *Dev Cell* 17(6):849-60.
- Song SY, Gannon M, Washington MK, Scoggins CR, Meszoely IM, Goldenring JR, Marino CR, Sandgren EP, Coffey RJ, Jr., Wright CV and others. 1999. Expansion of Pdx1-expressing pancreatic epithelium and islet neogenesis in transgenic mice overexpressing transforming growth factor alpha. *Gastroenterology* 117(6):1416-26.
- Soon-Shiong P. 1999. Treatment of type I diabetes using encapsulated islets. *Adv Drug Deliv Rev* 35(2-3):259-270.
- Soon-Shiong P, Feldman E, Nelson R, Heintz R, Yao Q, Yao Z, Zheng T, Merideth N, Skjak-Braek G, Espevik T and others. 1993. Long-term reversal of diabetes by the injection of immunoprotected islets. *Proc Natl Acad Sci U S A* 90(12):5843-7.
- Soonshiong P, Feldman E, Nelson R, Komtebedde J, Smidsrod O, Skjakbraek G, Espevik T, Heintz R, Lee M. 1992. Successful Reversal of Spontaneous Diabetes in Dogs by Intraperitoneal Microencapsulated Islets. *Transplantation* 54(5):769-774.
- Srikanta S, Ricker AT, McCulloch DK, Soeldner JS, Eisenbarth GS, Palmer JP. 1986. Autoimmunity to insulin, beta cell dysfunction, and development of insulin-dependent diabetes mellitus. *Diabetes* 35(2):139-42.
- Stabler C, Wilks K, Sambanis A, Constantinidis I. 2001. The effects of alginate composition on encapsulated betaTC3 cells. *Biomaterials* 22(11):1301-10.
- Steiner H, Teppner R, Brenn G, Vankova N, Tcholakova S, Denkov N. 2006. Numerical simulation and experimental study of emulsification in a narrow-gap homogenizer. *Chemical Engineering Science* 61(17):5841-5855.

- Stevenson KS, McGlynn L, Hodge M, McLinden H, George WD, Davies RW, Shiels PG. 2009. Isolation, characterization, and differentiation of thy1.1-sorted pancreatic adult progenitor cell populations. *Stem Cells Dev* 18(10):1389-98.
- Stokke BT, Draget KI, Smidsrod O, Yuguchi Y, Urakawa H, Kajiwara K. 2000. Small-angle X-ray scattering and rheological characterization of alginate gels. 1. Ca-alginate gels. *Macromolecules* 33(5):1853-1863.
- Storrs R, Dorian R, King SR, Lakey J, Rilo H. 2001. Preclinical development of the Islet Sheet. *Bioartificial Organs* Iii: Tissue Sourcing, Immunoisolation, and Clinical Trials 944:252-266.
- Storz H, Muller KJ, Ehrhart F, Gomez I, Shirley SG, Gessner P, Zimmermann G, Weyand E, Sukhorukov VL, Forst T and others. 2009. Physicochemical features of ultra-high viscosity alginates. *Carbohydr Res* 344(8):985-95.
- Storz H, Zimmermann U, Zimmermann H, Kulicke WM. 2010. Viscoelastic properties of ultra-high viscosity alginates. *Rheologica Acta* 49(2):155-167.
- Strand BL, Gaserod O, Kulseng B, Espevik T, Skjak-Baek G. 2002. Alginate-polylysine-alginate microcapsules: effect of size reduction on capsule properties. *J Microencapsul* 19(5):615-30.
- Strand BL, Morch YA, Syvertsen KR, Espevik T, Skjak-Braek G. 2003. Microcapsules made by enzymatically tailored alginate. *Journal of Biomedical Materials Research Part A* 64A(3):540-550.
- Strand BL, Ryan L, Veld PI, Kulseng B, Rokstad AM, Skjak-Braek G, Espevik T. 2001. Poly-L-lysine induces fibrosis on alginate microcapsules via the induction of cytokines. *Cell Transplantation* 10(3):263-275.
- Street C. 2004. Enriched human pancreatic ductal cultures obtained from selective death of acinar cells expressing Pancreatic and Duodenal Homeobox gene-1 in an age-dependent manner. Not in press yet.
- Street CN, Lakey JRT, Shapiro AMJ, Imes S, Rajotte RV, Ryan EA, Lyon JG, Kin T, Avila J, Tsujimura T and others. 2004a. Islet graft assessment in the Edmonton Protocol - Implications for predicting long-term clinical outcome. *Diabetes* 53(12):3107-3114.
- Street CN, Sipione S, Helms L, Binette T, Rajotte RV, Bleackley RC, Korbitt GS. 2004b. Stem cell-based approaches to solving the problem of tissue supply for islet transplantation in type 1 diabetes. *Int J Biochem Cell Biol* 36(4):667-83.
- Strobel O, Dor Y, Alsina J, Stirman A, Lauwers G, Trainor A, Castillo CF, Warshaw AL, Thayer SP. 2007. In vivo lineage tracing defines the role of acinar-to-ductal transdifferentiation in inflammatory ductal metaplasia. *Gastroenterology* 133(6):1999-2009.
- Sugiura S, Oda T, Izumida Y, Aoyagi Y, Satake M, Ochiai A, Ohkohchi N, Nakajima M. 2005. Size control of calcium alginate beads containing living cells using micro-nozzle array. *Biomaterials* 26(16):3327-3331.
- Sun Y, Ma X, Zhou D, Vacek I, Sun AM. 1996. Normalization of diabetes in spontaneously diabetic cynomolgus monkeys by xenografts of microencapsulated porcine islets without immunosuppression. *J Clin Invest* 98(6):1417-22.

- Suzuki A, Nakauchi H, Taniguchi H. 2004. Prospective isolation of multipotent pancreatic progenitors using flow-cytometric cell sorting. *Diabetes* 53(8):2143-52.
- Szabat M, Johnson JD, Piret JM. 2010. Reciprocal modulation of adult beta cell maturity by activin A and follistatin. *Diabetologia*.
- Takahashi K, Yamanaka S. 2006. Induction of pluripotent stem cells from mouse embryonic and adult fibroblast cultures by defined factors. *Cell* 126(4):663-76.
- Tam SK, Dusseault J, Polizu S, Menard M, Halle JP, Yahia L. 2005. Physicochemical model of alginate-poly-L-lysine microcapsules defined at the micrometric/nanometric scale using ATR-FTIR, XPS, and ToF-SIMS. *Biomaterials* 26(34):6950-6961.
- Tatarkiewicz K, Garcia M, Lopez-Avalos M, Bonner-Weir S, Weir GC. 2001. Porcine neonatal pancreatic cell clusters in tissue culture: benefits of serum and immobilization in alginate hydrogel. *Transplantation* 71(11):1518-26.
- Tateishi K, He J, Taranova O, Liang G, D'Alessio AC, Zhang Y. 2008. Generation of insulin-secreting islet-like clusters from human skin fibroblasts. *J Biol Chem* 283(46):31601-7.
- Tcholakova S, Denkov ND, Lips A. 2008. Comparison of solid particles, globular proteins and surfactants as emulsifiers. *Physical Chemistry Chemical Physics* 10(12):1608-1627.
- Teta M, Long SY, Wartschow LM, Rankin MM, Kushner JA. 2005. Very slow turnover of beta-cells in aged adult mice. *Diabetes* 54(9):2557-67.
- Teta M, Rankin MM, Long SY, Stein GM, Kushner JA. 2007. Growth and regeneration of adult beta cells does not involve specialized progenitors. *Dev Cell* 12(5):817-26.
- Tezel E, Nagasaka T, Tezel G, Nakao A. 2002. Characterization of scattered neuroendocrine cells in ductal carcinoma of the pancreas. *Pancreas* 25(2):136-41.
- Thanos CG, Bintz BE, Bell WJ, Qian H, Schneider PA, MacArthur DH, Emerich DF. 2006. Intraperitoneal stability of alginate-polyornithine microcapsules in rats: an FTIR and SEM analysis. *Biomaterials* 27(19):3570-9.
- Thanos CG, Calafiore R, Basta G, Bintz BE, Bell WJ, Hudak J, Vasconcellos A, Schneider P, Skinner SJ, Geaney M and others. 2007. Formulating the alginate-polyornithine biocapsule for prolonged stability: evaluation of composition and manufacturing technique. *J Biomed Mater Res A* 83(1):216-24.
- Thu B, Bruheim P, Espevik T, Smidsrod O, SoonShiong P, SkjakBraek G. 1996a. Alginate polycation microcapsules .1. Interaction between alginate and polycation. *Biomaterials* 17(10):1031-1040.
- Thu B, Bruheim P, Espevik T, Smidsrod O, SoonShiong P, SkjakBraek G. 1996b. Alginate polycation microcapsules .2. Some functional properties. *Biomaterials* 17(11):1069-1079.
- Thu B, Gaserod O, Paus D, Mikkelsen A, Skjak-Braek G, Toffanin R, Vittur F, Rizzo R. 2000. Inhomogeneous alginate gel spheres: An assessment of the polymer gradients by synchrotron radiation-induced x-ray emission, magnetic resonance microimaging, and mathematical modeling. *Biopolymers* 53(1):60-71.
- Thu B, SkjakBraek G, Micali F, Vittur F, Rizzo R. 1997. The spatial distribution of calcium in alginate gel beads analysed by synchrotron-radiation induced X-ray emission (SRIXE). *Carbohydrate Research* 297(2):101-105.

- Todorov I, Nair I, Ferreri K, Rawson J, Kuroda A, Pascual M, Omori K, Valiente L, Orr C, Al-Abdullah I and others. 2005. Multipotent progenitor cells isolated from adult human pancreatic tissue. *Transplant Proc* 37(8):3420-1.
- Todorov I, Omori K, Pascual M, Rawson J, Nair I, Valiente L, Vuong T, Matsuda T, Orr C, Ferreri K and others. 2006. Generation of human islets through expansion and differentiation of non-islet pancreatic cells discarded (pancreatic discard) after islet isolation. *Pancreas* 32(2):130-8.
- Trautmann B, Schlitt HJ, Hahn EG, Lohr M. 1993. Isolation, culture, and characterization of human pancreatic duct cells. *Pancreas* 8(2):248-54.
- Treutelaar MK, Skidmore JM, Dias-Leme CL, Hara M, Zhang L, Simeone D, Martin DM, Burant CF. 2003. Nestin-lineage cells contribute to the microvasculature but not endocrine cells of the islet. *Diabetes* 52(10):2503-12.
- Trivedi N, Hollister-Lock J, Lopez-Avalos MD, O'Neil JJ, Keegan M, Bonner-Weir S, Weir GC. 2001. Increase in beta-cell mass in transplanted porcine neonatal pancreatic cell clusters is due to proliferation of beta-cells and differentiation of duct cells. *Endocrinology* 142(5):2115-22.
- Tsang WG, Zheng T, Wang Y, Tang J, Rind HB, Francki A, Bufius N. 2007. Generation of functional islet-like clusters after monolayer culture and intracapsular aggregation of adult human pancreatic islet tissue. *Transplantation* 83(6):685-93.
- Tsirogianni A, Pipi E, Soufleros K. 2009. Specificity of islet cell autoantibodies and coexistence with other organ specific autoantibodies in type 1 diabetes mellitus. *Autoimmun Rev* 8(8):687-91.
- Tuch BE, Keogh GW, Williams LJ, Wu W, Foster JL, Vaithilingam V, Philips R. 2009. Safety and viability of microencapsulated human islets transplanted into diabetic humans. *Diabetes Care* 32(10):1887-9.
- Tziampazis E, Sambanis A. 1995. Tissue Engineering of a Bioartificial Pancreas - Modeling the Cell Environment and Device Function. *Biotechnology Progress* 11(2):115-126.
- Uludag H, De Vos P, Tresco PA. 2000. Technology of mammalian cell encapsulation. *Adv Drug Deliv Rev* 42(1-2):29-64.
- Valdes-Gonzalez RA, Dorantes LM, Garibay GN, Bracho-Blanchet E, Mendez AJ, Davila-Perez R, Elliott RB, Teran L, White DJ. 2005. Xenotransplantation of porcine neonatal islets of Langerhans and Sertoli cells: a 4-year study. *Eur J Endocrinol* 153(3):419-27.
- van Schilfgaarde R, de Vos P. 1999. Factors influencing the properties and performance of microcapsules for immunoprotection of pancreatic islets. *J Mol Med* 77(1):199-205.
- Vandenberg GW, De La Noue J. 2001. Evaluation of protein release from chitosan-alginate microcapsules produced using external or internal gelation. *J Microencapsul* 18(4):433-41.
- Vankova N, Tcholakova S, Denkov ND, Ivanov IB, Vulchev VD, Danner T. 2007. Emulsification in turbulent flow - 1. Mean and maximum drop diameters in inertial and viscous regimes. *Journal of Colloid and Interface Science* 312(2):363-380.

- vanSusante JLC, Buma P, vanOsch GJVM, Versleyen D, vanderKraan PM, vanderBerg WB, Homminga GN. 1995. Culture of chondrocytes in alginate and collagen carrier gels. *Acta Orthopaedica Scandinavica* 66(6):549-556.
- Vantyghem MC, Marcelli-Tourvieille S, Fermon C, Duhamel A, Raverdy V, Arnalsteen L, Kerr-Conte J, Noel C, Fontaine P, Pattou F. 2009. Intraperitoneal insulin infusion versus islet transplantation: comparative study in patients with type 1 diabetes. *Transplantation* 87(1):66-71.
- Vendrame F, Pileggi A, Laughlin E, Allende G, Martin-Pagola A, Molano RD, Diamantopoulos S, Standifer N, Geubtner K, Falk BA and others. 2010. Recurrence of type 1 diabetes after simultaneous pancreas-kidney transplantation, despite immunosuppression, is associated with autoantibodies and pathogenic autoreactive CD4 T-cells. *Diabetes* 59(4):947-57.
- Venkat RV, Stock LR, Chalmers JJ. 1996. Study of hydrodynamics in microcarrier culture spinner vessels: A particle tracking velocimetry approach. *Biotechnology and Bioengineering* 49(4):456-466.
- Vila MR, Nakamura T, Real FX. 1995. Hepatocyte growth factor is a potent mitogen for normal human pancreas cells in vitro. *Lab Invest* 73(3):409-18.
- Vizzardelli C, Molano RD, Pileggi A, Berney T, Cattani P, Fenjves ES, Peel A, Fraker C, Ricordi C, Inverardi L. 2002. Neonatal porcine pancreatic cell clusters as a potential source for transplantation in humans: characterization of proliferation, apoptosis, xenoantigen expression and gene delivery with recombinant AAV. *Xenotransplantation* 9(1):14-24.
- Vogelsang C, Wijffels RH, Ostgaard K. 2000. Rheological properties and mechanical stability of new gel-entrapment systems applied in bioreactors. *Biotechnol Bioeng* 70(3):247-53.
- Wang N, Adams G, Buttery L, Falcone FH, Stolnik S. 2009. Alginate encapsulation technology supports embryonic stem cells differentiation into insulin-producing cells. *J Biotechnol* 144(4):304-12.
- Wang X, Ye K. 2009. Three-dimensional differentiation of embryonic stem cells into islet-like insulin-producing clusters. *Tissue Eng Part A* 15(8):1941-52.
- Weber LM, Hayda KN, Haskins K, Anseth KS. 2007. The effects of cell-matrix interactions on encapsulated beta-cell function within hydrogels functionalized with matrix-derived adhesive peptides. *Biomaterials* 28(19):3004-11.
- Wei J, Russ MB. 1977. Convection and Diffusion in Tissues and Tissue-Cultures. *Journal of Theoretical Biology* 66(4):775-787.
- Weir GC, Quickel RR, Yoon KH, Tatarkiewicz K, Ulrich TR, Hollister-Lock J, Bonner-Weir S. 1997. Porcine neonatal pancreatic cell clusters (NPCCs): a potential source of tissue for islet transplantation. *Ann Transplant* 2(3):63-8.
- Wells JM. 2003. Genes expressed in the developing endocrine pancreas and their importance for stem cell and diabetes research. *Diabetes Metab Res Rev* 19(3):191-201.
- Wernersson ES, Tragardh C. 1999. Scale-up of Rushton turbine-agitated tanks. *Chemical Engineering Science* 54(19):4245-4256.
- Wilson JT, Chaikof EL. 2008. Challenges and emerging technologies in the immunoisolation of cells and tissues. *Adv Drug Deliv Rev* 60(2):124-45.

- Wilson JT, Cui W, Chaikof EL. 2008. Layer-by-layer assembly of a conformal nanothin PEG coating for intraportal islet transplantation. *Nano Lett* 8(7):1940-8.
- Wislet-Gendebien S, Hans G, Leprince P, Rigo JM, Moonen G, Rogister B. 2005. Plasticity of cultured mesenchymal stem cells: switch from nestin-positive to excitable neuron-like phenotype. *Stem Cells* 23(3):392-402.
- Wolfe-Coote SA, Louw J, Woodroof CW, Heydenrych JJ, du Toit DF. 1998. Induction of cell proliferation and differentiation in the pancreas of the adult Vervet monkey (*Cercopithecus aethiops*): preliminary results. *Pancreas* 16(2):129-33.
- Wolters GHJ, Fritschy WM, Gerrits D, Vanschilfagaarde R. 1992. A Versatile Alginate Droplet Generator Applicable for Microencapsulation of Pancreatic-Islets. *Journal of Applied Biomaterials* 3(4):281-286.
- Woods EJ, Liu J, Zieger MA, Lakey JR, Critser JK. 1999. The effects of microencapsulation on pancreatic islet osmotically induced volumetric response. *Cell Transplant* 8(6):699-708.
- Wu P, Ray NG, Shuler ML. 1993. A Computer-Model for Intracellular Ph Regulation in Chinese-Hamster Ovary Cells. *Biotechnology Progress* 9(4):374-384.
- Xiu-Dong L, Wei-Ting Y, Jun-Zhang L, Xiao-Jun M, Quan Y. 2007. Diffusion of acetic acid across oil/water interface in emulsification-internal gelation process for preparation of alginate gel beads. *Chemical Research in Chinese Universities* 23(5):579-584.
- Xu C, Breedveld V, Kopecek J. 2005. Reversible hydrogels from self-assembling genetically engineered protein block copolymers. *Biomacromolecules* 6(3):1739-49.
- Xu XB, D'Hoker J, Stange G, Bonne S, De Leu N, Xiao XW, De Castele MV, Mellitzer G, Ling ZD, Pipeleers D and others. 2008. beta cells can be generated from endogenous progenitors in injured adult mouse pancreas. *Cell* 132(2):197-207.
- Yang J, Goto M, Ise H, Cho CS, Akaike T. 2002. Galactosylated alginate as a scaffold for hepatocytes entrapment. *Biomaterials* 23(2):471-9.
- Yang YG, Sykes M. 2007. Xenotransplantation: current status and a perspective on the future. *Nat Rev Immunol* 7(7):519-31.
- Yatoh S, Dodge R, Akashi T, Omer A, Sharma A, Weir GC, Bonner-Weir S. 2007. Differentiation of affinity-purified human pancreatic duct cells to beta-cells. *Diabetes* 56(7):1802-9.
- Yoon KH, Quickel RR, Tatarikiewicz K, Ulrich TR, Hollister-Lock J, Trivedi N, Bonner-Weir S, Weir GC. 1999. Differentiation and expansion of beta cell mass in porcine neonatal pancreatic cell clusters transplanted into nude mice. *Cell Transplant* 8(6):673-89.
- Yoon SK, Choi SL, Song JY, Lee GM. 2005. Effect of culture pH on erythropoietin production by chinese hamster ovary cells grown in suspension at 32.5 and 37.0 degrees C. *Biotechnology and Bioengineering* 89(3):345-356.
- Zekorn T, Endl C, Horcher A, Siebers U, Bretzel RG, Federlin K. 1995. Mixed lymphocyte islet culture for assessment of immunoprotection by islet microencapsulation. *Transplantation Proceedings* 27(6):3362-3363.
- Zhang C, Wang M, Racine JJ, Liu H, Lin CL, Nair I, Lau J, Yu-An C, Todorov I, Atkinson M and others. 2010. Induction of chimerism permits low-dose islet grafts in the liver or pancreas to reverse refractory autoimmune diabetes. *Diabetes*.

- Zhang XJ, Bury S, Dibiasio D, Miller JE. 1989. Effects of Immobilization on Growth, Substrate Consumption, Beta-Galactosidase Induction, and by-Product Formation in *Escherichia-Coli*. *Journal of Industrial Microbiology* 4(3):239-246.
- Zhao M, Amiel SA, Christie MR, Rela M, Heaton N, Huang GC. 2005. Insulin-producing cells derived from human pancreatic non-endocrine cell cultures reverse streptozotocin-induced hyperglycaemia in mice. *Diabetologia* 48(10):2051-61.
- Zhao M, Christie MR, Heaton N, George S, Amiel S, Cai Huang G. 2002. Amelioration of streptozotocin-induced diabetes in mice using human islet cells derived from long-term culture in vitro. *Transplantation* 73(9):1454-60.
- Zhao XY, Li W, Lv Z, Liu L, Tong M, Hai T, Hao J, Guo CL, Ma QW, Wang L and others. 2009. iPS cells produce viable mice through tetraploid complementation. *Nature* 461(7260):86-90.
- Zhi ZL, Liu B, Jones PM, Pickup JC. 2010. Polysaccharide multilayer nanoencapsulation of insulin-producing beta-cells grown as pseudoislets for potential cellular delivery of insulin. *Biomacromolecules* 11(3):610-6.
- Zhou D, Sun AM, Li X, Mamujee SN, Vacek I, Georgiou J, Wheeler MB. 1998. In vitro and in vivo evaluation of insulin-producing beta TC6-F7 cells in microcapsules. *Am J Physiol* 274(5 Pt 1):C1356-62.
- Zhou Q, Brown J, Kanarek A, Rajagopal J, Melton DA. 2008. In vivo reprogramming of adult pancreatic exocrine cells to beta-cells. *Nature* 455(7213):627-32.
- Zhu L, Shi G, Schmidt CM, Hruban RH, Konieczny SF. 2007. Acinar cells contribute to the molecular heterogeneity of pancreatic intraepithelial neoplasia. *Am J Pathol* 171(1):263-73.
- Zimmermann H, Zimmermann D, Reuss R, Feilen PJ, Manz B, Katsen A, Weber M, Ihmig FR, Ehrhart F, Gessner P and others. 2005. Towards a medically approved technology for alginate-based microcapsules allowing long-term immunoisolated transplantation. *J Mater Sci Mater Med* 16(6):491-501.
- Zulewski H, Abraham EJ, Gerlach MJ, Daniel PB, Moritz W, Muller B, Vallejo M, Thomas MK, Habener JF. 2001. Multipotential nestin-positive stem cells isolated from adult pancreatic islets differentiate ex vivo into pancreatic endocrine, exocrine, and hepatic phenotypes. *Diabetes* 50(3):521-33.

APPENDIX A - SUPPLEMENTARY METHODS

A1. SIMPLIFIED CALCULATION OF CaCO₃ AND ACETIC ACID REQUIREMENTS FOR COMPLETE INTERNAL GELATION OF 1.5% ALGINATE

The following is a sample calculation for 1.5% Sigma A0682 alginate, which has 67% guluronic acid content.

Guluronic acid (G) molecular weight = 175 g/mol

$$[G] = 1.5 \frac{\text{g}}{100\text{mL}} \times \frac{1000\text{mL}}{\text{L}} \times \frac{\text{mol}}{175\text{g}} \times \frac{67}{100} = 0.057\text{M}$$

The stoichiometry between Ca²⁺ and G is 1:2. Therefore, the amount of free Ca²⁺ required to fully cross-link the available G residues is:

$$[\text{Ca}^{2+}] = [G] / 2 = 0.029\text{M}$$

The equilibrium concentrations of H₂CO₃, HCO₃⁻, CO₃²⁻, CH₃COOH, CH₃COO⁻ and H⁺ can then be solved using the following system of 6 equations:

$$K_{SP, \text{CaCO}_3} = [\text{Ca}^{2+}] [\text{CO}_3^{2-}]$$

$$K_{a, \text{HCO}_3^-} = 10^{-10.3} = \frac{[\text{CO}_3^{2-}] [\text{H}^+]}{[\text{HCO}_3^-]}$$

$$K_{a, \text{CO}_3^{2-}} = 10^{-6.35} = \frac{[\text{HCO}_3^-] [\text{H}^+]}{[\text{CO}_3^{2-}]}$$

$$K_{a, \text{CH}_3\text{COOH}} = 10^{-4.74} = \frac{[\text{CH}_3\text{COO}^-] [\text{H}^+]}{[\text{CH}_3\text{COOH}]}$$

Since the amount of Ca²⁺ released is equal to the sum of all forms of carbonate in the system (neglecting CO₂ formation):

$$[\text{Ca}^{2+}] = [\text{H}_2\text{CO}_3] + [\text{HCO}_3^-] + [\text{CO}_3^{2-}]$$

The last of the 6 equations is based on overall charge neutrality:

$$2[\text{Ca}^{2+}] - [\text{HCO}_3^-] - 2[\text{CO}_3^{2-}] + [\text{H}^+] - [\text{CH}_3\text{COO}^-] = 0$$

The solution of these equations results in $[\text{CO}_3^{2-}] = 2.09 \times 10^{-7} \text{M}$, $[\text{HCO}_3^-] = 0.0066 \text{M}$, $[\text{H}_2\text{CO}_3] = 0.022 \text{M}$, $[\text{CH}_3\text{COOH}] = 0.00415 \text{M}$, $[\text{CH}_3\text{COO}^-] = 0.0508 \text{M}$ and $\text{pH} = 5.8$ (in the absence of HEPES buffer). Therefore, the minimum total amount of acetic acid (ionized and acid form) required in the aqueous phase for complete internal gelation of 1.5% alginate is 0.055M. Based on the distribution coefficient (K_d) of acetic acid between mineral oil and water of ~ 0.04 (mol/mol) at 20°C and $\text{pH} 5.8$ (Reinsel et al. 1994), the total amount of acetic acid needed for a 10.5 mL aqueous phase and a 30 mL organic phase was 0.000643 mol, or 36.8 μL . This was increased to 40 μL based to replicate the process described by Poncelet et al. (1992). For the same purpose of replicating the previously published methodology by Poncelet et al. (1992), 25 mM CaCO_3 were used rather than the 29 mM obtained in the calculations above.

It should be noted that three reactions were not included in these calculations to simplify the problem: (1) the equilibrium between alginic acid, sodium alginate and calcium alginate, (2) the equilibrium within the buffer system (e.g. HEPES) and (3) CO_2 generation. In addition, the emulsion and internal gelation is actually more complex, as described in Section 1.4.3, due to acetic acid partitioning, CaCO_3 dissolution and ion/alginate diffusion effects, leading to gel and calcium inhomogeneity within beads and likely between beads of different sizes.

Also, it should be noted that rather than changing the amounts of CaCO_3 and acetic acid for process optimization, the buffer system was adjusted, allowing control over the process pH without significantly affecting the rate of acetic acid partitioning into the aqueous phase. Thus, the CaCO_3 and acetic acid amounts were not increased as alginate concentration was increased in order to avoid changes in reaction rates and pH that may impact cell survival.

A2. ISLET-LIKE CELL CLUSTER GENERATION BY MATRIGEL OVERLAY

This method was reported by Bonner-Weir et al. (2000) and Gao et al. (2003) to yield insulin+ islet-like cell clusters starting from islet-depleted human pancreatic tissue. The method was

the same as reported by Gao et al. except for testing different initial cell concentrations and comparing the use of non-dispersed initial cell aggregates with dispersed cell aggregates. Briefly, on day 0, aggregates were washed and seeded at 0.11 μL PCV/ cm^2 or 7.12×10^4 cells/ cm^2 dispersed cells. This corresponded to the same total seeding density based on standard curves of cells/PCV (see Figure B8 in Appendix B). The cells were cultured in 0.26 mL/ cm^2 CMRL-10FBS (described in Section 5.2.1) for 6 days with medium changes on days 1 and 4. On day 6, the medium was changed to DMEM/F12⁺ containing a 50:50 mixture of DMEM and F12 media (Invitrogen) + 5 mg/L insulin + 5 mg/L transferrin + 5 $\mu\text{g/L}$ selenite, (I-1884 from Sigma) + 10 mM nicotinamide + 0.2% BSA (both from Stem Cell Technologies). The next day, the medium was removed and 50 $\mu\text{L}/\text{cm}^2$ of Matrigel diluted 1:2 with cold DMEM/F12⁺ medium was added to the cultures placed on ice. The dishes were incubated at 37°C and 5% CO₂ and 90% relative humidity overnight before adding 0.26 mL/ cm^2 DMEM/F12⁺ medium the next morning. The cells were further cultured for 4 weeks (until day 35) with half medium exchanges. To collect RNA samples, the entire culture was disrupted with a cell scraper and sampling was performed as described in Section 3.3.8. Care had to be taken to avoid disrupting Matrigel when handling the plates (typically individual 3.5 cm tissue culture treated Petri dishes) and medium changes (careful suction with a P1000 pipette from the side of the dish to remove ~1/2 the medium, then slow addition of pre-warmed medium).

A3. CELLOMICS IMAGING AND ANALYSIS

Imaging was performed on a Cellomics ArrayScan VTI system. The band-pass filters used (excitation(bandpass)/emission(bandpass) in nm) were 365(50)/535(45) for Channel 1, 475(40)/535(45) (Channel 2) and 575(25)/640(30) (Channel 3). For live cell imaging of YoPro/Ca19-9, 24 images were acquired for each well using the 20X objective. For fixed cell imaging, 16 images were acquired with the 10X objective, which covered the entire well surface. The default auto-focus algorithm was applied once per well based on Channel 1 intensities. The cells were identified as objects based on Hoechst or DAPI staining captured

by the images in Channel 1. Each object was used to define a nuclear region of the same size as the original object to quantify the BrdU staining intensity in Channel 2. A cytoplasmic region was defined by an annulus placed at a distance of 1 pixel from the nuclear region and extending 2 pixels outward, which was used to quantify amylase, CK19 or vimentin staining intensity in Channel 3 (see also Figure B13 in Appendix B). Object identification and enumeration of BrdU, amylase, CK19 and/or vimentin+ cells was done using the Cellomics Compartmental Analysis Version 3 algorithm using the parameters shown in Table SII. Cells “positive” or “negative” for a given stain were defined as cells with average pixel intensity in the corresponding channel higher than a given threshold. These thresholds were based on scatter plots (Figure S3) of Channel 2 average intensities and Channel 3 average intensities of ~1000 cells cultured in CMRL-10FBS for wells that included 2 stains (e.g. BrdU and CK19) compared to single stained (e.g. staining done without adding the BrdU primary antibody or without adding the CK19 primary antibody) controls. The maximum acceptable rate of false positives was set to 2%. The Cellomics image acquisition parameters are detailed in Table B5.

A4. QUANTIFICATION OF STAINED CELLS BY IMAGEJ

Positive and negative cells were quantified by using a custom-programmed ImageJ plug-in that first enumerates cell nuclei using DAPI, then quantifies the pixel intensity of the other stains in the nuclear region for each cell to set a threshold for “positive” and “negative” cells. Even though the stains are generally cytoplasmic, some intensity is detected in the nuclear region since the cells do not significantly spread on the slide during the 15 min of adhesion. The results obtained by this method were not significantly different from counting the cells manually. For each stain, an average of ~2000 total cells was assessed by this method.

APPENDIX B - SUPPLEMENTARY DATA

B2. SUPPLEMENTARY TABLES

Table B1. Protocols to expand adult human pancreatic tissue

Max. culture time (months)	Overall expansion*	Culture steps (numbers) and alternatives (letters)			Growth factors and additives	Characteristics after given culture steps	References
		Adherent	Suspension	3D			
2	N/A	(2) 2 - 3w UD, TCTD or collagen;	(1) 3d fibroblast removal	(3) Overlay with 2 nd collagen layer	–	(initial) Hand-picked islets Ins+ cells observed 3d after step (3)	(Lucas-Clerc et al. 1993)
1.25	N/A	Manual fibroblast removal at passages	–	–	NaPyruvate, dexamethaso-ne, FBS	(Initial) Main duct & first-degree branches Differentiation not attempted	(Trautmann et al. 1993)
0.25	N/A	TCTD or HTB-9 matrix	–	–	FBS, Gen, HGF (4X ↑ BrdU+)	(Initial) Non-islet fraction Differentiation not attempted	(Vila et al. 1995)
0.3	> 1	–	(1) 24 h fibroblast pre-plating (2) 48h culture of handpicked islets	(3) 1 w in collagen , matrigel , or agarose	FBS	(Initial) Islet-rich (At 24 h) 49% endocrine, 30% CK19+ (3) 5.6% endocrine cells in ILCs in Matrigel; no ILCs in agarose or type 1 collagen	(Kerr-Conte et al. 1996)
1	N/A	(2a) 1w TCTD (2b) 1w on 804GM	(1) 4 to 16 days (2c) 7 days UD	–	(1) BSA (2) pooled AB human serum, HGF (↑ CK19+ division)	(Initial) Islet-rich After step (1): 25% duct, 63% ins+ (2) Layers of ins + cells covered by CK19+ cells; 42% ins+	(Lefebvre et al. 1998)
2	30000	(1) On HTB-9 matrix (2) re-seed, 1w on HTB-9	(3) UD	–	(1) FBS + HGF (2) & (3) BSA, ITS	(Initial) Islet “inner” cells (76% ins+) (2) No ↑ ins mRNA, but PDX-1+ at 30% mRNA levels found in islets; cells do not survive in mice	(Beattie et al. 1999)

Table B1. Protocols to expand adult human pancreatic tissue

Max. culture time (months)	Overall expansion*	Culture steps (numbers) and alternatives (letters)			Growth factors and additives	Characteristics after given culture steps	References
		Adherent	Suspension	3D			
1.5	0.2 (cell loss)	(2a) 10d UD (2b) gelatin (3) ~1w serum-free	(1a) 2-4d pre-plating on UD (remove fibroblasts) (1b) Select NCAM- cells (MACS)	(4) Matrigel overlay 2~6w	(1) BSA (2a) FBS (2b) (3 & 4) ITS, NIC, KGF, with or without HGF	(Initial) islet-depleted (1a) 3.5% ins+ (1b) 0.3% endocrine, 50% CK19+ (2 & 3) CK19+ or nestin+ and some CK19+/PDX-1+ (4a) ILCs: 50% ins+, GRIP, 15 fold ↑ ins/DNA, ins mRNA 5% of fresh islets, ins ↑ after 3m in mice (4b) No ↑ ins after Matrigel	(Bonner-Weir et al. 2000; Gao et al. 2007; Gao et al. 2005; Gao et al. 2003)
0.75	(a) 1/3 (b) 1.7 (c) 4	(1a) TCTD or collagen (2b) Dissociated ILCs: TCTD or 804GM (1c) TCTD 7d	–	(1b) Collagen	(1a) FBS (1b) NuSerum + EGF (2b) FBS (1c) FBS + ITS	(a) main duct (b) Islet-rich (c) Acinar-rich (2) No ILCs (not attempted) except in (b): ILCs are 80% CK19+, CHA+, dithizone+; digested ILCs: Ki67/CK7 +/+	(Gmyr et al. 2001)
8	~10 ⁷	(2) TCTD (3) Re-seeding of hand-picked clusters	(1) 4d on ConA to remove non-islet cells, handpick islets	–	(1) FBS, β-mercEtOH (2) Medium 1 + rLIF or EGF, bFGF (3) β-mercEtOH, GLP1 or exendin4	(Initial) handpicked islets (1) high purity islets (2) nestin+, ins- (3) When confluent, form ILCs: CK19+, PDX-1+, 5-30% ins+ (if GLP1 is added), respond to secretagogues, 5X ↑ ins/mL in presence of exendin4	(Abraham et al. 2002; Zulewski et al. 2001)
7	Max. 2X in 9d	(a) TCTD & various coatings		(b) In collagen or Matrigel	(a) & (b) FBS	(Initial) islet fraction, 70-90% dithizone+ (End) Small cells (<1% of cells): low granulation, ins+, glu+, PP+, PDX-1+, synapt+, nestin–, not GRIP	(Petropavlovskaia et al. 2002 & 2007; Bodnar et al. 2005)
4	3	Alternate 1w with 1w suspension	Alternate 1w with 1w monolayer		FBS	(Initial) islet fraction: 42% ins, 30%CK19, 19% glu, 5% amy (In monolayer) undetectable ins protein (End) Suspension clusters: 1/10 initial ins content, 1/3 initial # β-cells, GRIP, restore glycemia of diabetic mice	(Zhao et al. 2002)

Table B1. Protocols to expand adult human pancreatic tissue

Max. culture time (months)	Overall expansion*	Culture steps (numbers) and alternatives (letters)			Growth factors and additives	Characteristics after given culture steps	References
		Adherent	Suspension	3D			
>3	10 ¹²	(1) TCTD 3m (2) re-seeding in serum-free culture			(1) FBS (2) BSA, ITS	(Initial) islet fraction (1) 94% vim+, 75% nestin+, 98% smooth muscle actin+, C-peptide-, low PDX-1 (2) ILCs: PDX-1+, 27%ins+, GRIP, 1000X ↑ preproins mRNA but 1/5000 of fresh islets, human C-peptide in 3/6 mice 14d post transplant	(Gershengorn et al. 2004; Hardikar et al. 2003) not reproduced by (Kayali et al. 2007)
~1	~10 ⁴	(1) 1d TCTD (2) long-term TCTD (3) re-plating of ILCs in neurobasal differentiation medium			(1) FBS (2) EGF, BPE, N-acetyl-L-cysteine, ascorbic acid (3) N2 & B27 supplement, NIC, exendin-4, LY294002.	(Initial) Pancreas remnants (2) ILCs form spontaneously and express glu but not ins (3) ILCs express insulin at 1/400 the level of human islets	(Linning et al. 2004)
4	10 ⁷	(1) 12w TCTD (2) 4w low serum (3) Matrigel			(1) & (3) 10% FBS (2) 1% FBS	Nestin+ expanding cells re-express insulin after ~4m ILCs in Matrigel secrete more ins than on TCTD	(Maria-Engler et al. 2004)
6	0.5		(1) 2d 37°C then 28°C		(1) ZnSO ₄ , ITS, BSA, linoleic acid	6m islets: unaltered SI and normalize glycemia in diabetic mice	(Rush et al. 2004)
1						ILCs: GRIP, respond to secretagogues, de novo insulin based on ins reporter gene, human c-peptide in blood of transplanted mice	(Atouf et al. 2005)

Table B1. Protocols to expand adult human pancreatic tissue

Max. culture time (months)	Overall expansion*	Culture steps (numbers) and alternatives (letters)			Growth factors and additives	Characteristics after given culture steps	References
		Adherent	Suspension	3D			
0.75	N/A 45%+ for MCM2 replica- tion protein		(1) 7-15d (2) 1w		(1) B27, EGF, bFGF (2a) exendin gastrin, NIC (2b) brain-derived neurotrophic factor	(Initial) Islet-depleted: 0.3% ins+ (2) ILCs contain 10% C-peptide+ cells, GRIP, 5% of ins content of fresh islet, human c-peptide in transplanted mice ↑ over 4m, + for neural markers	(Todorov et al. 2005)
0.75	2	(1) 10-14d TCTD (2) re-seed, 5d on Matrigel	(3) 5d		(1) FBS, β-nerve growth factor, EGF (2) & (3) ITS, BSA, linoleic acid	(Initial) dissociated islets (1) E-cadh+/CK19+ & vim+/nestin+ cells, undetectable PDX-1 (2) ↑ ins, PDX-1, ngn3 mRNA versus (1) (3) ILCs: PDX-1+, up to 34% preproins mRNA of initial islets, not GRIP but respond to KCl	(Lechner et al. 2005)
2	1.5	(2) 4w (3) pIRES-NI + lipofectamine - mediated transfection with pdx1	(1) 5d elimination of □-cells (4) 12h no factors, 3h GLP-1 (5) 4-10d (1) UD		(1) FBS, treptozotocin (2) FBS, G418 (3) serum-free + GLP-1 (5) activin, NIC, betacellulin (1) Low serum	(Initial) Islet-depleted (1) 0% ins+, 79% amy+, 15% CK19+ (2) 20%CK19+, 50% vim+, 60% nestin+ (5) ILCs: 12-fold ↑ preproins mRNA, but no ins protein before transplant, restore glycemia in 40% of 42 diabetic mice transplanted, 15% ins+ in 6w grafts (Initial) Duct epithelium: no ins+ Dithizone+ ins+ cells (2) ↑ differentiation with ↑ aggregation	(Zhao et al. 2005) (Boretti and Gooch 2006)
8	10 ¹⁷	(3) UD	(1) 2d (2) 4d, re-plating floating mass twice	(4) 4w Matrigel	(1) FBS (2), (3) & (4) heparin, putrescine, progesterone, EGF, bFGF, HGF, ITS	(Initial) Duct tissue (3) express several mesenchymal stem cell surface markers (4) ILCs in Matrigel: dithizone+, ins mRNA; 7X increase in ins/DNA	(Lin et al. 2006)

Table B1. Protocols to expand adult human pancreatic tissue

Max. culture time (months)	Overall expansion*	Culture steps (numbers) and alternatives (letters)			Growth factors and additives	Characteristics after given culture steps	References
		Adherent	Suspension	3D			
1.25m	<2	(1) 4-7d collagen	(2) 1m on orbital shaker		(1) 10% FBS, NIC (2) 2% FBS CaCl ₂ , NIC, gastrin, KGF, IGF-1, exendin 4, ascorbic acid	(1) Islet-depleted: 75% amy+, 29% ck19+, 0.3% ins+ (2) Suspension ILCs : 13% ins+, GRIP, respond to theophylline, contain up to 20% ins of fresh islets; human c-peptide detected 4m after transplantation in mice	(Todorov et al. 2005)
0.5	3	(3) 7-10d on HTB9, re-seed on HTB-9, culture 4-6d	(1) islet hand-picking (2) 2-3d + 4d G418		(1) FBS (2) G418 (3) FGF10, KGF	(Initial) Islet-depleted (1) 0.2% ins+ (2) 0.05% ins+, ck19+, vim-, nestin- (3) <0.1% ins+, ck19+, vim+, nestin+ before transplant, 10%ins+ after 3m <i>in vivo</i> co-transplanted with fetal islets	(Hao et al. 2006)
4	65000	(1) 5w TCTD	(2) 1-7d		(1) FBS (2) ITS, betacellulin	(Initial) Islets: 15% ins+ after 3d culture (1) 0.5% ins+, 100% vim+, PDX-1- (2) 11% ins+, PDX-1+, GRIP, ins/total protein in physiological range	(Ouziel-Yahalom et al. 2006)
3	10 ¹³	(2) TCTD 2m (3) 3d (4) 3d (5) 3d	(1) 4d (6) 4d		(1) 10% FBS (2) 10% FBS, bFGF, EGF, NaPyruvate, β-mercEtOH (3) 1% FBS (4) 1% FBS + NIC (5) Medium 4 + exendin 4 (6) Medium 5 + TGFβ-1	(Initial) Islet-depleted, 82% CK19+, 7% amy+, 2% ins+ (2) CK19-, ins-, PDX-1-, express several mesenchymal stem cell markers (CD13, CD29, CD44, CD49b, CD54, CD90 and CD105), can undergo adipogenic, osteogenic, chondrogenic & hepatic differentiation (6) ins, PDX-1, neuroD, glucagon, ngn3, pax4 mRNA but not protein	(Seeberger et al. 2006)

Table B1. Protocols to expand adult human pancreatic tissue

Max. culture time (months)	Overall expansion*	Culture steps (numbers) and alternatives (letters)			Growth factors and additives	Characteristics after given culture steps	References
		Adherent	Suspension	3D			
1.25	<2	(1) 4-7d collagen	(2) 1m on orbital shaker		(1) 10% FBS, NIC (2) 2% FBS CaCl ₂ , NIC, gastrin, KGF, IGF-1, exendin-4, ascorbic acid	(Initial) non-islet, 75% amy+, 29% ck19+, 0.3% ins+ (1) 93% CK7+, 96% PDX-1+ (2) ILCs : 13% ins+, GRIP, up to 20% ins/DNA of fresh islets, human C-peptide detected 4m after transplantation in mice	(Todorov et al. 2006)
0.5	Cell losses			(1) 8d in collagen (2) 6 additional days	(1) 10% FBS, ins, dexamethazone, EGF, cholera toxin (2) Medium 1 + gastrin, INGAP, HGF, -cholera toxin	(Initial) Islet-depleted (1) Duct-like structures: amy-, CK19+ (2) 2-6% PDX-1+ cells in the duct-like structures, dithizone+/C-peptide+ buds appear in 6% of the duct-like structures	(Lipsett et al. 2007)
1.25	2.2	(1) seed 4000 IE per 10 cm dish (2) 23d with passage at d10 & d17		(3) 1-3w alginate poly-L-lysine capsules; liquefied alginate	(1) EGF, ITS among others (SM95 custom medium), 1% FBS (2) SM95 no serum	(Initial) >80% islet by dithizone staining (1) 10-50% plating efficiency (2) ~300X ↓ insulin/actin mRNA just before the first passage compared to fresh islets; remain GRIP up to 3 rd passage (3) ILCs: insulin+ core; CK19+ mantle. C-peptide detected in diabetic mice; 100% normoglycemia achieved in 5 weeks	(Tsang et al. 2007)

Table B1 legend:

amy – amylase (acinar marker); BPE – bovine pituitary extract; β -mercEtOH - β -mercaptoethanol; BrdU – bromodeoxyuridine; CA – carbonic anhydrase II (duct marker); CHA – Carbohydrate antigen 19-9 (duct marker); CK – cytokeratin (duct marker); ConA – concanavalin A; d – day; dith – dithizone (stains ins granules in viable β -cells); FBS – fetal bovine serum; Gen – Geneticin (inhibits fibroblast growth); glu – glucagon (α -cell marker); HGF – hepatocyte growth factor; IGF – insulin-like growth factor; ILC – islet-like cluster; ins – insulin; ITS – insulin, transferrin, selenium; m – months; MUC1 – mucin glycoprotein 1 (duct marker); NAD – nicotinamide adenine dinucleotide; NaPyruvate – sodium pyruvate; NIC – nicotinamide; PP – pancreatic polypeptide; rLIF – recombinant leukemia inhibitory factor; SI – stimulation index in response to a step change in glucose concentration; synapt. – synaptophysin (marker for neurosecretory granules); TGF – transforming growth factor; TCTD – tissue culture treated dishes; t_d – doubling time; UD – untreated dishes; vim – vimentin (fibroblast marker); w – week; 804GM – 804 G matrix from 804G rat cells.

* Total number of cells at the maximum culture time divided by the initial number of cells seeded.

Table B2. q-PCR primers

Gene	Forward primer	Reverse primer
Human aldolase	CGGGAAGAAGGAGAACCTG	CCGCTTAATAGGCGTGGTTA
Human amylase	TCAGACCTTGGTGGGAAAGA	GCACTCACAGCGTTACCAC
Human CK19	GGCCTCCTACCTGGACAAG	TGTCGATCTGCAGGACAATC
Human gapdh	CCCATCACCATCTTCCAGGAG	CTTCTCCATGGTGGTGAAGACG
Human insulin	GGAGCGTGGCTTCTTCTACA	CAGTGCCAAGGTCTGAAGGT
Human pdx-1	TGAAATCCACCAAAGCTCAC	GAATTCCTTCTCCAGCTCCA
Human vimentin	GGCTCAGATTCAGGAACAGC	AGCCTCAGAGAGGTCAGCAA

Table B3. Human pancreas donor information

Isolation numbers	Date of isolation (dd/mm/yy)	Cold Preservation Time (min)	Age	Body Weight (kg)
H1035	Received 22/09/05	N/A	N/A	N/A
H1041	30/10/05	390	55	N/A
BC75	Received 30/11/06	N/A	N/A	N/A
BC79	Received 18/01/07	257	42	70
BC90	15/06/07	180	17	80
BC107	05/03/08	225	56	55
BC109	20/06/08	165	18	70
BC110	30/06/08	185	54	53.5
BC116	01/11/08	140	22	75
BC117	28/11/08	627	50	92
123	07/02/09	272	23	77
127	04/05/09	720	64	77
129	10/08/09	164	17	80
130	23/09/09	185	58	73
148	27/08/10	N/A	44	N/A

Legend: cold preservation time is the time from when cross clamping of aorta at organ retrieval to time of start of islet isolation; culture time is the time the isolated islets were cultured in suspension prior to receiving samples; islet purity was assessed by dithizone staining by islet transplant lab (N/A: non-available)

Table B4. Yield of islet equivalents from the non-islet fraction by adherent culture followed by alginate-immobilized culture in emulsion-generated beads

Description	Value	Relative to	Section in thesis providing value
Insulin expression after alginate differentiation	3.50%	Islet-enriched fraction	3.3.8
Insulin expression of islet-enriched fraction	70%	Pure islets	3.2.12
Number of islet-depleted cells	50 fold	Number of islets/pancreas	1.1
Yield during adherent culture step	140%	Day 6 versus day 0 in 10% FBS for non-dispersed aggregates	Figure B15
Survival of emulsion process	71%	On day 7	3.3.8
Survival in alginate	40%	Day 17 versus day 7	Figure B4
Overall yield of "islet equivalents" from the non-islet fraction	50%	Islets available per pancreas	Multiplication of all above values

Table B5. Cellomics algorithms and parameters

Compartmental Analysis parameters, fixed cells		Compartmental Analysis parameters, live cells		Object identification parameters**		
Parameter	Value	Parameter	Value	Parameter	Minimum	Maximum
Obejctive magnification	10X	Obejctive magnification	20X	ObjectAreaCh1 (10X images)	10	200
UseReferenceWells	0	UseReferenceWells	0	ObjectAreaCh1 (20X images)		
MinRefAvgObjectCountPerField	2	MinRefAvgObjectCountPerField	2	ObjectShapeP2ACh1	0.5	1.3
UseMicrometers	0	UseMicrometers	0	ObjectShapeLWRCh1	0	2
PixelSize	2.048	PixelSize	4.096	ObjectAvgIntenCh1	50	4095
ChannelToDeriveRingOverlay	3	ChannelToDeriveRingOverlay	3	ObjectTotalIntenCh1	0	1E+10
ChannelToDeriveCircOverlay	2	ChannelToDeriveCircOverlay	2	RingAvgIntenCh2	0	32767
ChannelToDeriveRingSpotOverlay	3	ChannelToDeriveRingSpotOverlay	3	CircAvgIntenCh2	0	32767
ChannelToDeriveCircSpotOverlay	2	ChannelToDeriveCircSpotOverlay	2	CircRingAvgIntenDiffCh2	-32767	32767
Type_1_EventDefinition***	90302.062	Type_1_EventDefinition***	90302.062	CircRingAvgIntenRatioCh2	0	1E+12
ObjectTypeCh1	0	ObjectTypeCh1	0	RingSpotTotalAreaCh2	0	1E+12
BackgroundCorrectionCh1	70	BackgroundCorrectionCh1	70	RingSpotAvgIntenCh2	0	32767
ObjectSmoothFactorCh1	0	ObjectSmoothFactorCh1	0	CircSpotTotalAreaCh2	0	1E+12
ObjectSegmentationCh1 (images acquired day 2)	3.73	ObjectSegmentationCh1	5.5	CircSpotAvgIntenCh2	0	32767
ObjectSegmentationCh1 (images acquired day 7)	4.1	RejectBorderObjectsCh1	1	AvgIntenCh2	0	32767
RejectBorderObjectsCh1	1	BackgroundCorrectionCh2	70	TotalIntenCh2	0	1E+12
BackgroundCorrectionCh2	70	CircModifierCh2	0	RingAvgIntenCh3	0	32767
CircModifierCh2	0	CircAvgIntenCh2LevelHigh (YoPro)****	70 to 217	CircAvgIntenCh3	0	32767
CircAvgIntenCh2LevelHigh (BrdU)****	70 to 150	CircAvgIntenCh2LevelLow	0	CircRingAvgIntenDiffCh3	-32767	32767
CircAvgIntenCh2LevelHigh (amylase)****	78 to 145	CircAvgIntenCh2LevelHigh_CC	1	CircRingAvgIntenRatioCh3	0	1E+12
CircAvgIntenCh2LevelLow	0	CircAvgIntenCh2LevelLow_CC	1	RingSpotTotalAreaCh3	0	1E+12
CircAvgIntenCh2LevelHigh_CC	1	MaskModifierCh2	0	RingSpotAvgIntenCh3	0	32767
CircAvgIntenCh2LevelLow_CC	1	BackgroundCorrectionCh3	70	CircSpotTotalAreaCh3	0	1E+12
MaskModifierCh2	0	RingDistanceCh3	1	CircSpotAvgIntenCh3	0	32767
BackgroundCorrectionCh3	70	RingWidthCh3	2	AvgIntenCh3	0	32767
RingDistanceCh3	1	CircModifierCh3	0	TotalIntenCh3	0	1E+12
RingWidthCh3	2	RingAvgIntenCh3LevelHigh (Ca19-9)****	285 to 545			
CircModifierCh3	0	RingAvgIntenCh3LevelLow	0			
RingAvgIntenCh3LevelHigh (CK19)****	100 to 178	RingAvgIntenCh3LevelHigh_CC	1			
RingAvgIntenCh3LevelHigh (vimentin)****	80 to 100	RingAvgIntenCh3LevelLow_CC	1			
RingAvgIntenCh3LevelLow	0	MaskModifierCh3	0			
RingAvgIntenCh3LevelHigh_CC	1					
RingAvgIntenCh3LevelLow_CC	1					
MaskModifierCh3	0					

*Only parameters relevant to the analysis are shown here. All others have no impact on the results and the default values were used.

**The type 1 event was defined as: CircAvgInt Ch2 AND RingAvgInt Ch3.

***For Channel 1 (Ch1), the fixed threshold method (threshold 50) was used, while isodata thresholds values of 0 were used for channels 2 and 3, i.e. object selection was performed solely based on Channel 1.

****These values were different for each day of imaging and set manually based on scatter plots of Channel 3 (Ch3) average intensities plotted as a function of Channel 2 (Ch2) average intensities and allowing at most 2% false positives based on controls omitting the corresponding primary antibody.

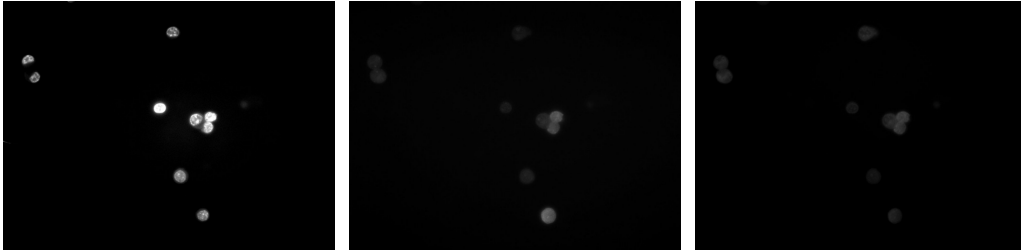
B3. SUPPLEMENTARY FIGURES

Day 1

DAPI

Insulin (green)

CK7 (red)



Day 18 (8 days of suspension culture + 10 days of culture in the AHFBR)

DAPI

Insulin (green)

CK7

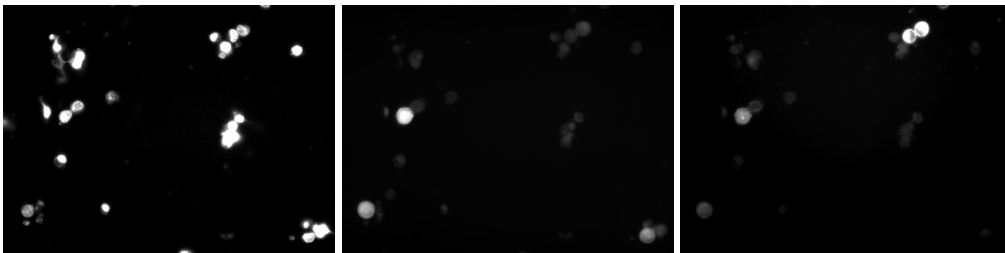


Figure B1. Insulin staining of NPCCs in the AHFBR.

Cells received (day 0) had 8% insulin⁺ cells. After 8 days of suspension culture, this fraction was $4.4 \pm 0.7\%$ (images not shown). After 10 days of alginate-immobilized culture (day 18), the fraction of insulin⁺ cells measured for slab cultures was $12 \pm 3\%$. The fraction of insulin⁺ cells recovered from the AHFBR (7%) was not significantly different based on 95% confidence intervals. However, the intensity of positive cells was higher at day 18 than at day 0. Also, many cells positive for both CK7 and insulin were observed at this time point. Slides with single staining were used to set thresholds for counting cells as positively stained.

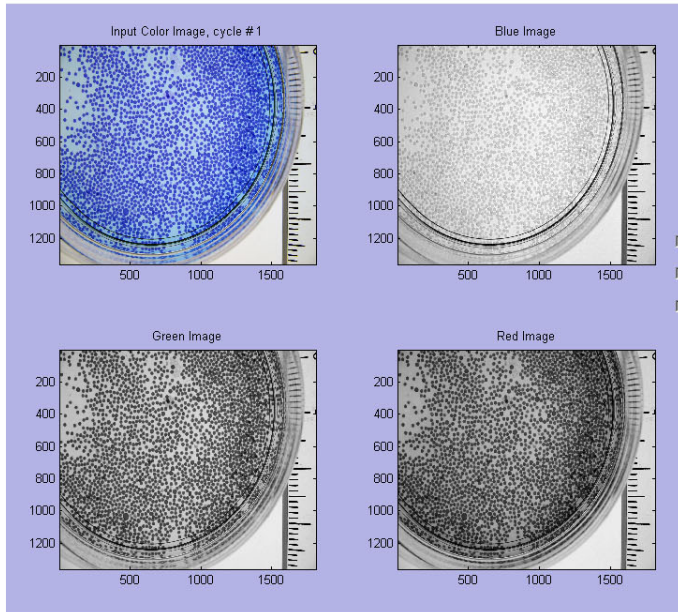
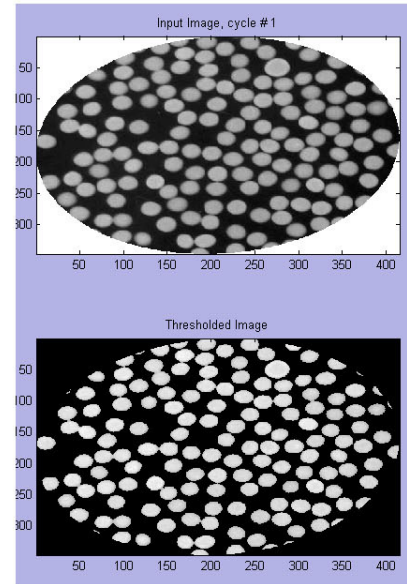
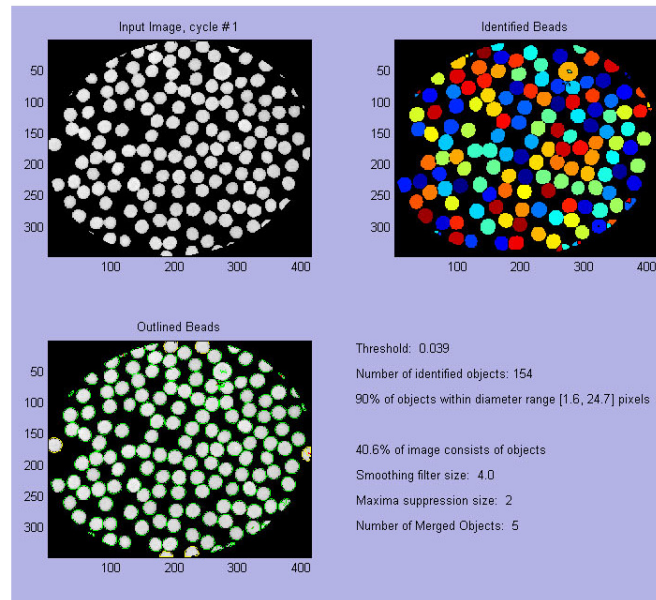
A**B****C**

Figure B2. Bead image analysis by Cell Profiler after toluidine blue staining.

(A) Original image of alginate beads produced by extrusion and external gelation (0.75% LVM + 0.75% MVG alginate) stained for toluidine blue-O and selection of the green filtered image for analysis. (B) Thresholding to separate beads from the background. (C) Bead object identification based on the IdentifyPrimAutomatic module with Otsu-Amada thresholding and object segmentation based on shape.

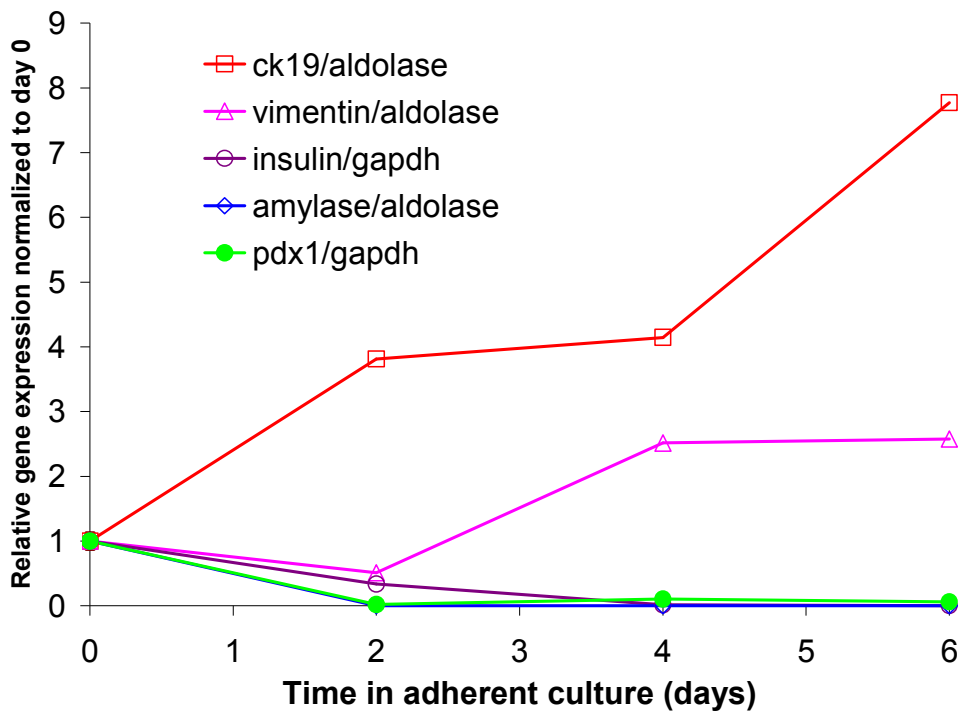


Figure B3. Time course q-PCR data for dispersed human non-islet tissue during adherent culture.

The cells are dissociated into single cells and cultured in CMRL + 10% FBS. Non-dispersed islet-depleted cell clusters followed similar patterns. The data represents N=1 pancreas with triplicate analytical replicates performed for the day 0 samples.

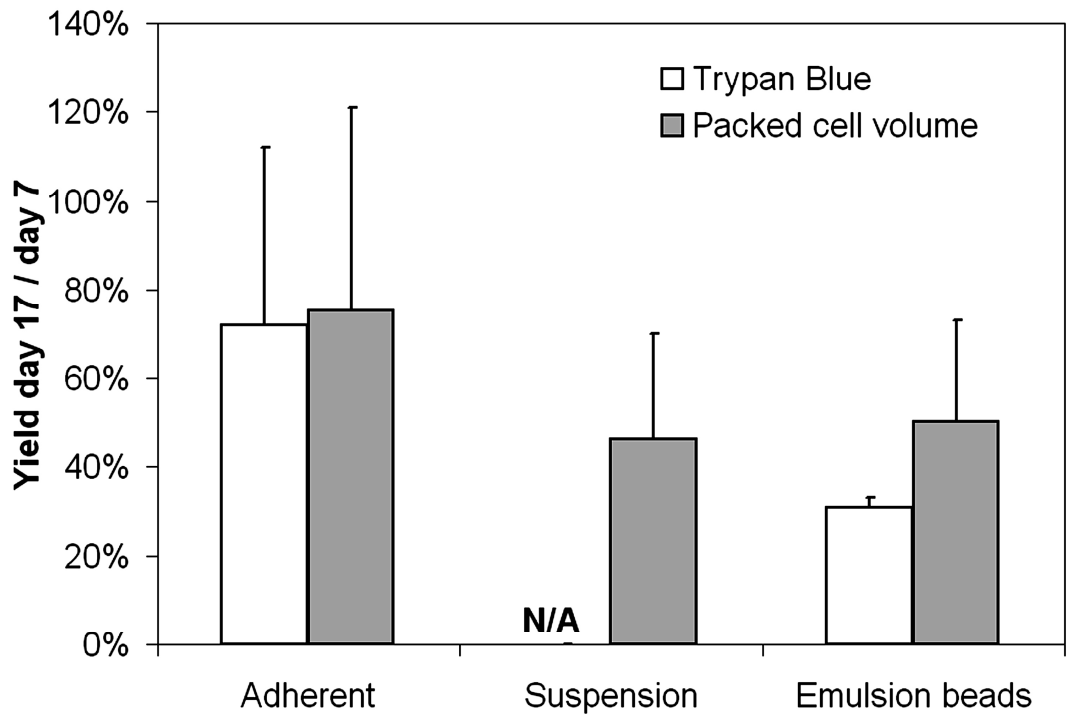


Figure B4. Human islet-depleted cell survival during serum-free culture between day 7 and day 17.

The survival is compared between adherent cultures, suspension cultures or alginate-immobilized cultures in 1.5% alginate beads produced by the MOPS emulsion process. The cell number was assessed either by trypan blue enumeration (live cells) or packed cell volume (total cells). Trypan blue live cell counts were not performed for suspension cultures where large cell aggregates were observed. N=2 for adherent and suspension cultures, while N = 4 for the emulsion-generated beads.

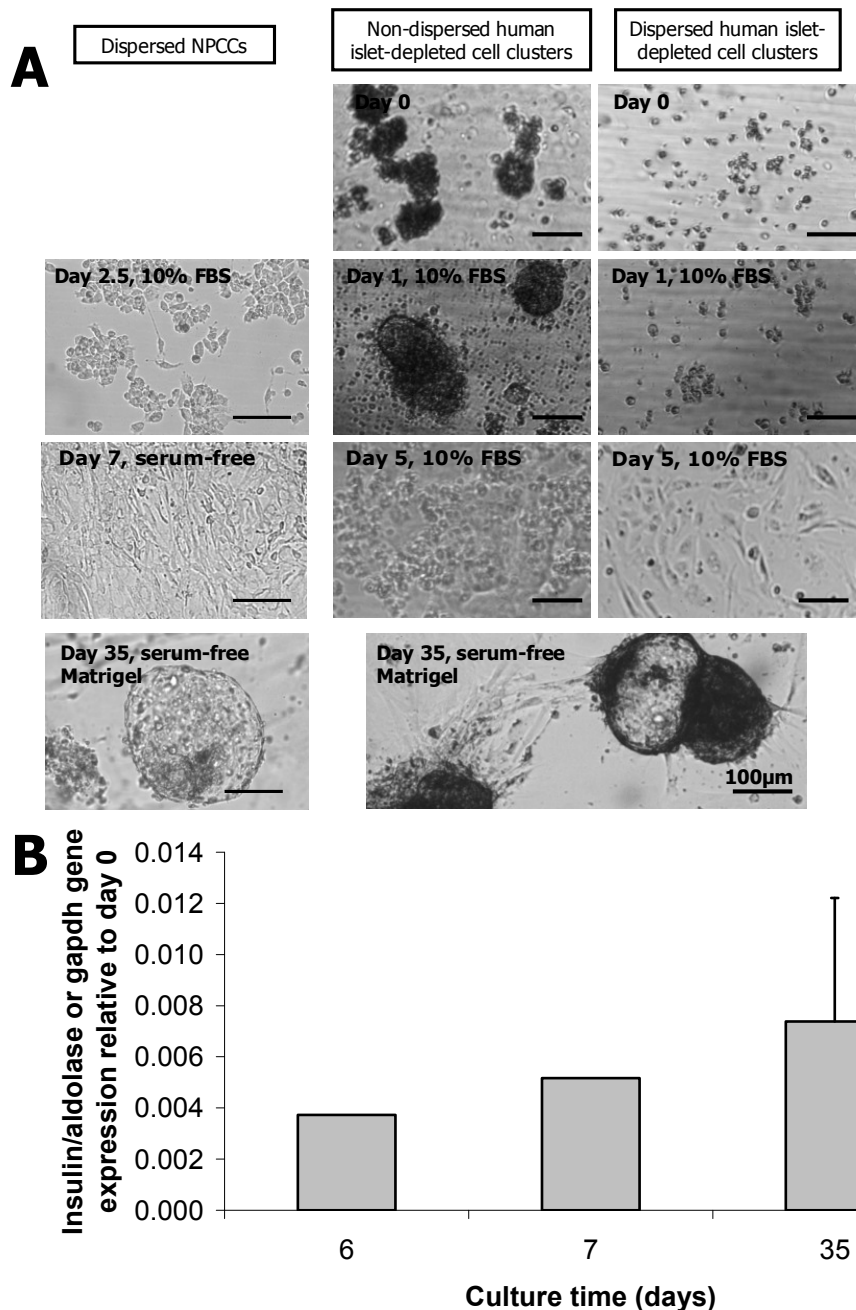


Figure B5. Cell morphology and insulin expression during Matrigel-induced islet-like cluster formation by NPCCs and human islet-depleted pancreatic cells.

(A) Cell morphology changes during the culture steps for islet-like cluster formation by the protocol described by Bonner-Weir et al. (2000). The protocol is detailed in Section B1 and consists in 6 days of culture of dispersed or non-dispersed pancreatic cell clusters in medium containing 10% FBS (days 0-6), 1 day culture in serum-free medium (until day 7), Matrigel overlay of the cultures on day 7 and overnight gelling, addition of serum-free medium on day 8 and serum-free Matrigel-overlaid culture until day 35 during which cell spheroids are generated. (B) Insulin/aldolase A or insulin/gapdh expression levels normalized to day 0. On day 35, the insulin/aldolase A or gapdh expression level was equivalent to $0.004 \pm 0.003\%$ of the expression measured for the islet-rich fraction. The error bar represents the average \pm SEM of $N = 2$ pancreata. Scale bars all represent $100 \mu\text{m}$.

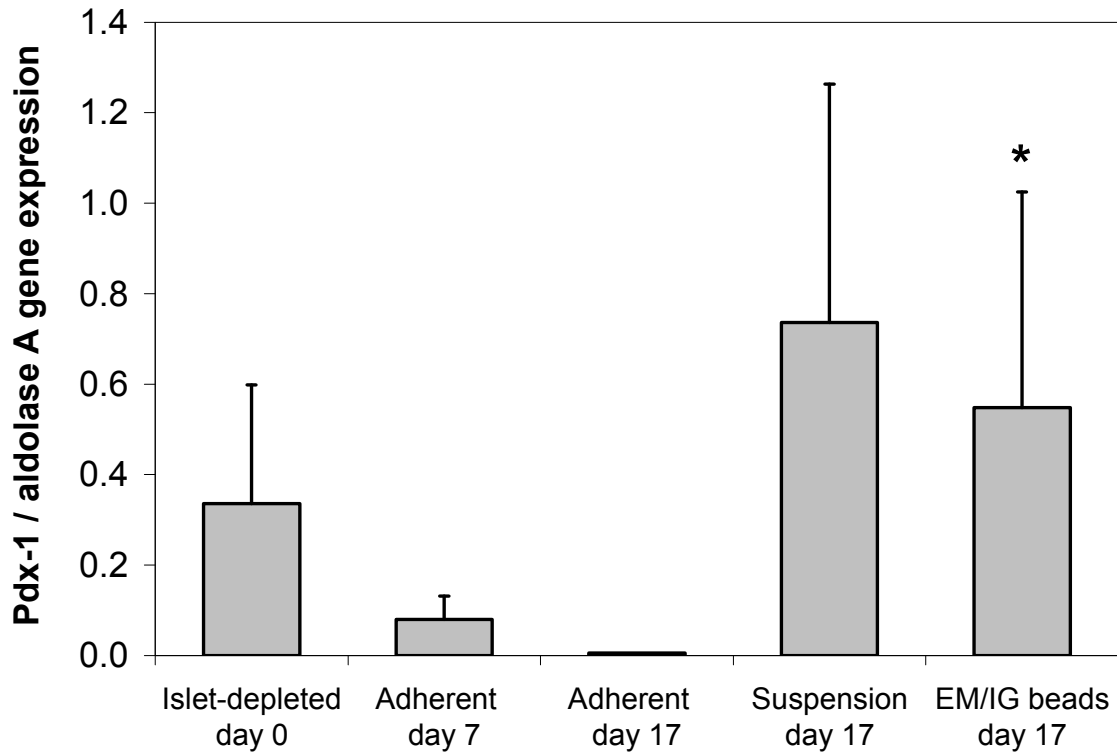


Figure B6. Pdx-1 gene expression of islet-depleted human pancreatic tissue before and after 10 days of immobilized culture in emulsion-generated alginate beads.

Pdx-1 gene expression was quantified by q-PCR and normalized to the aldolase A housekeeping gene. Islet-depleted pancreatic tissue aggregates were first cultured under adherent conditions for 7 days and then split into adherent, suspension and MOPS emulsion (EM/IG) immobilized serum-free cultures for 10 days. N = 2 pancreata (islet-depleted day 0 and suspension day 17), N = 3 pancreata (adherent day 7 and EM/IG beads day 17) or N = 1 (adherent day 17).

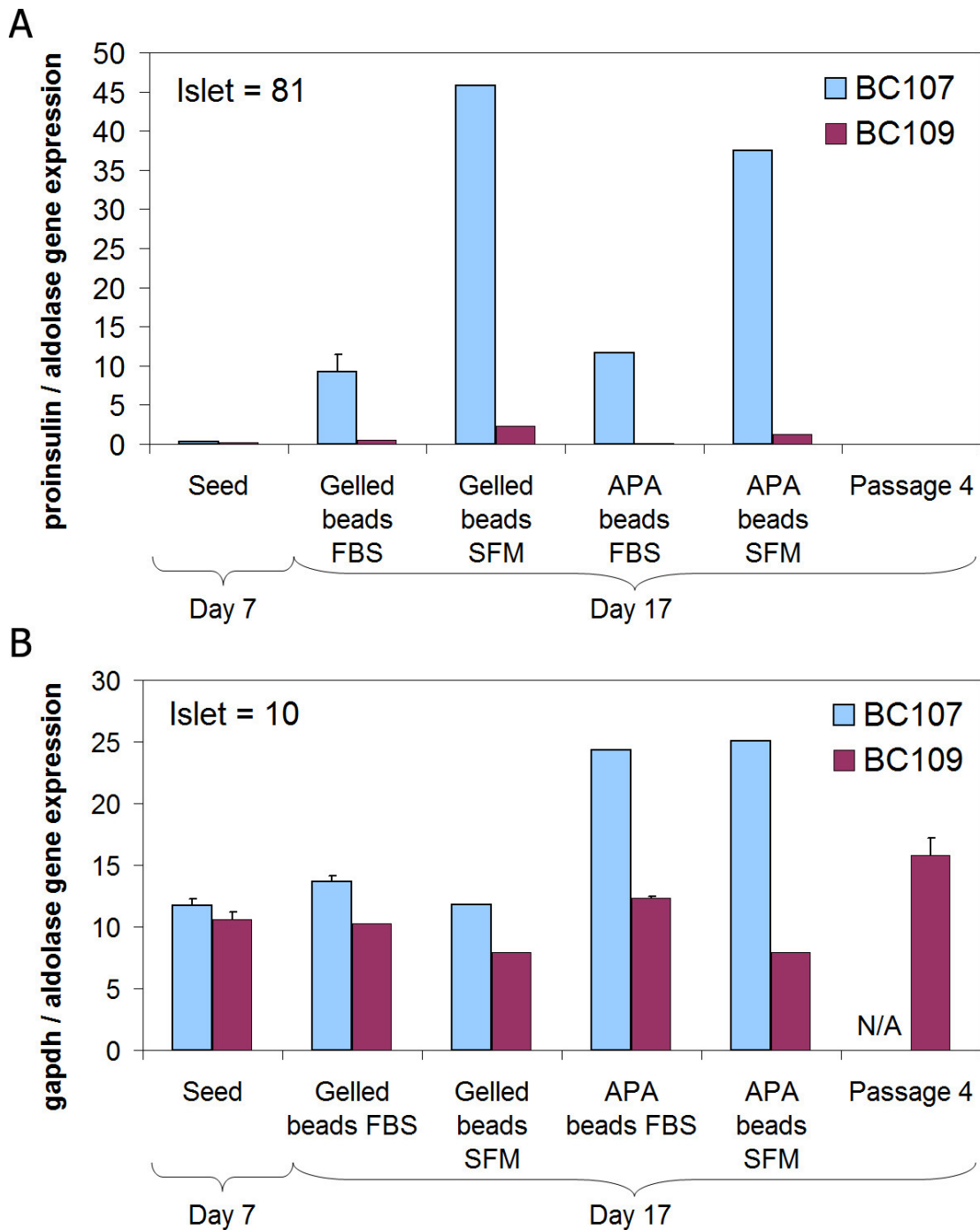


Figure B7. Insulin and gapdh gene expression of islet-depleted human pancreatic tissue before and after 10 days of immobilized culture in emulsion-generated alginate beads with or without poly-L-lysine and FBS.

Islet-depleted tissue was immobilized in emulsion/internal gelation alginate beads (gelled beads) and in certain cases coated for 5 min with 0.05% poly-L-lysine (PLL, Sigma P2658), washed with saline, coated for 8 min with 0.09%, washed again with saline, then incubated in degelling solution (final citrate concentration = 46 mM), followed by washing with medium to generate alginate-PLL-alginate (APA) beads. The serum-free medium (SFM) and serum-containing medium were those described in Section 3.2.12.

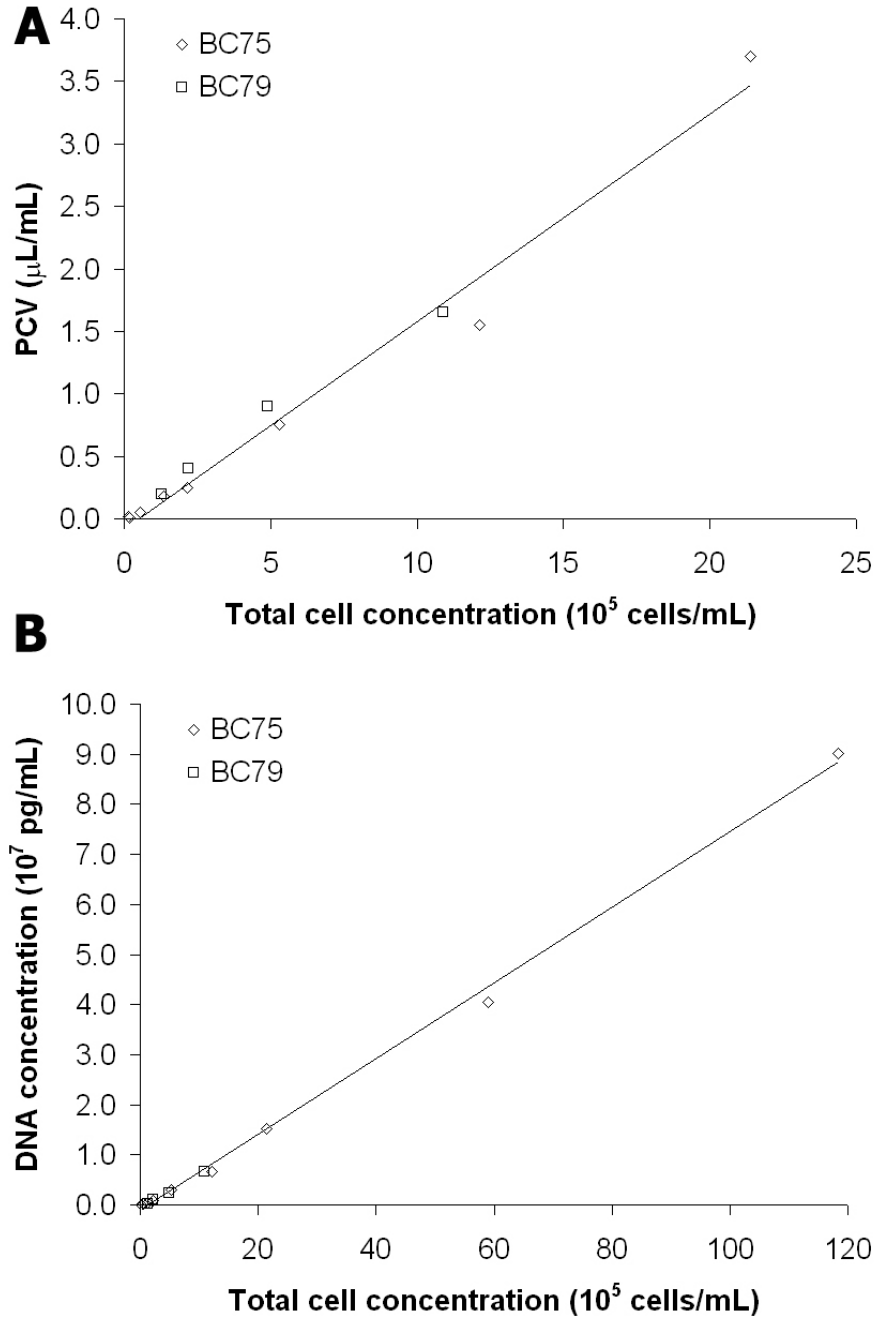


Figure B8. Correlation between total dispersed human islet-depleted pancreatic cell concentrations (live + dead cells), packed cell volume and DNA.

On day 0, pancreatic islet-depleted cell clusters were dispersed by the method described in Section 5.2.3 and the packed cell volume was measured as described in Section 3.2.5, as well as the DNA concentration as described in Section 2.1.14. The average slope of the curves for the 2 pancreata tested were (A) 6.28×10^5 cells/ μL PCV and (B) 7.6 pg DNA/cell. There was no significant difference in the DNA/PCV ratio between dispersed and non-dispersed cell clusters.

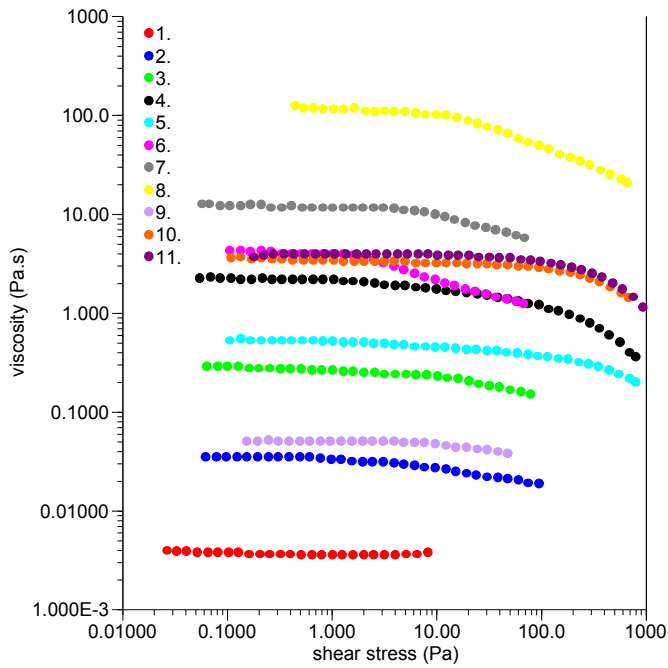


Figure B9. Dynamic viscosity of alginate samples as a function of shear stress.

The samples shown are: (1) 0.5% Sigma alginate, (2) 1.5% Sigma alginate, (3) 3% Sigma alginate, (4 to 6) 3 different batches of 5% Sigma alginate, (7) 7% Sigma alginate, (8) 10% Sigma alginate, (9) 1.5% LVM:MVG alginate (used for transplant), (10) 5% LVM:MVG alginate (used for transplant), (11) 5% alginate from different manufacturer lots.

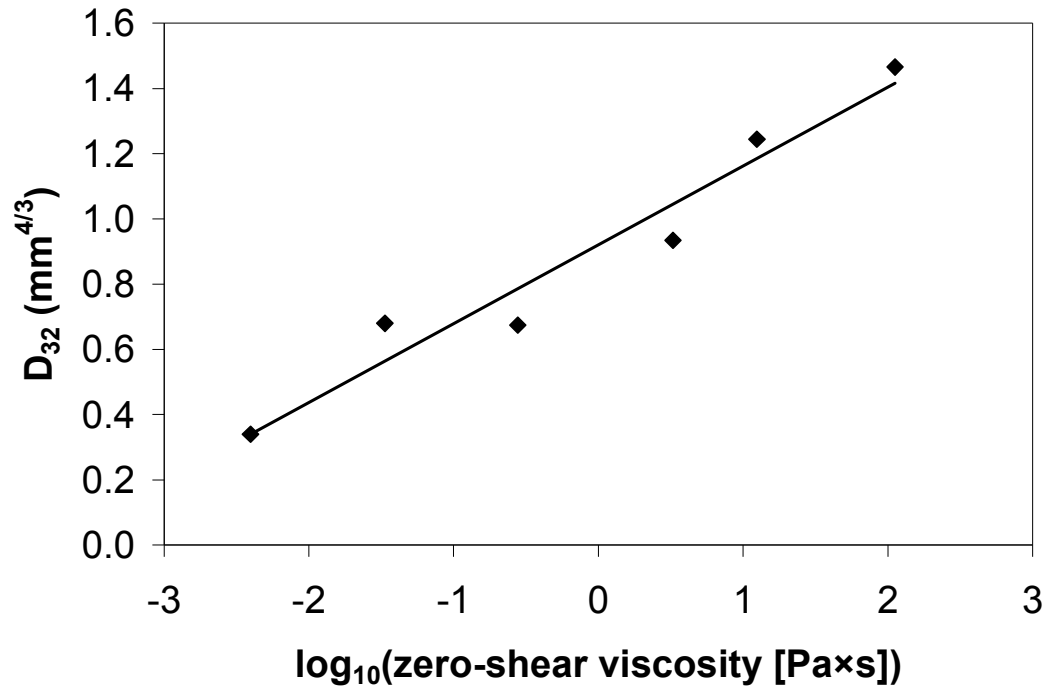


Figure B10. Relationship between the log of the zero-shear viscosity and the surface area moment average emulsion bead diameter.

The data plotted are for Sigma A0682 alginate concentrations of 0.5%, 1.5%, 3%, 5%, 7% and 10%. The coefficient of determination R^2 was 0.95.

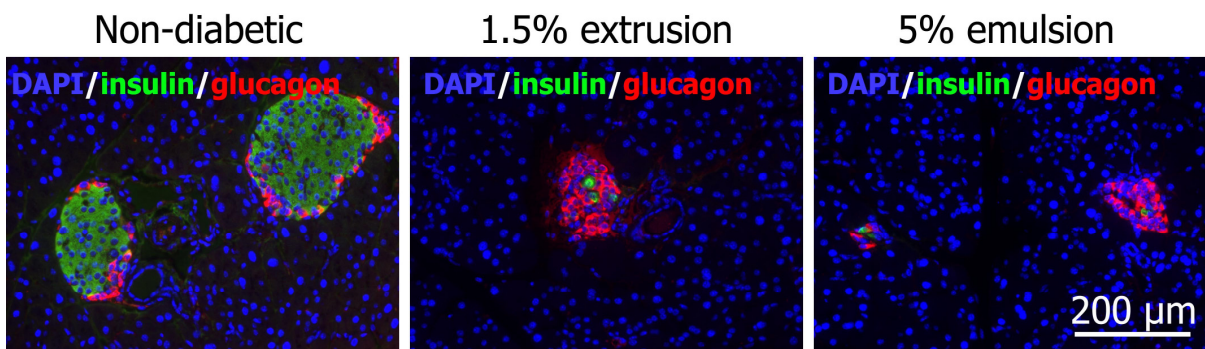


Figure B11. Insulin and glucagon stained pancreas sections obtained after sacrificing the mice on day 19.

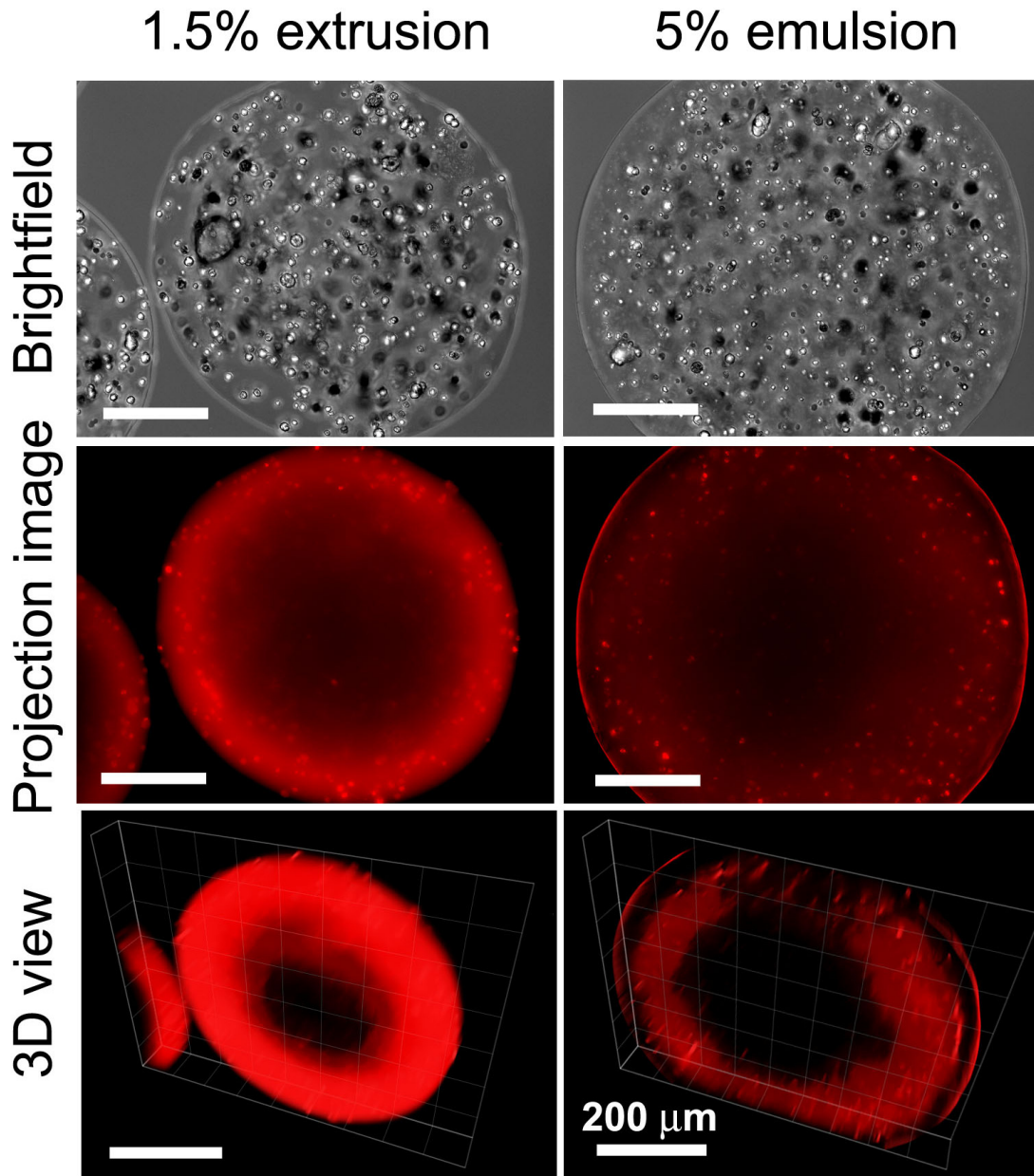


Figure B12. Visualization of mouse immunoglobulins (IgGs) in alginate beads.

Beads from two mice transplanted with 5% emulsion beads and one mouse transplanted with 1.5% extrusion beads, as well as control beads kept *in vitro* were used to visualize IgGs bound to the cells or beads. The beads (25 μL /sample) were washed with 1 mL HEPES buffered saline solution, the supernatant was removed to obtain 100 μL total volume, to which 100 μL of Alexa 568-conjugated goat anti-mouse IgG (Invitrogen) diluted 1:100 in the same solution were added. Beads from *in vitro* cultures were used as negative controls. After 1 h incubation at room temperature and 75 rpm orbital agitation in the dark, the beads were washed twice with HEPES buffered saline solution and immediately imaged on an inverted Olympus IX81 microscope. Stacks of 26 images acquired at 4 μm intervals were analyzed using Slidebook.

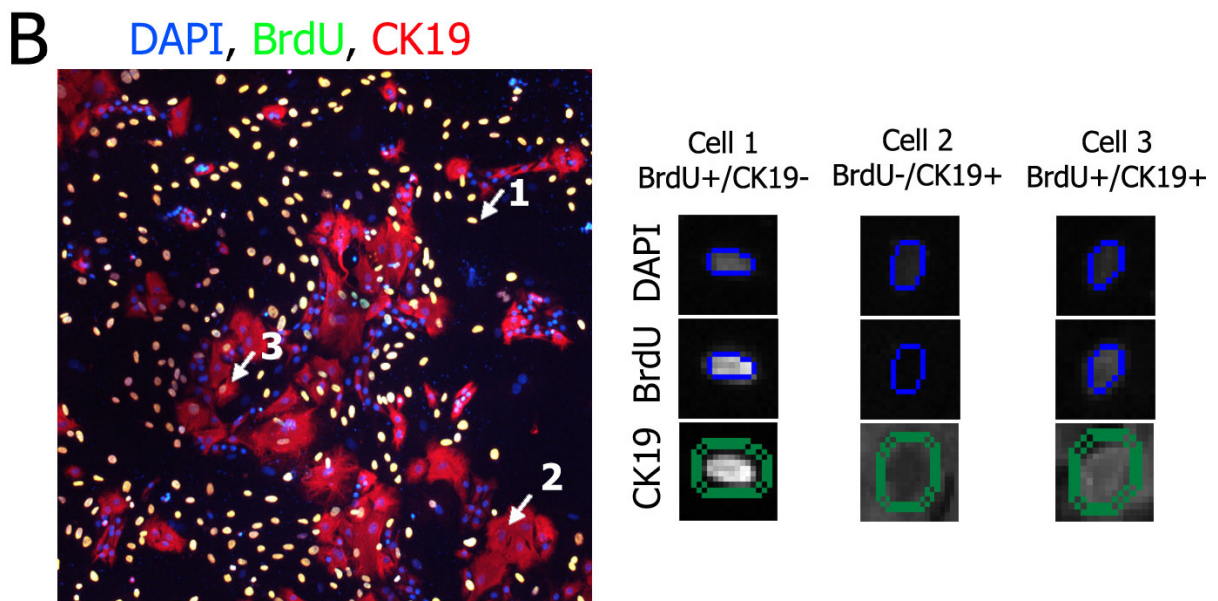
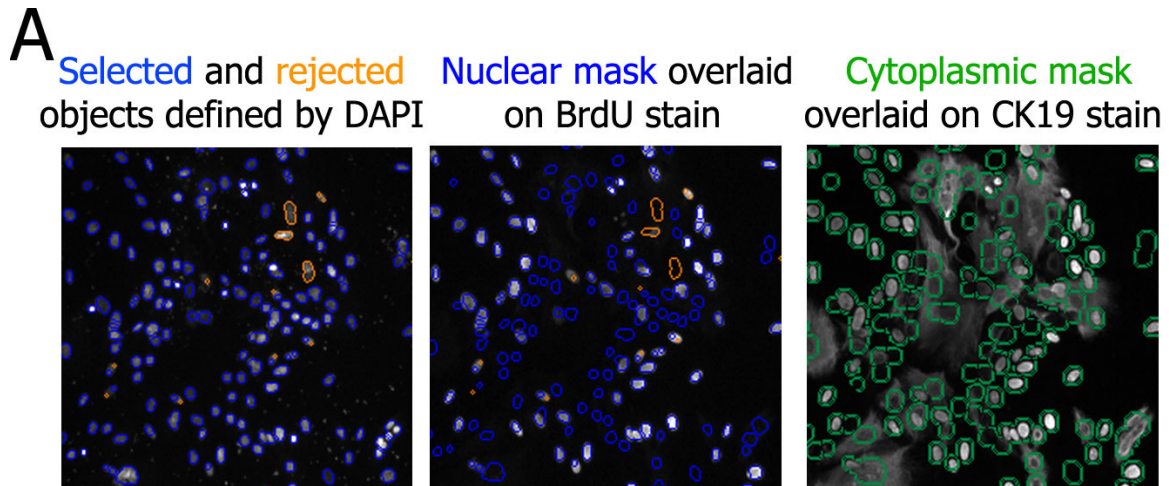


Figure B13. Cellomics image analysis.

(A) Object identification based on the shape and intensity of nuclei stained with DAPI in the UV fluorescence Channel 1. This nuclear region was used to quantify Ki67, BrdU or YoPro staining intensity in the green fluorescence Channel 2. The cytoplasmic mask was defined by tracing an annulus that started 1 pixel outside the nuclear region and extended 2 pixels further. This cytoplasmic region was used to quantify amylase staining intensity in Ch2, as well CK19, vimentin or Ca19-9 staining intensity in the red fluorescence Channel 3. (B) Sample Cellomics image with examples of a BrdU+/CK19- cell, a BrdU-/CK19+ cell and a BrdU+/CK19+ cell. The nucleus of the BrdU+/CK19+ cell is fluorescent because of the BrdU -> CK19 sequential staining sequence and because both primary antibodies were raised in mouse. However, no staining is found in the cytoplasmic region where CK19 staining is quantified.

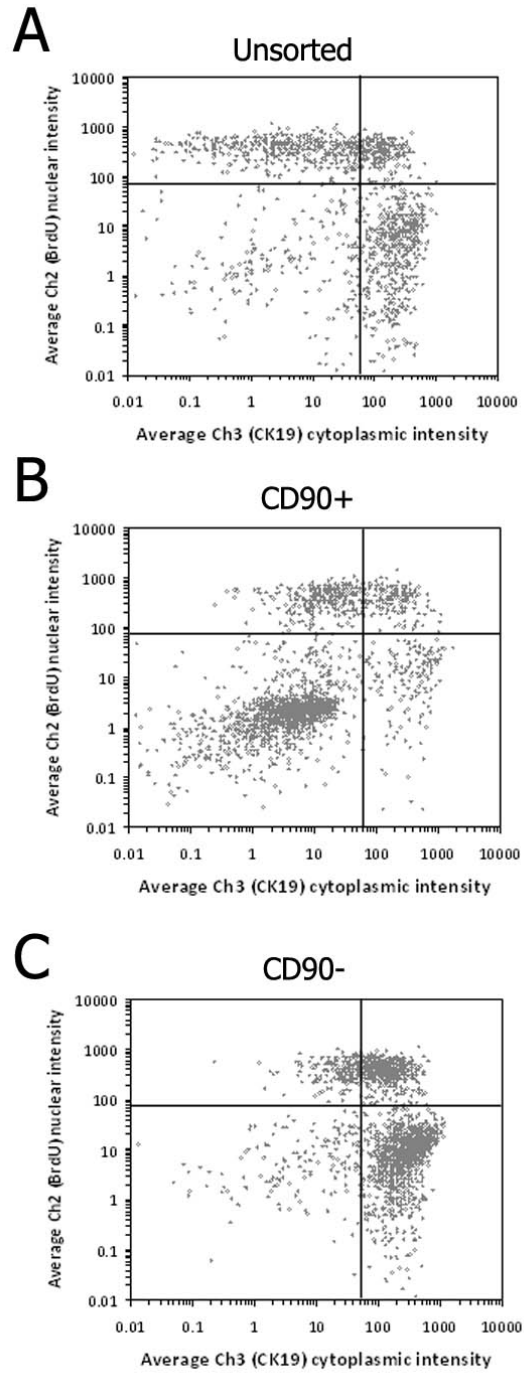
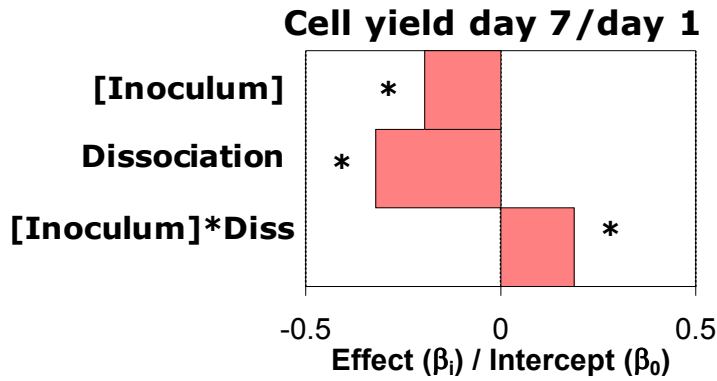


Figure B14. Quantification of BrdU and CK19 staining by the Cellomics algorithm.

(A) Unsorted, (B) CD90-enriched and (C) CD90-depleted populations analyzed by fixing the cells on day 8. Unsorted cells were plated on day 0, while CD90 sorting was performed on day 1. The quadrants were generated manually but allowing for at most 2% false positive cells in single stained controls. The results shown are for the BC130 pancreas.

A)



B)

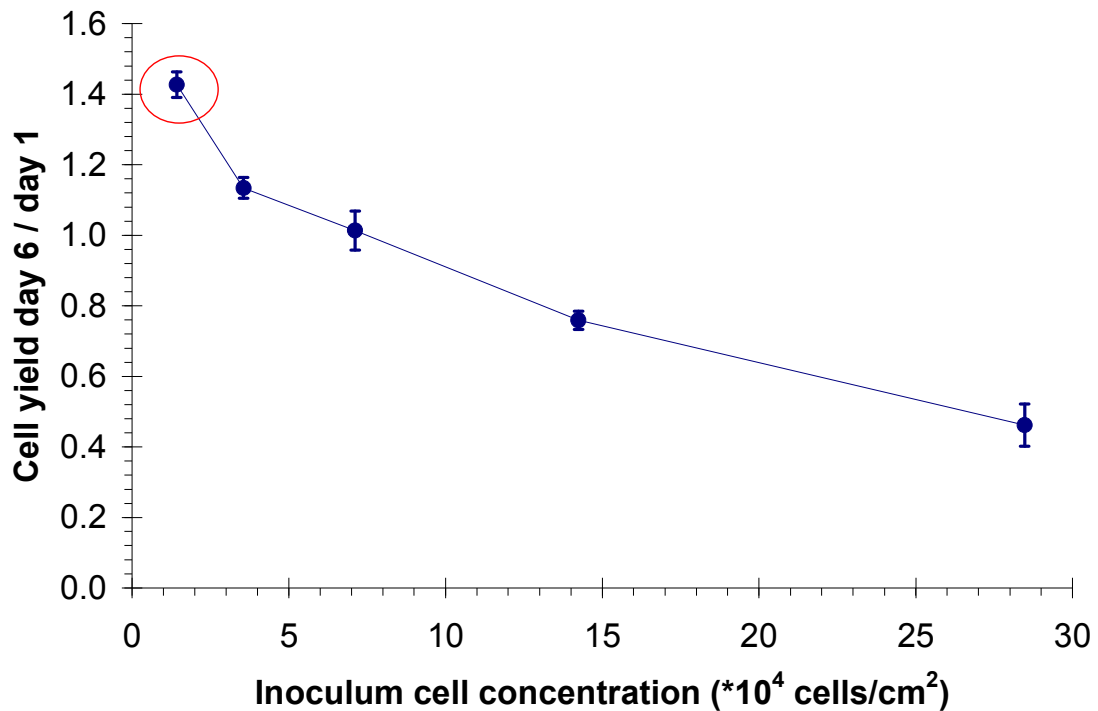


Figure B15. Impact of seeding density and dissociation into single cells on the yield of cells during monolayer culture.

(A) When considering the cell yield after the expansion step, seeding density was shown to have a negative effect on non-dissociated cell clusters. (B) A dose response curve for different seeding densities performed on non-dissociated cells from another pancreas confirmed the tremendous impact of seeding density on the yield of cells during monolayer culture. * $p < 0.05$

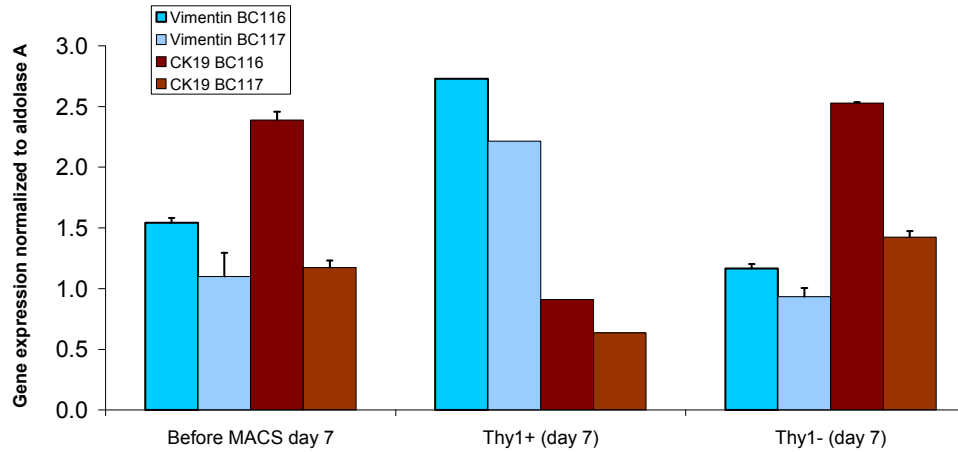


Figure B16. CK19 and vimentin expression levels in CD90-sorted populations.

The CD90 MACS was performed after 7 days of adherent culture of unsorted non-dispersed islet-depleted pancreatic clusters cultured in CMRL-10FBS. This culture step increased the number of CD90+ cells that could be used for mRNA extraction compared to the CD90+ cell numbers present on day 0 or day 1. Immediately after MACS, cells were sampled and gene expression levels were determined by q-PCR. The experiment was repeated for 2 pancreata (BC116 and BC117) and the error bars represent culture replicates.

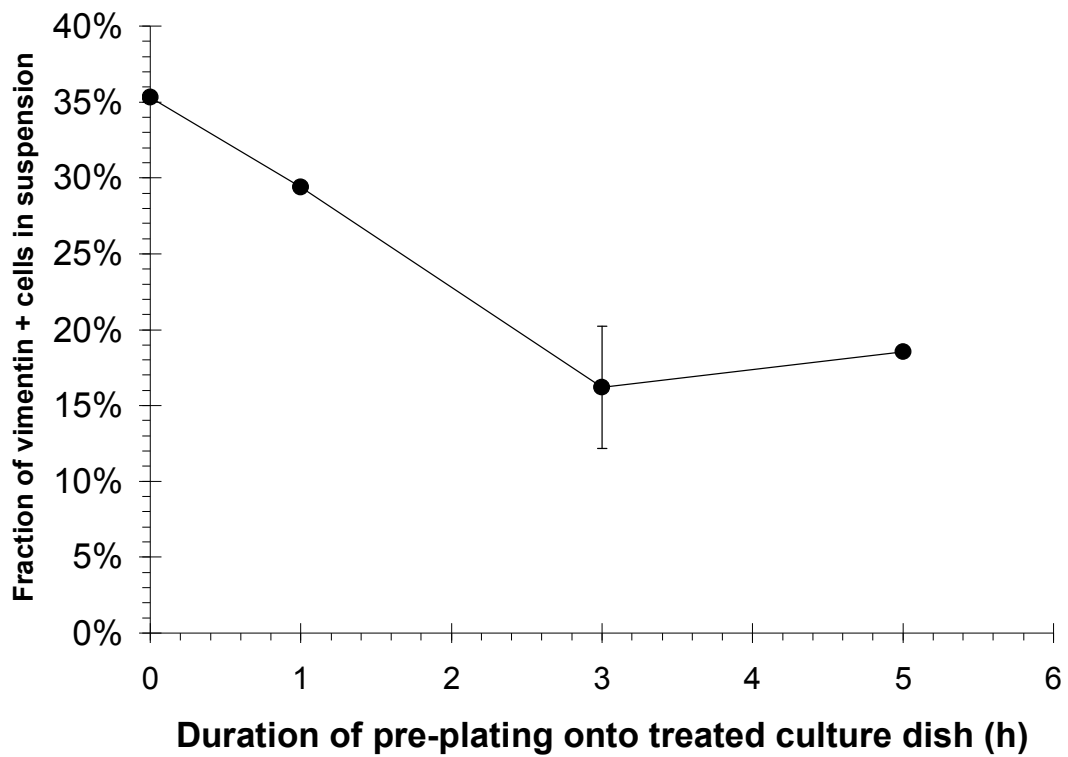


Figure B17. Pre-plating to eliminate vimentin+ cells from human islet-depleted pancreatic tissue

The cells that remain in suspension are then transferred to another tissue culture treated dish for experimentation. The cells used were single cells obtained from the dissociation of a whole neonatal porcine pancreas.

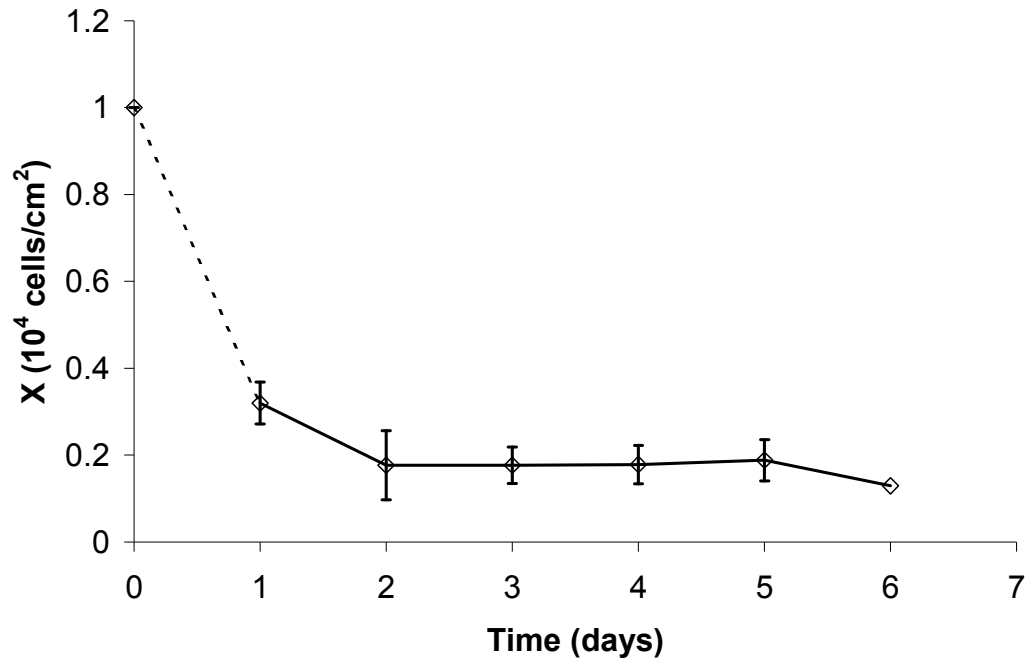


Figure B18. Changes in total cell number with time for unsorted dispersed islet-depleted pancreatic cells cultured in 96-well screening plates.

The cells were plated on day 0 in CMRL-10FBS, followed by medium change to CMRL-0.1XITS on day 1 and day 4. The dotted line represents the change between the total cell number seeded and the number of cells adherent one day later (i.e. the plating efficiency based on total live cells). The total live cell number was quantified by trypsinizing wells at each time point, followed by trypan blue cell enumeration. The data shown is the average of N=2 pancreata \pm SEM.

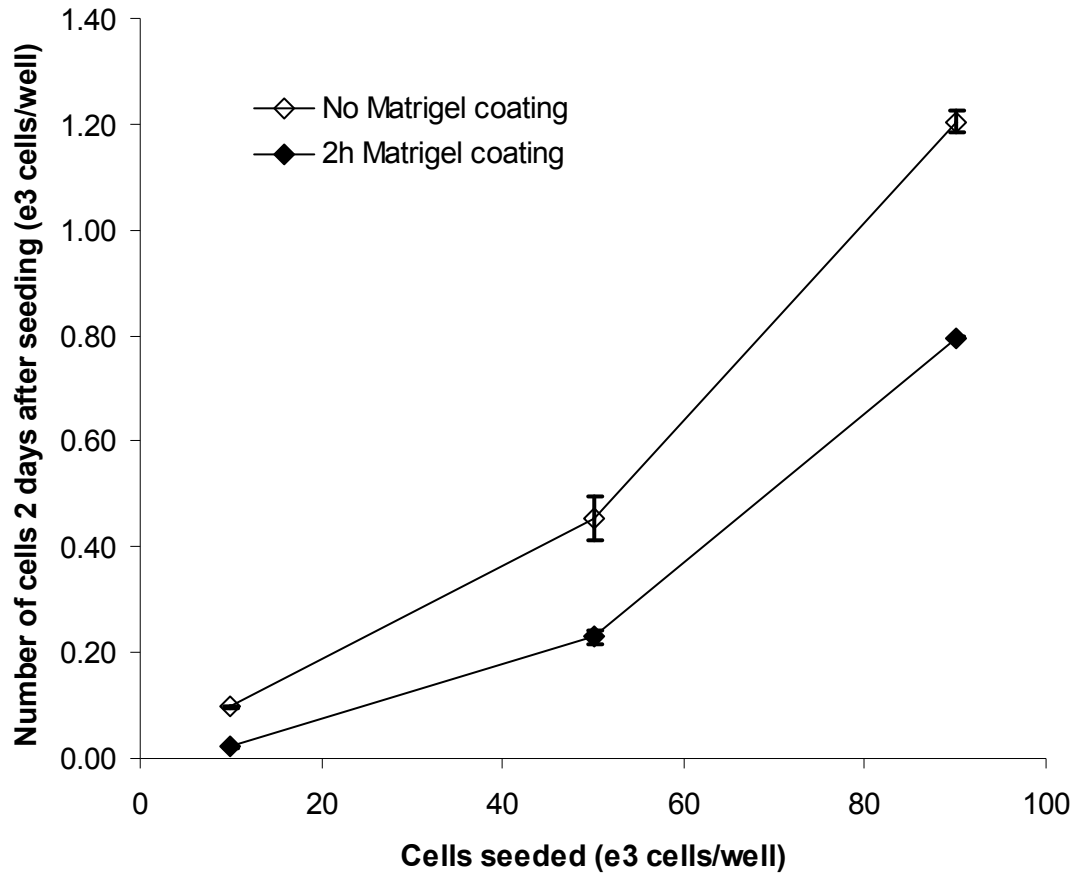


Figure B19. Effect of Matrigel surface coating on the seeding efficiency of CD90-depleted cells.

Total number of cells attached to the surface of uncoated or Matrigel-coated 96 well plates 24 h after adding 10 000, 50 000 or 90 000 CD90- cells/well on day 1. The results shown were obtained from a single pancreas (BC123) and represent the average \pm SEM of 3 replicate wells per condition.

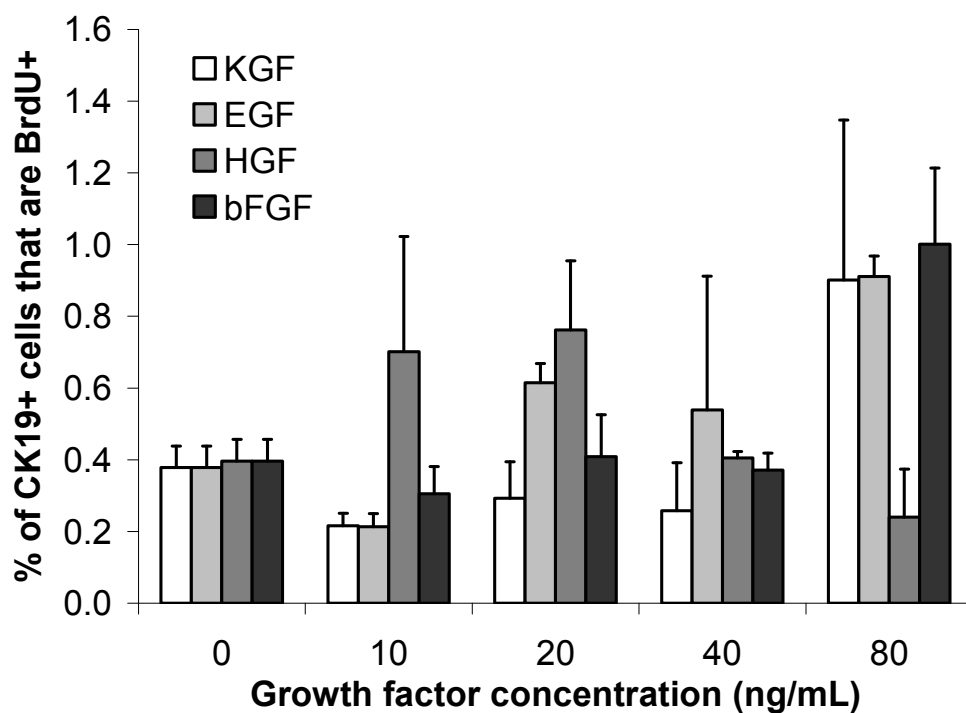
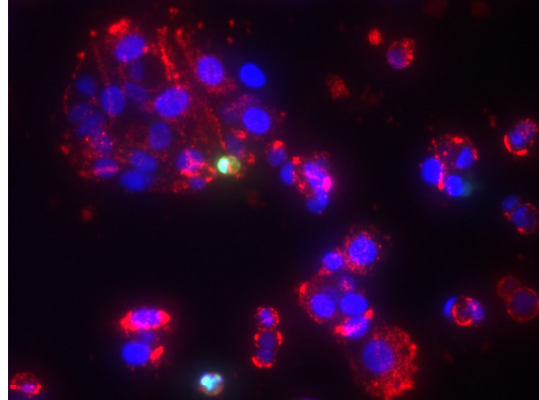


Figure B20. bFGF, EGF, KGF and HGF dose-dependent effects on the proliferation of human CK19+ pancreatic cells.

The results shown represent the average \pm SEM of the result measured in 3 replicate wells, but using a single pancreas (BC130).

A Hoechst, YoPro, Ca19-9



B

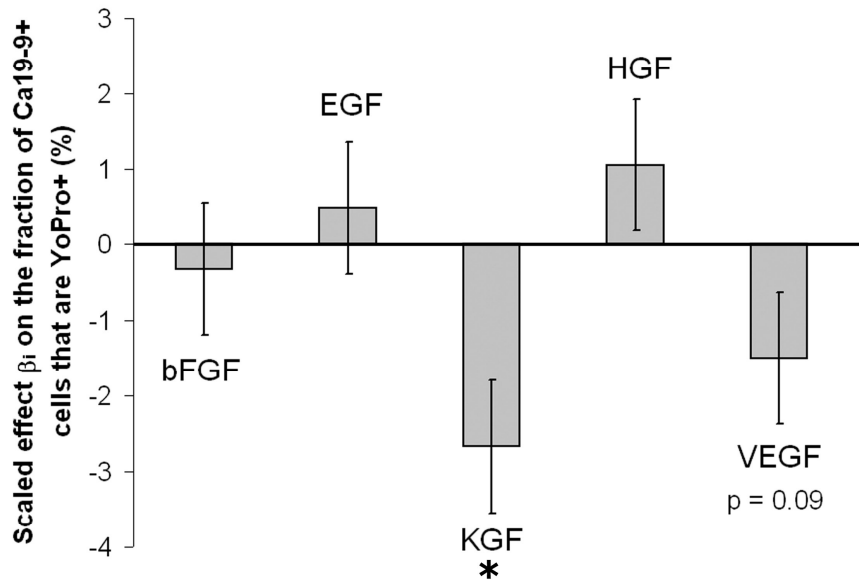


Figure B21. Effects of bFGF, EGF, KGF, HGF and VEGF on apoptosis measured on day 3 based on YoPro permeability of the Ca19-9+ cells.

(A) Sample image of live CD90- cells plated on day 1 in CMRL-10FBS, cultured in CMRL-0.1X ITS basal medium with 10% FBS added on day 2, then stained for YoPro and Ca19-9 on day 3. YoPro clearly labelled a subset of the Ca19-9+ cells. (B) The effects and interactions of the five growth factors were tested in a full factorial experiment including 8 centre points, but the whole model was not significant except for the KGF main effect ($p = 0.0483$). The whole model was therefore reduced to include only the main five growth factor effects, shown here. The model intercept value (at the centre point values of 10 ng/mL of each of the factors) was $24.9 \pm 0.8\%$ YoPro+ cells among the Ca19-9+ cells. Again, only the KGF negative effect was significant. The model prediction in the presence of KGF alone was $22.5 \pm 4.3\%$ YoPro+ cells among the Ca19-9+ cells. The fraction of YoPro+ cells among Ca19-9+ cells was $28 \pm 4\%$ in basal medium and $8 \pm 1\%$ in basal medium + 10% FBS. * $p < 0.05$ for the reduced model based on the whole model ANOVA.